AD NUMBER: AD0910452

LIMITATION CHANGES

TO:

Approved for public release; distribution is unlimited.

FROM:

Distribution authorized to U.S. Government agencies only; Administrative/Operational Use; 1 Apr 1973. Other requests shall be referred to Space and Missile Systems Organization, Los Angeles, CA 90045.

AUTHORITY

SAMSO ltr dtd 17 Jun 1977

SAMSO TR 73-65, Vol II

Final Report

SYSTEM 621B USER EQUIPMENT DEFINITION AND EXPERIMENTS PROGRAM

TASK VI – PHASE II

Volume II – Test and Equipment Description

Grumman Aerospace Corporation

Technical Report SAMSO TR 73-65, Vol. II
April 1973

Space and Missile Systems Organization
Air Force Systems Command
Los Angeles, California 90045

ERRATA

for

Technical Report SAMSO TR 73-65, Vol. II

1. Page 7, equation (20), now reads; "$W = M^{-1} \partial \rho_i$".
Should read; "$W = M^{-1} \delta \rho_i$".

2. Page 11, para. 2.1, second line now reads; "...antennas bottom and top), and interface . . .".
Should read; "...antennas (bottom and top), an interface...".

Page 11, para. 2.1.1., fifth line now reads; "...621B Receiver Power Supply..."
Should read; "...621B Receiver, Power Supply..."

3. Page 79, para. 3.1, third line now reads; "...by the 6586th Test Group...".
Should read; "...by the 6585th Test Group...".

4. Page 81, Figure 53, 12th entry now reads; "Installed Rcvr in MCS".
Should read; "Installed Rcvr in MCS at Northrop Strip".

5. Page 94, para. 3.2.1, third and fourth lines now read; " The 43-ft pole lengths were decided on as a result of a study to eliminate possible multipath due...".
Should read; "The pole lengths were decided on as a result of a study to eliminate possible ground multipaths due...".

6. Page 133, dash under sixth bullet now reads; "...lock-on on first try with $\dot{R}$ Zero and...".
Should read; "...lock-on on first try with $\dot{R} \simeq$ Zero and...".

7. Page 204, third and fourth lines from bottom now read;
"$BW_{code} = 5.6$"
"$BW_{carr} = 43.6$"
Should read;
"$BW_{code} = 2.8$"
"$BW_{carr} = 21.8$"

8. Page 228, second paragraph, second line now reads; "...covariance equations, see Ref. 1."
Should read; "...covariance equations, see Ref. 28".

SAMSO TR 73-65, Vol II

Final Report

SYSTEM 621B USER EQUIPMENT DEFINITION AND EXPERIMENTS PROGRAM

TASK VI – PHASE II

Volume II – Test and Equipment Description

Prepared by

Grumman Aerospace Corporation
Bethpage, New York 11714

For

Space and Missile Systems Organization
Air Force Systems Command
Los Angeles, California 90045

April 1973

FOREWORD

This report dated 11 April 1973, contains the findings of a program titled "System 621B User Equipment Definition and Experiments Program, Phase II Field Test". The work was accomplished by Grumman Aerospace Corporation (GAC), Grumman Data Systems Corp. (GDSC), both of Bethpage, N.Y. and the Hazeltine Corporation (HC) at Greenlawn, N.Y. and complies with all the requirements of Contract Number F04701-71-C-0176. In addition to the receivers which were designed and built under this contract, the Air Force provided an additional receiver designed and built by the Magnavox Research Laboratory (MRL) of Torrance, California which was also flight tested.

System 621B is a concept for a global satellite - based precision navigation system designed to meet the requirements of land, sea and air military forces in an advantageous cost effective manner. One of the most important elements in this system is the user receiver. This report summarizes a series of flight and ground tests conducted at the White Sands Missile Range to evaluate the performance of a four-channel receiver in typical flight and field environments in order to solidify confidence in the predicted performance of System 621B receivers.

The report is published in three (3) volumes and bears the Air Force report number SAMSO-TR 73-65. Volume I is an Executive Summary, presenting in concise form a description of the program, the ground and flight equipment and an overview of the test results. Volume II contains the detailed program history, equipment description and data processing approach. Volume III contains a detailed presentation of the data taken during the program and a discussion of the results and conclusions to be drawn therefrom.

Grumman wishes to acknowledge the assistance of Lt. Col. V.L. Denninger, Program Manager, and Capt. D. Wilson, the Air Force Space and Missile System Organization and of Messrs. W. Melton, F. Butterfield, T. Connor, A. Gillogly, W. Feese, Dr. J. Clifford, and Dr. L. Hagerman, of the Aerospace Corporation.

This report was prepared by Messrs. J. Courtney, R. Laho, I. Kadar, P. Richards, M. Moore of Grumman, R. Regis of Hazeltine, and B. Glazer of Magnavox.

John J. Courtney, Jr.
621B Director

Edward Z. Gray, Director
Special Projects

Publication approval of this technical report does not constitute Air Force approval of the report's findings or conclusions. It is published only for exchange and stimulation of ideas.

Valentine L. Denninger, Lt. Col., USAF
Program Manager
System 621B

ABSTRACT

System 621B is a concept for a global satellite-based precision navigation system designed to meet the requirements of land, sea and air military forces in an advantageous cost effective manner. One of the most important elements in this system is the user receiver. This report summarizes a series of flight and ground tests conducted at the White Sands Missile Range to evaluate the performance of a four-channel receiver in typical flight and field environments in order to solidify confidence in the predicted performance of System 621B receivers.

TABLE OF CONTENTS

TABLE OF CONTENTS (Cont)

LIST OF ILLUSTRATIONS

LIST OF ILLUSTRATIONS (Cont)

LIST OF ILLUSTRATIONS (Cont)

LIST OF TABLES

SECTION I

INTRODUCTION

1.1 REPORT CONTENT

This report documents the results of Phase II of the 621B User Equipment Definition and Experiment Program, which was the flight test of two four-channel receivers in a simulated operational environment at the White Sands Missile Range.

Volume I is an executive summary, containing a short overview of the entire test program. Significant test results such as system accuracy, major error sources, and major new findings of system operation are concisely presented; conclusions of the test program and recommendations for future work are also included.

Volume II describes the program objectives and system configuration, test facilities, 621B hardware and software, and the various tests used to evaluate the system. The primary purpose of Volume II is to present the background necessary for an understanding of the results discussed in Volume III. Additionally, certain aspects of the field test program which were an integral part of the program but do not directly impact the test results are also presented. These aspects concern the areas in which testing resulted in a better understanding of system behavior, and where, as a consequence, test configurations or procedures were modified.

Volume III presents the test data and an analysis of the data showing system behavior, error sources, and conclusions which can be derived from the data.

1.2 TEST OBJECTIVES

The primary objective of the field test program was to evaluate the performance of two four-channel receivers in typical flight and field environments. To achieve this goal a simulated satellite constellation geometry with typical receiver power profiles was established at White Sands Missile Range (WSMR). Ephemeris and ionosphere errors were not included in the test configuration. The flight profiles flown over the simulated satellite cluster of transmitters represented compressed time flights at representative satellite-to-user look angles. The test system accuracy including user dynamics in the presence of multipath, was to be demonstrated, both in Area Navigation and Instrument Landing System (ILS) flight configurations.

The integrity of the tests was to be established by calibration and accurate survey of the location of the transmitting antennas and ground systems, and by comparison of the derived trajectories with WSMR provided best estimate trajectories (BET's). The WSMR best estimate trajectory is a position and velocity solution obtained by combining data from optical and rf trackers, (see section 4.6).

Two correlation receivers were developed, differing in the design details but both capable of performing the measurements of range and range rate relative to each of the transmitters necessary for the unique determination of user's position and velocity coordinates. In particular, it was important to verify the predicted (both theoretical and laboratory measured) receiver performance parameters in an operational environment with dynamics, low signal levels and in the presence of multipath.

1.3 PASSIVE USER NAVIGATION

There are two major approaches to deriving three-dimensional passive position location information from a navigation satellite system: range differencing, and pseudo ranging.

In range differencing, the user measures the difference in the time of arrival of signals broadcast from a network of time synchronized satellites. With the satellite ephemerides and system time available to the user, simultaneous measurements from four satellites are necessary to solve for the three-dimensional position and velocity coordinates. Since the user's clock is not synchronized with respect to the satellite's clock, there is an apparent bias between the user and satellite clocks. The clock bias measurement is eliminated in the range differencing solution resulting in the intersection of three hyperbolic surfaces which locates position.

In pseudo ranging, the user also measures the time of arrival of signals simultaneously received from time-synchronized satellites. By performing four simultaneous measurements, the user establishes four independent pseudo ranges which differ from the geometrical ranges by the difference between the satellite oscillator phase and the user oscillator phase. The user, knowing the satellite ephemerides, can solve four equations in four unknowns for his position in three dimensions and the common bias of the range measurements. A similar computation algorithm enables the user to determine his three-dimensional velocity coordinates based upon doppler (pseudo doppler) measurements derived from the navigation signal.

The advantage of pseudo ranging is that the clock bias and bias rate are computed rather than eliminated, thus providing an independent source for estimating clock parameters, and allows smoothing of position and velocity computations. The pseudo ranging technique is therefore preferred in systems having accurate clocks and requiring high accuracy navigation. This technique was used in the field test.

The measurements are performed by a four-channel correlation receiver operating at L-band, receiving signals phase-shift keyed by unique pseudo random sequences, providing code division multiplexing of signals.

The measurement errors introduced into the system are a function of the signal design, the receiver implementation, and the time varying channel characteristics described by the relative system geometry and by the properties of the propagation medium. The errors affecting range and range rate measurements include ionospheric and tropospheric uncertainties, multipath, receiver noise, receiver precision, receiver dynamics and time varying biases introduced by the receiver. Other system error sources include calibration station location, range measurements, satellite clock drift and calibration station clock drift.

Only the user-to-satellite line-of-sight components of these errors contribute to "system" errors with the major contribution being the satellite position errors, ionospheric uncertainties and residual uncompensated biases.

The system implementation, in part consisting of ground based receivers at known locations and a master calibration station, provides for calibration of many of the error sources associated with the satellites, atmosphere, and clocks resulting in the computation of error correction parameters which are sent to the user over the satellite-to-user ranging link so that he may improve the accuracy of his position and velocity.

1.3.1 Theory

To determine his position and velocity a user cross-correlates pseudo random (PRN) codes (locally generated in the receiver) with the code-division-multiplexed navigation signals simultaneously emitted at the same carrier frequency by the satellites. The relative phase or equivalent time displacement between his local code and the incoming code is measured allowing determination of the relative range. Since, in general, the user is not synchronized to satellite time, the measurements just made (at least four) are not equivalent to the geometrical ranges to the satellites but rather to what are called pseudo ranges (ρ_i), where a pseudo range is a range differing from the geometrical range by a distance equivalent to the common receiver and the satellite time bias.

Simultaneous with range measurements, the user is measuring range rate in each channel from the doppler on the carrier frequency. Again, since the user's oscillator frequency is, in general, not synchronized to the satellite's oscillator frequency, a pseudo range rate rather than true range rate is measured. This information is sufficient for the calculation of user position and velocity given the satellites (R_i) ephemerides and the time of day of the satellites (GMT). The system provides these data as each satellite transmits its own ephemerides and Greenwich Mean Time as part of the navigation signal.

For this discussion, assume Earth Centered Relative (ECR) coordinates will be the basic computational reference system for System 621B. (See Figure 1.)

The pseudo range from the i^{th} satellite to the user is

$$\rho_i = \bar{\epsilon}_i \cdot (\bar{R}_i - \bar{R}_\mu) + b_\mu + b_i \qquad i = 1, \ldots, 4, \ldots, N$$

$$\bar{\epsilon}_i = \frac{\bar{R}_i - \bar{R}_\mu}{\rho_i - b_i - b_\mu} \tag{1}$$

where

b_u = user oscillator phase bias (ft); to be determined by user

b_i = satellite oscillator phase bias (ft); transmitted to user

In the same fashion the pseudo range rate from the i^{th} satellite to the user is

$$\dot{\rho}_i = \bar{\epsilon}_i \cdot (\dot{\bar{R}}_i - \dot{\bar{R}}_\mu) + \dot{b}_\mu + \dot{b}_i \qquad i = 1, \ldots, 4, \ldots, N \tag{2}$$

where

$\dot{b}_u$ = user oscillator frequency bias (fps); to be determined by user

$\dot{b}_i$ = satellite oscillator frequency bias (fps); transmitted to user

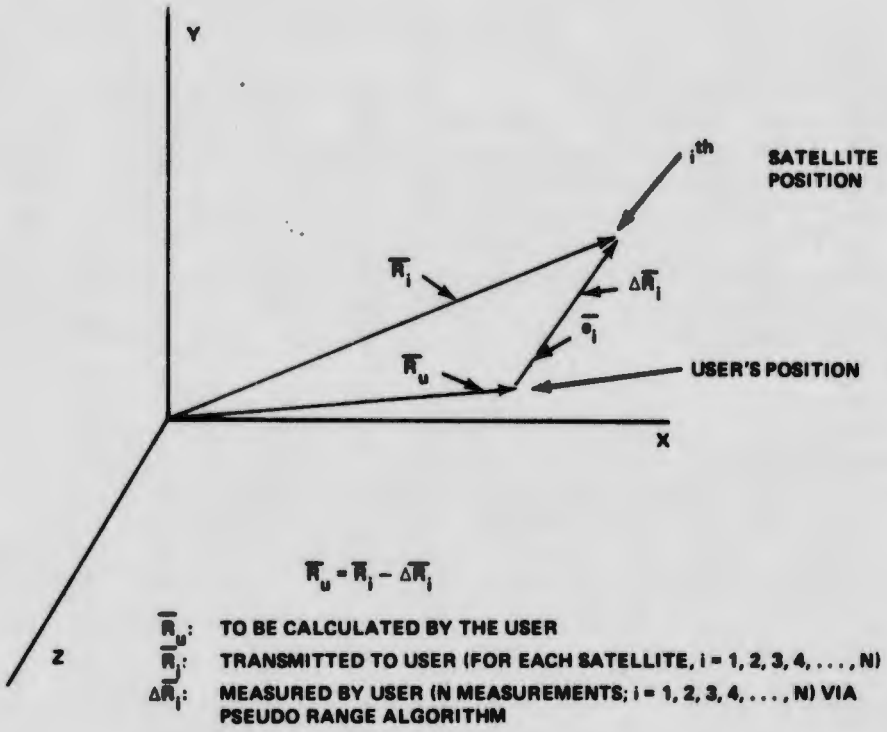

Figure 1 ECR Coordinates

Rearranging the above equations

$$\bar{\epsilon}_i \cdot \bar{R}_\mu - b_\mu = \bar{\epsilon}_i \cdot \bar{R}_i + b_i - \rho_i \tag{3}$$

$$\bar{\epsilon}_i \cdot \dot{\bar{R}}_\mu - \dot{b}_\mu = \bar{\epsilon}_i \cdot \dot{\bar{R}}_i + \dot{b}_i - \dot{\rho}_i \tag{4}$$

The matrix equation for the four satellites becomes

$$\underset{(4\times4)}{\begin{bmatrix} \bar{\epsilon}_1^T & -1 \\ \bar{\epsilon}_2^T & -1 \\ \bar{\epsilon}_3^T & -1 \\ \bar{\epsilon}_4^T & -1 \end{bmatrix}} \underset{(4\times1)}{\begin{bmatrix} R_\mu \\ b_\mu \end{bmatrix}} = \underset{(4\times16)}{\begin{bmatrix} \bar{\epsilon}_1^T & 1 & 0000 & 0000 & 0000 \\ 0000 & \bar{\epsilon}_2^T & 1 & 0000 & 0000 \\ 0000 & 0000 & \bar{\epsilon}_3^T & 1 & 0000 \\ 0000 & 0000 & 0000 & \bar{\epsilon}_4^T & 1 \end{bmatrix}} \underset{(16\times1)}{\begin{bmatrix} R_1 \\ b_1 \\ R_2 \\ b_2 \\ R_3 \\ b_3 \\ R_4 \\ b_4 \end{bmatrix}} - \underset{(4\times1)}{\begin{bmatrix} \rho_1 \\ \rho_2 \\ \rho_3 \\ \rho_4 \end{bmatrix}} \tag{5}$$

$$G_\mu \bar{X}_\mu = B_\mu \bar{X}_s - \bar{\rho} \tag{6}$$

where the direction cosine matrices G_u and B_u are known to sufficient accuracy.

The system measurements become

$$\bar{\rho} = B_\mu \bar{X}_s - G_\mu \bar{X}_\mu \tag{7}$$

$$\bar{\dot{\rho}} = B_\mu \bar{\dot{X}}_s - G_\mu \bar{\dot{X}}_\mu \tag{8}$$

with the resulting measurement error equations

$$\delta\bar{\rho} = B_\mu \delta\bar{X}_s - G_\mu \delta\bar{X}_\mu + \bar{d} + \bar{n}_1 \tag{9}$$

$$\delta\bar{\dot{\rho}} = B_\mu \delta\bar{\dot{X}}_s - G_\mu \delta\bar{\dot{X}}_\mu + \bar{\dot{d}} + \bar{n}_2 \tag{10}$$

where

$B_u \delta\bar{X}_s$, $B_u \delta\bar{\dot{X}}_s$ = projection of the error due to satellite orbit determination and satellite oscillator errors in the line-of-sight directions

$G_u \delta\bar{X}_u$, $G_u \delta\bar{\dot{X}}_u$ = projection of the error vector due to user position and velocity error together with user oscillator errors in the line-of-sight directions

$\bar{d}$, $\bar{\dot{d}}$ = measurement error due to environment (ionosphere signal delay correction, multipath delay, troposphere signal delay correction, and vehicle dynamics)

n_1, n_2 = measurement error due to uncorrelated receiver noise

In reference to the Earth Centered Coordinates given in Figure 1, the user by performing four simultaneous pseudo range ρ_i, and pseudo range rate $\dot{\rho}_i$, measurements can compute his three-dimensional position and velocity coordinates by the solution of Eqs. (1) and (2) for $\bar{R}_u$ and $\bar{\dot{R}}_u$ respectively.

1.3.1.1 Position Solution

Starting with Eq. (1) one can write, defining $b = b_u + b_1$;

$$\bar{R}_i \cdot \bar{R}_\mu = -\frac{(\rho_i - b)^2}{2} + \frac{\bar{R}_i \cdot \bar{R}_i + \bar{R}_\mu \cdot \bar{R}_\mu}{2} \tag{11}$$

$$\bar{f} = \text{col}\left[R_{\mu x}, R_{\mu y}, R_{\mu z}, b\right]$$

Subtracting pairs of equations for i=1, 2, 3, 4 one can define a vector $\bar{f}$ in terms of the unknowns as:

$$D\bar{f} = C \tag{12}$$

where

$$D = \begin{bmatrix} (\bar{R}_2 - \bar{R}_1)^T (\rho - \rho_2) \\ (\bar{R}_3 - \bar{R}_2)^T (\rho_2 - \rho_3) \\ (\bar{R}_4 - \bar{R}_3)^T (\rho_3 - \rho_4) \end{bmatrix}, C = \frac{1}{2} \begin{bmatrix} \rho_1^2 - \rho_2^2 + \bar{R}_2 \cdot \bar{R}_2 - \bar{R}_1 \cdot \bar{R}_1 \\ \rho_2^2 - \rho_3^2 + \bar{R}_3 \cdot \bar{R}_3 - \bar{R}_2 \cdot \bar{R}_2 \\ \rho_3^2 - \rho_4^2 + \bar{R}_4 \cdot \bar{R}_4 - \bar{R}_3 \cdot \bar{R}_3 \end{bmatrix}$$

Equation (12) is solved satisfying the constraint (from Eq. (11) by selecting i=4 for reference; i.e., the 4th transmitter)

$$\bar{R}_4 \cdot \bar{R}_\mu = -\frac{(\rho_4 - b)^2}{2} + \frac{\bar{R}_4 \cdot \bar{R}_4 + \bar{R}_\mu \cdot \bar{R}_\mu}{2} \tag{13}$$

This solution satisfying the constraint, results in a quadratic. The appropriate roots are selected based upon physical realizability (Ref 1).

1.3.1.2 Velocity Solution

The velocity solution is obtained from Eq. (2) containing a set of four linear equations in four unknowns;

$$\bar{\epsilon}_i (\dot{\bar{R}}_i - \dot{\bar{R}}_\mu) = -\dot{\rho} + \dot{b} \tag{14}$$

let,

$$\dot{\bar{f}} = \text{col}\left[\dot{R}_{\mu x}, \dot{R}_{\mu y}, \dot{R}_{\mu z}, \dot{b}\right] \tag{15}$$

where

$$M\dot{\bar{f}} = I\rho_i + A \tag{16}$$

$$M = \begin{bmatrix} \epsilon_{11} & \epsilon_{12} & \epsilon_{13} & \epsilon_{14} \\ \epsilon_{21} & \epsilon_{22} & \epsilon_{23} & \epsilon_{24} \\ \epsilon_{31} & \epsilon_{32} & \epsilon_{33} & \epsilon_{34} \\ \epsilon_{41} & \epsilon_{42} & \epsilon_{43} & \epsilon_{44} \end{bmatrix} \qquad A = \begin{bmatrix} \bar{\epsilon}_1^T \cdot \dot{\bar{R}}_1 \\ \bar{\epsilon}_2^T \cdot \dot{\bar{R}}_2 \\ \bar{\epsilon}_3^T \cdot \dot{\bar{R}}_3 \\ \bar{\epsilon}_4^T \cdot \dot{\bar{R}}_4 \end{bmatrix}$$

$$\dot{\bar{f}} = M^{-1}\left[I\dot{\rho}_i + A\right] \tag{17}$$

provided that M is nonsingular.

1.3.1.3 Static Geometric Dilution of Precision

The apparent time-of-arrival and apparent doppler measurements are corrupted by errors caused both by the propagation medium and by the receiver error sources which are a strong function of the signal design.

Starting with noisy measurements, the solution algorithms for position and velocity in three dimensions (based upon pseudo range and pseudo doppler) will result in noisy position and velocity solutions. The position and velocity solutions in three dimensions obtained directly by linear transformations of pseudo range and pseudo range rate measurements respectively are called the "Static" position and velocity solutions (Ref. 2).

The sensitivity of the position solution to unity measurement errors as a function of the linear transformation (a function of the relative position of the user with respect to the satellites) is a measure of the reduction (or dilution) of the system precision. The covariance of the transformation to unity measurement error variances is called the Geometric Dilution of Precision (GDOP), which is a measure of the degree to which measurement errors are amplified by system geometry effects to produce position errors.

The sensitivity equations for position follow from Eq. (1) with $\partial\bar{R}_1 = \bar{0}$ as:

$$\bar{\epsilon}_i \cdot \delta\bar{R}_\mu + \delta b = \delta\rho_i \qquad i = 1,2,3,4 \tag{18}$$

$$M\begin{bmatrix}\delta\bar{R}_\mu \\ \delta b\end{bmatrix} = \delta\rho_i \tag{19}$$

where

$$M = \begin{bmatrix}\epsilon_{11} & \epsilon_{12} & \epsilon_{13} & 1 \\ \epsilon_{21} & \epsilon_{22} & \epsilon_{23} & 1 \\ \epsilon_{31} & \epsilon_{32} & \epsilon_{33} & 1 \\ \epsilon_{41} & \epsilon_{42} & \epsilon_{43} & 1\end{bmatrix}$$

$$W = \text{col}\left[\delta\bar{R}_\mu, \delta b\right]$$

Define W = col

$$W = M^{-1}\,\delta\rho_i \tag{20}$$

Taking expected values of both sides of Eq. (20);

$$E\left\{WW^T\right\} = M^{-1} E\left\{\delta\bar{\rho}_i\, \delta\bar{\rho}_i^T\right\}(M^{-1})^T \tag{21}$$

If $E\left\{\delta\bar{\rho}_i\, \delta\bar{\rho}_i^T\right\} = I$ (Identity Matrix), the static GDOPs are given by:

$$GDOP\begin{bmatrix} X \\ Y \\ Z \\ b \end{bmatrix} = \left\{DIAGONAL\left[M^{-1}(M^{-1})^T\right]\right\}^{\frac{1}{2}} \tag{22}$$

The purpose of filtering the static solution is to obtain the best linear estimate in some sense (i.e., least squares) of the noisy position and velocity solution by taking advantage of the relationships among independent measurements (observables) the physics of the measurement process and the dynamics of motion. The Kalman filter provides a recursive procedure for providing a linear, statistically optimum estimate of the parameters involved.

1.3.2 Experiment Program Implementation

The principal elements of the System 621B Field Test Navigation System consist of the ground transmitters, calibration receiver segment and the airborne receiver (user) segment. Both the ground and airborne segments utilize four-channel correlation receivers to extract apparent time of arrival and doppler history of the incoming signals. Each ground transmitter generates a navigation signal consisting of a PRN code modulated on an L-band rf carrier.

The test program was designed with certain constraints with respect to the final operational concept in order to keep the overall execution time of the test program within reasonable bounds. The prime areas where constraints were applied are:

- The 621B signal did not contain "satellite" or time information but consisted only of the PRN modulated range code signal
- Hardware synchronization of the transmitters was not attempted. Instead, a time history of the transmitted signals was recorded and synchronization of the data accomplished post-flight via software
- The operational environment was simulated by scaling the distance down and inverting the system. The test range space available at WSMR, and the flight envelope of the test aircraft limited realistic simulation and data collection regions to narrow corridors approximately 6 n mi long x 2 n mi wide

By taking and recording eight simultaneous measurements of pseudo-range and pseudo-range rate to each of the four transmitters at both the ground and airborne receivers and knowing the location of the ground transmitters, aircraft position and velocity in three dimensions, and bias and bias rates can be determined by post-flight data processing. The pseudo-range measurements are derived by tracking the phase of the PRN code while the pseudo-doppler measurements are derived from the reconstructed rf carrier.

The airborne and ground recorded pseudo-range and pseudo-doppler data are brought together (post-flight) using WSMR time as a basis for aligning the two data sets. The test system is synchronized in the software by tracking the change of the apparent range and range rate in the transmitter signal histories recorded by the calibration receiver. The total pseudo range and psuedo dopplers were formed by subtracting the airborne components of pseudo range and pseudo doppler from the ground components (adjusted to common sample intervals based upon WSMR time) and used as described in paragraph 1.3 to compute user position and velocity in a convenient coordinate frame for WSMR tests.

SECTION II

EQUIPMENT DESCRIPTION

This section describes the 621B experimental equipment developed by the Grumman Aerospace Corporation, the Hazeltine Corporation (HC) and the Magnavox Research Lab (MRL) to support the system 621B Experiments Program. For a more detailed description of the Magnavox Research Lab 621B receiver refer to Ref. 3.

2.1 FLIGHT VEHICLE EQUIPMENT

The airborne 621B experimental equipment consists of two 621B receivers (HC and MRL), two antennas (bottom and top), and interface unit, on-board data recorders and an IRIG "B" timing system. A control panel was supplied to provide antenna selection and signal distribution to the receivers. A remote controlled signal attenuator in the received signal line was used to aid in initial acquisition of the 621B signal and provide for adjusting the signal levels into the receivers during the various flight profiles.

2.1.1 Receiver (Hazeltine Corp.)

Two interchangeable receivers were provided, one for use in the aircraft and the other for use in the Mobile Calibration Station (MCS). The main function of the receivers is to provide digitally formatted data which are related to range and range rate of the receiver relative to each of the four transmitters. (Figure 2 shows the Hazeltine 621B Receiver Power Supply, Displays and Controls)

Certain analog and discrete signals are also provided which are of use during post-flight data reduction to determine the status of the receiver.

A modular design was selected to permit quick fault isolation and module replacement as an aid in maintenance and to provide rf shielding within the unit. The receiver consists of eight modules (four processor modules, RF/IF module, frequency source module, distribution module, and a self test module) as shown in the block diagram of Figure 3. The functions are briefly described below.

The received signal, code division multiplexed from the four transmitters, are amplified by the rf and IF amplifiers and applied to the processors and matched filter.

When the processors are not in synchronization, the matched filter outputs are used to start the processor code generators at the approximate code state (a fraction of a code bit) of the incoming signal. When the processor is in sync, the matched filter outputs are disregarded. Each processor has a unique M-sequence code generator which is the same as the code generator in the respective transmitter so that each processor will track one, and only one, transmitter.

The processors utilize coherent phase lock loops for carrier and code tracking. The main outputs of the processor are digital words giving coarse pseudo range (100 nanosecond increments), fine pseudo range (0.5 nanosecond increments), and coarse

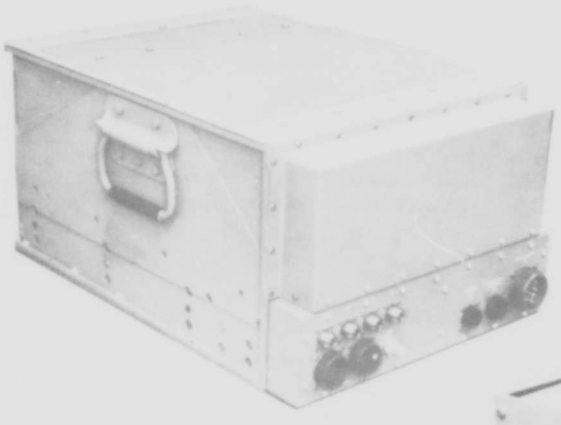

RECEIVER
DIMENSIONS: 10 x 14 x 18 IN.
82 LB
1575 MHz

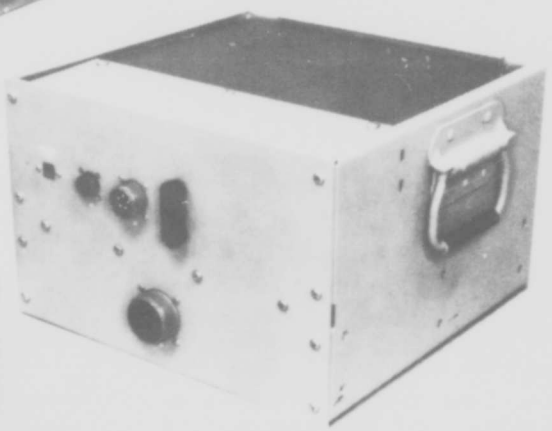

POWER SUPPLY
DIMENSIONS: 9 x 14 x 13.5 IN.
64 LB

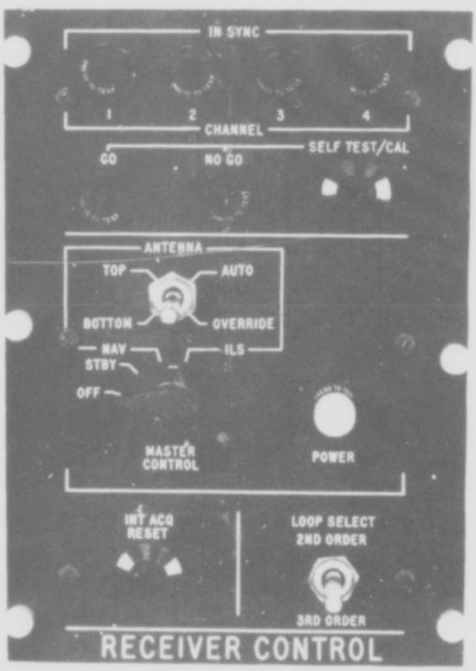

AIRBORNE RECEIVER
CONTROL PANEL
DIMENSIONS: 8.25 x 5.75 x 3 IN.
2.5 LB

Figure 2 Hazeltine Navigation Receiver, Power Supply, and Controls

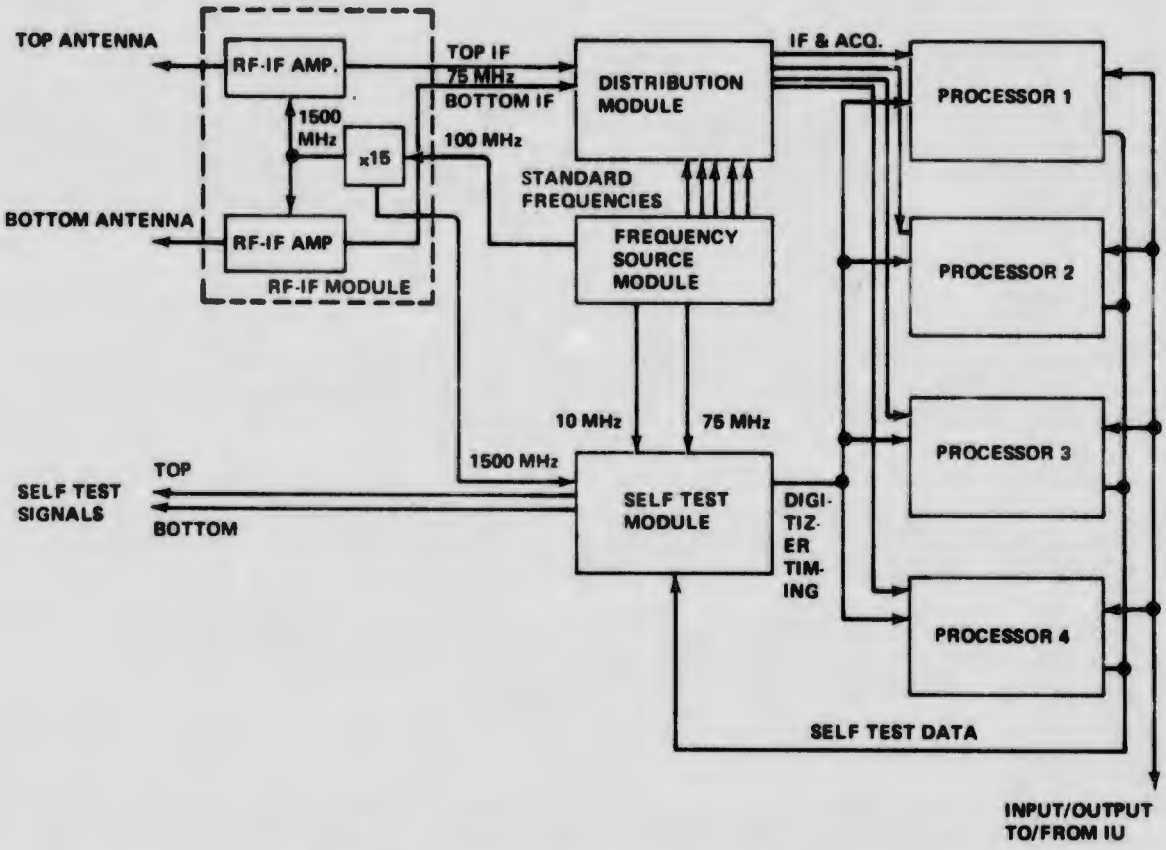

Figure 3 Hazeltine Receiver, Block Diagram

and fine pseudo doppler (0.05 fps). These words are available at any time and rate, on request from the Interface Unit (IU). In the test program, the airborne receiver supplied data sets on request at intervals of 0.2 seconds for all four processors, providing a navigation update rate of five times per second. The ground (MCS) receiver responded to data requests at a rate of once per second. In the test configuration, these outputs were supplied via interface units to digital tape recorders.

2.1.1.1 RF/IF Module

The RF/IF module receiver, selects and amplifies the incoming protected signals, and down-converts the incoming rf signal to an IF signal for processing. There are two separate RF/IF modules incorporated into the receiver because the original intent was to perform ILS tests using an F-4 aircraft. The three ground transmitters and one balloon-borne transmitter would have not been visible to a single antenna for the complete ILS approach. It was planned to switch the inputs to the processors from the top and the bottom antenna, to the top antenna at a point in the approach where the top antenna has a view of all four transmitters. Therefore, two antennas would be required. To avoid phase cancellation between signals received from a common source by both antennas (the top and bottom aircraft antennas), separate RF/IF processing is required for each antenna. Thus two separate, but identical, RF/IF modules are provided in the receiver. However, the NC-135A actually used as the test aircraft has an antenna location which provided a view of all four transmitters for the entire ILS approach. This eliminated the need for antenna switching.

2.1.1.2 Frequency Source Module

This module consists of the stable 5 MHz oscillator and a frequency synthesizer. The oscillator uses a precision F-C cut quartz crystal in a double oven. The frequency synthesizer provides the seven separate frequencies (1.125 MHz, 10 MHz, 10.05 MHz, 15 MHz, 75 MHz, 90 MHz and 100 MHz) used by the RF/IF, processor and self test modules.

2.1.1.3 Distribution Module

This module contains two matched filters (one for each of the two RF/IF channels), their related amplifiers and filters, IF channel switching for the two antennas, IF distribution, and distribution of the various reference frequencies.

A lithium niobate surface acoustic wave matched filter generates a synchronizing (sync) pulse in response to the acquisition portion of the received signal code. The sync pulse is used to time the start of the internally generated reference code which is used to track and demodulate the received signal.

The antenna switching and control circuits determine which antenna and RF/IF module is used to provide each of the four processors with an IF signal. This is selectable at the control box for various operating modes.

2.1.1.4 Processor Module

Four identical and interchangeable processor modules are used in each receiver. Each processor module contains a reference code generator, code tracking loop, carrier tracking loop, reacquisition circuitry and pseudo-range and pseudo-doppler digitizer to perform a complete signal tracking and measurement function for a receiver channel.

The reference code generator provides the protected signal code for range tracking and for demodulation to provide a reconstituted carrier for doppler tracking. The code generator consists of a 25-stage shift register with taps to provide a pseudo-random code sequence, identical to that generated at the corresponding transmitter, at the nominal rate of 10 Mbps. The code repeats at about 3.3 seconds. The code generator also provides a code, used internally by the receiver, to achieve additional cw jamming resistance.

The reacquisition circuitry was originally intended to provide a technique in each channel to automatically reacquire the signal if it is briefly interrupted. The scheme was as follows: Upon loss of signal, the reacquisition circuitry jumps the code ahead and scans back sequentially searching until lock is acquired. If lock is not acquired in the initial scan the search is repeated until the signal is acquired; or, if the signal is not acquired in a preset time, the initial acquisition mode is activated. However, the reacquisition circuitry was not made fully operational as the initial acquisition technique (using the matched filter) adequately accomplished the reacquisition function.

The code tracking loop is a third-order loop during tracking. It is automatically switched to second-order loop for acquisition. One-half bit early-late coding is utilized in the code tracking loop to develop the phase error used to correct its VCXO. The VCXO output drives the code generator and range digitizers.

The carrier tracking loop is also a third-order loop during tracking and is automatically switched to a second-order loop for acquisition. The carrier tracking loop VCXO maintains an offset frequency equal to the doppler shift on the incoming signal. The output of the carrier VCXO determines the exact processor IF frequency and input to the doppler digitizers to provide coarse and fine doppler outputs.

The pseudo-range digitizers provide coarse and fine range data words to the IU. Coarse pseudo-range information for each channel is digitized in a 25-bit counter which is driven in synchronism with the code generator. Fine range is determined by a heterodyne type of vernier technique which provides a pseudo-range resolution 0.5 ft. The fine range is digitized in an 8-bit counter. One additional bit is provided to resolve a potential ambiguity between the coarse and fine digitizer outputs. Pseudo range is shifted from the counters upon command by the transfer pulse from the IU, stored by 26 and 8-bit shift registers, and read out at a 200 KHz rate upon reception of the associated read pulse. The serial data transfer rate is arbitrary, and any rate up to about 5 MHz could be used for the receiver.

The pseudo-doppler digitizer provides a fine and coarse doppler output to the IU. Each digitizer converts the pseudo-doppler information of its corresponding channel to binary format with resolution of 0.05 fps. The coarse and fine pseudo-doppler information is stored and transferred to 20-bit and 15-bit shift registers, respectively, and read out serially at a 200 KHz rate upon receipt of the associate read pulse from the IU.

2.1.1.5 Self Test Module

The self test module contains the standard clock digitizer, digitizer timing and control circuits, self test signal generator, self test code generator, signal strength power monitor and Go/No-Go decision circuitry.

The standard clock digitizer is provided to measure the state of the 10 MHz standard frequency in a 25-stage counter upon receipt of the transfer pulse. This is transferred to the IU at a 200 KHz rate upon receipt of a read pulse. The pseudo-range words are subtracted from this clock word to obtain the pseudo range used in the navigation solution. Use of the clock word removes constraints on when the receiver may be interrogated for range data.

The digitizer timing and control circuits determine the overall digitizer timing for each of the channels.

The self test signal generator provides a coded 1575 MHz signal which can be tracked by all processors when in the self test mode. A 75 MHz carrier is biphase modulated, amplitude modulated (power boosted) during the acquisition code, and upconverted to 1575 MHz utilizing a sample of the receiver 1500 MHz local oscillator carrier. Normal operation is for approximately 21 seconds after the self test cycle is initiated, after which the signal is disabled to prevent interference with the incoming signals. Extended testing and troubleshooting is facilitated by switching to the calibration mode which provides a continuous signal. CW operation is also provided for test purposes.

The self test code generator is identical to those used in the processors and transmitters. It nominally generates a fifth code, the self test code, as determined by a program connector. Modifications to the control lines enable the code generation and gates required for the self test/calibrate cycle.

The signal strength monitor and decision circuits are used to monitor the receiver power applied to the antenna inputs. During the self test cycle a GO status is indicated if all gains in the RF/IF and processors are within a preset "window". An excessive loss in gain or self test signal power will cause a NO GO indication. An analog voltage representation of the received power is provided to the IU during self test, as well as during normal operation.

2.1.1.6 Receiver Power Supply

The receiver power supply contains a purchased special module and control circuitry to enable Off, Standby and Operate modes of operation. The power supply module, operating from 400 Hz, three-phase power, provides all voltages required for receiver operation with current-limiting and over-voltage protection. Only the 28 vdc is provided in the standby mode to operate the receiver ovens. A three-phase circuit breaker is provided on the front panel for local short circuit protection.

2.1.1.7 Receiver Airborne Control Panel

This unit provides all manual controls for the receiver required during operation, see Figure 2. This box also provides the visual indication of lock-on for each of the four channels as well as the Go/No-Go indication for the self test circuits.

Additional information of the receiver is provided as necessary in this report to understand the test results. A comprehensive discussion of receiver operation can be found in the Operation and Maintenance Manual (Ref. 4).

2.1.2 Airborne Receiver Functional Design (Magnavox Research Labs)

This section is adapted from the Magnavox Research Lab (MRL) report (Ref. 3) and is included here in order to provide a convenient reference for discussing test results in Volume III. A complete description of Magnavox Research Lab's contribution to the 621B Experiment Program may be found in the referenced report.

The MX-450 Navigation Receiver was designed to acquire, track, and process a composite signal consisting of four unique pseudo-noise (PN) modulated, L-band carrier signals for the purpose of deriving very accurate estimates of signal arrival times and doppler frequencies relative to a local frequency time standard. These pseudo-range and range-rate measurements are combined with various receiver status indicators (such as automatic gain control levels) and formatted in a manner suitable for transfer to an incremental digital tape recorder for subsequent off-line data reduction and processing.

The receiver was designed and fabricated to withstand the environmental rigors associated with actual flight testing in the field. Figure 4 illustrates the physical appearance and dimensions of the various units which comprise the receiver and associated peripheral equipments.

A typical transmitter signal consists of an L-band carrier biphase modulated at a 10 Mbps rate with a pseudo-random code sequence. This code sequence has a period of 2^{25} bits so that it repeats approximately every 3.36 seconds. The initial signal acquisition technique implemented at the transmitter consists of inserting a special 255-bit sequence at the beginning of the transmit period and transmitting at a boosted

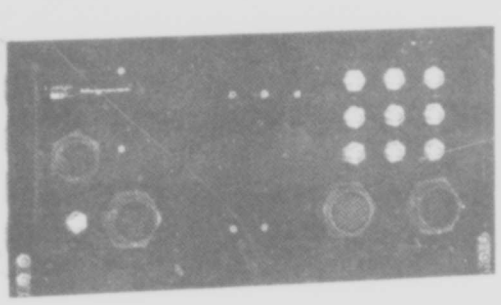

SIGNAL PROCESSOR
DIMENSIONS: 15 x 18 x 8 IN.
1.25 CU. FT.
36 LB

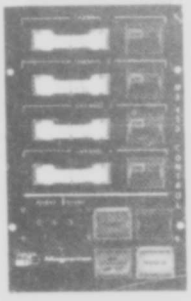

CONTROL DISPLAY PANEL
DIMENSIONS: 5-3/4 x 4-1/2 x 9 IN.
.135 CU. FT.
4-1/2 LB

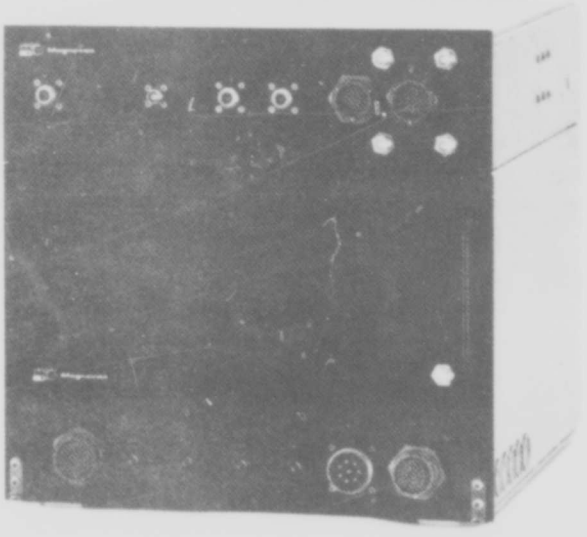

MICROWAVE RECEIVER
DIMENSIONS: 15 x 18 x 4 IN.
0.625 CU. FT.
16-1/4 LB

POWER SUPPLIES
DIMENSIONS: 15 x 18 x 9 IN.
1.4 CU. FT.
88 LB

Figure 4 MRL Navigation Receiver, Power Supply and Control/Display

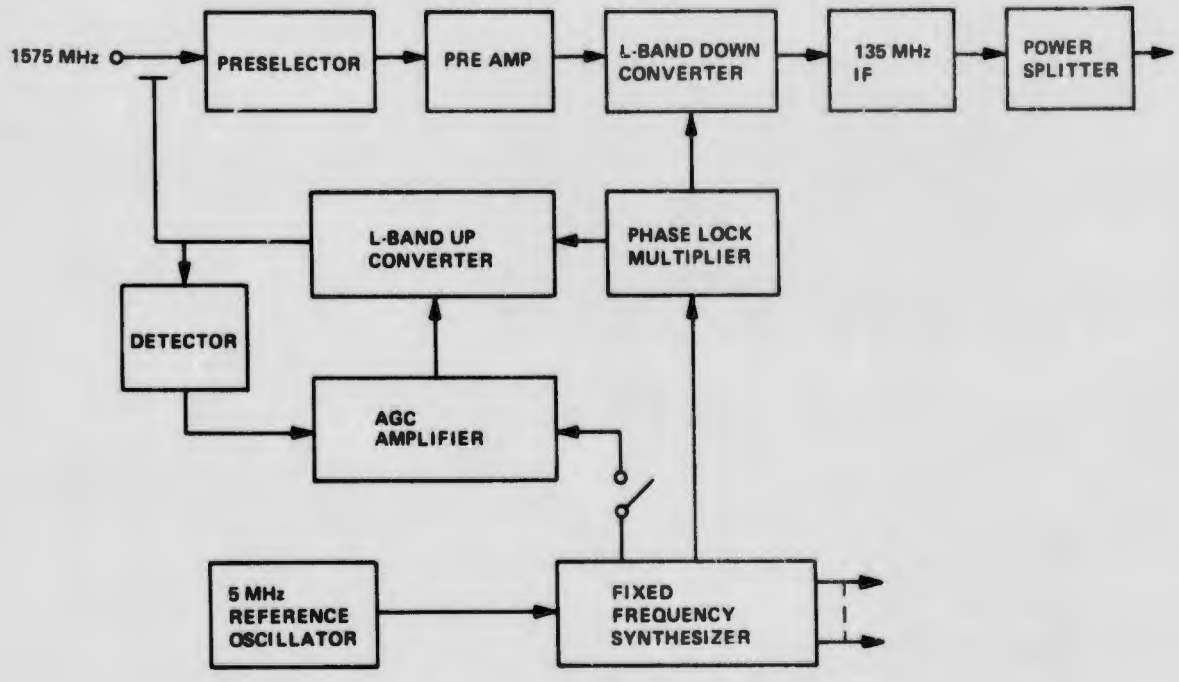

Figure 5 L-Band Microwave Receiver

power level for the duration of this special short sequence. Immediately following this short sequence, the last 2^{25} -255 bits of a long code generated by a 25-stage, maximal-length, linear-code generator is transmitted at nominal power level. The MRL receiver initial acquisition procedure uses a very effective radio-metric type detection technique to detect the increase in received power during the 25- μ s period of power boosted initial sync signal. The relatively small amount of initial time uncertainty remaining after the detection of power boost is resolved by means of a short reacquisition search. Finally each of the transmitter long codes are generated by a sequence generator with different feedback arrangements which uniquely identifies each individual emitter and which in turn, permits each of the four signal processors in the airborne receiver to track only the intended transmitter signal.

Figure 5 illustrates the essential functions performed by the L-band microwave receiver. The incoming 1575 MHz composite signal is first bandpass filtered by the fixed-tuned preselector prior to rf amplification. The preselector's frequency response is less than 1 db down within 10 MHz, 3 db down within 15 MHz and 80 db down within 60 MHz of the center frequency. The preamplifier has a noise figure of approximately 3.5 db and provides a signal gain of 30 db. The down-converter generates the 135 MHz, IF signal by mixing the received 1575 MHz signal with the 1440 MHz, local-oscillator signal. This 1440 MHz signal is derived from a fixed-reference frequency by means of a phase-lock multiplier which helps to ensure the generation of a local-oscillator signal characterized by a high degree of spectral purity.

The 135 MHz, IF module performs three essential functions within the receiver. It provides controlled IF gain prior to correlation through both non-coherent (or total power) agc as well as through what will be referred to as max-channel coherent agc. Since noncoherent agc is required in any case, it is a relatively simple extension to detect the increase in total receiver power level during the 25 μ s power

boost period by ac-coupling the output of the square-law detector in the noncoherent agc loop to a threshold device. For example, during the long-code, transmit period, the agc square-law detector will effectively see only the front-end noise power at -96 dbm since the received signal level will be at the nominal level of -123 dbm or lower. When the power-boost signal is received at -100 dbm the square-law detector sees an apparent increase of approximately 33% in the total receiver power level for 25 μs which is more than adequate for the threshold device to detect signal presence reliably.

The remaining function, shown in Figure 6, is associated with the calibration and self-test modes of the receiver. In either of these modes the switch closure provides either a modulated or unmodulated 135 MHz signal as desired. This signal is up converted to 1575 MHz and applied to the preselector input through a coupler as a method of simulating a transmitter signal. The purpose of the agc loop is to control the calibrate-signal power level to something on the order of 1 dbm.

At this point in the signal flow, the composite 135-MHz IF signal is separated into its constituent elements by means of the correlation process in order to perform the necessary parameter estimation tasks on each of the unique pseudo-noise signals. If we now consider a typical signal processing channel as depicted functionally in Figure 6, we see that each channel basically consists of two loops; one is a carrier-tracking, third-order, phase-locked loop while the second is a delay-lock, code-tracking, third-

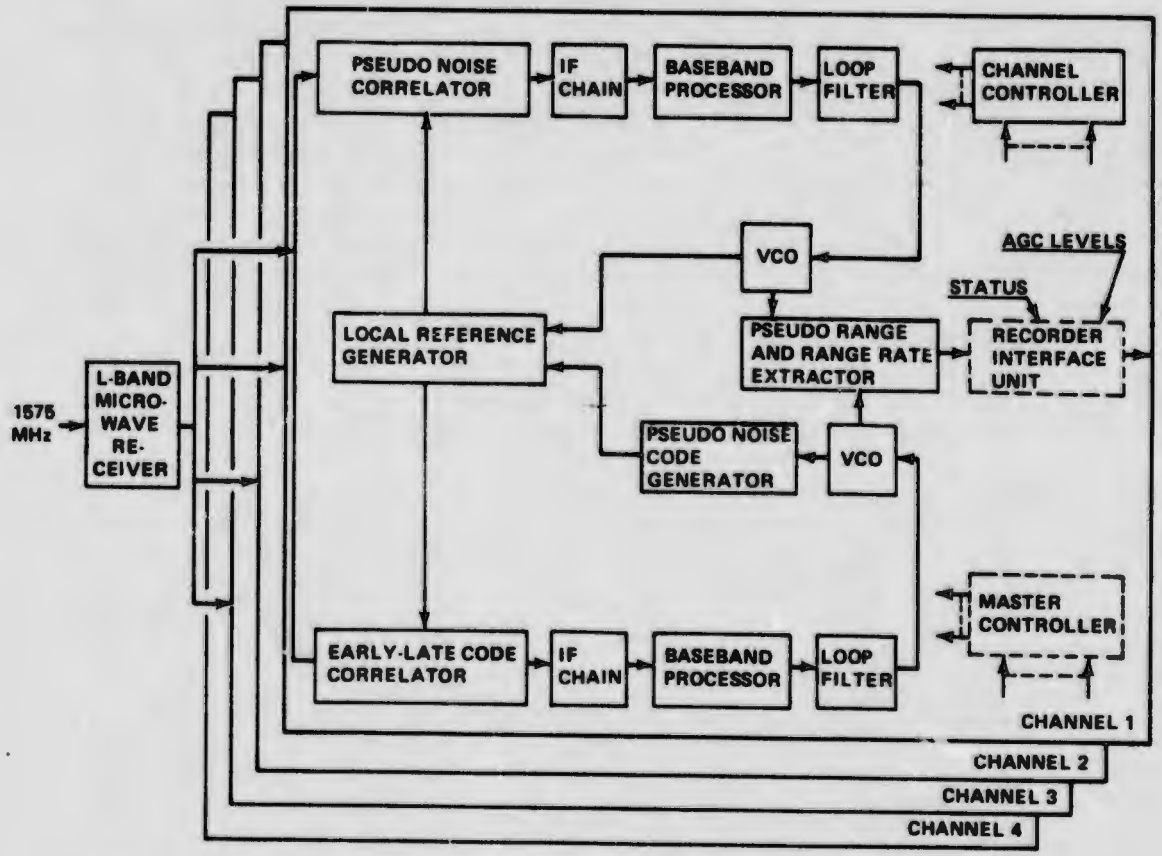

Figure 6 Functional Block Diagram of Delay Lock Correlation Receiver

order loop. The fundamental operation performed by the carrier loop is the generation of a phase-coherent, local replica of the receiver carrier signal while the code loop generates a time synchronized local replica of the received-code signal.

Assuming, for the moment, that the particular channel of interest has acquired frequency, phase, and time synchronization with respect to the received signal, the local reference at the pseudo-noise correlator will consist of a biphase modulated carrier whose frequency, except for an offset equal to the IF, is identical to the received carrier frequency including doppler and doppler rate and whose modulating code is aligned exactly in time with the received code. The correlation properties of pseudo-noise codes are such that once the local code is time aligned with the corresponding received code, a cw signal appears at the correlator output and all other received codes will be discriminated against and appear as wideband noise at the relatively narrowband, intermediate-frequency input. The cw signal is then amplified, down converted and filtered before being applied to the baseband processor which, among other things, derives the tracking-loop-error signal by synchronously demodulating the cw signal at its input. This error signal is then operated upon by the loop filter before it is applied to the voltage-controlled oscillator (vco) to maintain phase coherence with the received carrier. Biphase modulating this regenerated carrier with the synchronized code from the code-tracking loop and applying it to the correlator closes the carrier-tracking loop.

The functional operation of the code tracking loop is not very different from that described for the carrier tracking loop. The major difference is the way the correlation function is implemented to derive the appropriate code loop error function. The delay-lock technique which has been implemented for tracking the pseudo-noise signals is theoretically far superior to the more traditional approaches such as tau-jitter although it is somewhat more complex to mechanize. The operation of the delay-lock loop can be readily visualized by means of the baseband model as shown in Figure 7. There are some serious problems associated with the practical implementation of the baseband, delay-lock loop. For example, it does require an excessive amount of circuitry and power and considerable care must be exercised to match the two correlation channels. The particular implementation incorporated in the MX-450 design produces the desired results while avoiding the problems just cited by delaying the local code separately by a full-code chip and by a half-code chip. If this latter code (i.e., one-half chip delayed) is now applied as the local code replica to the carrier channel, then once code correlation is achieved in the carrier channel we see that the undelayed local code is one-half of a chip early while the full chip delayed local code is one-half of a chip late. Performing a differencing operation on these local early and late codes

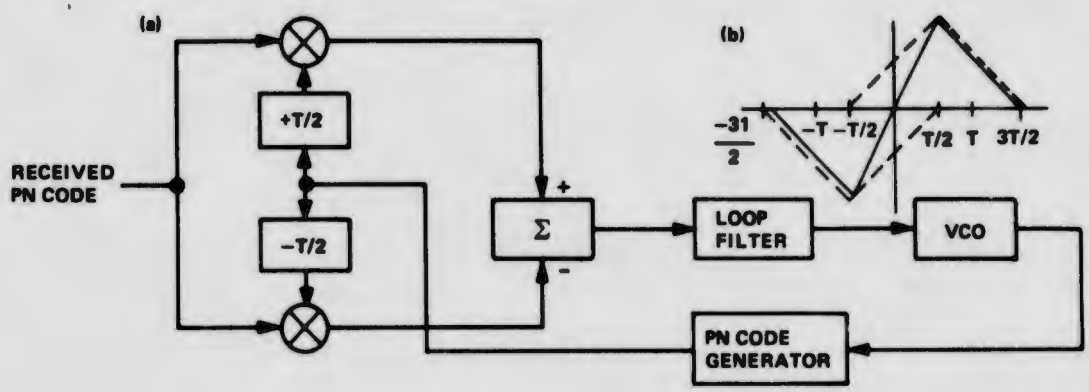

Figure 7 Baseband Delay Lock Model

gives rise to a three-level waveform which, when correlated with the incoming received code, produces exactly the same error characteristic curve as obtained for the base-band model. These functional operations are illustrated in Figure 8.

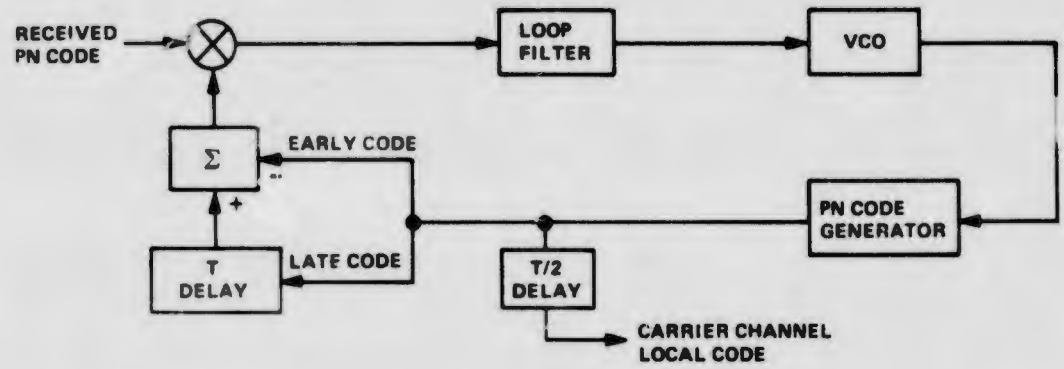

Figure 8 IF Delay-Lock Correlator

Since each channel generates a local replica of the received carrier and code signals, it only remains to derive estimates of the pseudo-range and pseudo-doppler frequency for the receiver to complete its primary function. In order to describe the method used to accomplish this task, consider the receiver as being in the calibrate mode. In this mode, each of the four channels simultaneously tracks a common code and a carrier frequency derived from the local frequency reference. During this process the receiver measures the relative delays between the locally simulated transmitter code and the individual channel codes resulting from the difference in the electrical path length traversed by the simulated transmitter code. These delays are accumulated in what will be referred to as range registers until the end of the calibrate mode at which point in time the range registers are reset to zero and thereby compensate for the static differential delay among the four channels. The receiver can now be considered to be in a coast mode until a power-boost signal is detected. In this coast mode, the local carrier frequency and coder clock are effectively derived from the local frequency reference and both the carrier and code voltage-controlled oscillator, which are essentially digital implementations, are inhibited from responding to their respective control signals until the initial acquisition mode begins upon detection of the power boost. At the end of the calibrate mode (which also happens to be the start of the coast mode), the pseudo-noise code generators are reset to their initial-state conditions and at the same time, a time-of-day counter is reset to zero. For the remainder of the coast mode, both the pseudo-noise generators and the time-of-day counter are stepped forward by a 10 MHz clock derived from the 5 MHz frequency standard. Once the power-boost, sync signal (which marks the beginning of the received sequence) is detected for the channel under consideration, the contents of the time-of-day counter represents the number of pseudo-noise chips by which the origin of the received pseudo-noise sequence and the origin of the local pseudo-noise sequence are separated in time. Since all four pseudo-noise codes in the receiver have a common time origin (i.e., end of calibrate) and at least in principle, since all four transmitted sequences also share a common time origin, the four time-of-day numbers derived at the receiver could be utilized to generate a coarse estimate of the differential slant ranges between the transmitter grid and the airborne platform. As soon as the power-boost event is detected the local pseudo-noise code generator is reset to its initial condition and a small aperture autosearch is begun to achieve code synchroni-

zation. As digital devices, the vco's (or as they are more properly referred to, incremental phase modulators) respond to digital control signals such that the carrier vco advances or retards its phase by 3^{0} per pulse and the code vco advances or retards its phase by 1/256th of a code bit per pulse in accordance with their respective sign information. Accumulating the algebraic sum of the code-loop, control pulses during the autosearch routine in the fine range register provides the pseudo-noise chip fractional count to the time-of-day count which, after suitable scaling, provides readings of signal arrival times relative to the local on-board clock. In a similar manner, the algebraic sum of the carrier-loop, control pulses is accumulated in the doppler register to provide readings of doppler measurements relative to the local frequency standard.

The contents of the pseudo-range registers are sampled every 0.2 seconds and stored in a 4096-bit, buffer memory. The doppler registers are also sampled every 0.2 seconds for their contents accumulated over the previous 0.1 seconds. Finally, the contents of the buffer memory are transferred every second to an incremental digital tape recorder for post-flight data reduction and processing.

To complete this overview discussion of the receiver functional design, a summary description of the acquisition (or reacquisition) mode peculiar to a particular channel is necessary. When in this mode, a channel attempts to verify the presence of a cw carrier signal in the 6 KHz bandwidth of its final 1.25 MHz, IF stage. The decision as to whether signal is present or not is based on a time-variable, sequential-decision strategy where the decision "signal not present" is manifested by a pulse. This pulse increments the phase of the local code by one-half a pseudo-noise chip and a signal-present decision is reviewed again. The sequential detector continues to generate pulses indicating the absence of signal as long as the received and local pseudo-noise codes are misaligned in time by a pseudo-noise chip or more. Sooner or later, by stepping the local code in half-chip increments, the two-code sequences become time aligned and a burst of cw energy appears at the IF amplifier output. The sequential detector finally decides that the signal is indeed present and advertises this decision by not creating a pulse. As a result, the local code hovers without any additional half-chip phase stepping so as to maintain the correlation which resulted in the appearance of cw at the intermediate-frequency. In the meantime, the in-phase and quadrature channels of the synchronous demodulator are monitored by a digital frequency discriminator to estimate the initial frequency uncertainty of the cw signal. This estimate, in turn, is applied to the digital-loop filter to aid the third-order-tracking loops' frequency pull-in until the point is reached where the loop automatically phase locks. At this point the code loop is closed and the time alignment of the received and local codes is further refined. On the occurrence of this event, the acquisition mode is terminated and the channel enters the tracking mode.

The overall tie-in of the various functions are shown in the system level block diagram of Figure 9.

2.1.3 Interface Unit

The Interface Unit (IU) is the major interface for the digital and digitized analog data from the Hazeltine receiver and the onboard data recorders. In addition, signal conditioning is provided for the auto pilot (rate gyro) signal outputs and various transducers which provide vibration, acceleration and vehicle touchdown informatior Figure 10 is a block diagram of the IU.

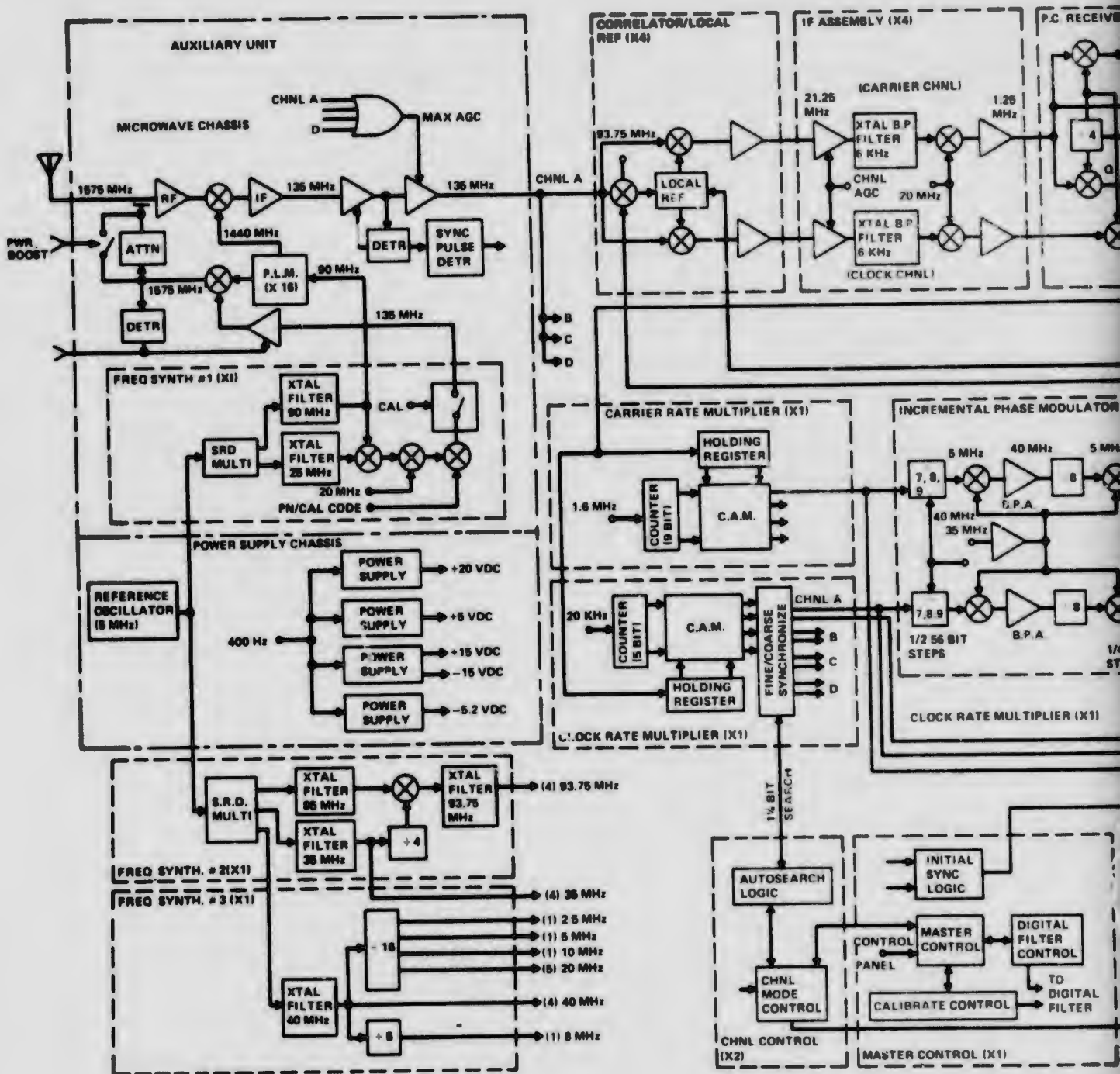
AUXILIARY UNIT
MICROWAVE CHASSIS
CHNL A
D
MAX AGC
1575 MHz
RF
IF
135 MHz
135 MHz
CHNL A
PWR BOOST
ATTN
1440 MHz
DETR
SYNC PULSE DETR
P.L.M. (X 16)
90 MHz
1575 MHz
DETR
135 MHz
B
C
D
FREQ SYNTH #1 (X1)
XTAL FILTER 90 MHz
CAL
SRD MULTI
XTAL FILTER 25 MHz
20 MHz
PN/CAL CODE
POWER SUPPLY CHASSIS
REFERENCE OSCILLATOR (5 MHz)
400 Hz
POWER SUPPLY
+20 VDC
POWER SUPPLY
+5 VDC
POWER SUPPLY
+15 VDC
-15 VDC
POWER SUPPLY
-5.2 VDC
S.R.D. MULTI
XTAL FILTER 85 MHz
XTAL FILTER 35 MHz
÷4
XTAL FILTER 93.75 MHz
(4) 93.75 MHz
FREQ SYNTH. #2(X1)
FREQ SYNTH. #3 (X1)
(4) 35 MHz
÷16
(1) 2.5 MHz
(1) 5 MHz
(1) 10 MHz
(5) 20 MHz
XTAL FILTER 40 MHz
(4) 40 MHz
÷5
(1) 8 MHz
CORRELATOR/LOCAL REF (X4)
93.75 MHz
LOCAL REF
IF ASSEMBLY (X4)
(CARRIER CHNL)
21.25 MHz
XTAL B.P. FILTER 6 KHz
1.25 MHz
CHNL AGC
20 MHz
XTAL B.P. FILTER 6 KHz
(CLOCK CHNL)
P.C. RECEIVE
CARRIER RATE MULTIPLIER (X1)
HOLDING REGISTER
1.6 MHz
COUNTER (9 BIT)
C.A.M.
INCREMENTAL PHASE MODULATOR
5 MHz
40 MHz
B.P.A.
40 MHz
35 MHz
7.8.9
1/2 56 BIT STEPS
B.P.A.
20 KHz
COUNTER (5 BIT)
C.A.M.
CHNL A
HOLDING REGISTER
FINE/COARSE SYNCHRONIZE
B
C
D
CLOCK RATE MULTIPLIER (X1)
CLOCK RATE MULTIPLIER (X1)
1¼ BIT SEARCH
AUTOSEARCH LOGIC
CHNL MODE CONTROL
CHNL CONTROL (X2)
INITIAL SYNC LOGIC
CONTROL PANEL
MASTER CONTROL
DIGITAL FILTER CONTROL
TO DIGITAL FILTER
CALIBRATE CONTROL
MASTER CONTROL (X1)

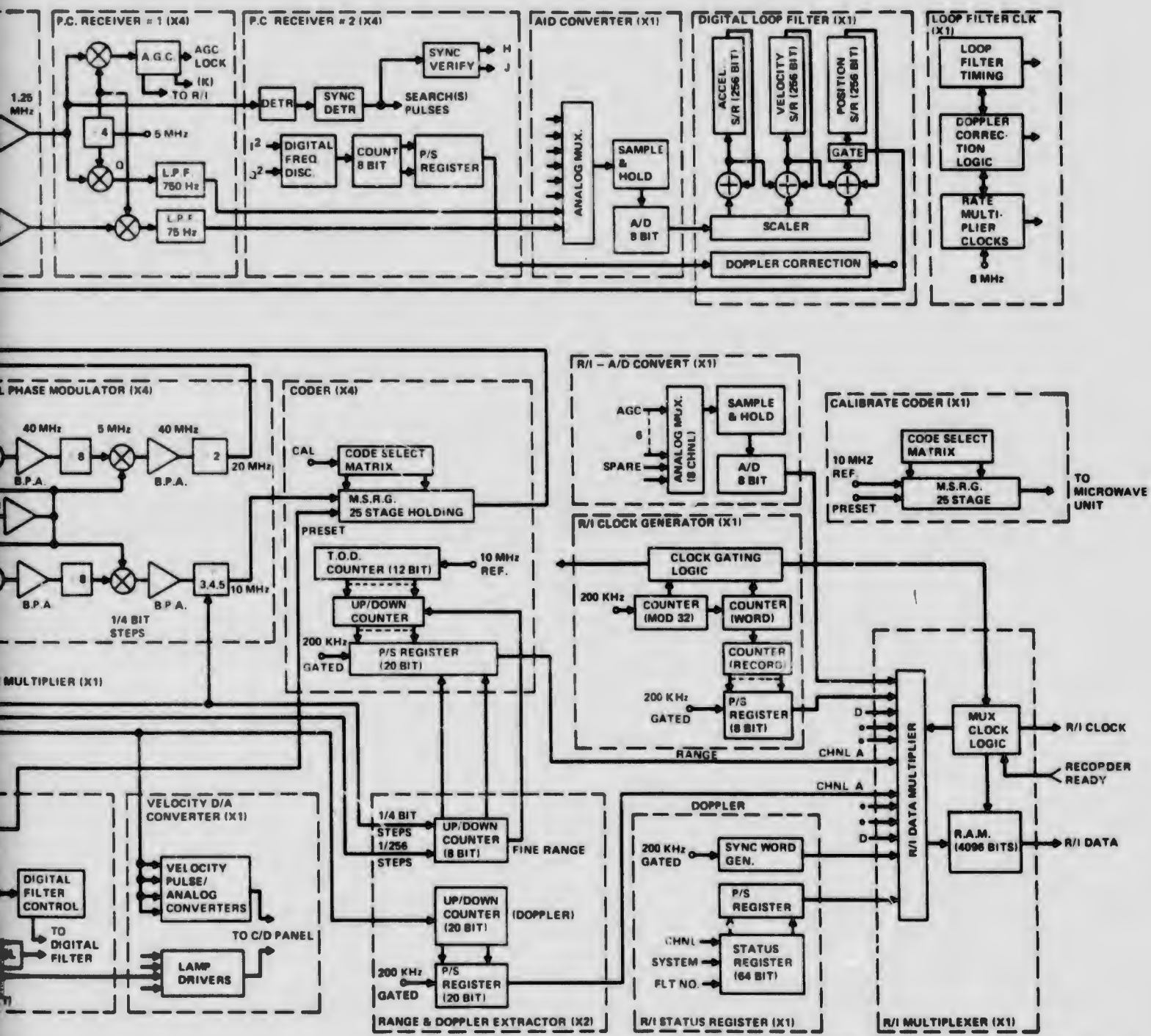

Figure 9 MRL Receiver, Block Diagram

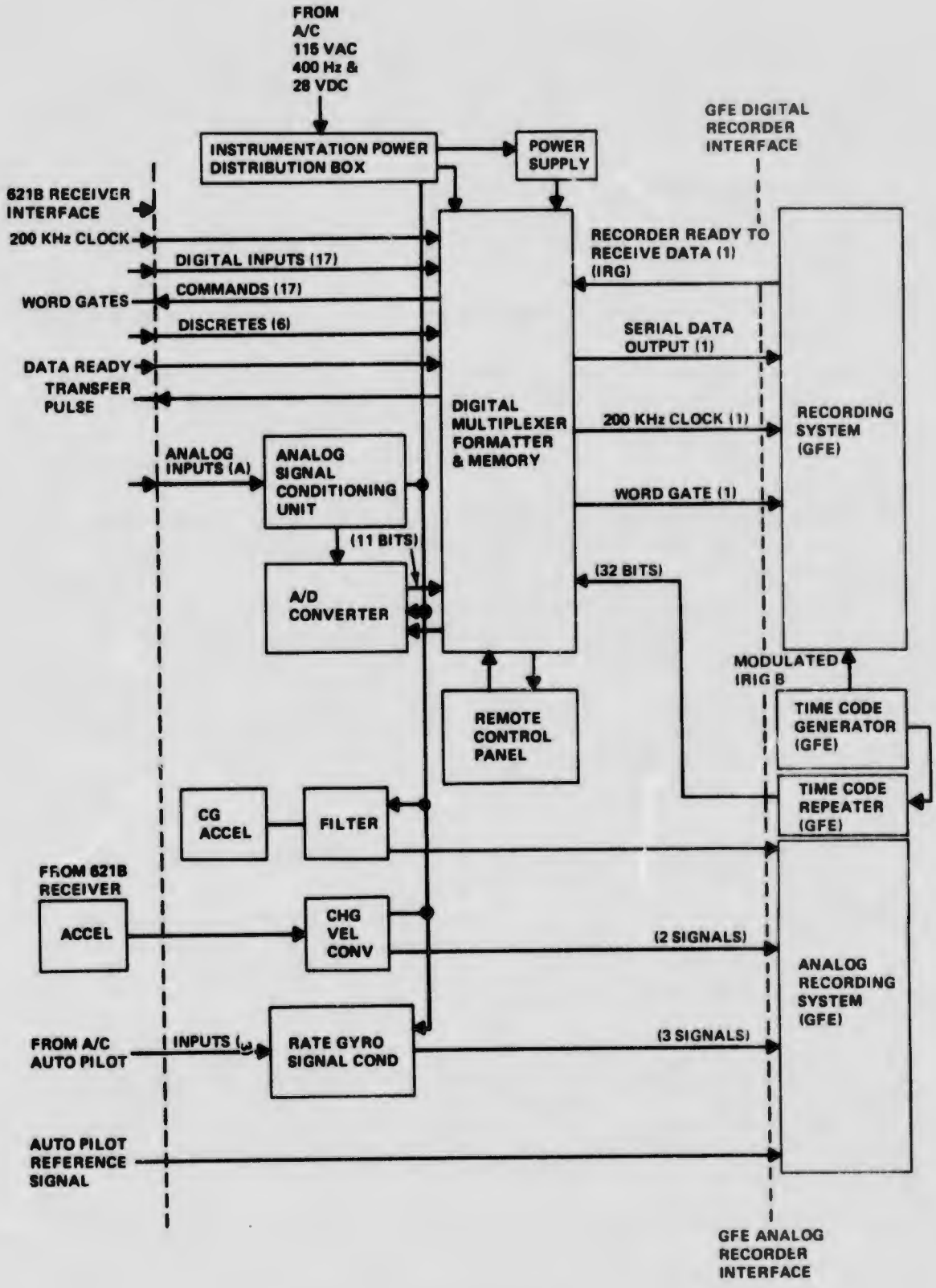

Figure 10 Interface Unit Block Diagram

The design of the multiplexer/formatter unit was influenced by the need to sample the receiver outputs 5 times/sec and the GFE on-board recording system's inability to accept the data at this rate. Thus, a storage capability (memory) was included in the multiplexer/formatter design to permit serial transfer of the data to the recording system once a second.

In brief, the system operates as follows:

- A transfer pulse is generated by the multiplexer and sent to the 621B receiver every 200 ms
- After a time interval of approximately 50 μs, the receiver returns a "data" ready signal
- Upon receipt of "data ready," the multiplexer begins a sequence of read commands that interrogate the various data registers in proper order. This results in the acquisition of a data group
- The data is loaded into a memory (shift register) contained within the multiplexer
- When five data groups have been acquired the memory is commanded to unload and the data are transferred to the recording system. These five data groups constitute a single data record
- As each data record is recorded on tape, the recording system returns an "END IRG" signal which is used to generate a system "OK" signal for display on a remote panel
- The various analog signals are routed to the A/D converter via the analog signal conditioner. The digital output from the A/D converter is then inserted in the data format.

2.1.3.1 Interface Unit Equipment Description

The following paragraphs describe the function of the IU as shown in Figure 10.

See Figures 89 and 90 for the IU installation in the aircraft. Detail design information and schematics for the IU are contained in Ref. 5.

2.1.3.2 Digital Multiplexer/Formatter

The digital multiplexer/formatter is the central interface for the digital and digitized analog data. This unit provides the electronics to receive, format and transfer data to the on-board recording system. In addition, the multiplexer/formatter generates transfer pulses which are used by the HC receiver to initiate transfer of data. A block diagram showing the implementation of the multiplexer is included in Figure 11.

Following is a summary of the major logic functions shown in the block diagram:

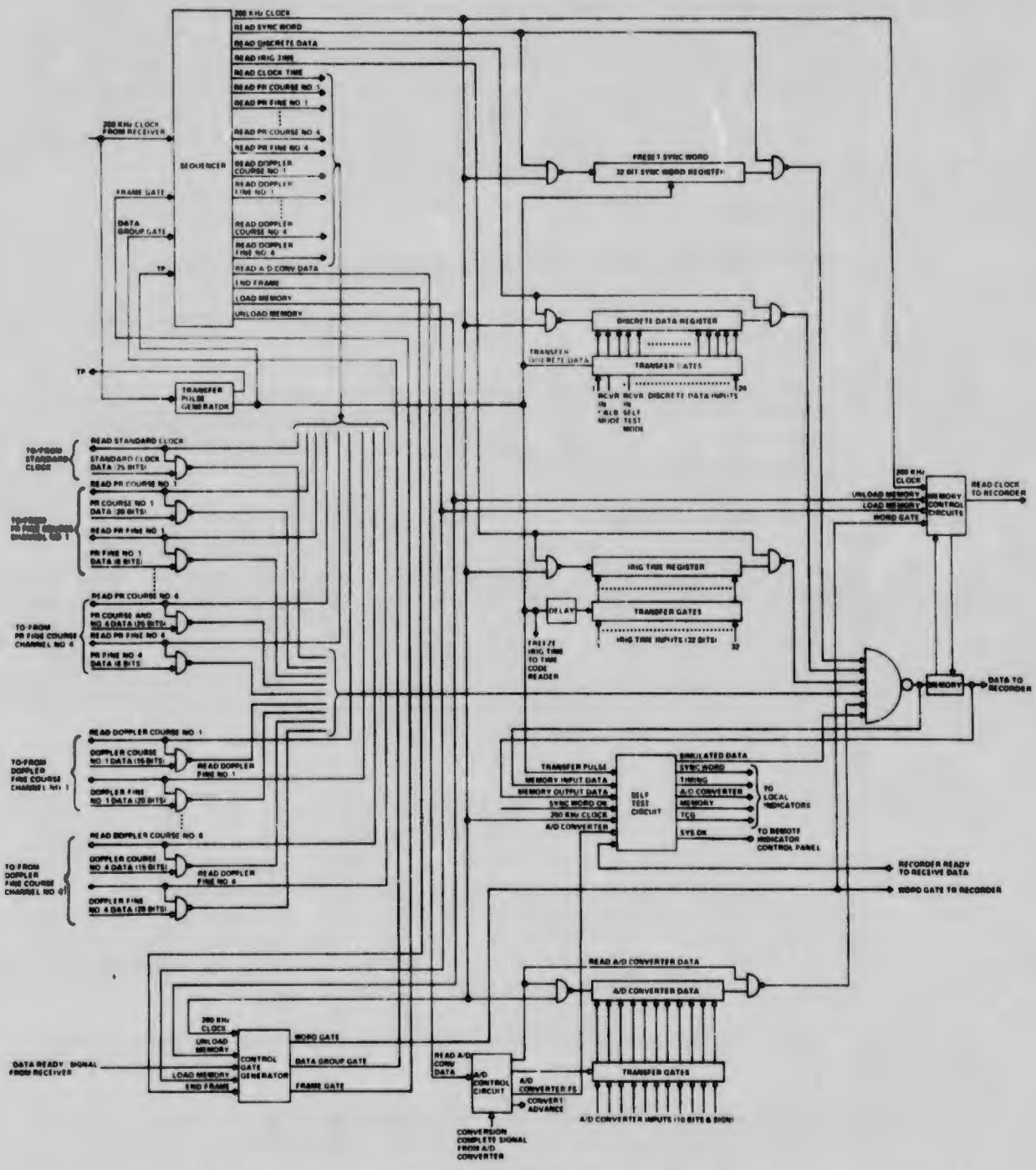

Figure 11 Digital Multiplexer Block Diagram

- **Memory and Memory Control - The memory consists of a 4096-bit bipolar unit with load and unload occurring sequentially. The memory control circuits are required to provide the various commands required for memory functions**

- Sequencer - This is the logic group that controls the timing and generation of the various read commands necessary for system operation. These read commands are timed to accept data for load into the memory in the proper sequence and stop accepting data when the particular register being interrogated is empty, i.e., the length of each read command is programmed for the bit length of the data word associated with that command, (5 μs/bit). The basis for all timing in the sequencer (and all other circuits) is the 200 KHz read clock supplied by the HC receiver

- Control Gate Generator provides:

  - A data gate to bracket data words being loaded into the memory

  - A word gate to bracket data words being unloaded from the memory. This output is supplied to the recording system

  - A data group gate which is used internally to bracket each data group being loaded into the memory. The falling edges of this signal are counted by the sequencer to initiate memory unload when five data groups have been stored

- Transfer Pulse Generator - Provides a transfer pulse (TP) every 200 ms as required by the HC receiver to initiate a transfer of data and send a "Data Ready" signal to the multiplexer/formatter. This in turn results in the acquisition of a data group. In addition to the receiver TP, another TP is generated for internal use and is used to set the sync word register, the discrete data register and the IRIG time register (i.e., freezes IRIG time)

- A/D Control Circuit - Generates commands required to cause the conversion of analog data into digital data, transfer this data into a register and allow it to be gated into the memory

- Self Test Circuit - Included in the design to provide a convenient means for flight line testing and also to provide an in-flight check of system operation by monitoring various key parameters within the multiplexer/formatter, A/D converter and time code generator output. The outputs from this circuit are indicator lamps on the front panel of the unit and dual outputs for a remote display "System OK" indicator. To insure that the self test switch is not inadvertently left in the activated position, the remote indicator will remain "OFF" unless this switch is in "Normal."

The front panel indicators display the "GO" - "NO-GO" status of the following information:

- Simulated Data - Indicates that the multiplexer is in the test mode and the output format consists of a normal sync word, simulated digital words (all zeros) and normal analog words

- TCG - Monitors the output of a holdover one shot which is driven by the 1 ms output of the Time Code Generator

- Timing - Indicates proper operation of the clock, transfer pulse, data ready command, synchronizer, word gate, and load/unload memory commands

- Sync - Checks the sync word at the input to the memory. The sync word data is shifted into a test register at the proper time and certain bits are compared with the known values. If they compare properly, a "Good" indication is displayed

- Memory - Performs the same check described above but at the memory output

- MUX-A/D - This indicator monitors the output of a full scale channel of the A/D converter which is held to full scale by applying +12 vdc to the input. This checks the analog multiplexer, A/D converter, ±15vdc power supply in the analog signal conditioner and the A/D converter logic circuits in the digital multiplexer

- The system "OK" indicator, labeled record indication, is located on the operators control panel (remote) and is operated by a signal obtained from the recording system's (IRG pulse) which is combined with all of the outputs, except simulated, described above. A good or "GO" indication consists of the indicator lamp flashing on and off at a one second rate. A steady on or off, or erratic flash rate indicates a system failure.

If for any reason, the HC receiver is not functioning at the time a test is desired, the self test mode can be selected by activating a switch on the front panel. When this switch is activated an internal clock will be substituted for the one normally received from the HC receiver, an internal "Data Ready" signal will be generated and all data words normally obtained from the HC receiver will become "all zeros." Other data outputs will be the same as in the "normal mode."

The timing diagram for the data at the multiplexer/formatter to recording system interface is shown in Figure 12.

2.1.3.3 Digital Test Unit

This unit is used to apply inputs to the test word register to obtain a known test word format for monitoring the multiplexer/formatter operation. The test word is introduced into the data stream once per second. The test word consists of 32 bits; twenty bits are fixed data and 12 bits are derived from the test word circuitry which monitors the recording system and timing system's operation.

2.1.3.4 Analog Signal Conditioner

The Analog Signal Conditioner (ASC) is the interface and signal conditioning unit for all analog signals. Low level signals are amplified and routed to the GFE analog recorder. Analog outputs from the HC receiver are routed to the A/D converter, where they are digitized. The ASC contains an integral power supply and calibration circuitry.

2.1.3.5 Analog to Digital Converter

This unit is a purchased item, DSE Model 440003. The equipment contains a multichannel analog multiplexer with random or sequential access, an A/D converter and an integral power supply. The basic capabilities are:

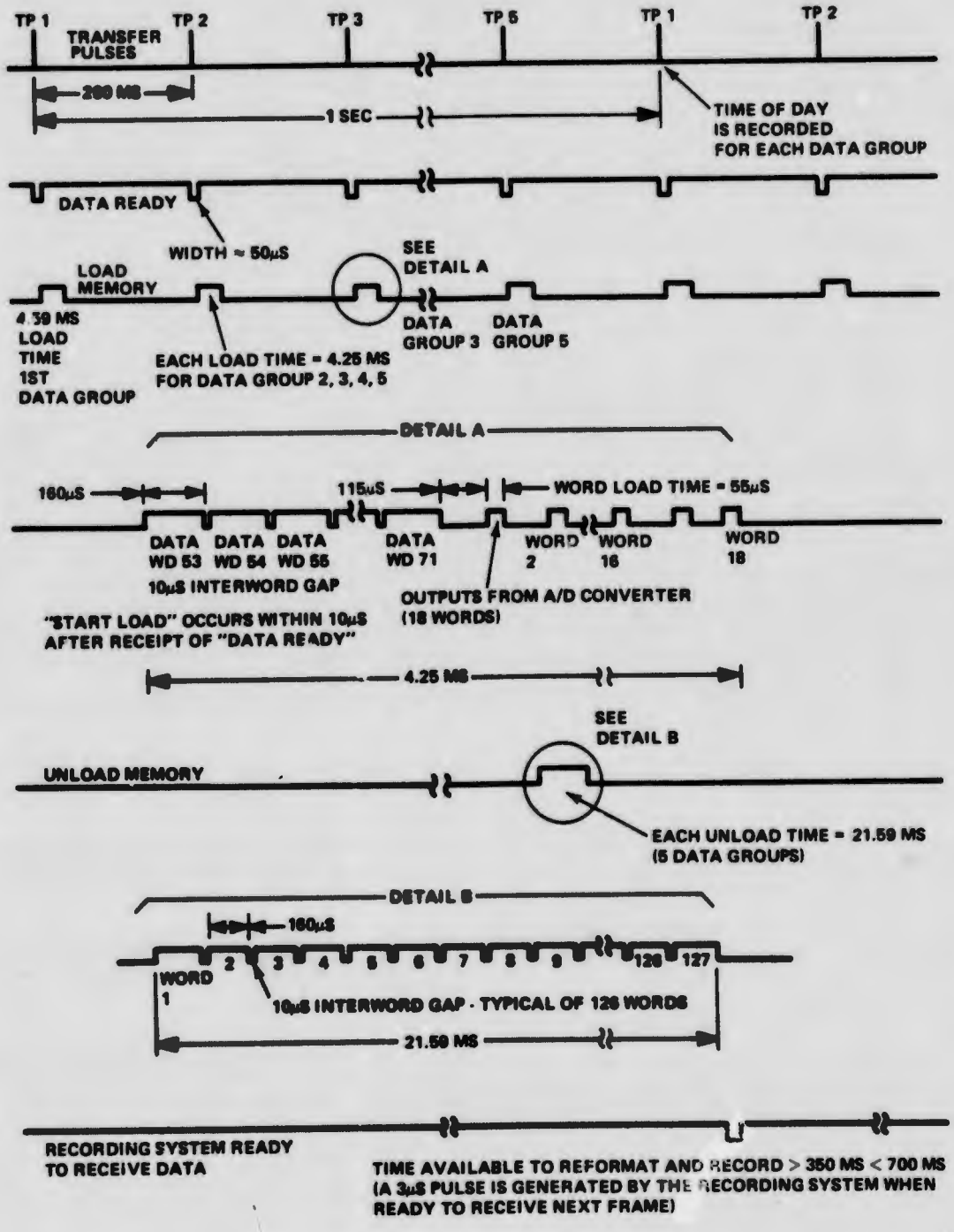

Figure 12 Timing Diagram, IU/Recorder

- Inputs
  - Analog Voltage: ±10 vdc
  - Input Impedance: >10 megohms at dc
  - Common Mode Rejection: 60 db at 400 Hz
  - Over Voltage: ±15 vdc
- Outputs
  - Data (absolute value and sign): 11 bits (including sign)
  - Accuracy: 1 part in 2^9
  - Isolation: signal and power isolated from chassis
  - Source Impedance: <5K ohm

2.1.3.6 Auto Pilot (Rate Gyro) Signal Conditioner

The Auto Pilot Signal Conditioner (APSC) unit accepts the signal outputs (roll, yaw and pitch) of the auto-pilot's rate gyros and converts them to linearly proportional high level bipolar dc voltages which are recorded by the on-board analog recorder. The data were used to aid in determining the true position of the aircraft receiving antenna, i.e., correct for aircraft dynamics.

The 26v 400 HZ reference excitation voltage for the rate gyros were monitored and recorded. Thus, a suitable correction could be made for variations in aircraft primary power levels, since it was found that the rate gyro outputs were affected by variations in excitation supply voltage.

The APSC contained provisions for calibration, the unit was calibrated prior to each flight.

2.1.3.7 Power Distribution Box and Power Supplies

This unit provided for the control, protection and distribution of aircraft primary power both 400 Hz ac and 28 vdc to the various components of the IU. In addition, over and under voltage protection circuitry were provided to protect voltage sensitive components. The logic power supply had a built-in over voltage protection.

2.1.3.8 Remote Control and Display Panel

This unit provides for remote control of the IU. Provisions for power control, reset of under and over-voltage conditions and remote control of data transfer to the on-board digital recording system are provided. In addition, the "System OK" indicator is located on this panel, Figure 90.

2.2 GROUND EQUIPMENT

This section describes the hardware used on the ground for this test program.

The equipment can be considered in two groups, one which is used to generate the experiment program data consisting of transmitters, antennas, calibration receivers and instrumentation, and the other used to evaluate the navigation solution data consisting of WSMR instrumentation hardware.

2.2.1 Transmitters

Four transmitters were provided (Figure 13), one of which has the capability of operating on batteries while carried aloft by a balloon. All transmitters were designed to radiate spread spectrum signals to simulate the type of signal which would be obtained from 621B satellites. The transmitter output signals are fed to two antennas; one, the uplink signal, was used for the link to the test aircraft and the other, the monitor link signal, was directed to the Mobile Calibration Station (MCS) (for some flights).

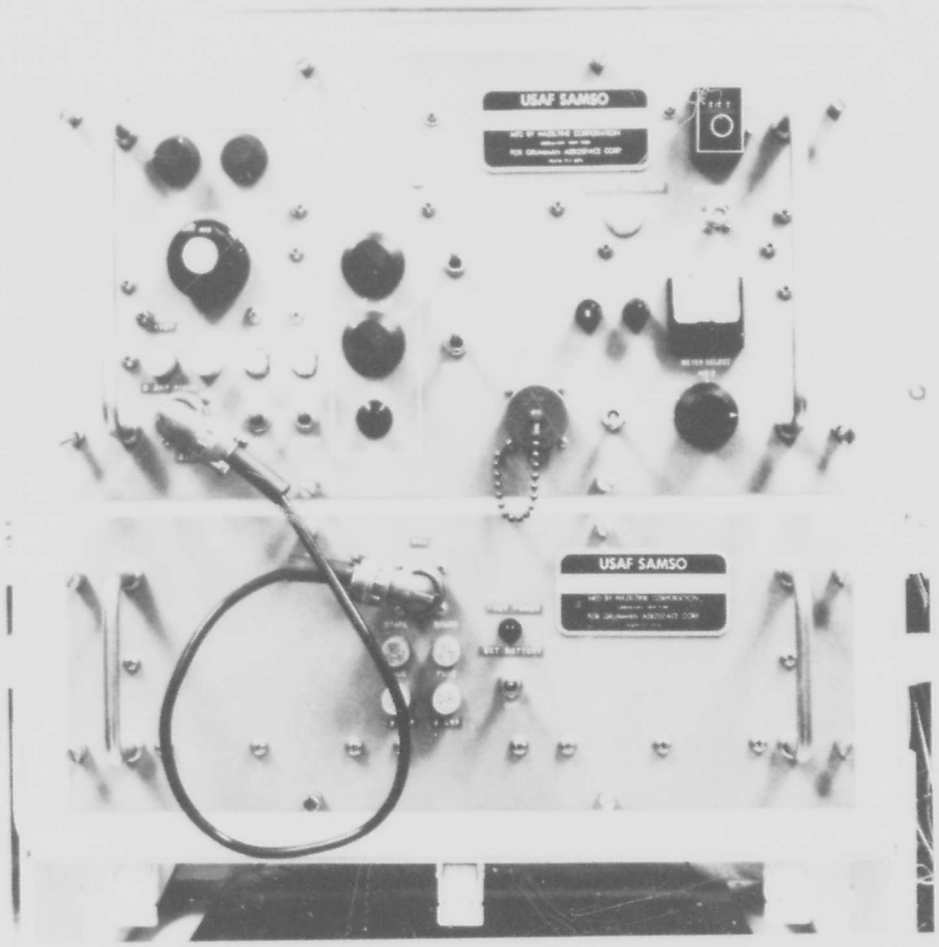

Figure 13 System 621B Transmitter

Each transmitter generates a distinctive 25-stage M-sequence code (truncated to 2^{25} -255 bits) which is combined with a common 8-stage M-sequence code to modulate an L-band carrier. The resulting 2^{25} bit sequence has a period of 3.3554432 seconds. The code clock frequency as well as the carrier frequency are generated from a stable crystal oscillator. The code rate is 10 Mbps. The code biphase modulates the carrier. The 8-stage common M-sequence (length of 25.5 μs) is power boosted by about 30 db to assure a received signal power of -100 dbm required for acquisition. Nominal power output of the transmitter for use by the aircraft receiver is adjustable to provide a received power level in the range of -80 dbm to -140 dbm. Nominal power output for use by the MCS is -106 dbm.

Long term stability of the transmitter oscillator is assured by operating on a standby mode (using battery power).

The interconnection of the various subassemblies is shown in block diagram form in Figure 14. At the top left of the diagram, the 5 MHz frequency standard is shown with the associated front panel frequency adjusting potentiometer R3. The 5 MHz output is coupled through a padded tee to the 5 MHz jack on the front panel and to the frequency multiplier assembly. The frequency multiplier assembly provides a 10 MHz output to the code generator and a 225 MHz output to the X7 multiplier.

The 1575 MHz output from the X7 multiplier is applied via a bandpass filter to a Microlab power splitter, which divides the carrier energy between the two balanced modulators. The balanced modulators driven by the monitor link and uplink outputs from the code generator via driver amplifiers in the performance monitor module, supply spread-spectrum-modulated signals to the monitor link rf amplifier and the uplink rf amplifier.

The monitor link rf amplifier feeds the monitor link antenna directly while the uplink rf amplifier provides two outputs, the Hi rf, and Lo rf outputs. These signals are sampled for monitoring in the performance monitor, and pass through isolation and filtering sections with appropriate padding to be combined in a circulator for transmission from the uplink jack.

The transmitter characteristics are summarized in Table I and the transmitter control functions tabulated in Table II.

Table I Summary of Transmitter Characteristics

Transmitter	
Carrier Frequency	1575 MHz
Coding	2^{25} bits PNR biphase
Code Repetition Period	3.3554432 seconds
Code Rate	10 Mbps
Uplink Power (Max)	+20 dbm (+27 dbm boost)
Monitor Link Power (Max)	−6 dbm (+4 dbm boost)

2.2.2 Calibration Receiver

The calibration receiver is functionally identical to the Hazeltine airborne receiver described in paragraph 2.1.1. The ground use of this receiver required a different control and display complement as described below.

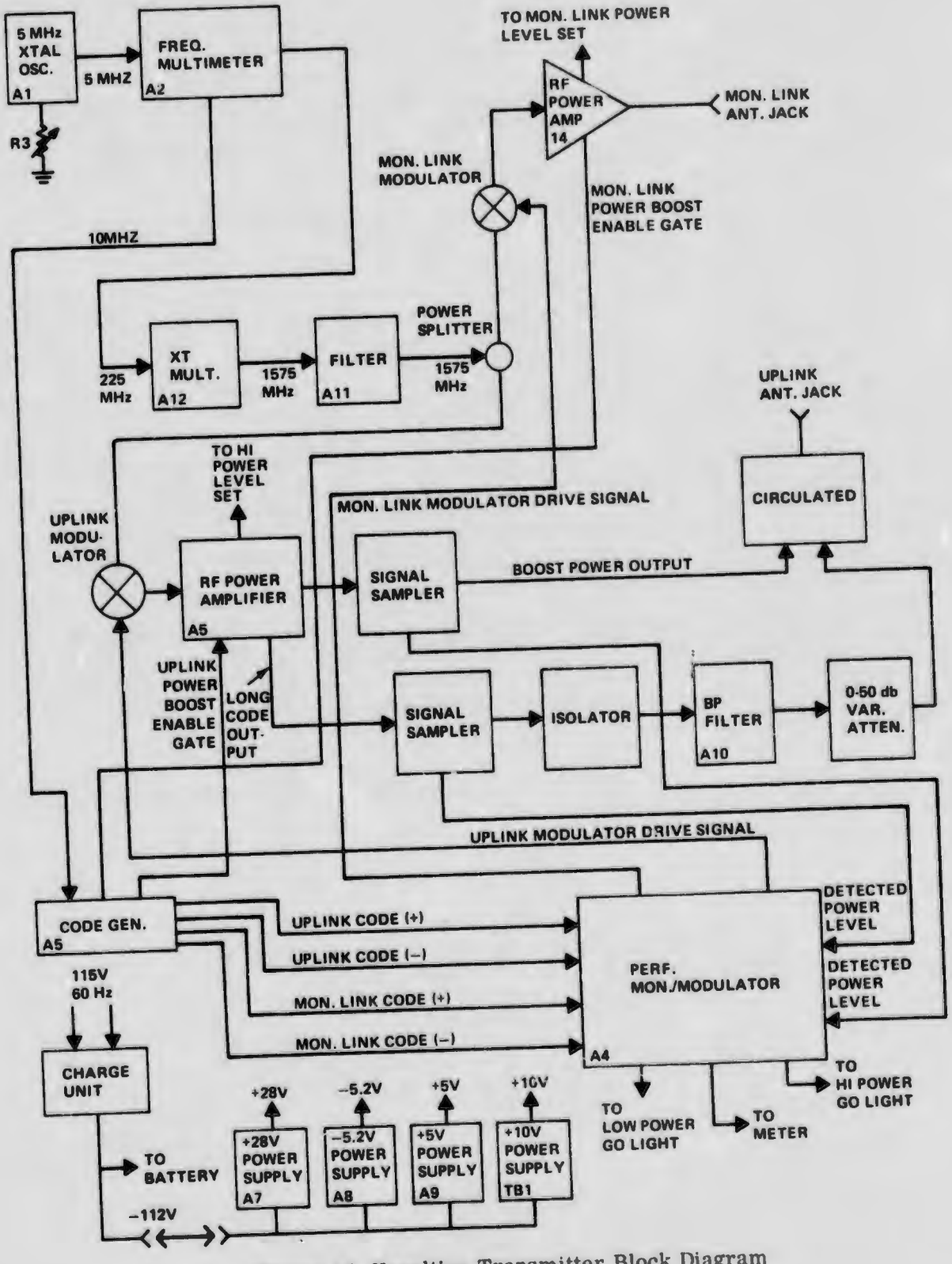

Figure 14 Hazeltine Transmitter Block Diagram

Table II Transmitter Control Functions

Control	Function
Power ON/OFF	Controls 115v ac power to transmitter
Operate/Standby	In Standby, only +28v is present for osc oven In Operate, all voltages supplied to unit
Control Local/Remote	Provides remote control of Operate/Standby function
Code Enable Start/Stop	Starts and Stops code
CW Test/OFF	When code enable switch is in start position placing CW test switch in CW test causes a CW signal to be transmitted at the long code power level
Code Slew Rate Initiate	These controls allow code to be slewed by number of bits selected
High Power Level Set	Controls boost power output level from +27 to +37 dbm
Monitor Link Level Set	Controls monitor link output power level
Low Power Adjust	Controls long code output power level from maximum of +22 dbm
Frequency Adjust	Adjusts 5 MHz osc frequency; full adjustment range is 1 part in 10^8
Meter Select	Provides test signals to meter
Low Power Indicator	Go light indicates maximum long code power > +18 dbm and < +24 dbm
High Power Indicator	Go light indicates boost power > +32 dbm
Standard Frequency Out	Provides sample of 5 MHz osc
Coarse Frequency Adjust	Adjusts 5 MHz osc frequency; full adjust range is 2 parts in 10^7
Charging Unit Ext Battery ON/OFF	Connect ext +12v battery across charger unit output
Norm/Self Test	In self test the normal transmitter code is replaced by the self test code (switch located inside unit)

2.2.2.1 Calibration Receiver Control

The calibration receiver control provides essentially the same controls as does the airborne control box, but also provides power level monitoring meters to indicate the relative signal strength for the signals being processed by each of the four receiver channels, and an audio alarm device, which sounds if any signal drops below a preset level, Figure 15.

2.2.2.2 Calibration Receiver Display

The calibration receiver display (Figure 15) provides a digital readout of a portion of the data transferred to the interface unit for recording. These data are used to monitor the performance of the receiver in the calibration installation and may be used to assist in multipath measurements and other diagnostic or investigative experiments. The data presented represents, depending on control setting, the fine range data for each of the four channels or, the fine doppler data represented by the eight least significant bits of the fine doppler output for each of the four channels.

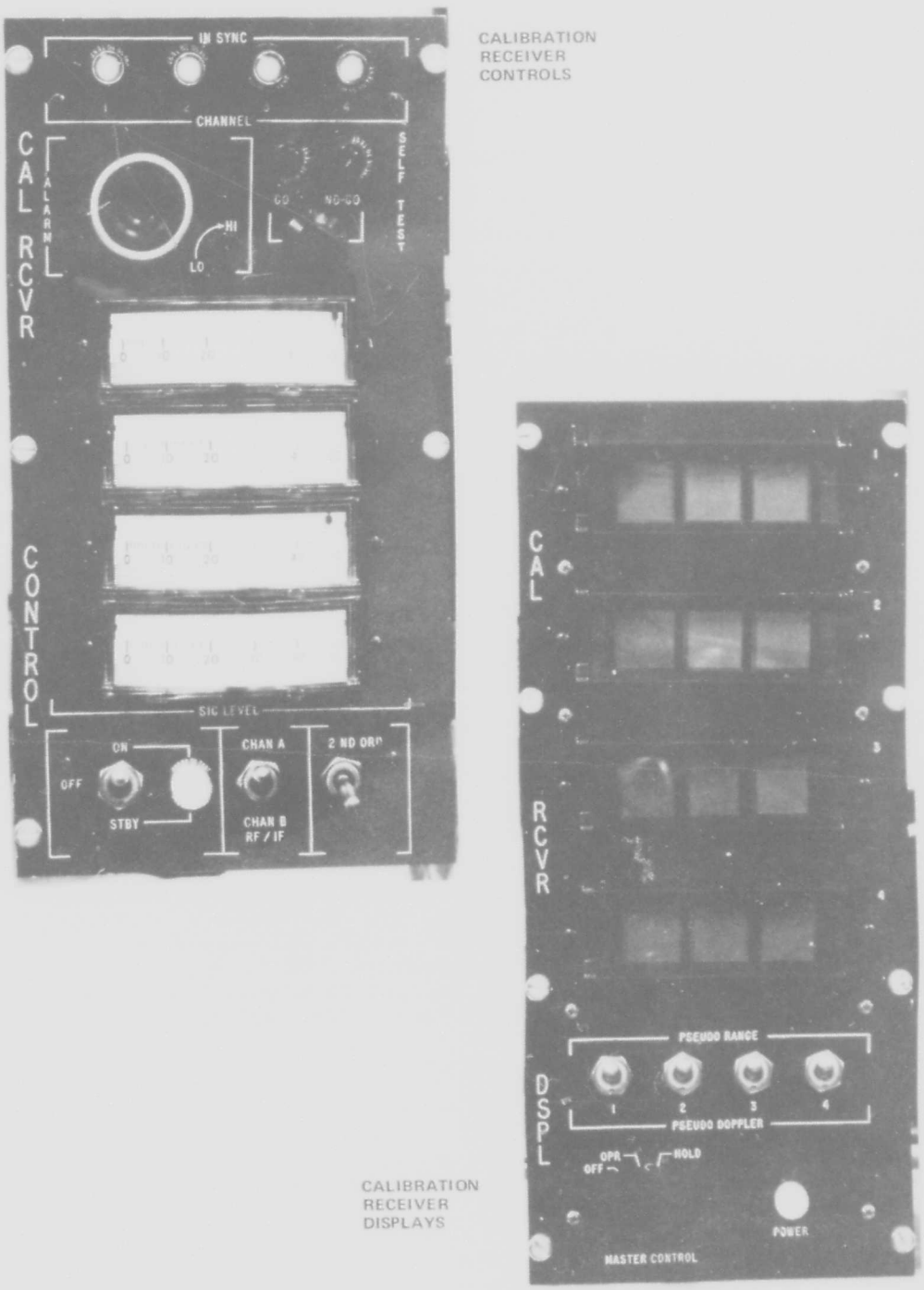

Figure 15 Calibration Receiver Controls and Calibration Receiver Displays

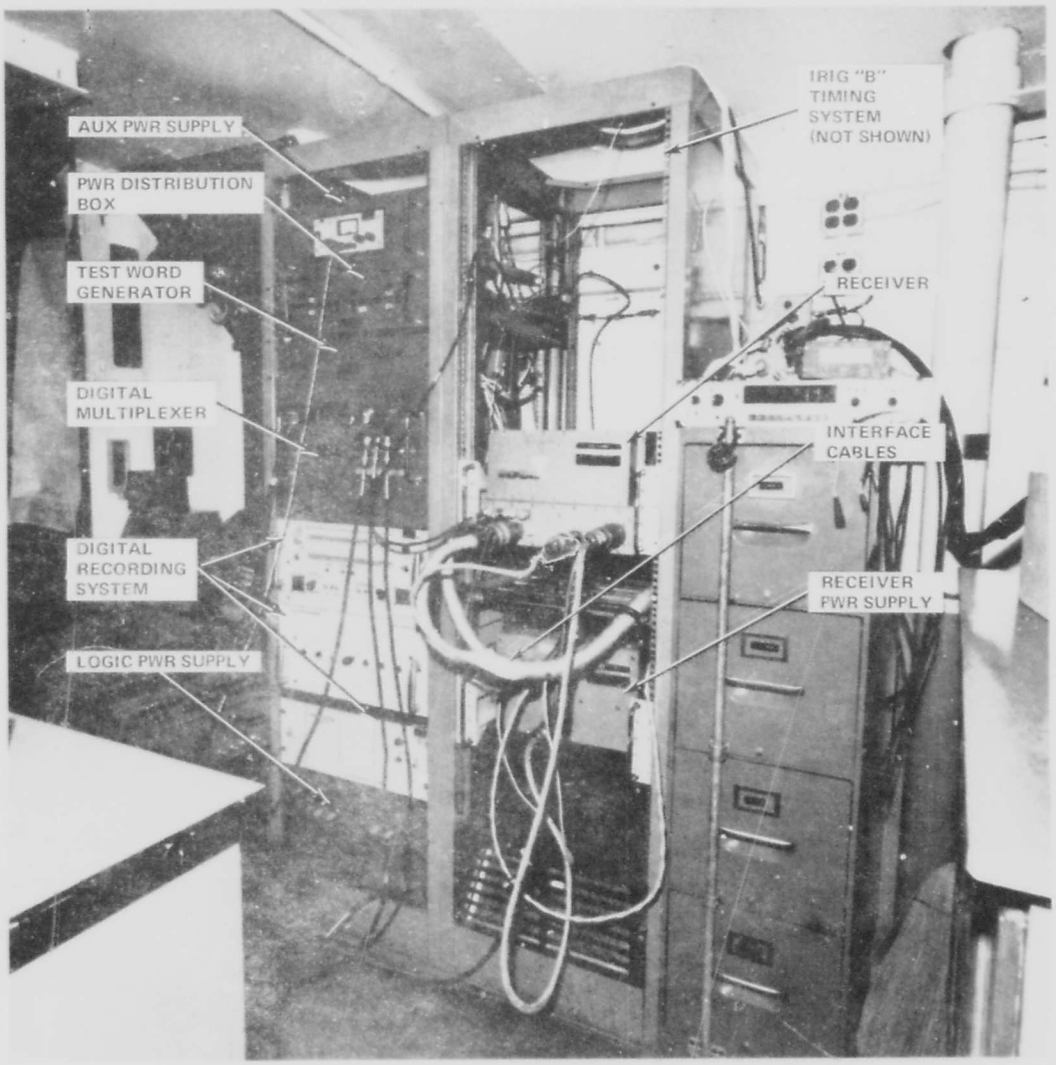

Figure 16 MCS Installation Hazeltine Receiver and Grumman Data Acquisition System

2.2.3 Instrumentation

The ground instrumentation as Data Acquisition System (DAS), is located at the calibration site (MCS), and is used to record the data from the 621B calibration receiver. Figure 16 shows the equipment installation. The WSMR timing equipment is not shown. The timing equipment is located above the calibration receiver in the right hand rack. Figure 17 is a block diagram of the DAS.

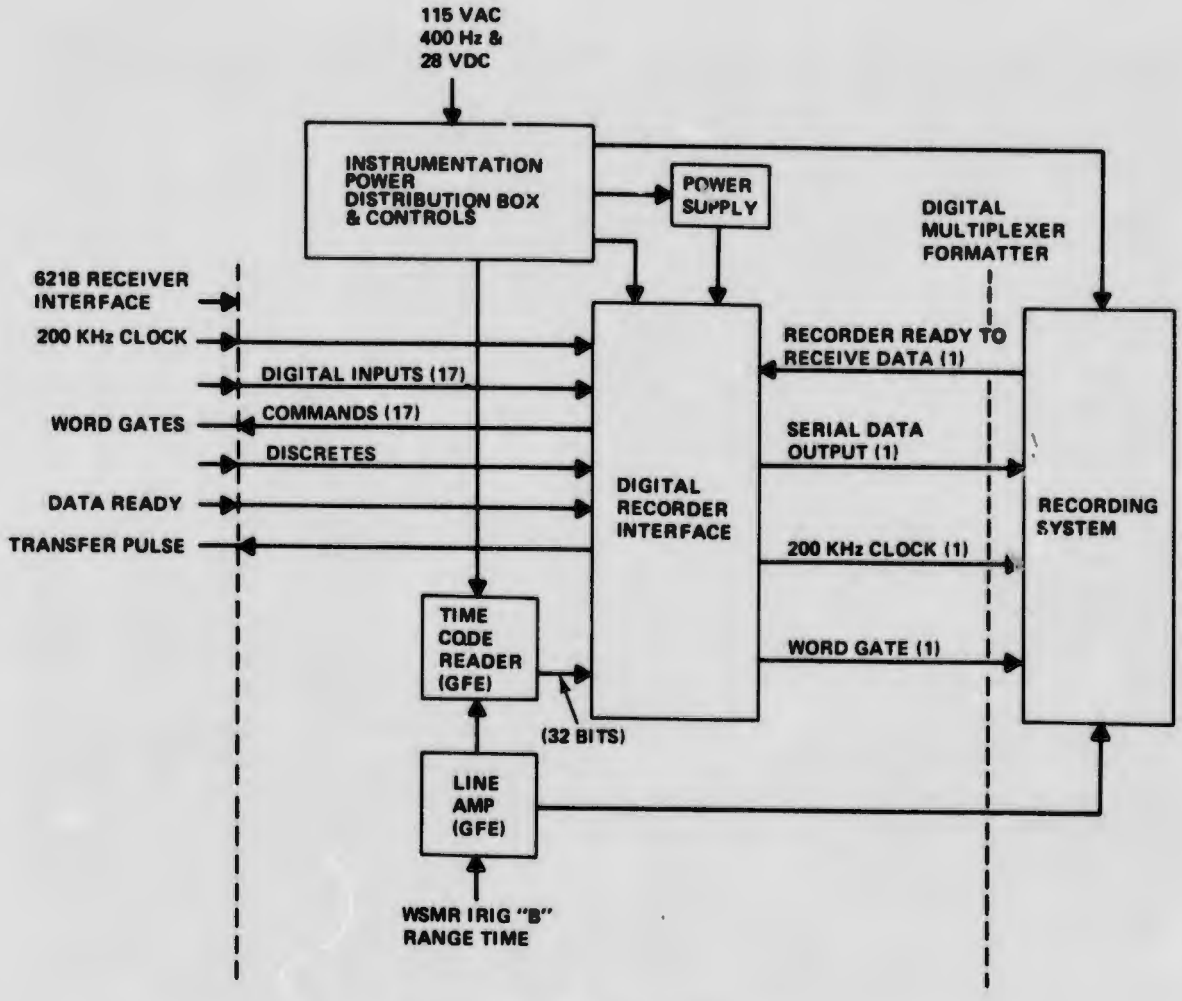

Figure 17 DAS Block Diagram

With a few exceptions, the DAS functions are similar to the airborne IU, described in paragraph 2.1.3. Detail design information and schematics for the DAS are given in Ref. 5. The following paragraphs discuss the pertinent differences between the DAS and the IU.

2.2.3.1 Digital Multiplexer/Formatter

The digital multiplexer/formatter for the ground site differs from the one in the aircraft in that a memory is not included in the ground site unit. This is possible because the data is sampled at a slower rate (1 sample/sec) and can be transferred directly to the recording system. Therefore, except for the references to the memory and its associated control and test circuitry the discussion of the airborne unit (paragraph 2.1.3.2) also describes the operation of the ground site unit.

2.2.3.2 Digital Test Unit (Test Word Generator)

This unit is identical to the airborne unit (paragraph 2.1.3.3) and serves the same function. The test word, however, consists of 32 bits of fixed data which may be changed prior to each flight, or for test purposes.

2.2.3.3 Power Distribution and Control Panel

At the ground site, operating personnel could readily monitor the operation of the DAS during the mission. A need for remote control of the equipment did not exist. Thus the operating controls and power distribution function were combined into one unit. The description of the airborne units in paragraph 2.1.3.7 and 2.1.3.9 are applicable to the ground equipment.

2.2.3.4 Digital Recording System

The recording system is a purchased item, Digital Products Model 214A1-1. This unit is identical to those used in the aircraft for recording 621B digital data. The major components of the recording system are:

- Digital Recorder
- Data Buffer and Tape Control Unit
- Memory Unit (Core Buffer)

The essential characteristics of the recording system are:

- Input data signal format:
  - Word Length: 48 bit max.
  - Frame Length: 127 48-bit words max.
  - Clock Rate: 1 MHz max.
  - Sync Word: unique repeatable word required once per frame.
  - Data Format: serial transfer of Manchester, Rz, or NRZ
  - Interface Circuitry: DTL compatible
- Output data format - The output data is in the form of a digital magnetic tape which is IBM-computer compatible:
  - Packing Density: 556 characters per in.
  - Record Head Configuration: 7 track in-line
  - Tape Width: 0.5 in.
  - Reel Size: 10-1/2 in. IBM type

- Tape Capacity: 2400 ft, 1.5 mil
- Recording Technique: NRZ Mark (NRZI)
- Slew Rate: 3 KHz

2.2.3.5 IRIG "B" Timing Equipment

The time code generator/reader was GFE by the 6585th Test Group at Holloman AFB and was the same type used in the aircraft. A line amplifier which conditioned the incoming IRIG "B" signal via telephone lines was supplied by the WSMR timing group. During the ILS tests, it was necessary to resort to a radio link in order to obtain a high quality timing signal. The WSMR timing group supplied the equipment.

2.2.4 Mobile Calibration Station

Since the same equipment was utilized in the Area Navigation, ILS, and Multipath tests, a mobile van was used to house this installation and provide ease of relocation. The Mobile Calibration Station (MCS) is shown at its site in the 50 mi area in Figure 18.

The calibration receiver and interface unit was installed in the MCS. The calibration receiver and its associated power supply are installed in a standard 19-in. rack within the MCS. An electrical harness within the MCS interconnects the calibration receiver, interface unit, recording system, control and display unit and power distribution panel.

Four rf cables connected the receiver to the external calibration link antennas via a signal combiner.

The calibration receiver and its associated power supply require forced air cooling. Blowers installed in the 19-in. rack (Figure 19) take MCS ambient air and blow it over the units exhausting the warmed air to the MCS interior. Cooling of ambient air is provided by an exhaust fan at the rear of the truck interior and by window unit air conditioners.

The receiver data acquisition system and recorder is shown installed in the MCS in Figure 16. The calibration receiver display, calibration receiver control and power control panel for the MCS is shown in Figure 20.

The MCS consists of a specially designed van mounted on a 1968 International Loadstar 1800 truck body. The MCS comes with its own external trailer-mounted diesel engine which drives three independent generators (60 Hz, 400 Hz, 28 vdc) satisfying all power requirements.

In addition to housing the calibration receiver and associated equipment, the MCS served as a focal point for all ground operations since it provided an excellent field repair facility and contained communications gear for use during test flights.

2.2.5 Antennas

Four distinct types of antennas evolved during the design period to satisfy the program objectives. A primary goal in the system simulation was to obtain a signal

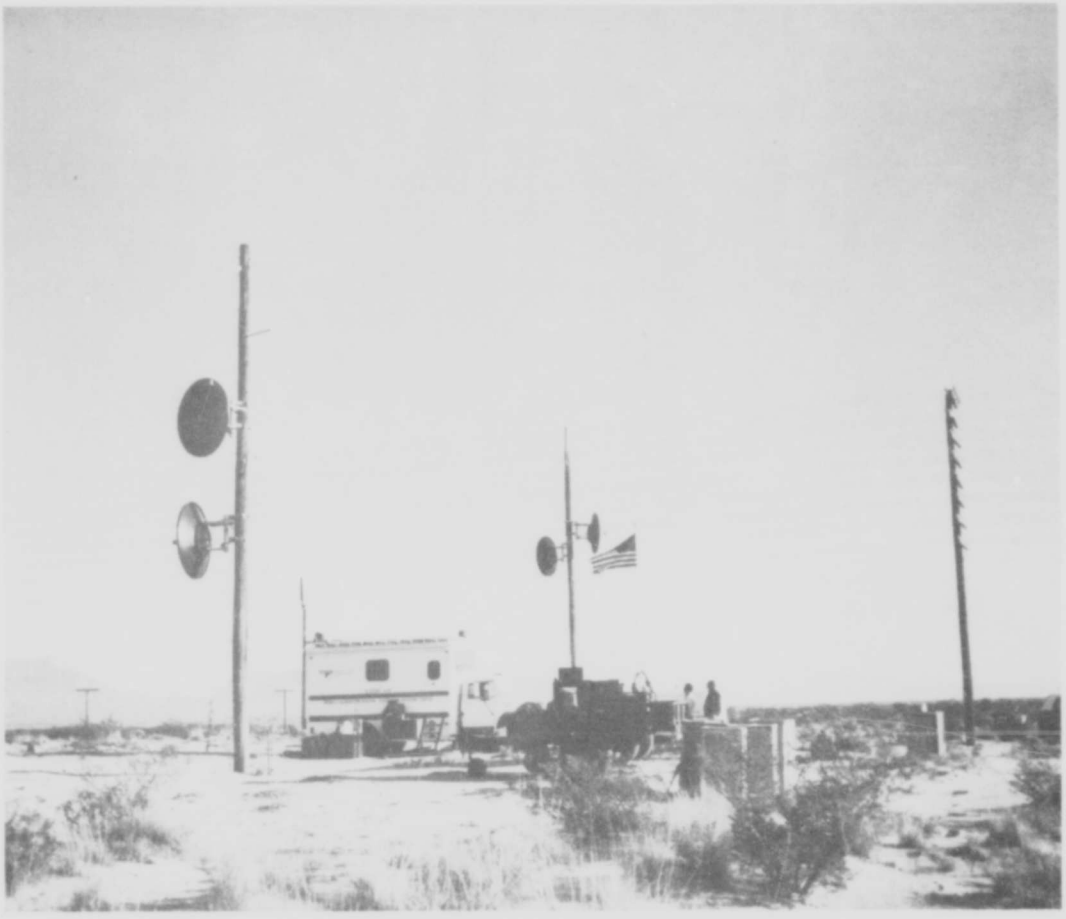

Figure 18 MCS Site (50 Mile Area)

profile at the aircraft which would be similar to that received from a satellite. To achieve this goal the system was configured with a transmitter uplink antenna with a pattern shaped to give a constant power level for constant altitude flight paths, an omni antenna at the aircraft, and parabolic dish antennas on the ground to route the signal from the transmitters to the calibration receiver. In addition, a simple test antenna was used in the WSMR field test to sample the rf field at various points to gain an understanding of the system antenna interactions with the actual installations.

As will be seen in the test results discussion in Volume III, we improved our understanding of some aspects of the antenna design requirements as the program progressed. This section will, therefore, discuss the details of the electrical and mechanical characteristics of the antenna as well as their utilization at WSMR so that the appropriate background is available for discussion of test results and antenna errors presented in Volume III.

The antenna utilization is best understood with respect to the type of test. Test categories are Area Navigation, ILS, and Ground User Multipath.

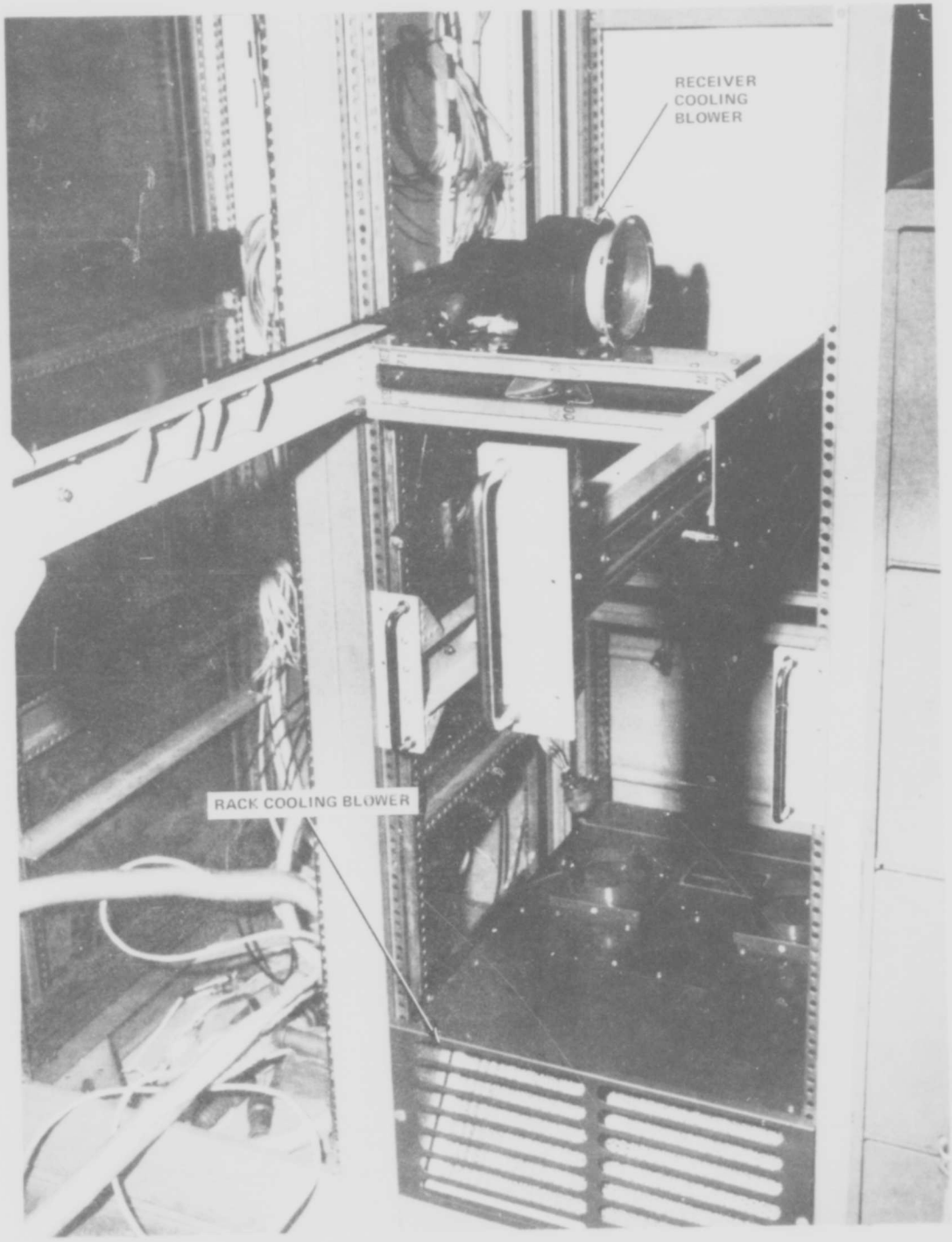

Figure 19 MCS Calibration Receiver Cooling Air Installation

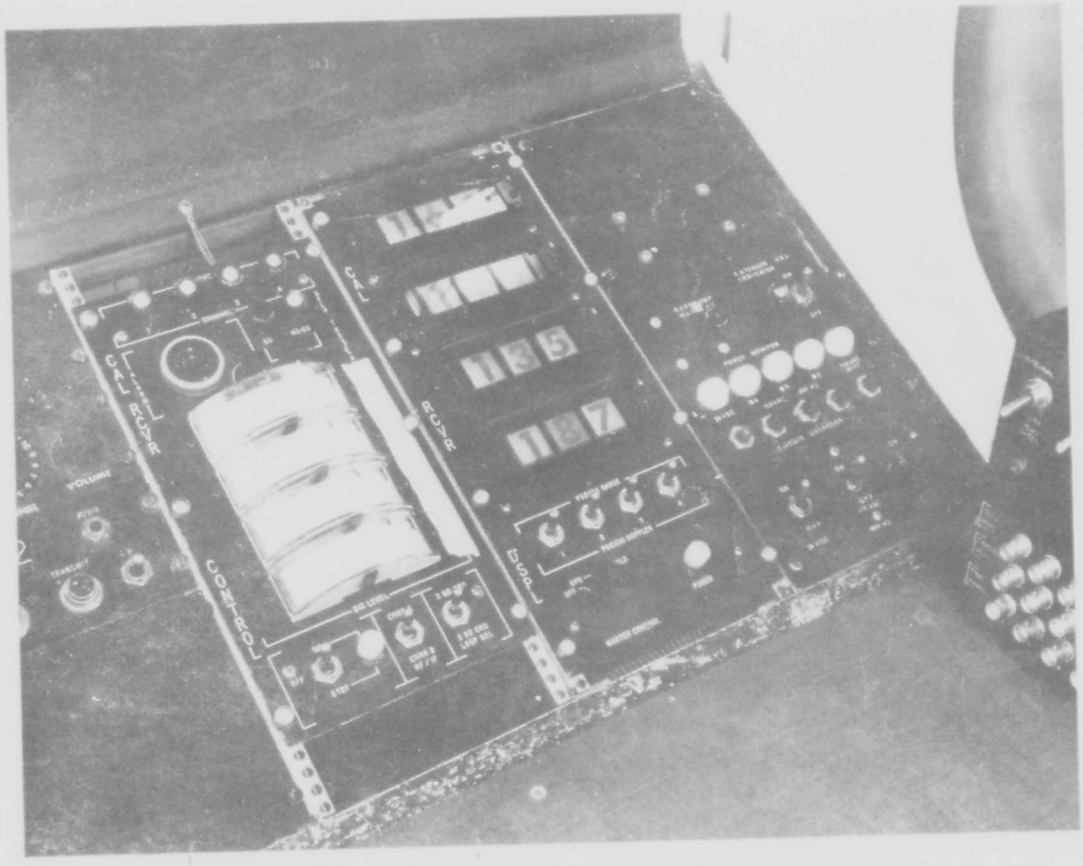

Figure 20 MCS Controls and Displays

2.2.5.1 Area Navigation Tests

Omni Antennas

- On the bottom centerline of the NC-135A at station 1050. It is the receiving antenna during System Demonstration testing
- In the 50 mi area, at EC-50 and WC-50 transmitter site for purposes of providing power illumination to the aircraft during the aircraft's System Demonstration "D" Flight Path. (Refer to paragraph 3.5.3.1 for description of flight paths, and to section 3.1 for site location and nomenclature.)

Uplink Antenna

The shaped beam uplink antennas were used only for area navigation flights to provide the desired power contour along the flight path. The primary flight paths were categorized as A or B. Different configurations and/or positioning of the uplink antennas were required for these paths.

At EC-50 and WC-50 transmitter sites two uplink antennas were used to provide power illumination to the aircraft during area navigation flights. One was oriented for the A flight path and the other for the B flight path. During part of the test program (Flights 17-22) these same antennas were also used to radiate to the MCS.

At Salt and SC-50 sites a single uplink antenna was used to radiate to the aircraft during area navigation flights. To accommodate the A and B flight paths, the antenna position was changed from "A" to "B" by removing ball lock pins from predrilled "A" azimuth and elevation holes and replacing the pins in the "B" holes. This was a manual change and required climbing the pole to accomplish. This same antenna was used to radiate to the MCS for flights 17-23.

Dish Antenna

The dish antennas were utilized in the 50 mi area at the MCS site, EC-50, SC-50, WC-50, and Salt transmitter sites. Four dish antennas were utilized at the MCS site to receive signals from similar dishes at each of the four transmitter sites. The ground rf links were changed for flights 17-23 so that the four MCS dish antennas received signals from the transmitter site uplink antennas rather than the dish antennas.

Test Antenna

The test antenna was used during field probe and multipath testing.

2.2.5.2 ILS Tests

For ILS testing the following antennas were used:

Omni Antenna

- On top centerline of the NC-135A aircraft vertical stabilizer aft of the aircraft's HF antenna for purposes of providing antenna coverage during ILS testing
- At A, C, D transmitter sites and on the balloon transmitter at Northrop Strip for purposes of providing power illumination to the aircraft during the aircraft's ILS flight path (Figure 56)
- At the MCS site at Northrop strip for purposes of providing antenna coverage during ILS testing.

2.2.5.3 Multipath Tests

For ground user multipath tests the antenna utilization was:

- Omni Antenna
  - At all transmitter locations during multipath testing
  - At the MCS location during multipath testing as the omnidirectional antenna.

- Dish Antenna

  - A dish antenna was mounted on a trailer and was used at the MCS location during multipath testing as the directional antenna.

2.2.5.4 Antenna Characteristics

Omni Antenna Electrical Characteristics

- Gain: +4 db with respect to RHCP isotrope
- 3 db beamwidth: 160^{o}
- Antenna input VSWR: 1.2:1
- Probe input VSWR: 1.5:1
- Probe coupling (cw): -20 db

Omni Antenna Mechanical Characteristics

The omni antenna was originally designed to provide nearly hemispherical radiation coverage and withstand RF-4C flight environments. A later investigation indicated that the antenna would meet the NC-135A environments. The omni antenna assembly consists of an antenna, hybrid and probe mounted within a radome, (Figure 21). The void between the antenna, probe and radome is filled with dielectric foam which aids structural integrity.

The omni antenna subassembly consists of three major sections:

- Shaped elements (radiating section)
- Quadrature hybrid (phasing section)
- Coupling probe (internal test section)

The radiating section consists of two mutually perpendicular modified dipoles shaped to provide circularity while maintaining a low profile.

The quadrature hybrid is incorporated within the antenna subassembly base and provides the phasing to the radiating elements necessary for right hand circular polarization.

The coupling probe is an electrically short monopole which radiates test signals to the antenna element allowing a true end to end system self test.

The cover radome is a hemispherical shaped hat covering the entire antenna subassembly. The radome is of sufficient thickness to survive steady state free-stream loads at Mach 1.4.

The omni antenna measures 7.5 in. diameter by 3.25 in. high.

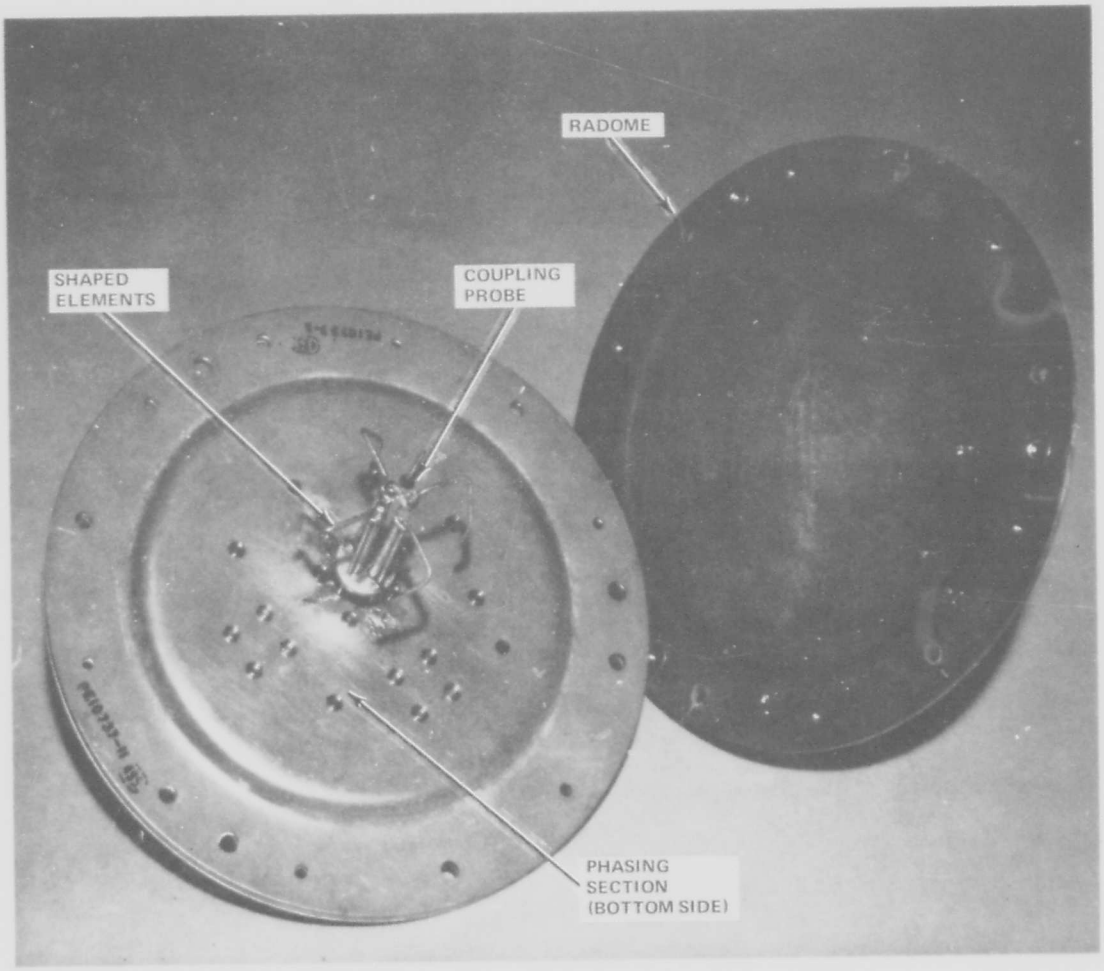

Figure 21 Omni Antenna

Omni Antenna Radiation Patterns

Formal scale model radiation patterns of a scale model omni antenna mounted on a scale model NC-135A aircraft were never performed. It was felt that a bottom antenna location on the NC-135A test aircraft would provide sufficient antenna coverage during system demonstration testing.

Without scale model antenna radiation patterns, satisfactory coverage during ILS testing was in question. Since the balloon antenna was to be above the aircraft, a top omni antenna location on the aircraft was dictated; however a top fuselage location was poor for providing coverage to the ground transmitters.

To answer the ILS question, a plastic scale model 707 (structural equivalent of the NC-135A) was constructed, painted black, back lighted and placed in a

darkened scale model ILS range. A mirror was placed at each scaled transmitter site and the proposed top vertical stabilizer location was clearly visible throughout the scaled ILS range.

The omni antenna location at the top of the vertical stabilizer provided sufficient coverage during actual ILS testing as indicated by the scale model ray test.

Uplink Antenna Electrical Characteristics

- Type: special shaped beam
- Frequency: 1575 $\pm$ 25 MHz
- Polarization: right hand circular
- Gain: approximately 4 db in respect to isotropic
- 3 db Beamwidth: 150° along flight path, 50° perpendicular to flight path

The uplink antenna coordinate system is shown in Figure 22. A typical smoothed three dimensional radiation pattern of the uplink antenna is shown in Figures 23 and 24.

The typical uplink antenna radiation pattern shown in Figure 23 was constructed from a single set of pattern data for the quadrant in which the aircraft is shown. The data presented for the quadrant behind the aircraft is the mirror image so that the fore and aft are geometrically identical.

The isometric pattern presentation causes an apparent foreshortening effect to the conical cuts which are basically elliptical in cross section.

While the pattern shown is geometrically correct, minor lobes and irregularities have been smoothed for clarity. This is especially true for the lower hemisphere.

Figure 24 shows an "envelope" half removed from the pattern in an attempt to integrate the presented data.

Uplink Antenna Mechanical Construction

The antenna is constructed of two phased array boards secured to either side of a metal "A" shaped ground plane which serves as a mounting frame. The phased array boards are separated at the proper distance from the ground plane by means of dielectric material. The base of the ground plane serves as a mounting surface for the phasing network, the external mounting tube and the base of the polycarbonate radome. Each of the phased array boards have eight crossed dipoles aligned in two banks of four. The phasing network has a single external input and four internal outputs, and one output is connected to each of the crossed dipole banks. The phasing network is terminated external of the radome. Figure 25 shows the antenna construction and provides approximate dimensions. After satisfactory initial electrical tests, the entire assembly was positioned into the polycarbonate radome and foamed in place.

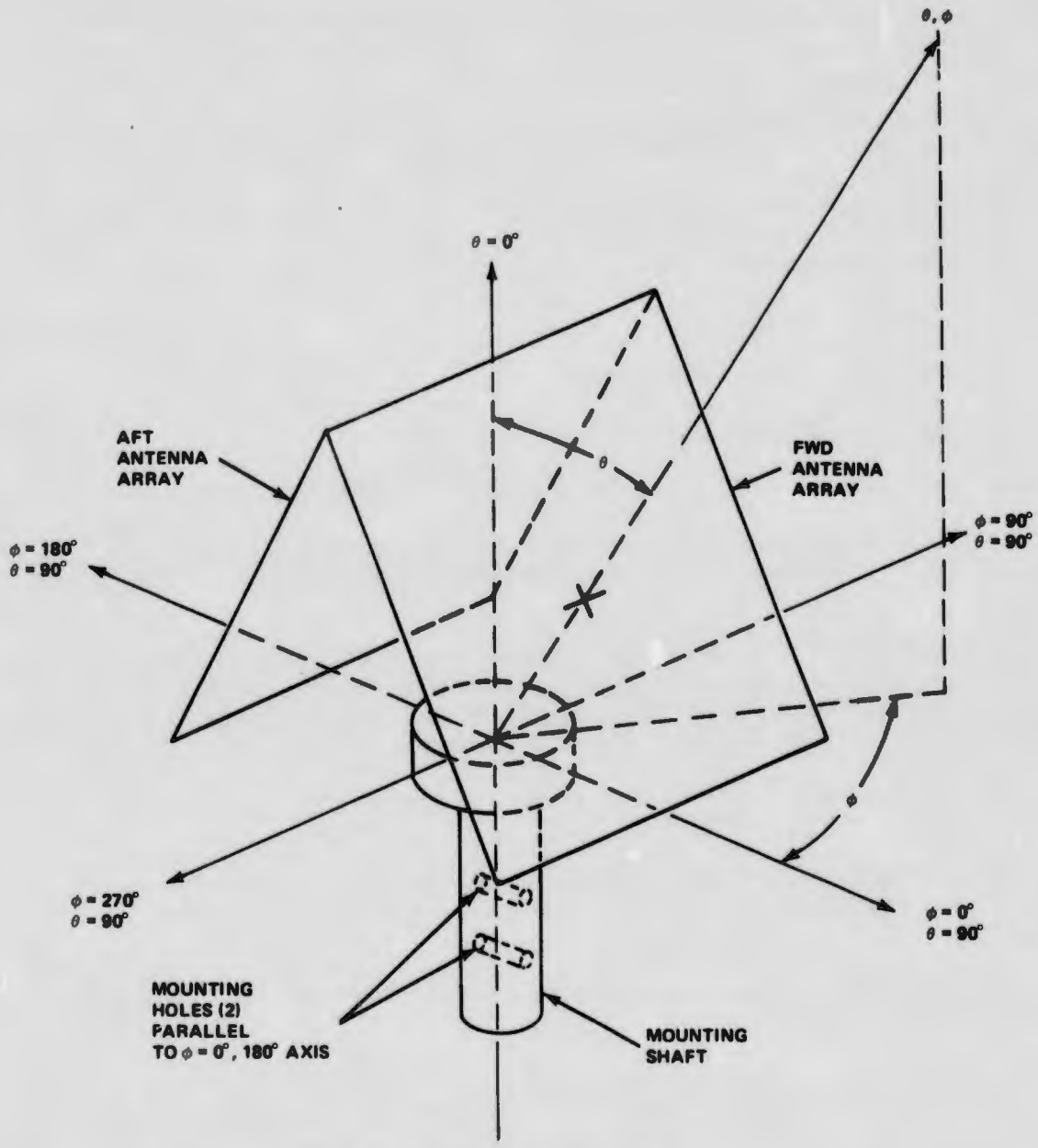

UPLINK ANTENNA COORDINATE SYSTEM

POSITION IS DETERMINED BY θ & ϕ
θ & ϕ AXES ARE MUTUALLY PERPENDICULAR
θ INCREASES CLOCKWISE
ϕ INCREASES ANTI-CLOCKWISE

Figure 22 Uplink Antenna Coordinate System

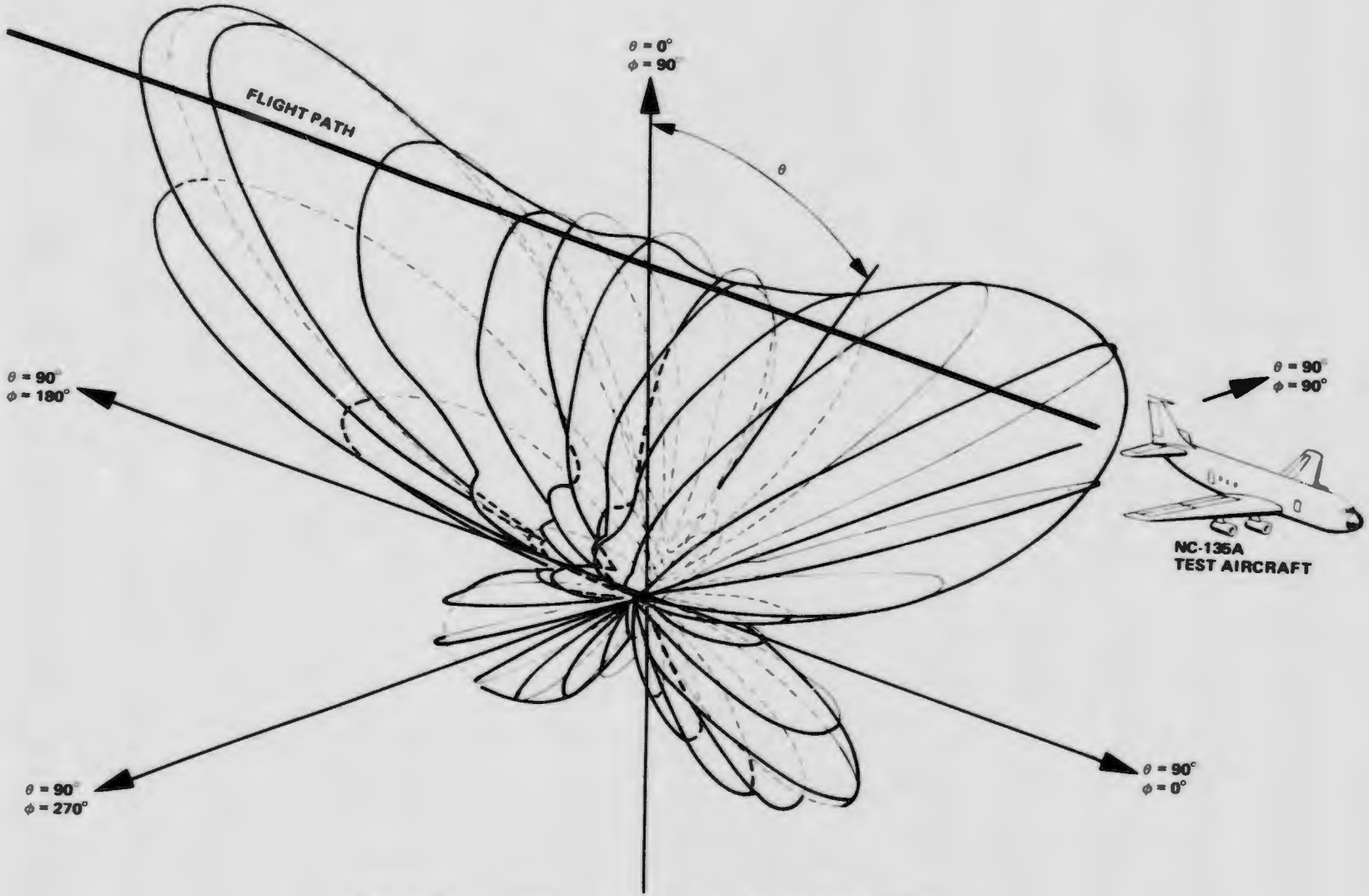

Figure 23 Typical Uplink Antenna Radiation Pattern

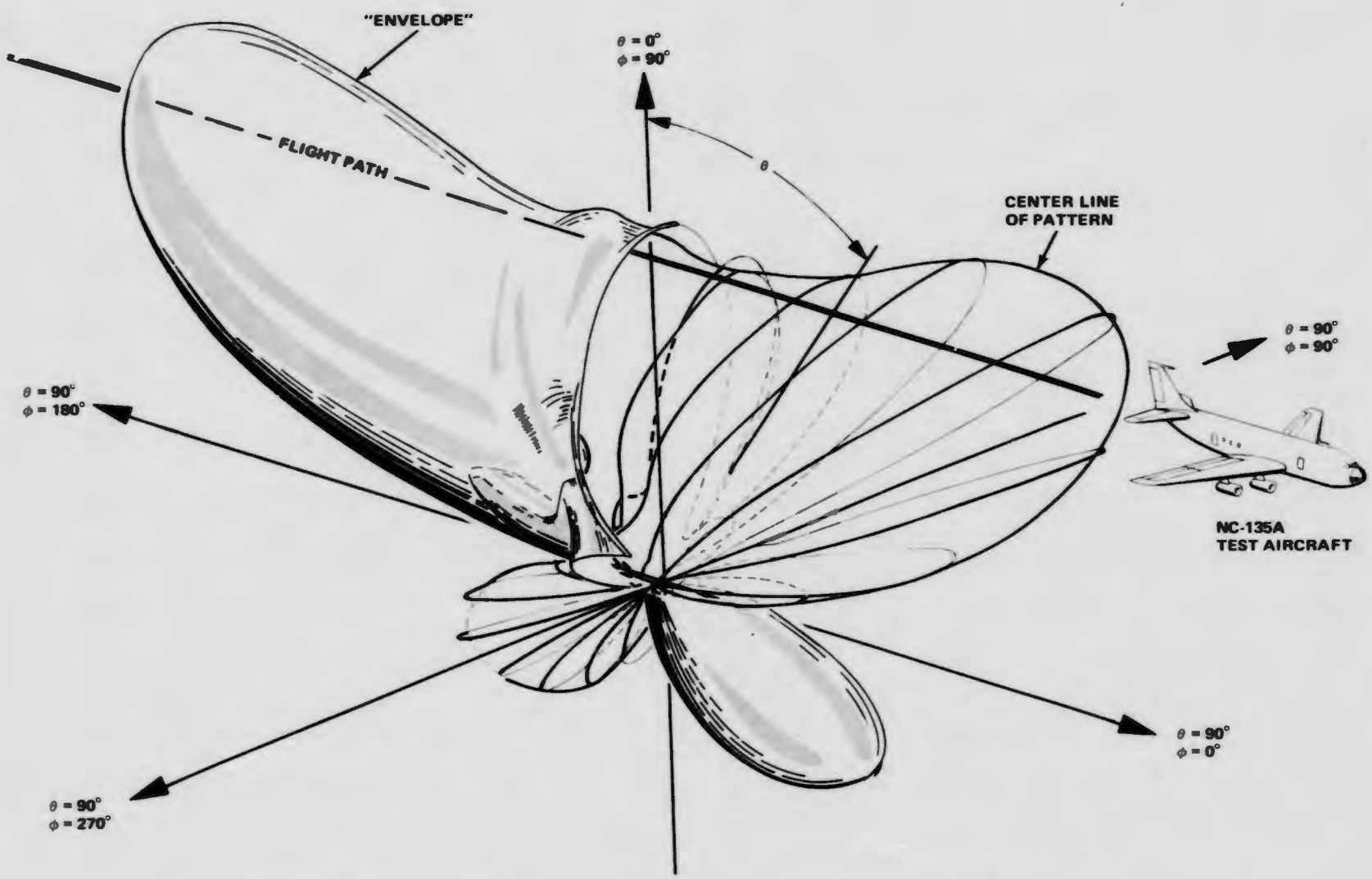

Figure 24 Typical Uplink Antenna Radiation Pattern Envelope Half Removed

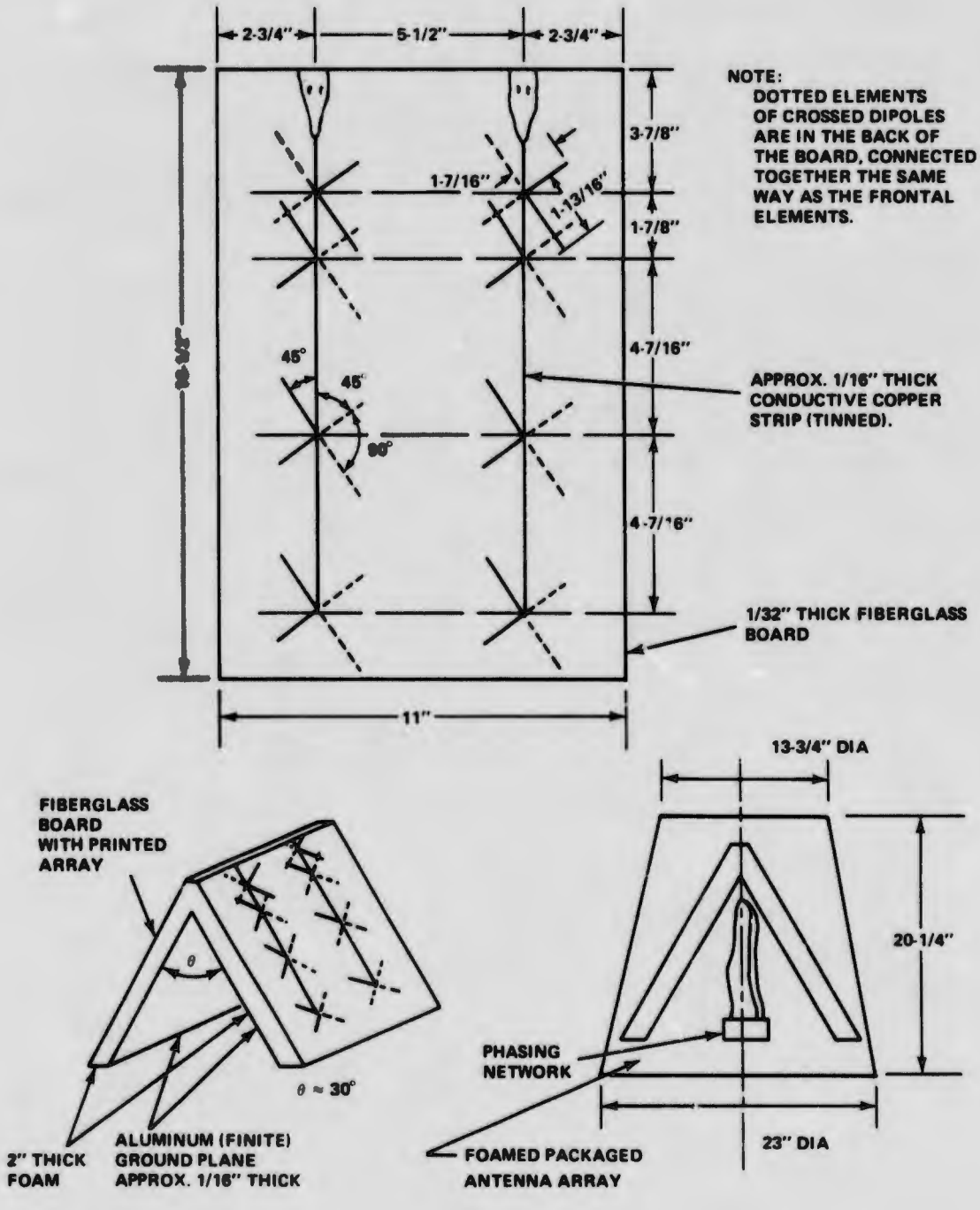

Figure 25 Uplink Antenna Construction

Uplink Antenna Mechanical Alignment

The maximum radiation is designed to be at approximately $\theta = 60^o$, $\phi = 0^o$, 180^o (the mounting shaft is attached to the antenna with the mounting holes parallel to the $\phi = 0^o$, 180^o axis, Figure 22).

Rf pattern tests were then utilized to redesignate boresight since nominal shifts were expected due to slight asymmetries in alignment and foam density. By taking successive great circle cuts, both the $\theta_e = 0$ axis, Figures 26, 27 and 28, the $\phi_e = 0$, 180^o axis and the α_e angle (coordinate system tilt in the plane formed by the $\theta m = 0$, $180^o / \phi = 0^o m$, 180^o axis) were determined, where the "e" subscript means electrically determined parameter and the "m" subscript means the mechanically determined parameters. By placing an optical theodolite immediately behind the transmitting test antenna, the antenna was then skewed in θ and ϕ until the mechanical boresight was achieved. The difference in θ and ϕ from the electrical boresight values are noted on the drive synchro displays of the pattern test equipment and represent the $\Delta\theta$ and $\Delta\phi$ as shown in Figure 26. The electrical boresight angles were then lightly scribed on the antenna/radome. The tilt mechanism was then placed in a fixture and the tilt mechanism coordinate system was aligned to the theodolite system. The tilt mechanism's mounting bolt hole pattern was then used for antenna shaft mounting and the antenna $\theta = 0^o$ axis were aligned with the $\theta_e = 0^o$ axis of the antenna/radome. If the elevation angle of the antenna was 0^o then the θ axis shaft was

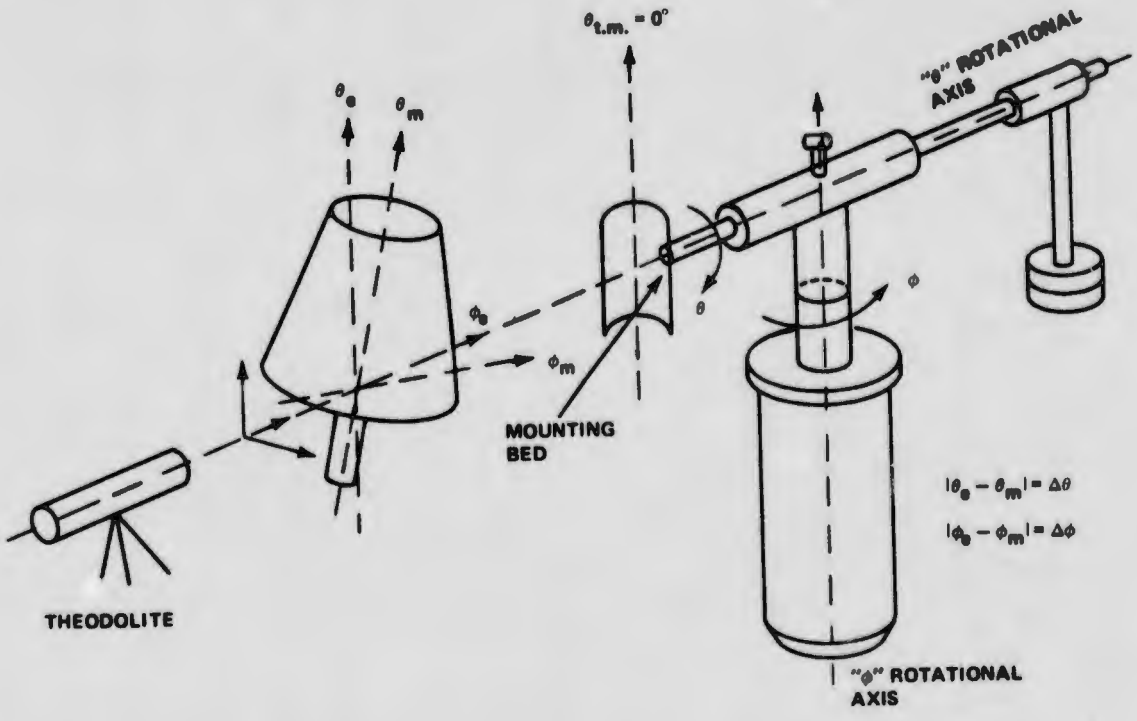

Figure 26 Uplink Antenna Electrical Boresight

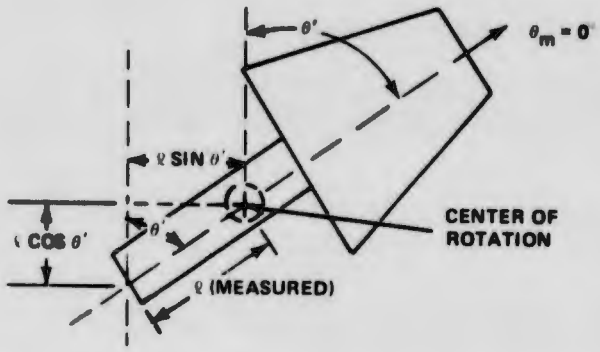

Figure 27 Uplink Antenna Off-Axis Alignment (Elevation)

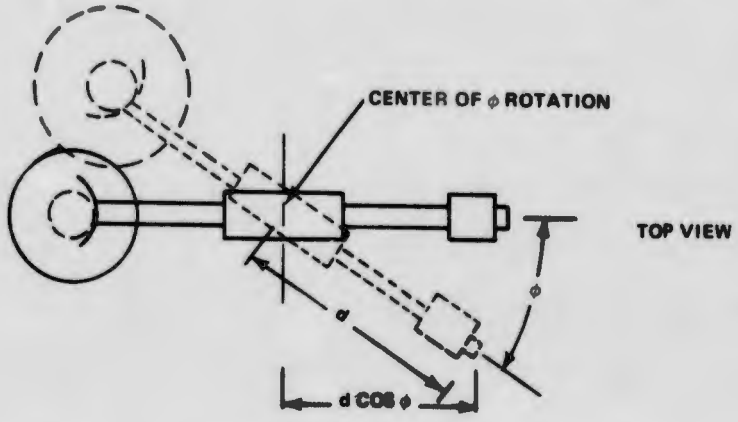

Figure 28 Uplink Antenna Off-Axis Alignment (Azimuth)

drilled and pinned. If the desired angle was other than 0^{o} a simple procedure was derived. Figure 27 shows the tilted antenna as seen through the theodolite. Knowing the desired tilt angle θ, observations were made to the mechanical axis where $0' = \theta'$ = $\theta_{desired} \pm \Delta\theta$ ($\pm\Delta\theta$ implying θ_e is rotary cw or ccw of θ_m axis). Since "ℓ" and θ are known, simple computations yield "$\ell \sin \theta$" and/or "$\ell \cos \theta$." Mechanically mounting a ruler vertical (zeroed at point θ), the theodolite horizontal cross hairs set to traverse the center of rotation, mark off "$\ell \cos \theta$." Adjustments of the angle set were made until the desired "$\ell \cos \theta$" measurement was obtained. The tilt mechanism was then drilled and pinned.

A similar technique was used for multiple azimuth angles. Figure 28 shows the technique of using the horizontal projection of the shaft length from center of rotation to end of shaft.

Here $\phi = (\phi$ desired), since $\Delta\phi$ has been corrected for in the mounting procedure of the antenna shaft to the tilt mechanism mounting bed.

In both the azimuth and elevation angle measurements, the angle error is less than 1^{o} because of the long measurement arm used.

Uplink Antenna Alignment on Poles at Sites

The A and B uplink antennas are electrically identical but mechanically different. The antennas are mechanically set in their own tilt mechanism at preset azimuth and elevation angles.

Once the antenna is joined to the tilt mechanism it becomes dedicated to a specific transmitter site. Figures 29 through 32 illustrate the alignment of the antennas at the various sites.

Dish Antenna Electrical Characteristics

A Prodelin Masar 73-741 6-ft diameter solid fiberglass parabolic dish with plane polarized feed was used.

- Frequency: 1575 ± 25 MHz
- Gain: +27.5 db
- 3 db beamwidth: 8.0°
- First sidelobe: -18 db
- Wide angle sidelobe: -24 db
- Front to back ratio: 30 db
- VSWR: 1.35:1 max

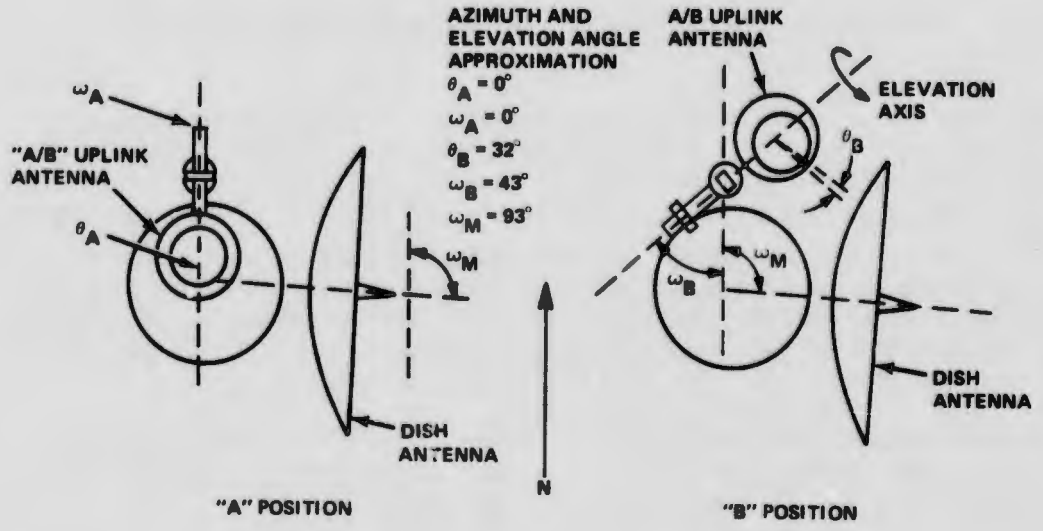

Figure 29 Antenna Orientation at Salt Site

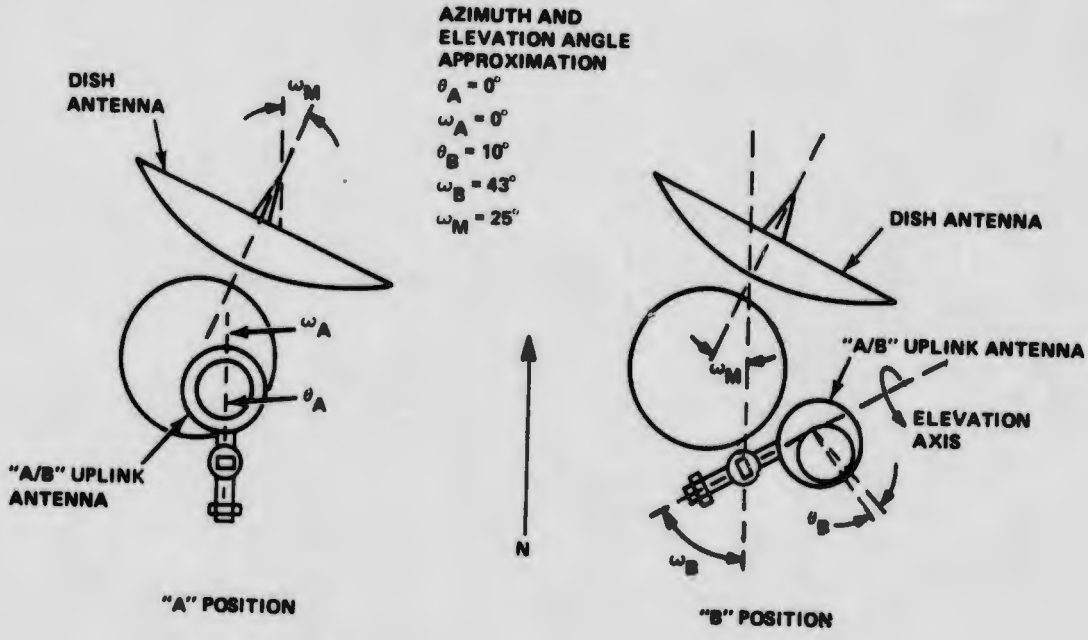

Figure 30 Antenna Orientation at SC-50 Site

Dish Antenna Mechanical Characteristics

The dish antenna differs from standard dishes in that the fiberglass dish weighs 48 lb, versus 100 lb for standard aluminum dishes. The lighter weight simplified handling and installation of the dishes at the various sites and on the multipath trailer. The dish antenna and mounting brackets were designed to withstand 125 mph winds.

Test Antenna Electrical Characteristic

- Type: short dipole 1/4 wavelength above fixed ground plane approximately 10 in. by 14 in. (dipole paralled to 10-in. dimension).
- Frequency: 1575 ± 25 MHz
- Beamwidth: approximately 110° between half power points
- Gain: approximately 4.5 db with respect to isotropic
- VSWR: approximately 1.20:1

Test Antenna Mechanical Characteristics

The test antenna consisted of the dipole sticking through the ground plane held in place by means of right angle bracket and a small cable clamp. To provide rigidity plastic tape was wrapped between the dipole and the ground plane. The test antenna was mounted to the field probe by means of "C" clamps.

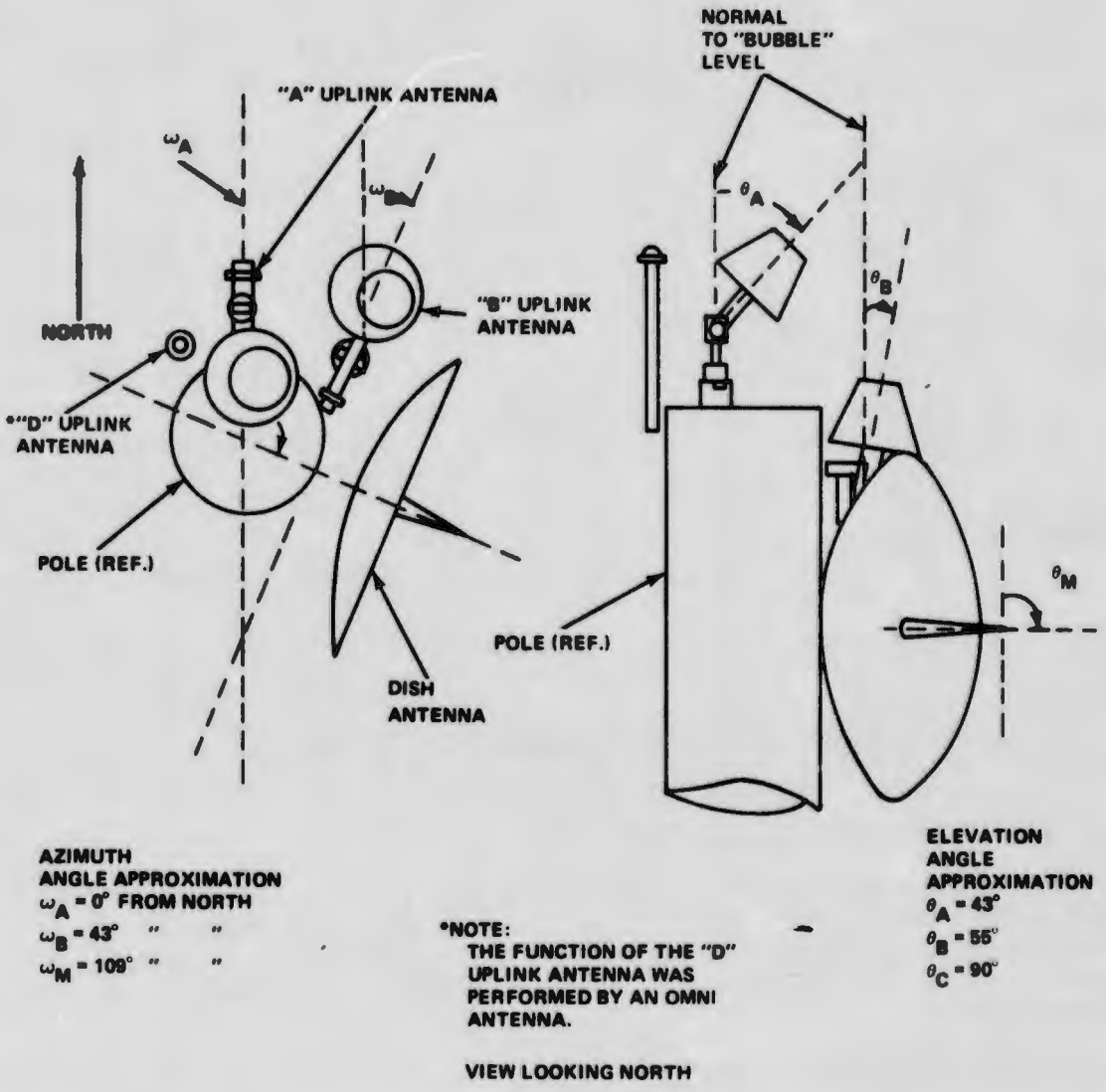

Figure 31 Antenna Orientation at WC-50 Transmitter Site

2.2.6 Balloon and Equipment

2.2.6.1 Balloon

ILS testing at Northrop strip utilized a balloon-borne transmitter. The tethered balloon used to suspend the transmitter was a 45,000 cu ft, helium filled, ballonet barrage type balloon. The balloon was tethered to a motorized winch that raised and lowered the transmitter during missions, Figure 33. On non-flight days, the balloon was moored to ground anchor points of the 240-ft diameter launch pad. The balloon was inflated and deflated a number of times depending on program flight schedule. On one occasion the balloon had to be lowered to repair holes torn in both the fabric and instrument by a lightning strike.

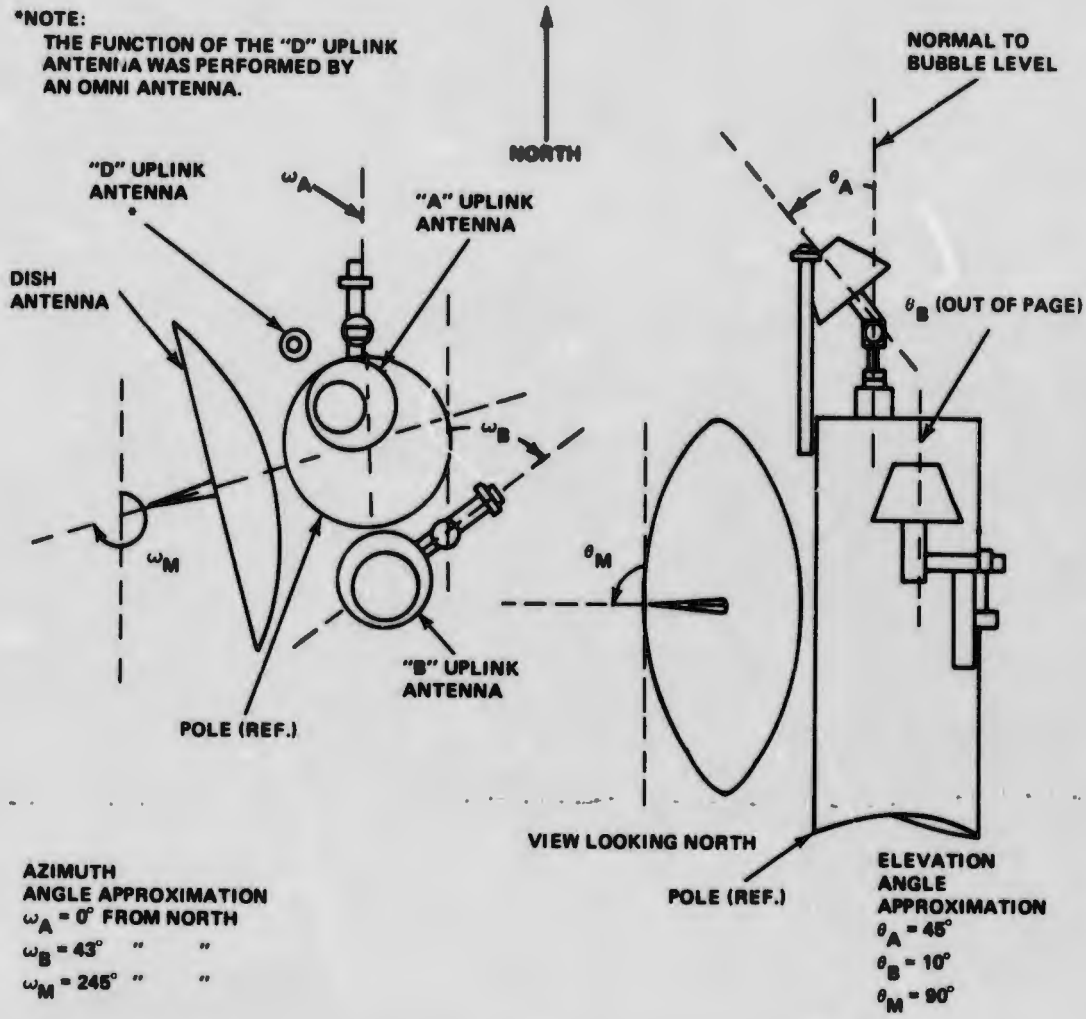

Figure 32 Antenna Orientation at EC-50 Transmitter Site

2.2.6.2 Balloon Package

The battery powered transmitter was mounted to a load bar suspended below the balloon, Figure 34. Plywood panels were mounted to the thermal shields of the transmitter with day-glo orange arrows, pointing to the omni antenna, painted on each of the five visible side panels. The object of the arrows and cloth tail tied to the omni antenna was to "flag" the spot of the signal origin, the omni antenna. During the flight, the balloon transmitter was tracked by four cinetheodolites and it was felt that the flagging would help optics track the antenna. The arrows also aided in the cine film data reduction. Figure 35 shows the transmitter at 5000 ft above ground level (AGL) during a mission, as seen by a cinetheodolite. Most flights required the balloon to be at 5000 ft AGL.

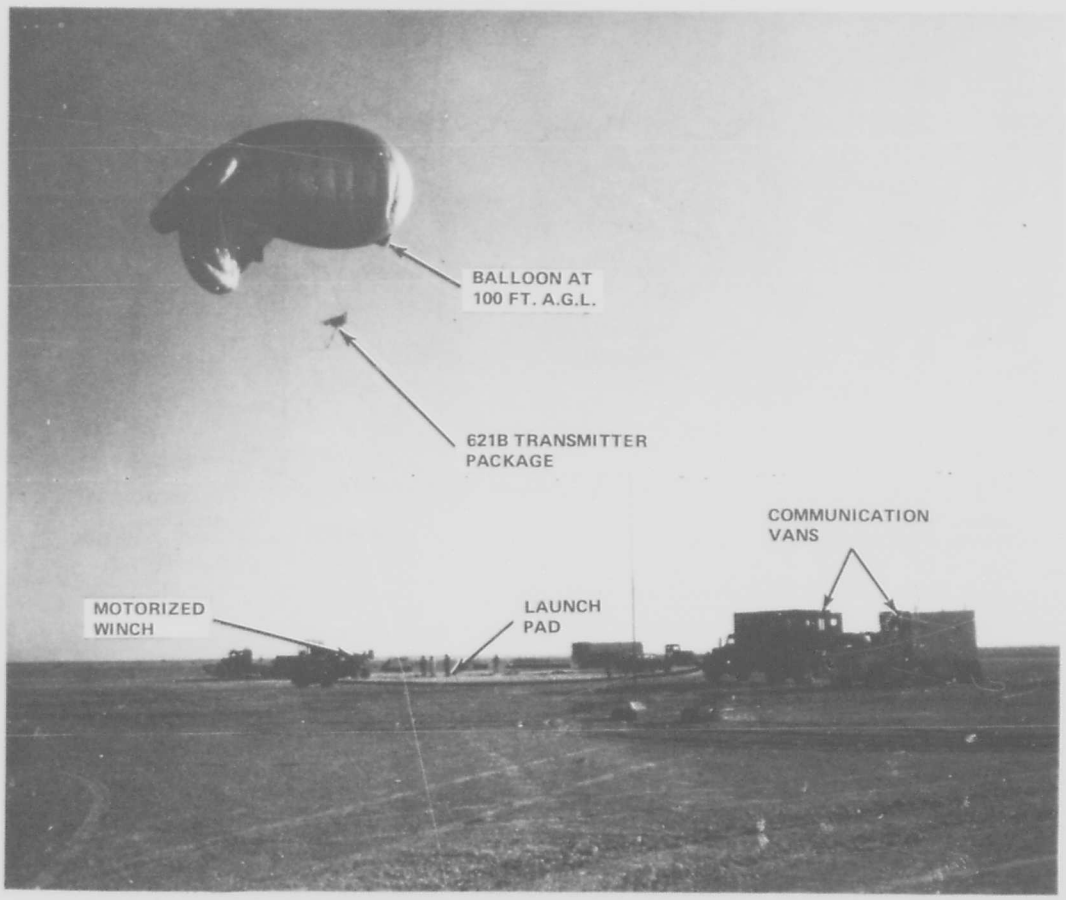

Figure 33 621B Balloon and Launch Pad Complex

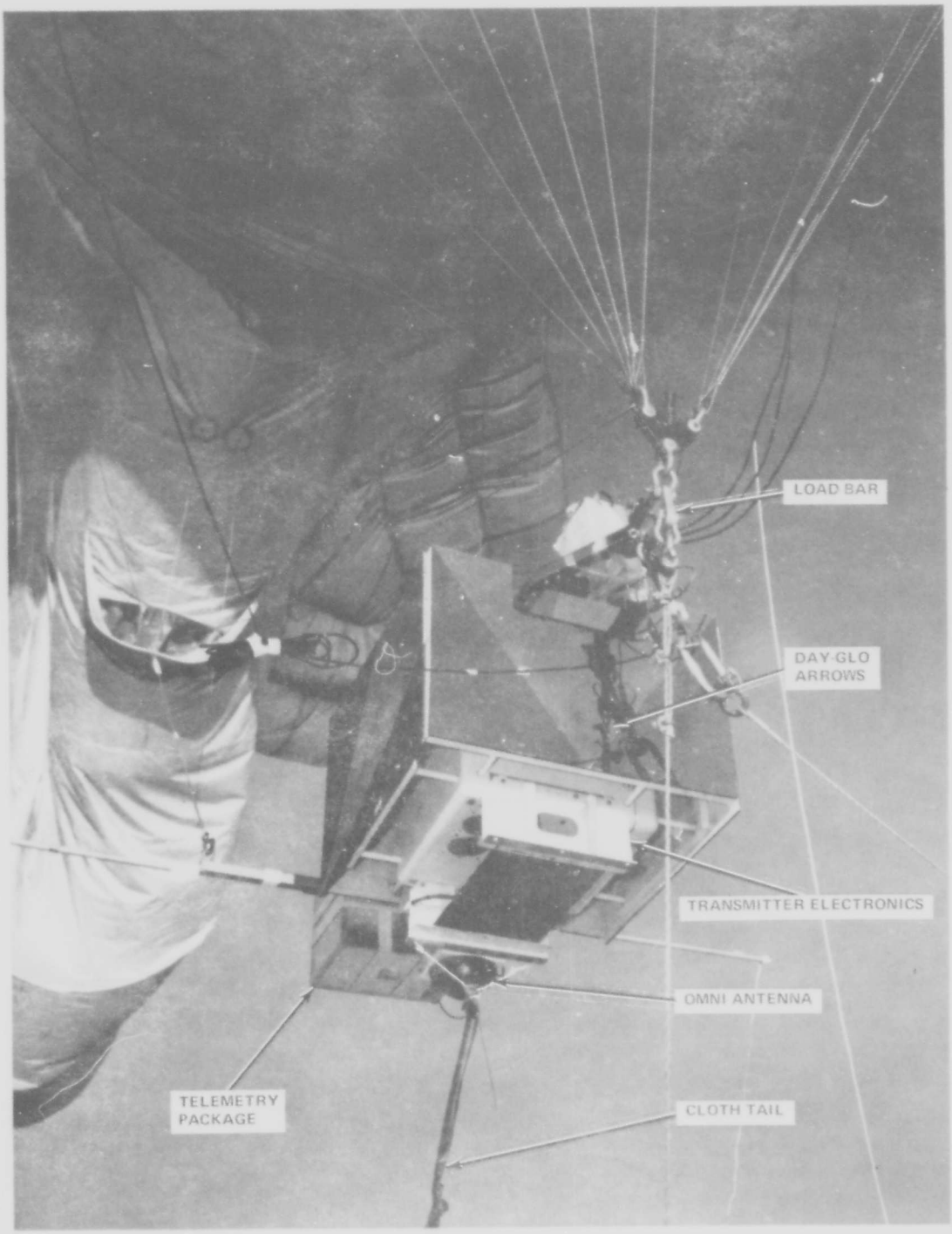

Figure 34 621B Transmitter Package in Flight Configuration

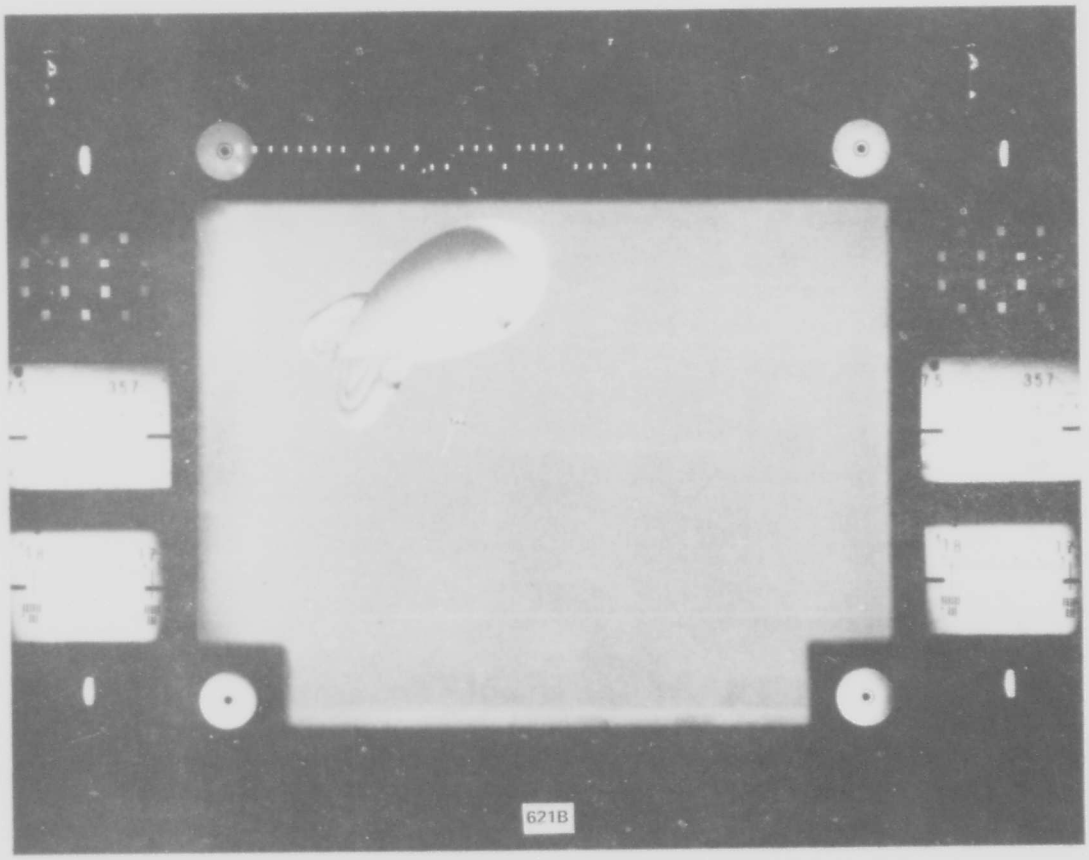

Figure 35 Flight 31 at 17:01:39:00 Station (G-267 Cinetheodolite) Run No. 7

The load bar also had a telemetry package (Figure 36) and a C-band radar beacon suspended from it. The telemetry package was used to command the 621B transmitter on and off, switch an internal (to transmitter) 20 db attenuator in and out and varying the transmitter output rf power in conjunction with external attenuators. The package also controlled squibs, and gas valves for balloon flight control. The C-band transponder, strapped below the telemetry package was energized on and off by the telemetry package. The transponder beacon allowed the balloon package to be tracked by FPS-16 radar, Figure 37. The radar data were intended to be used for "quick look" on the balloon position while the cine data were being reduced.

The same balloon-transmitter configuration was used for smooth and rough earth multipath testing. During these tests, the balloon was flown at 2000 ft AGL and moved from the balloon launch pad to the multipath sites (see paragraph 3.5.5 for a detailed description of multipath testing).

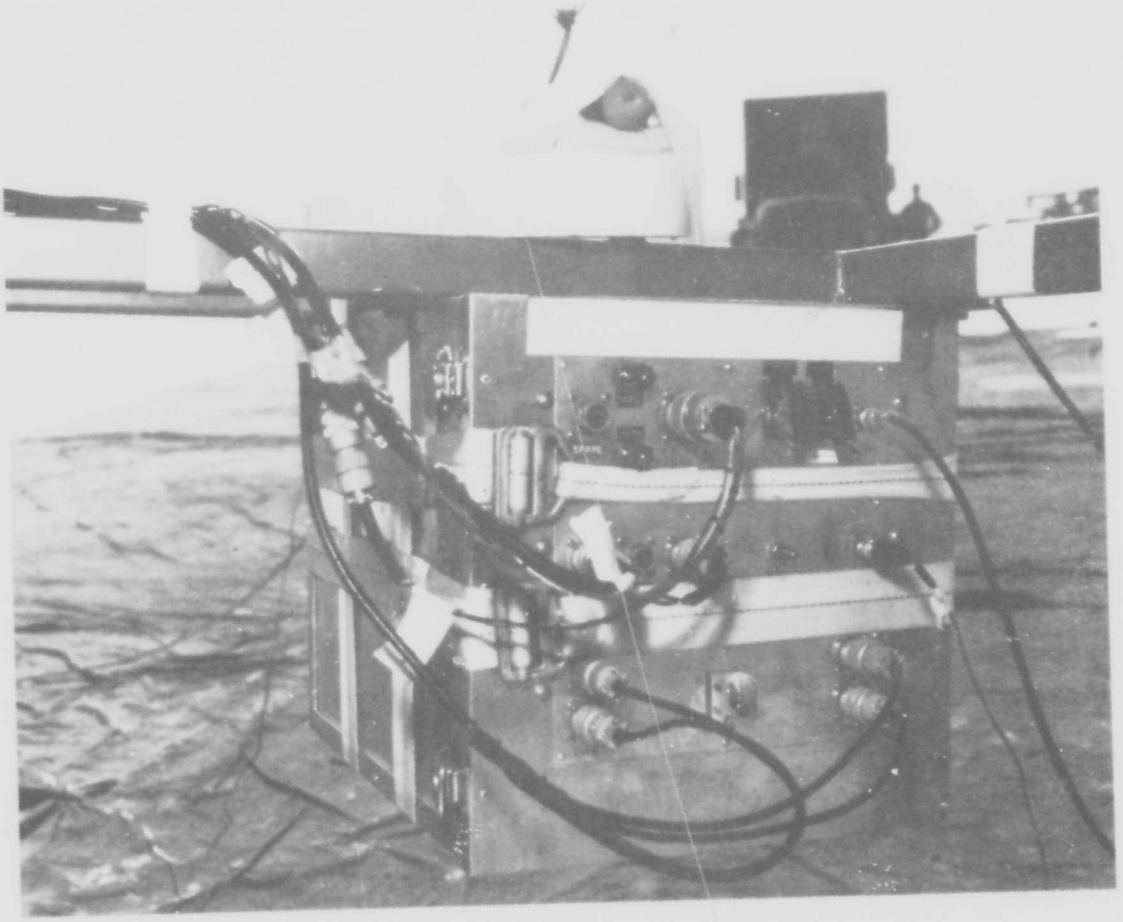

Figure 36 Balloon Telemetry Package Mounted on Load Bar

All balloon related functions were handled by the Air Force Cambridge Research Laboratories Bedford, Mass. (AFCRL) Holloman AFB Detachment. Grumman Aerospace Corporation was responsible for the function of the 621B transmitter and its installation and removal prior to and at the end of each mission.

2.2.7 WSMR Reference Trajectory Sensors

Most reference trajectories provided by WSMR are based on angle and/or range measurements from which position data are computed. Velocity and acceleration are usually obtained as derivative data from the position information. Thus velocity and acceleration "measurements" are not measurements at all but are mathematical derivations and are no more precise than the position data from which they are derived.

To enhance the WSMR Reference data to the accuracy considered necessary for our test program, four types of aircraft position instrumentation were utilized. The AN/FPS-16 radar, Askania Cinetheodolites, a Doppler Velocity and Position System (DOVAP), and an airborne LTN-51 Inertial Measuring Unit. Software packages have been developed to filter and merge various sensor data to produce a best estimate of trajectory (BET).

2.2.7.1 Radar

AN/FPS-16 radars normally scheduled for the 621B flights were R-113, R-123, and R-127, Figure 38. Other radars were sometimes used if one of the above was inoperative.

The FPS-16 radar is a C-band monopulse tracking radar capable of providing real-time data for vehicle control and flight safety purposes, acquisition data for range instrumentation, and vectoring data for drone and aircraft control. Skin and

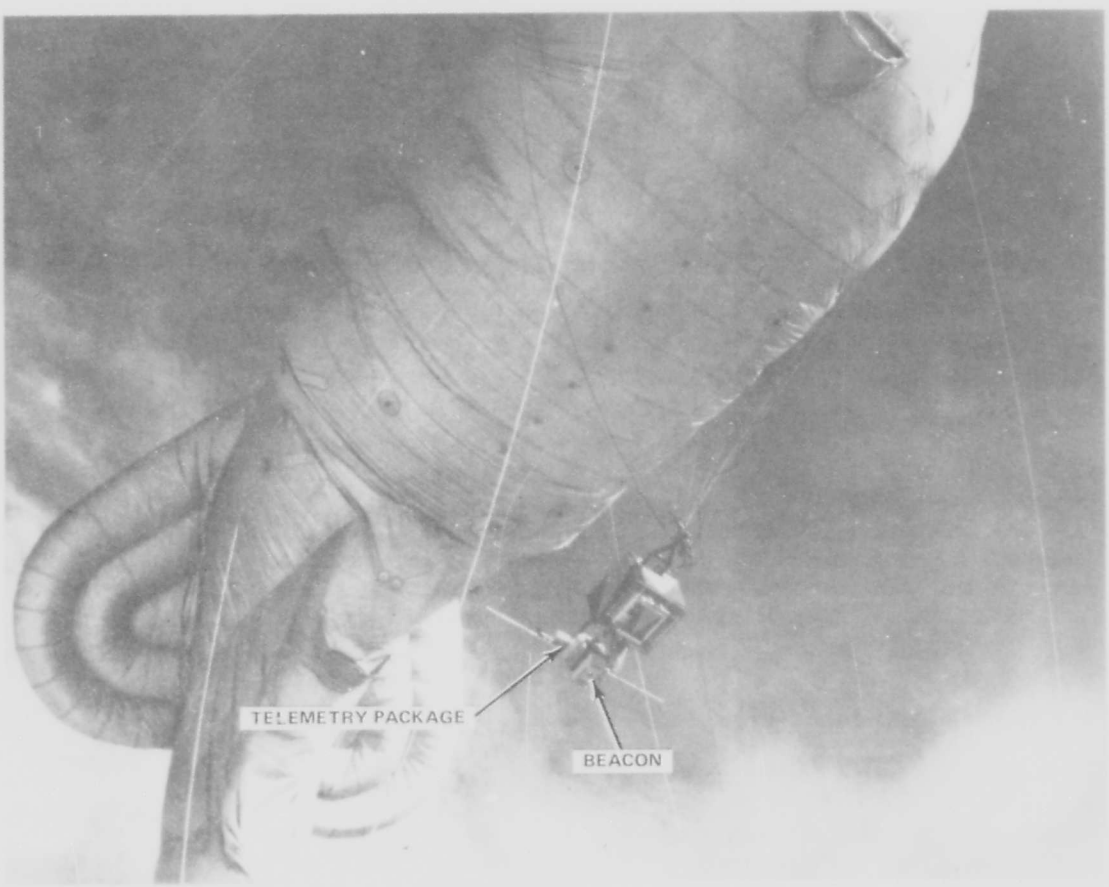

Figure 37 621B Balloon Package

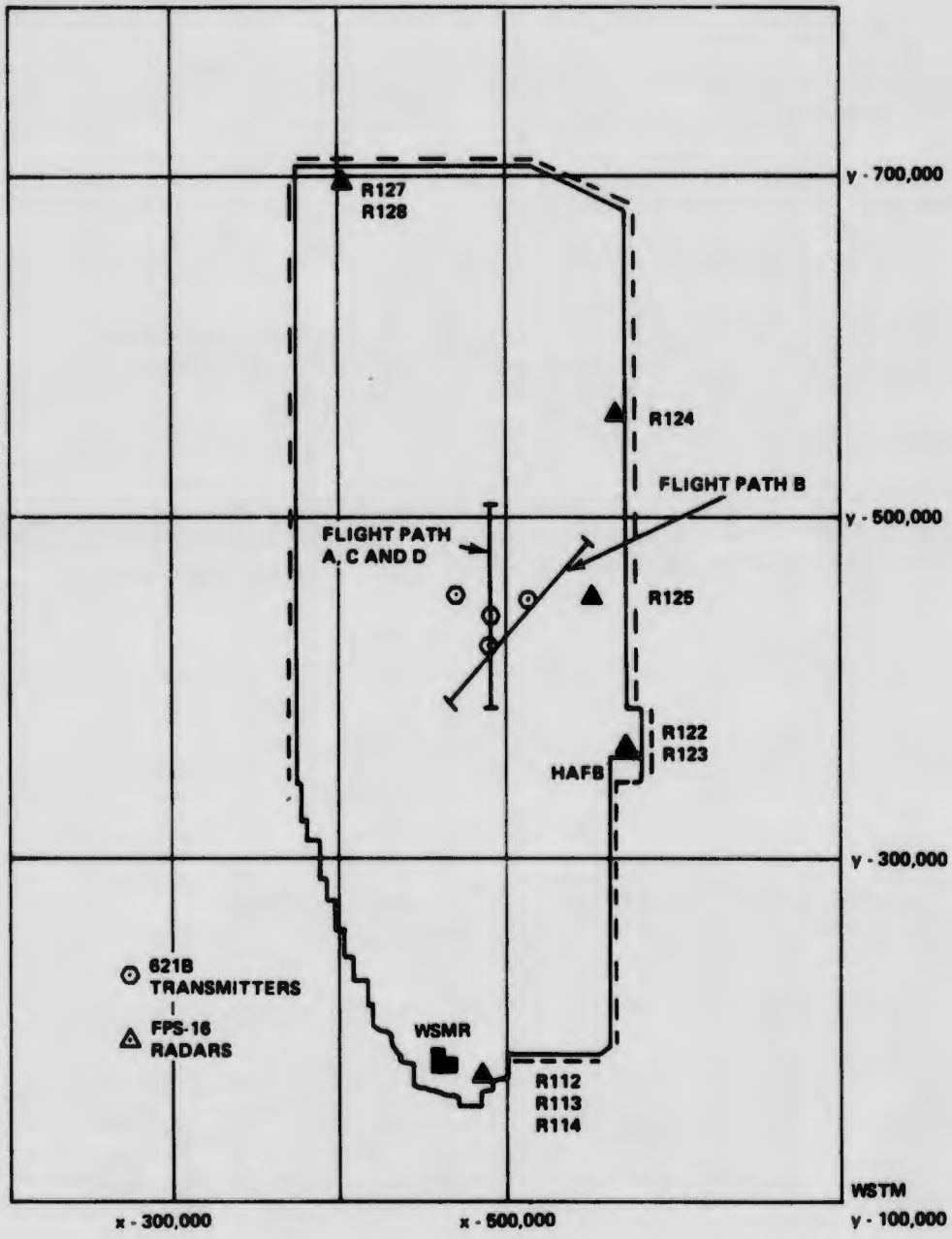

Figure 38 FPS-16 Radars Used for 621B as per White Sands Datum-71

beacon tracking modes can be used simultaneously and data output fed directly into digital and analog computing equipment. We used the radar data to vector the aircraft and also to provide "Quick Look" data for analysis purposes. Its characteristics are:

- System Precision
  - Position: ± 15 to ± 130 ft (function of range
  - Velocity (derivative): ± 15 to 60 ft/sec
  - Acceleration (derivation): ± 20 to ± 75 ft/sec^2

- System Coverage
  - Range: 500 yards to 2000 n mi
  - Azimuth: 300°
  - Elevation: -10° to 190°

A modification kit has been added to R-113, R-123, and R-127 called the Coherent Transmitter and Doppler Velocity System. Range rate measurement accuracies of ± 0.1 fps are expected to a range of 2000 mi, Figure 39.

2.2.7.2 Cinetheodolite

The cinetheodolite is an optical tracking instrument (Figure 40 and 41) designed to record on 35 mm film the following information: (1) angle data taken from elevation and azimuth shaft encoders; (2) IRIG timing; (3) frame number; and (4) target

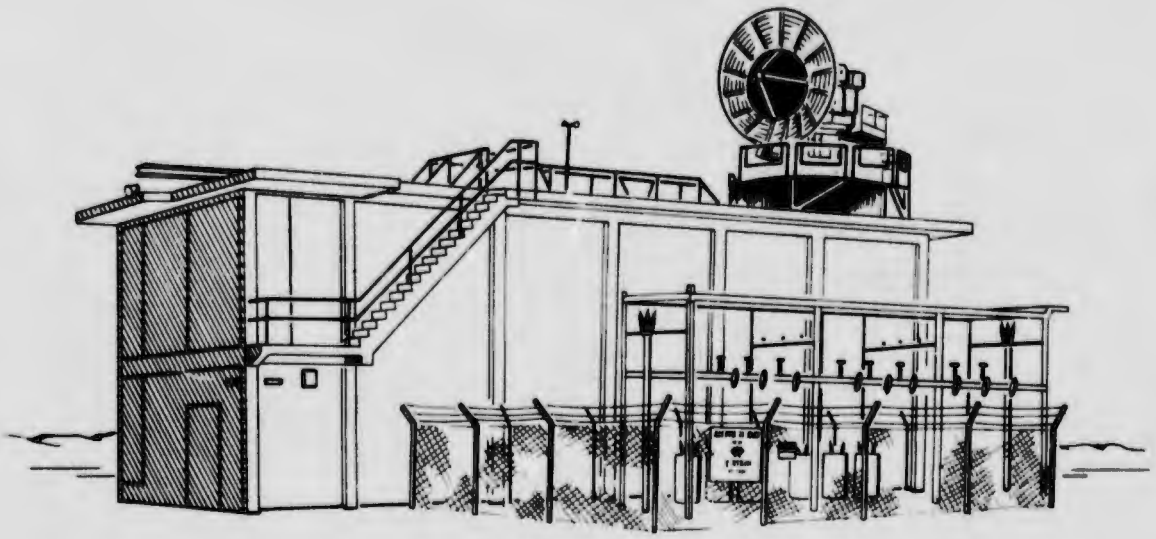

Figure 39 FPS-16 Radar With Optical Tracker as an Acquisition Aid

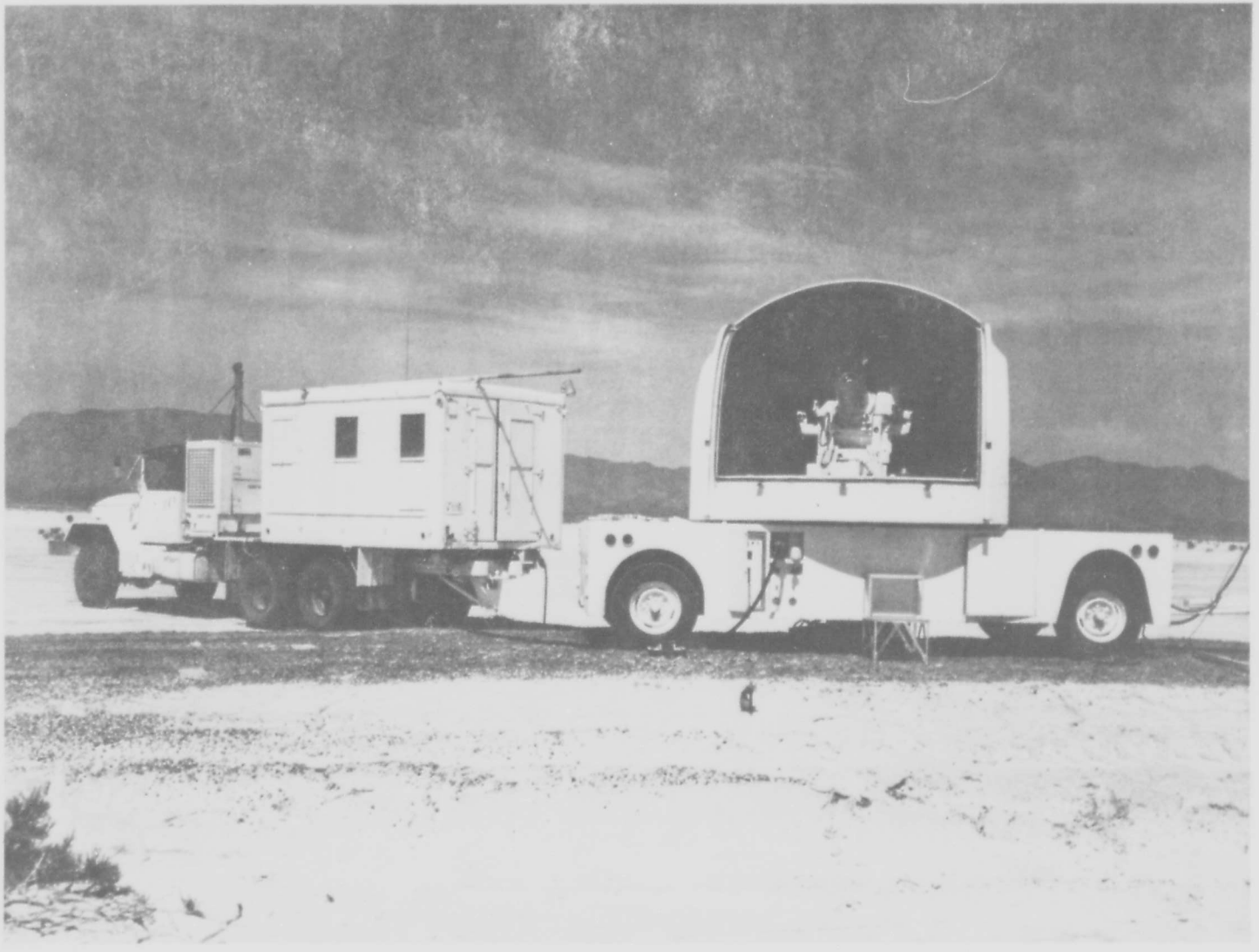

Figure 40 George 282, Mobile High Speed Askania Located West of Northrop Strip

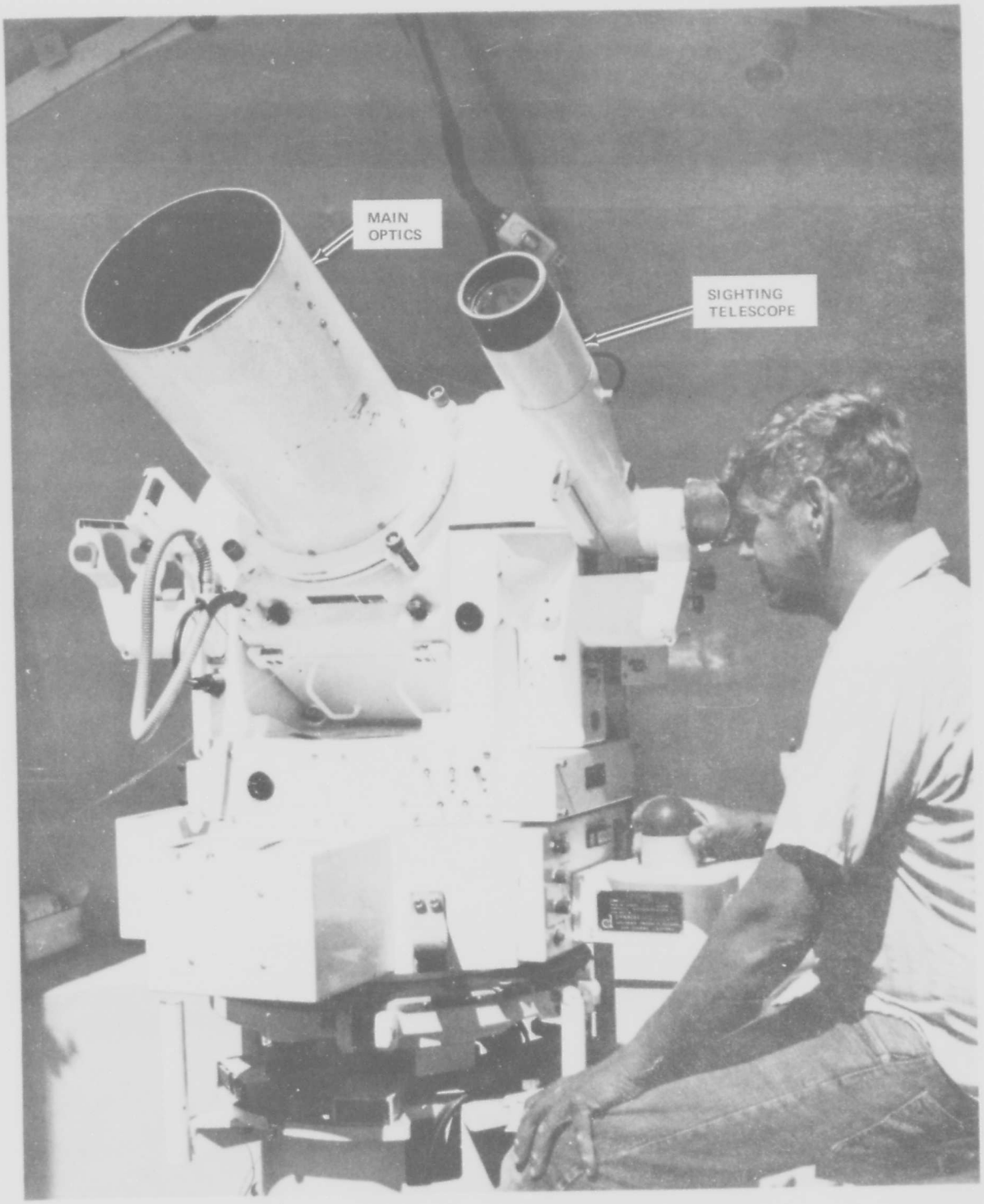

Figure 41 Typical High Speed Askania, 20 Frames per Second, Focal Length 44 Inches

vehicle image relative to fiducial marks superimposed on each frame of film. The film image is then read manually by measuring deviations of the aircraft from the center of the fiducials and adding these corrections to the readings taken from the azimuth and elevation dials. (Figure 42 illustrates the target vehicle and paint pattern utilized on the 621B flight test program. Figure 43 displays a single frame of data taken from the high speed Askainia G-267.) The maximum slant range of a cinetheodolite is approximately 60,000 ft depending upon atmospheric conditions. Precision of cinetheodolite position data varies with target size, slant range, elevation angle, and tracking acceleration rates. Position error is approximately ± 8 ft. Two stations are required to derive position data but four to nine are desired to provide the accuracy quoted above. (See Figures 44 and 45 for the cinetheodolite instrumentation plan utilized by WSMR). Figures 46 and 47 show the ILS Flight Path as viewed from a cinetheodolite.

2.2.7.3 Doppler Velocity and Position (DOVAP) System

The DOVAP System is comprised of 60 receiver stations, seven ground reference transmitters and ten receive/record stations deployable on 256 sites. The basic system consists of a ground reference transmitter, an airborne transponder and three or more ground dual-receiving stations. A reference signal from the ground transmitter is received by the aircraft beacon and by each of the ground receivers. In the aircraft the DOVAP signal is doubled in frequency and retransmitted to the receivers on the ground. At each receiving station the reference signal is doubled and compared with the signal received from the airborne transponder. The difference is a doppler frequency directly proportional to the velocity of the aircraft. The doppler frequency and time marks are recorded on magnetic tape. Integration of the doppler cycle over an interval of time represents a change in path length from the transmitter to the vehicle and then to the receiver. The data normally obtained includes three coordinate space positions, with the velocities being derived from position differentials. (See Figure 48 for locations and instrumentation geometry of the DOVAP stations used for 621B). Figures 49 and 50 illustrate the DOVAP system. Its characteristics are:

- System Precision
  - Position Precision: 0.5 to 14 ft depending upon altitude
  - Velocity Precision: 0.1 to 3 ft/sec
  - Acceleration Precision: 0.1 to 3 ft/sec^2

2.2.7.4 Telescope

During the ILS portion of the 621B flight test program, a mobile telescope was utilized to provide touch down event data. The telescope photographed the aircraft with a 46-in. lens at a rate of 250 frames per second. The image was recorded with IRIG A timing pulses on 35 mm film. WSMR read this film and provided time of touch down.

The Mobile Telescope (T-619) was colocated with the cinetheodolite G-278, Figure 45. (See Figure 51 for a photograph of station T-619, Mobile Telescope and Figure 52 for an example of one frame of telescope film.)

The discussion of WSMR reference trajectory sensors was extracted from Ref. 6.

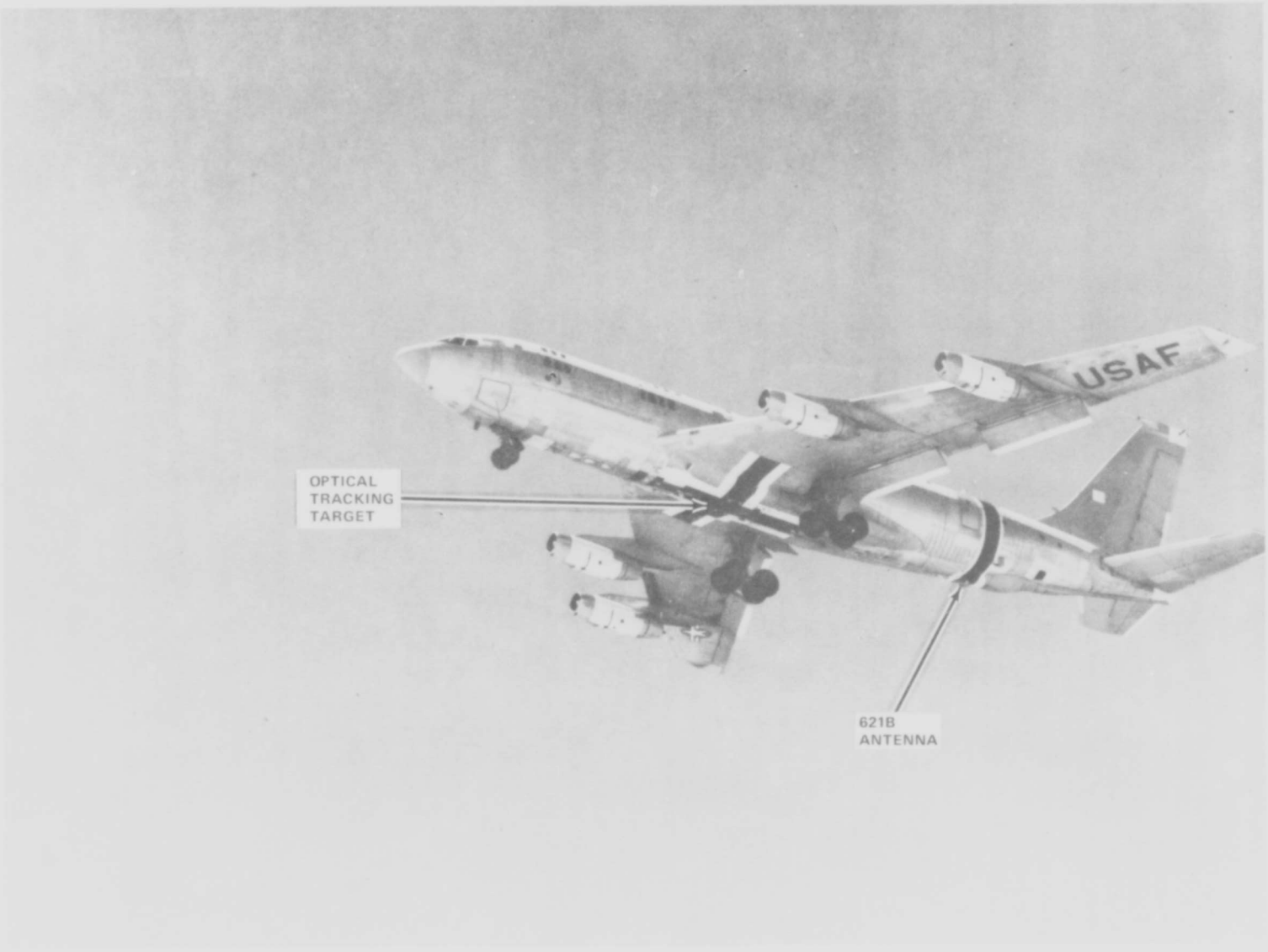

Figure 42 621B Paint Patterns

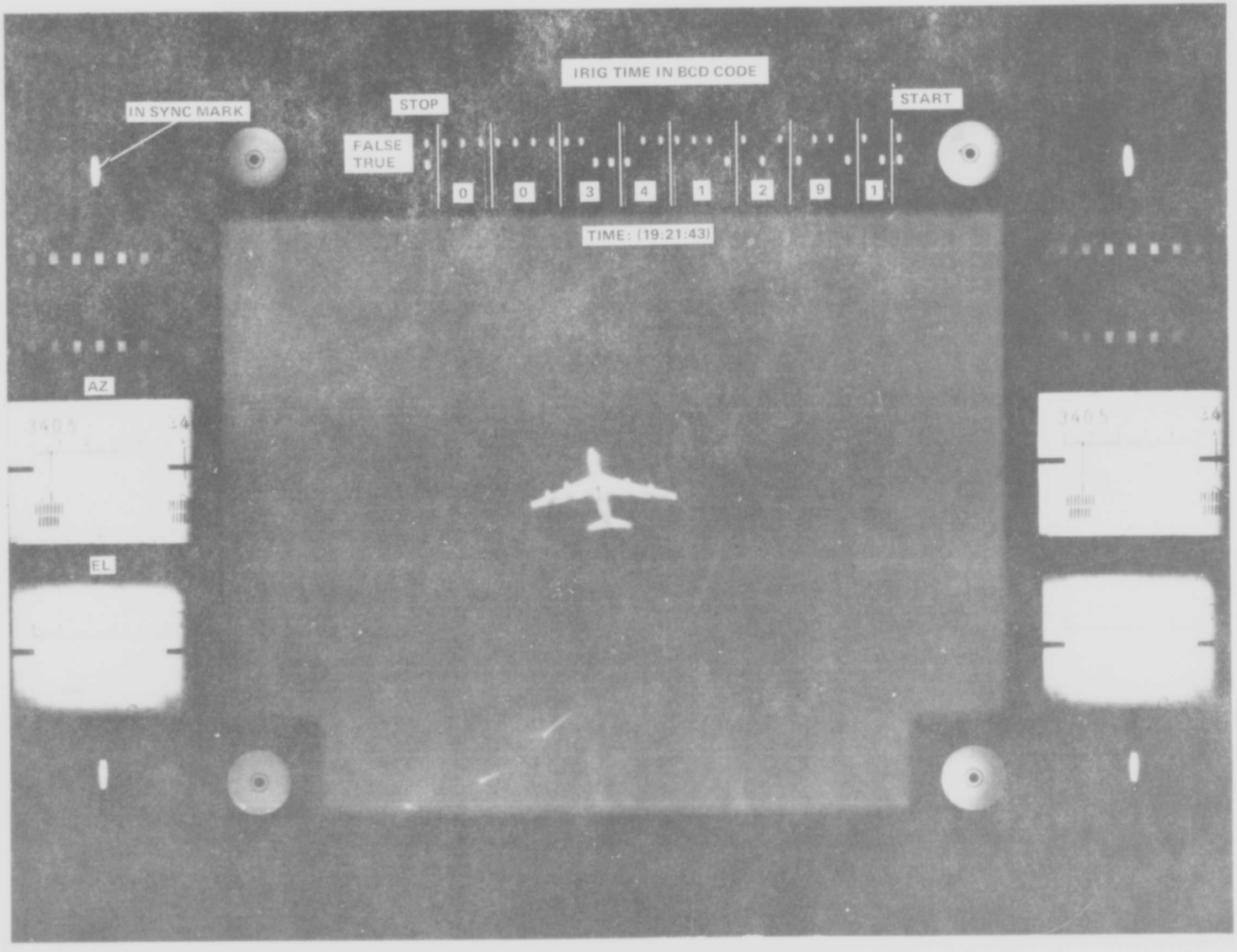

Figure 43 High Speed Askania G-267

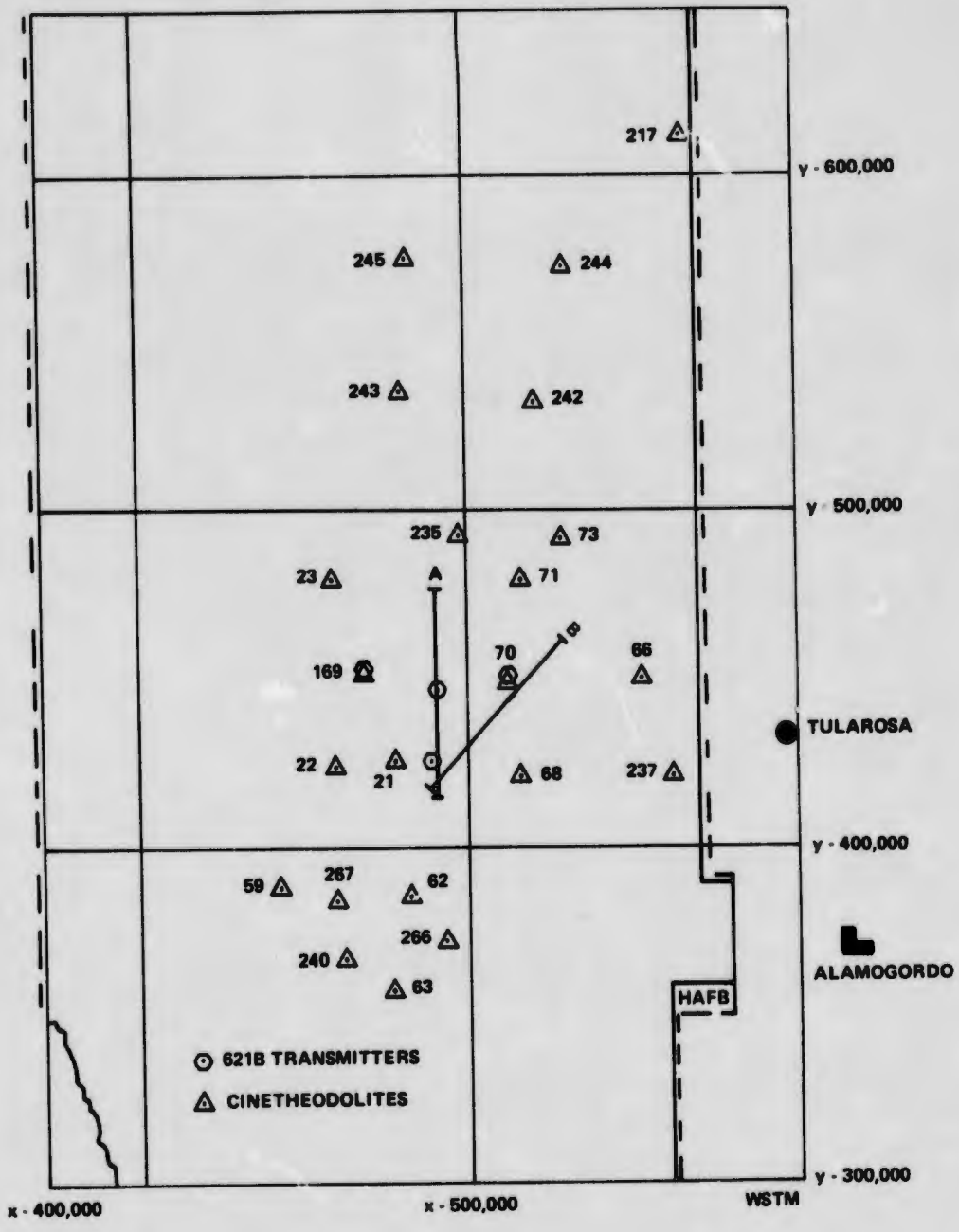

Figure 44 Area Navigation Cinetheodolite Coverage for 621B (Askania)

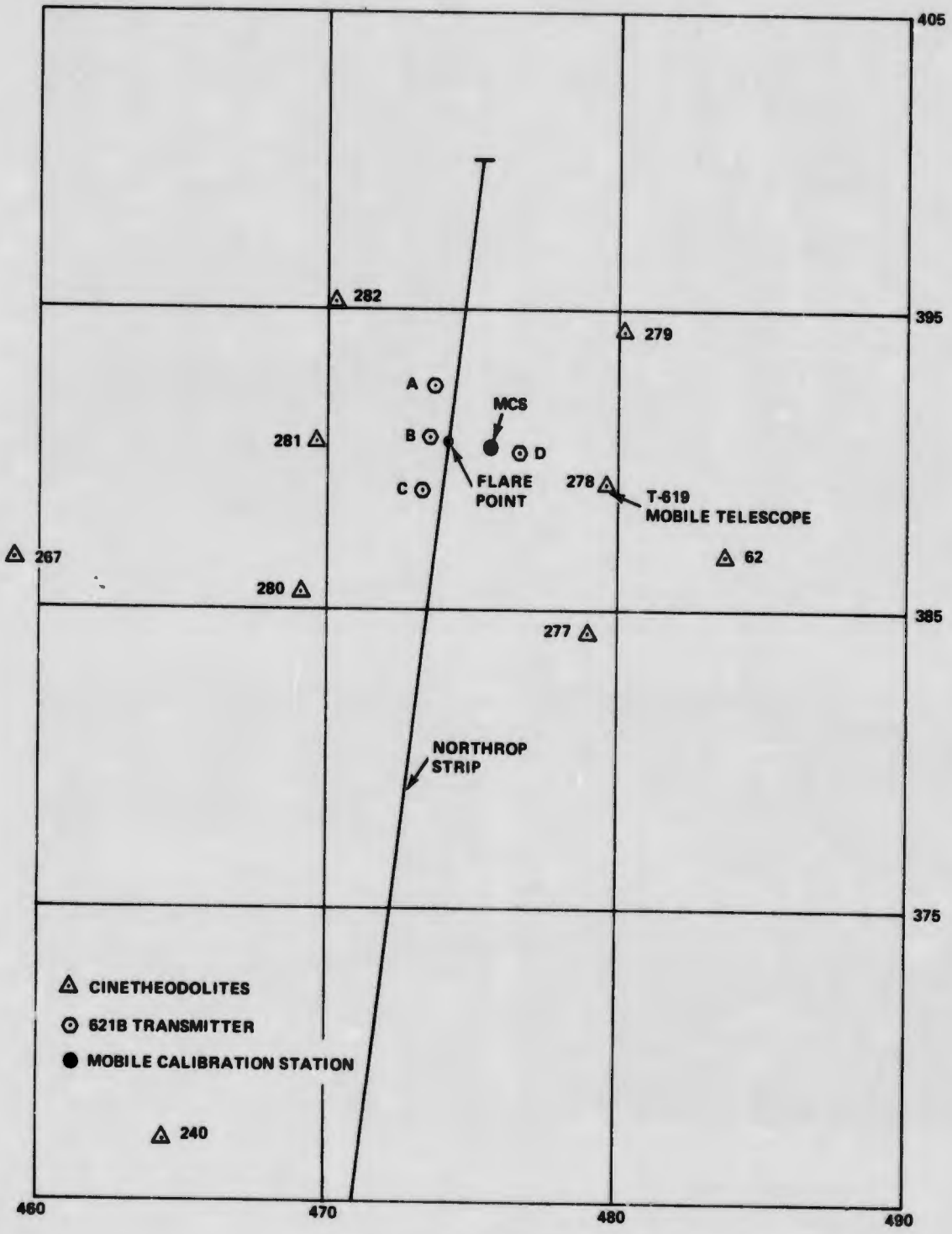

Figure 45 Cinetheodolite Stations Used for ILS

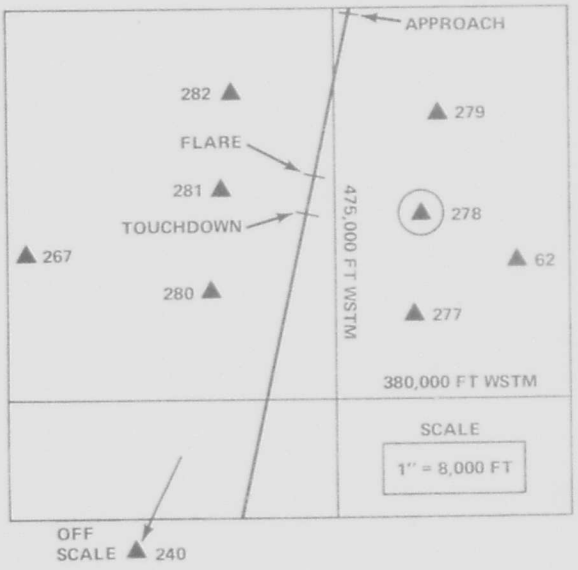

TIME = 16 08 03.00
40 SEC PRIOR TO FLARE

APPROACH

TIME = 16 08 43.20

AIRCRAFT FLARE

TIME = 16 08 49.00

TOUCHDOWN

Figure 46 ILS Touchdown, Flight 31, Run 02 as Viewed by G-278

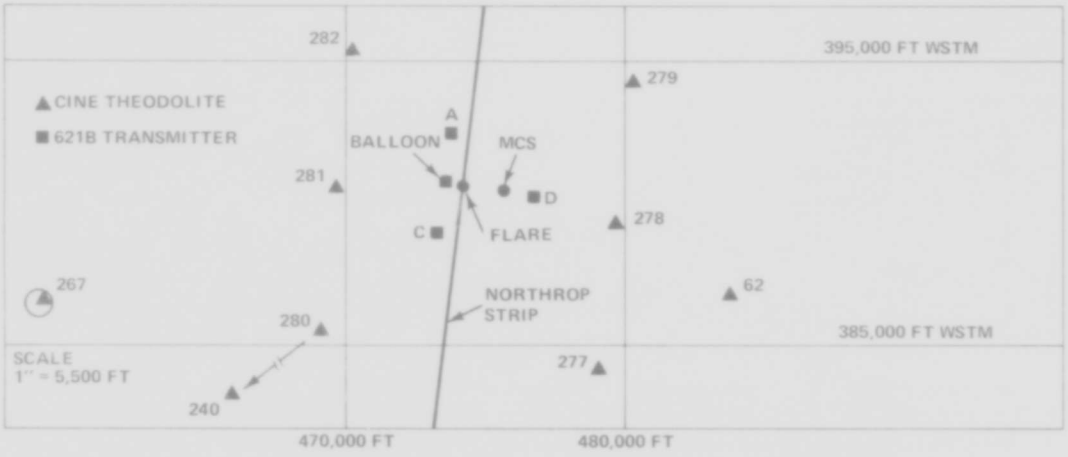

Figure 47 621B Balloon as Viewed by G-267 During Flight 27, Run 12

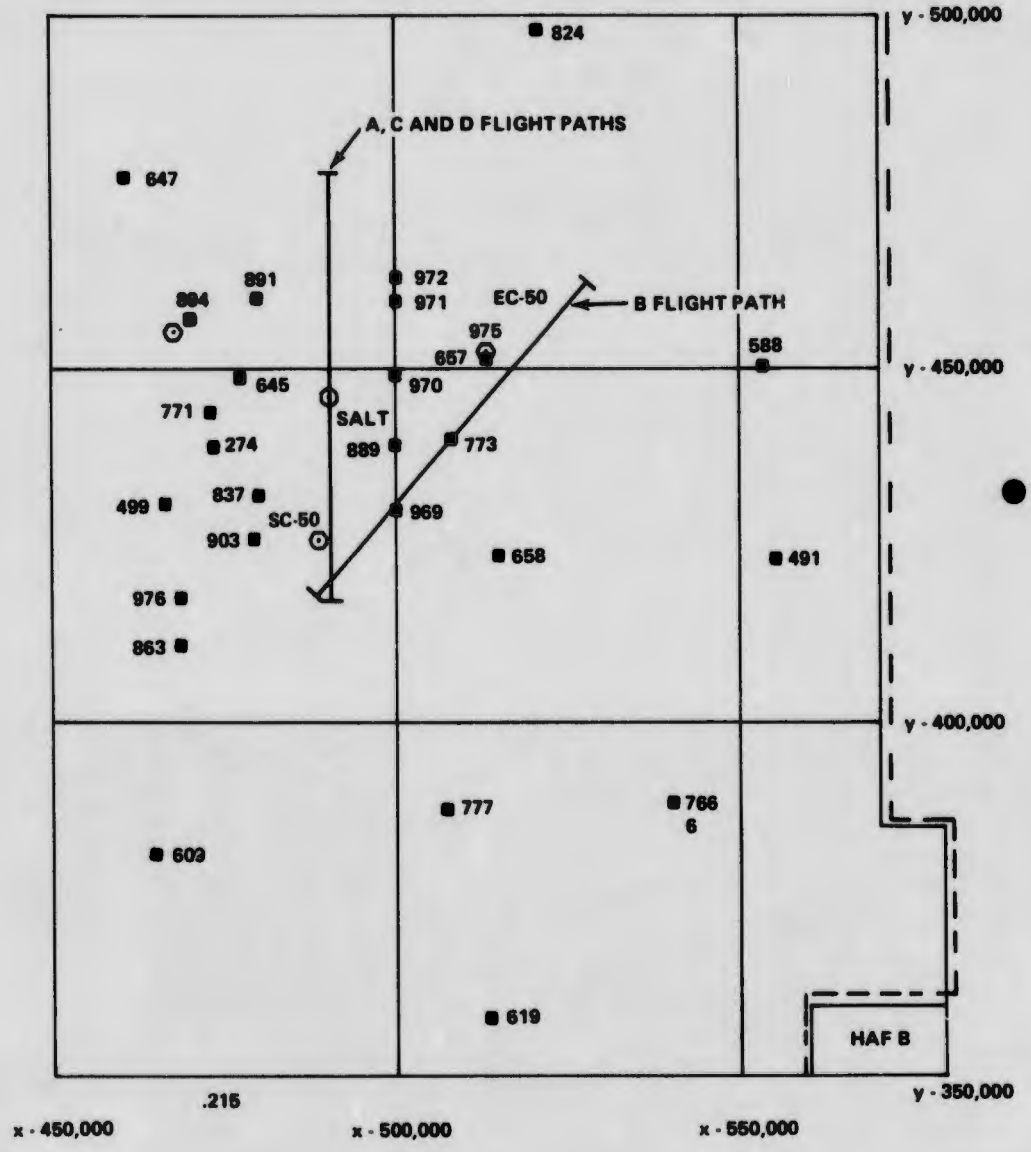

Figure 48 WSMR DOVAP Stations Used for 621B Tests

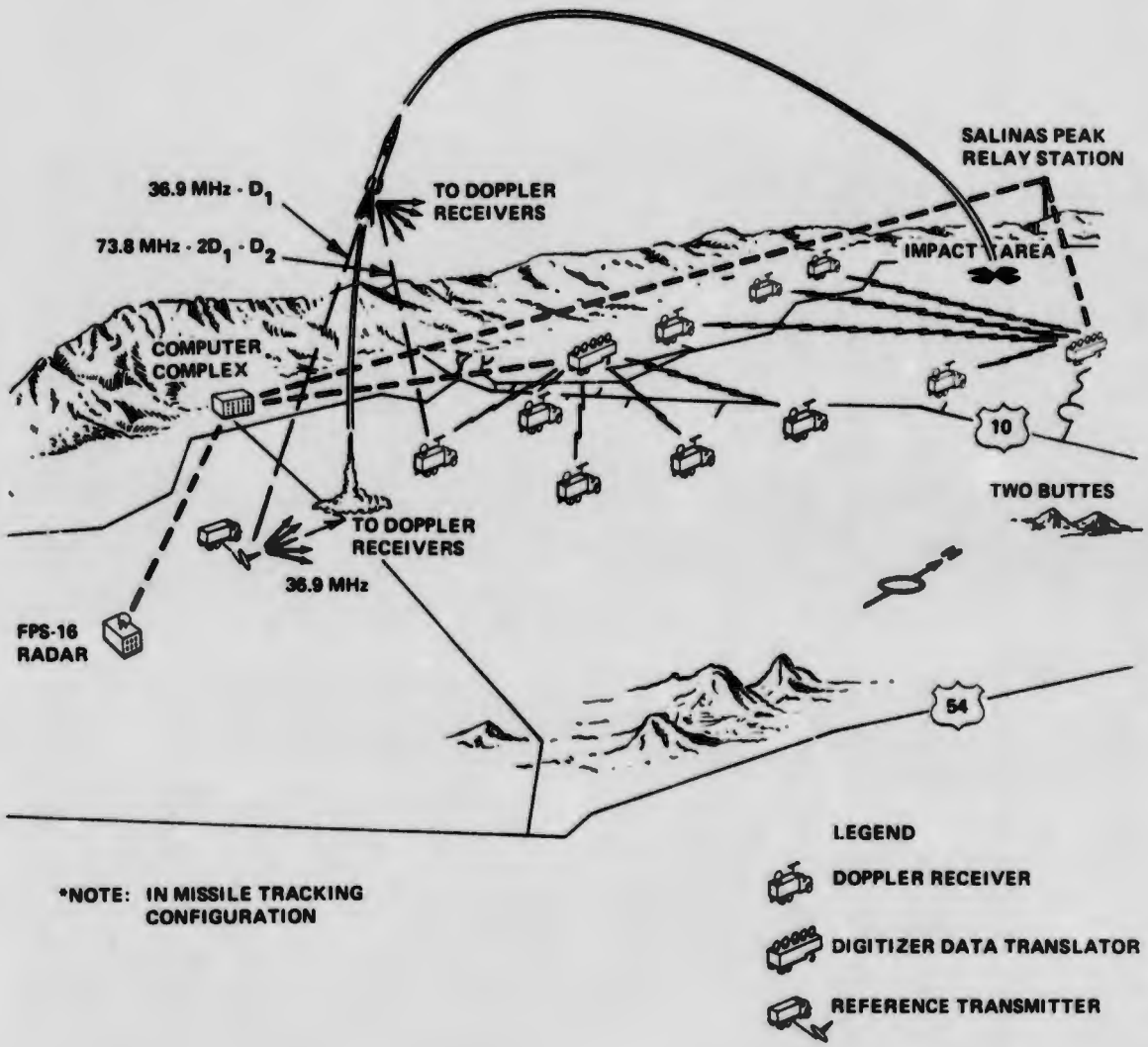

Figure 49 Typical Real Time DOVAP* System Used at WSMR

Figure 50 DOVAP Receiver Site

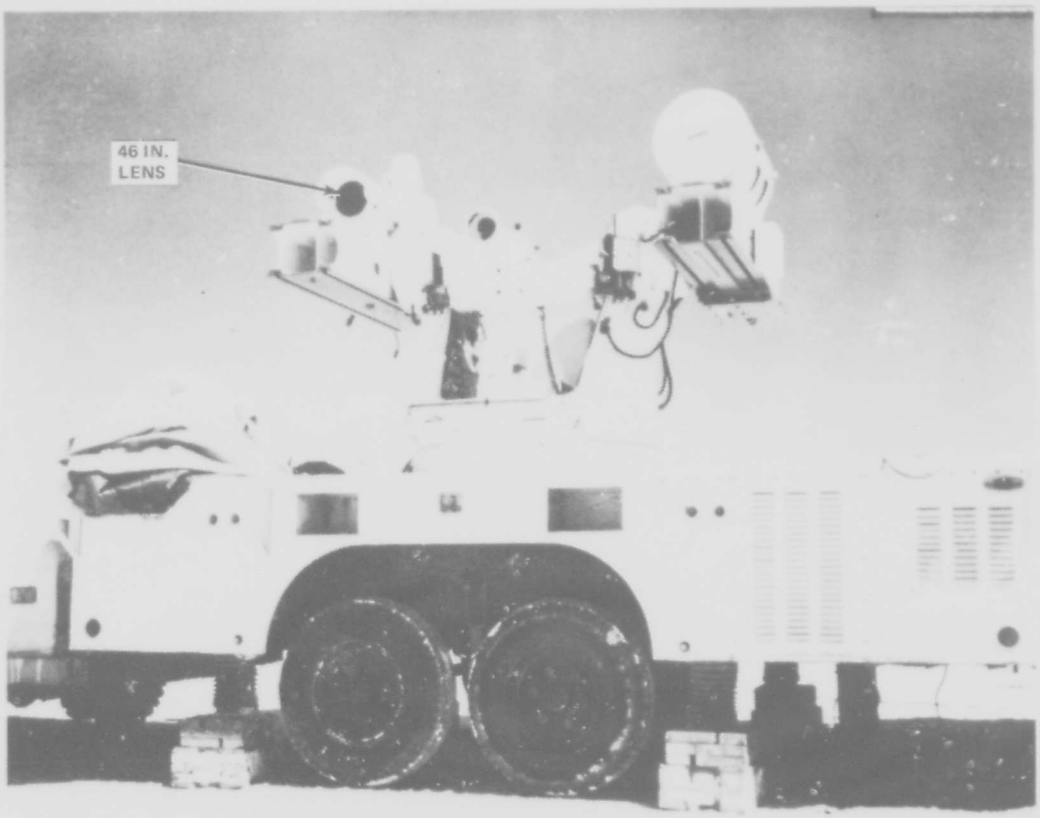

Figure 51 Station T-619, Mobile Telescope

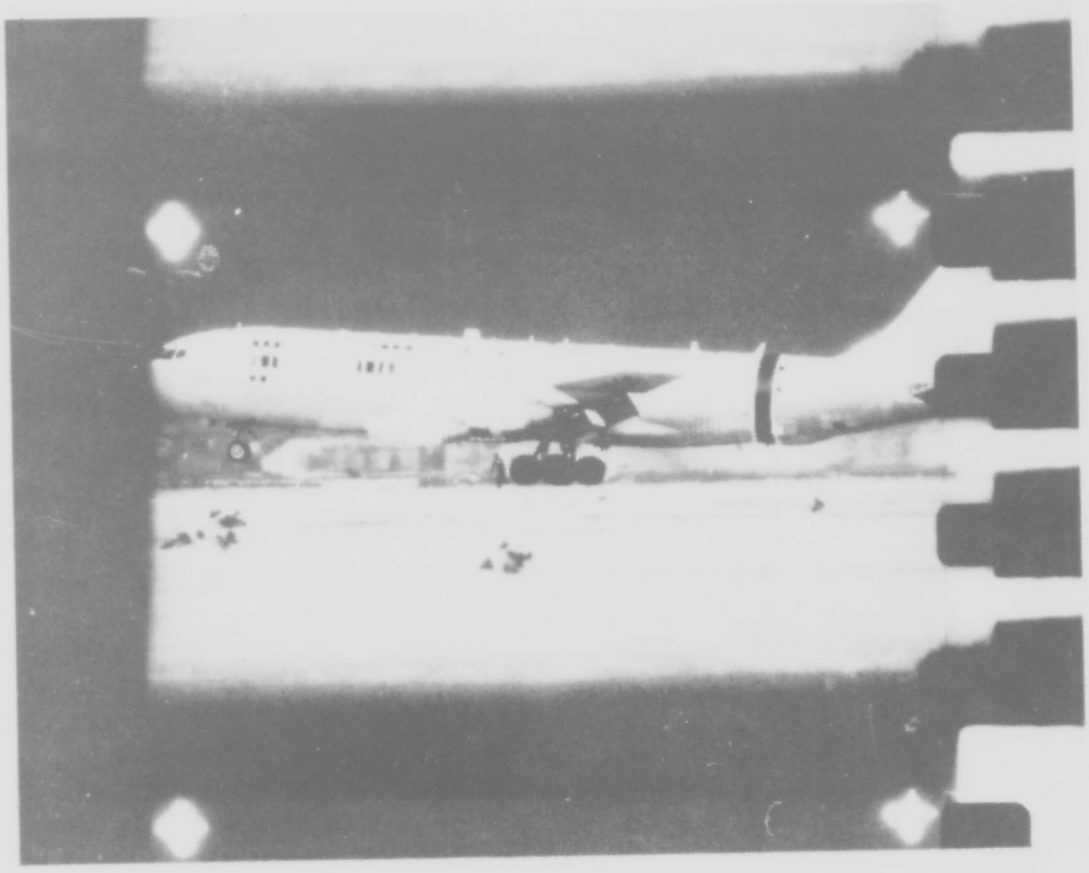

Figure 52 One Frame of Film at Touchdown From T-619 Mobile Telescope

SECTION III

EXPERIMENT PROGRAM HISTORY

This section deals with the ground site selection and preparation, ground equipment installation, and the chronology of the flight program. The approach taken in this section is to discuss the test program from an historical viewpoint so that the initial equipment design concepts and their subsequent modifications as the test program progressed can be clearly and logically treated. It is fair to state at this point that the ground system proved to be the "sleeper" in this program. Although great effort was applied towards the ground system design, we discovered that we did not fully understand all the error producing mechanisms. This resulted in further investigation of ground system components and configuration changes in order to isolate anomalous ground system effects. The impact of this on the test results and data accuracy is significant as will be seen in Volume III.

The flight chronology has been included in this section so that the interactions between the flight program and the ground system modifications can be clearly understood. Certain modifications caused us to rerun test flights to collect comparison data. The categorization of test flights in Volume III is a direct result of these events.

A summary chronology of significant experiment program events is presented in Figure 53. The System Demonstration Configurations for Area Navigation are shown on Figures 54, 55, and for ILS on Figure 56.

3.1 SITE SELECTION

The 621B Experiments Test Program was conducted at the White Sands Missile Range. This was a natural selection since it had the appropriate facilities; the program was coordinated by the 6586th Test Group at Holloman AFB, and the aircraft used for the tests staged out of Kirkland AFB. The program requirements involved an investigation of Area Navigation and landing guidance capabilities. Thus two distinct test configurations were identified and implemented at WSMR.

3.1.1 Area Navigation

A computer analysis conducted during the study phase indicated that a transmitter grid located on the ground in the form of a symmetrical Y would closely simulate the new earth rf environment generated by a stationary satellite of equal inclination and eccentricity rotating around it, Figure 57.

There were several instrumented and surveyed sites at WSMR that served as candidates for possible transmitter sites. (See Figure 58 for a 621B site map.) The Y was oriented so that flights over WSMR would be in a north-south direction, thereby insuring that the flight profiles were compatible with existing instrumentation. This narrowed the selection of sites considerably, and WC-50, EC-50, SC-50, and Salt sites were picked as shown on Figure 59. WC-50 and SC-50 have good

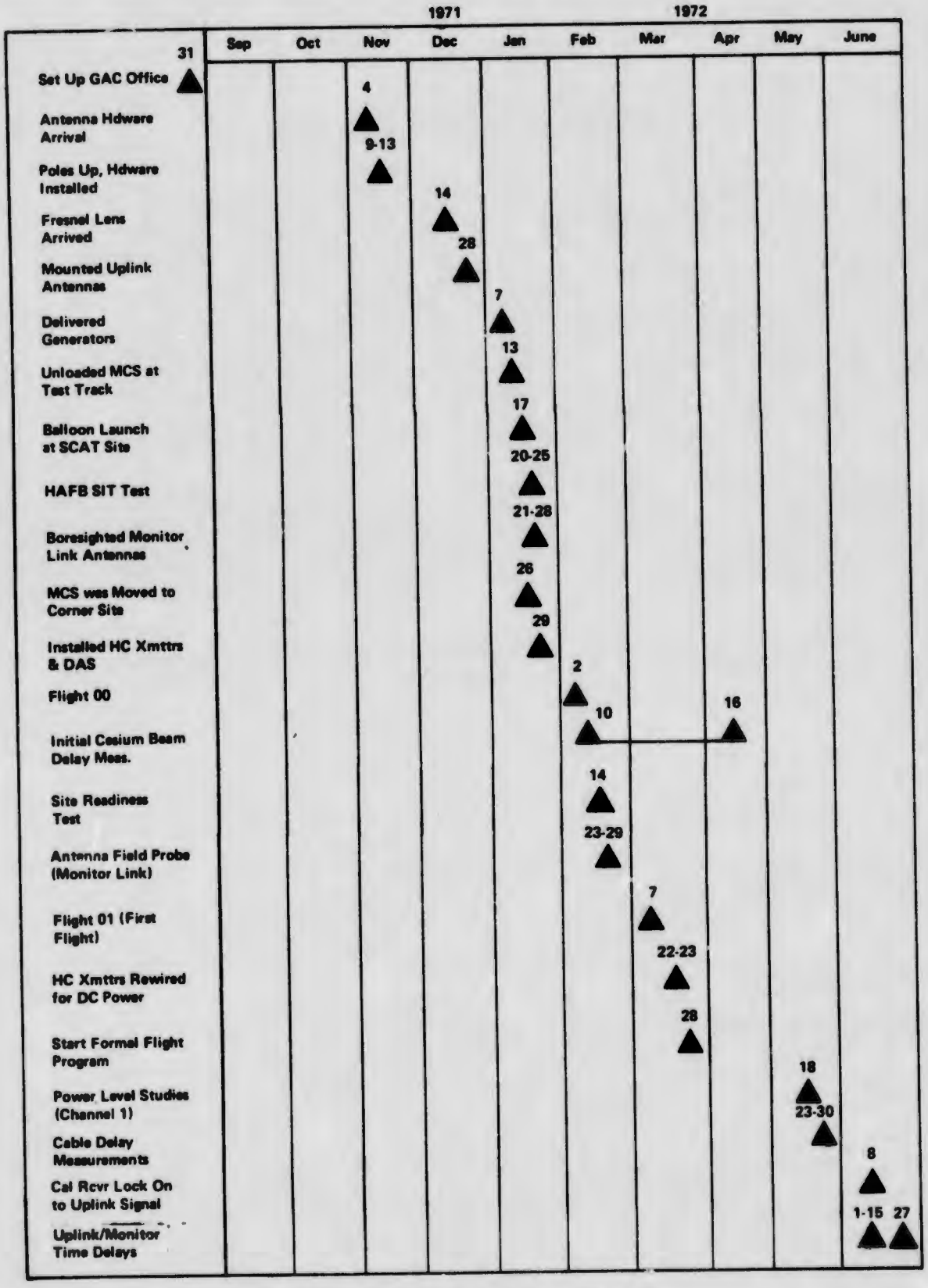

Figure 53 621B Program History

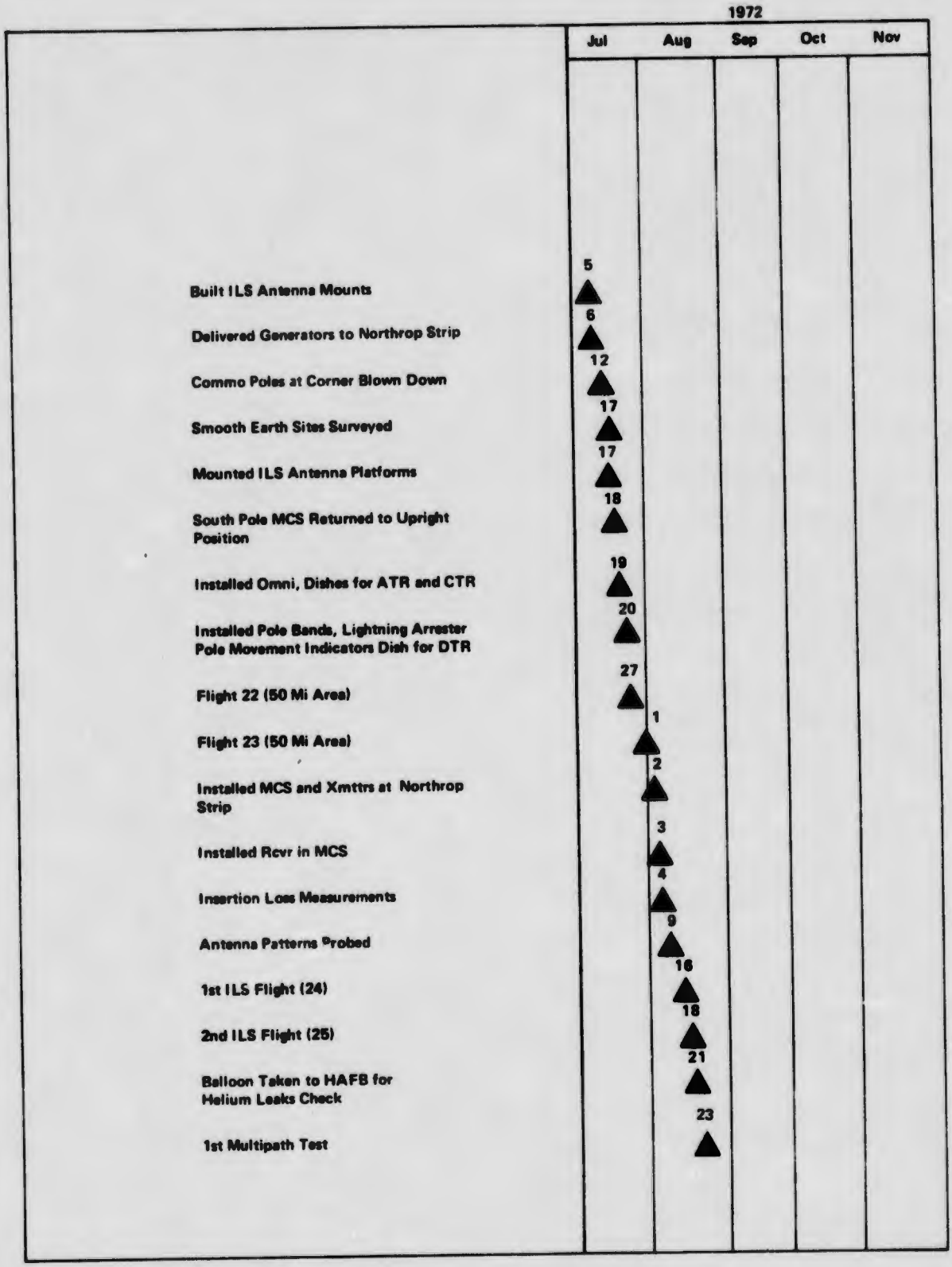

Figure 53 621B Program History (Continued)

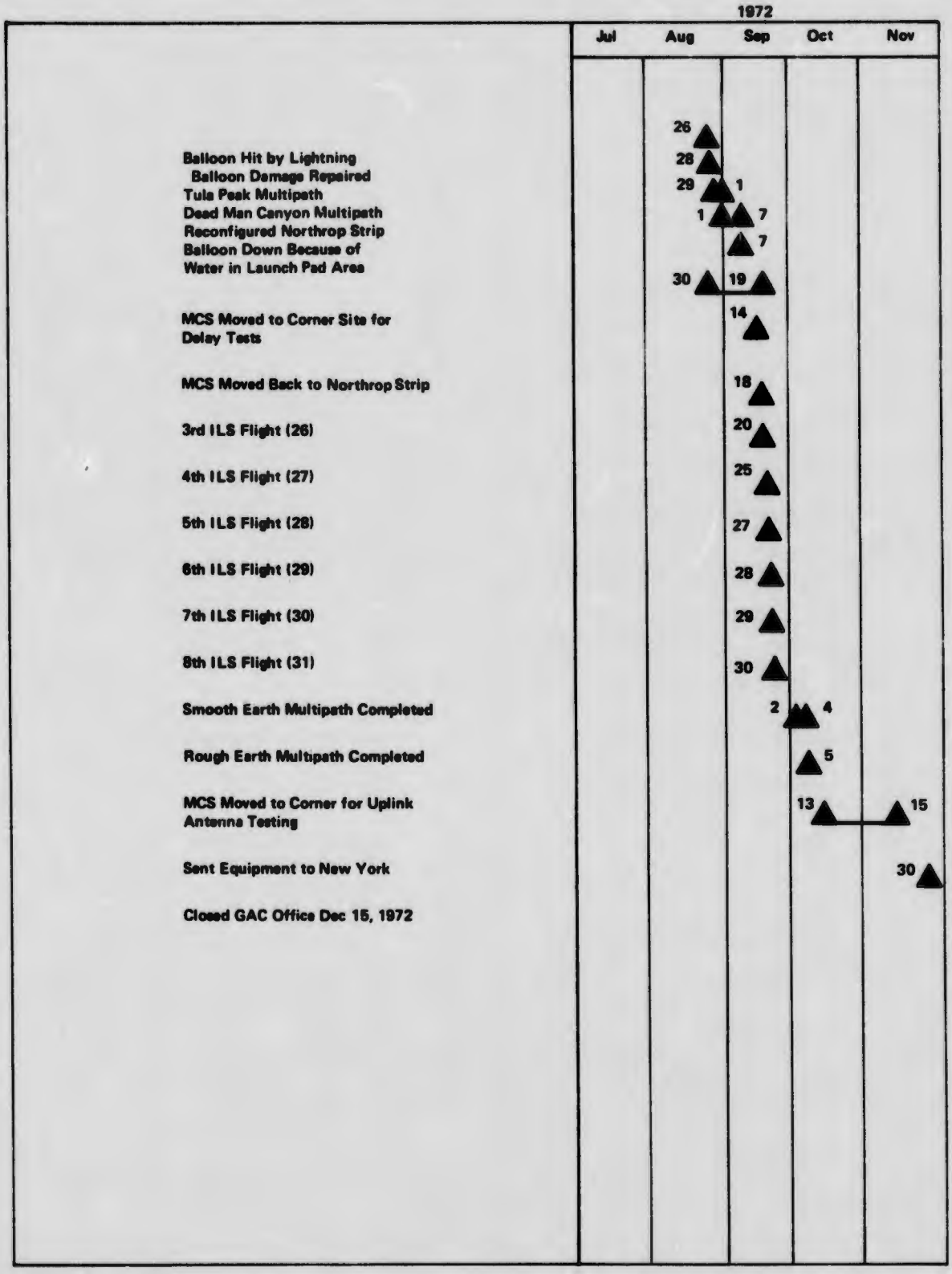

Figure 53 621B Program History (Concluded)

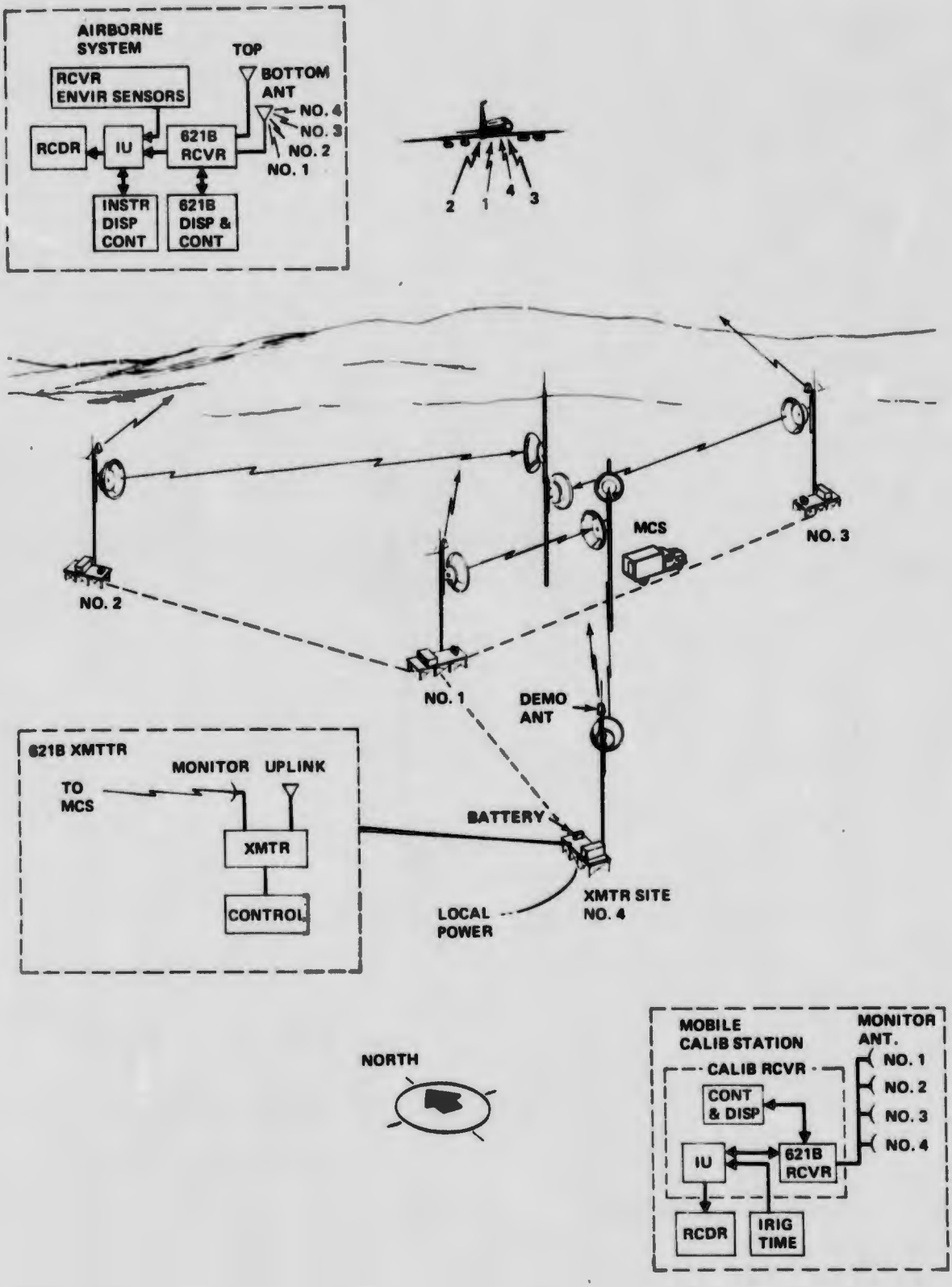

Figure 54 System Demonstration Configuration on Flights 1-15

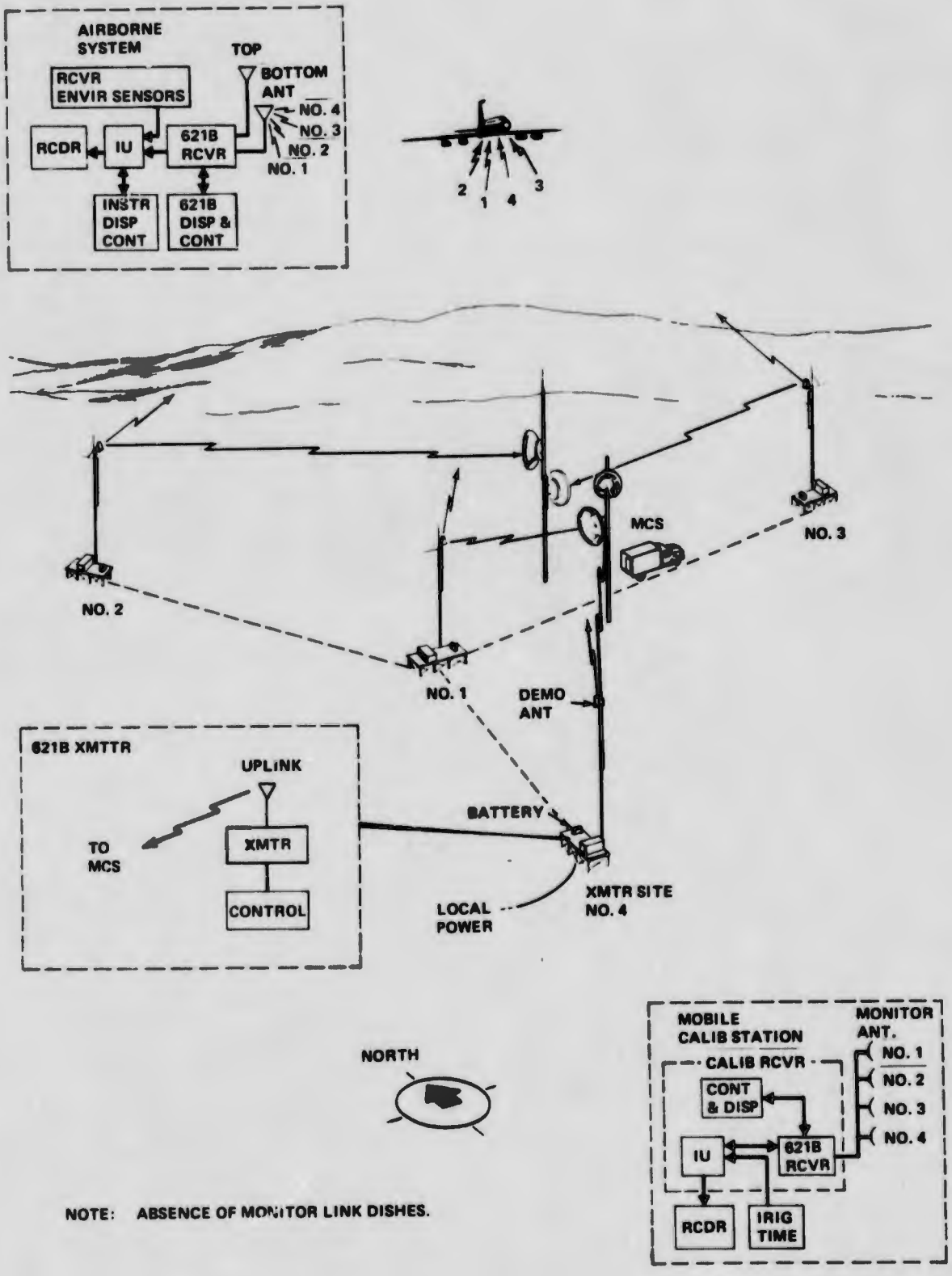

NOTE: ABSENCE OF MONITOR LINK DISHES.

Figure 55 System Demonstration Configuration on Flights 17-23

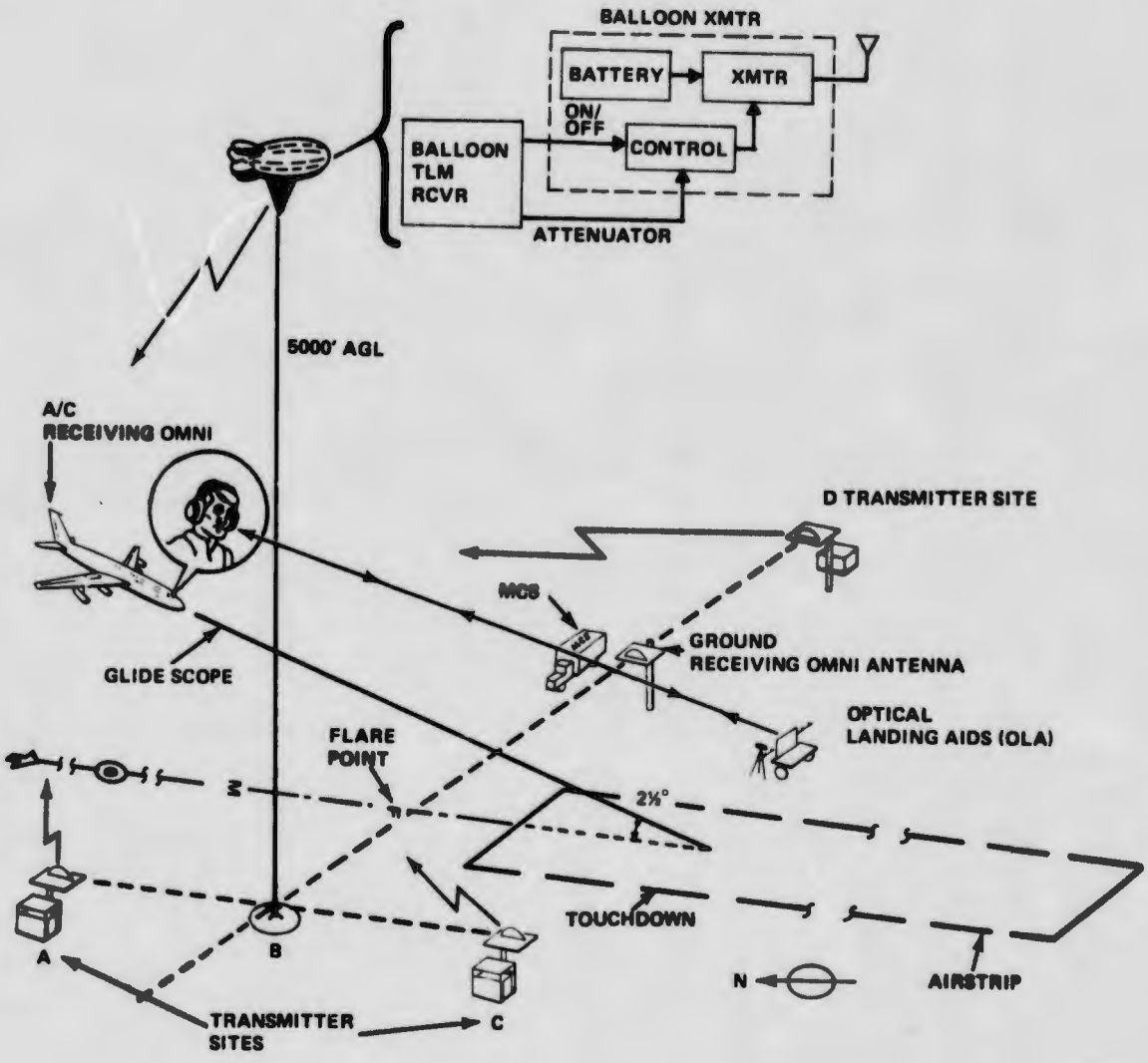

Figure 56 System Demonstration Configuration - ILS

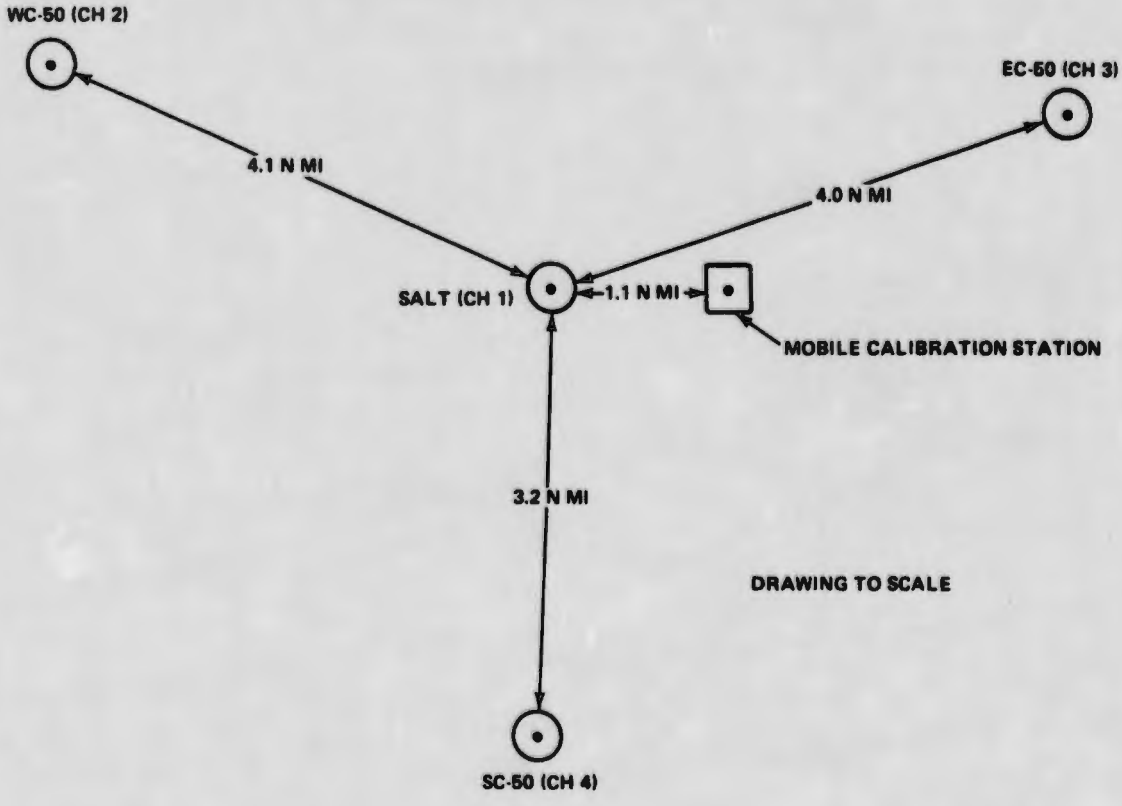

Figure 57 Sites Selected to Simulate a Rotating Y Satellite Configuration

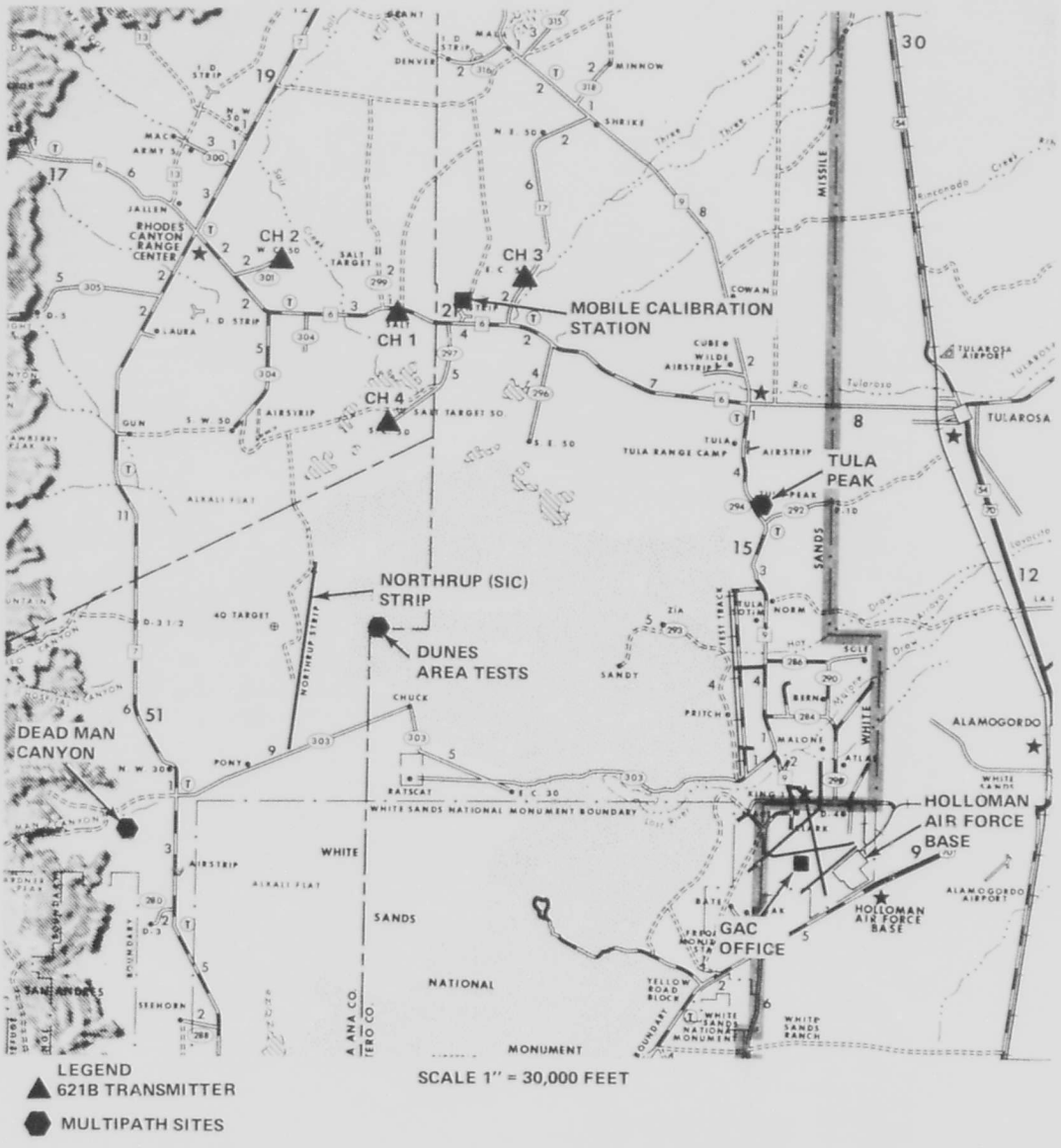

Figure 58 621B Site Locations

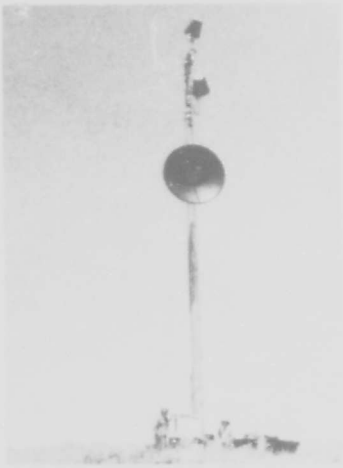

WC-50

EC-50

SALT

MCS

SC-50

Figure 59 621B Ground Site Configuration

access on secondary roads, but more importantly they both have a constant source of 60 Hz ac power. EC-50 has a paved road leading to it, but requires a 60 Hz generator to supply ac power to the transmitter. Salt site is the center of the Y and the transmitter grid. It is accessible via a dirt road, but also requires a 60 Hz generator for ac power. Dc power from external storage batteries actually powered the transmitters during a mission, but the generators provided the bulk of power during checkout and maintenance of the sites.

The Mobile Calibration Station (MCS) was located at Corner Site primarily because it had "line-of-site" with all the transmitter antennas.

The actual transmitter site locations were then processed in the computer simulation resulting in the system geometry contours shown in Figure 60. These contours show the geometrical reduction (GDOP) of the user position and velocity precision ($\sigma_X, \sigma_Y, \sigma_Z,$ etc.) as a result of the receiver measurement precision ($\sigma R, \sigma \dot{R}$).

The system factors considered in site selection are outlined in Figure 61. Practical considerations, however, limited ILS to providing high fidelity simulation of only the following system characteristics in the experiment program:

- Operational GDOP's
- Operational signal power levels
- Adequate data collection periods for system characterization.

3.1.2 ILS

The ILS portion of the flight test program was conducted at Northrop strip, an unimproved dry alkali salt flat area without electric power. The site configuration was developed with the following concepts in mind:

- Minimize altitude error at flare (Z=50 ft)
- Minimize sink rate error between flare and touchdown
- Maintain reasonably good horizontal accuracy.

It was determined that three ground transmitters forming an approximately symmetrical Y about the aircraft flare point would provide minimum horizontal GDOP and a fourth transmitter located directly above the flare point would provide the required Z-axis accuracy. In practice the fourth transmitter was 1000 ft horizontally from the flare point in order to keep the balloon tethering cable clear of the aircraft flight path zone. This did not appreciably affect the Z-axis GDOP. (For site configuration, see Figure 62.)

Although Northrop Strip was unimproved, it provided the best landing area for two reasons: first, the requirement to have a transmitter elevated 5000 ft above the terrain in the vicinity of the flight path could only be met by a tethered balloon or a helicopter. The high density altitudes involved made a helicopter impractical, and the tethered balloon was used. Investigations of various landing fields showed that none of them would permit flight operations with a balloon tethered within the airport airspace. At Northrop Strip this was not a problem since there was no flight

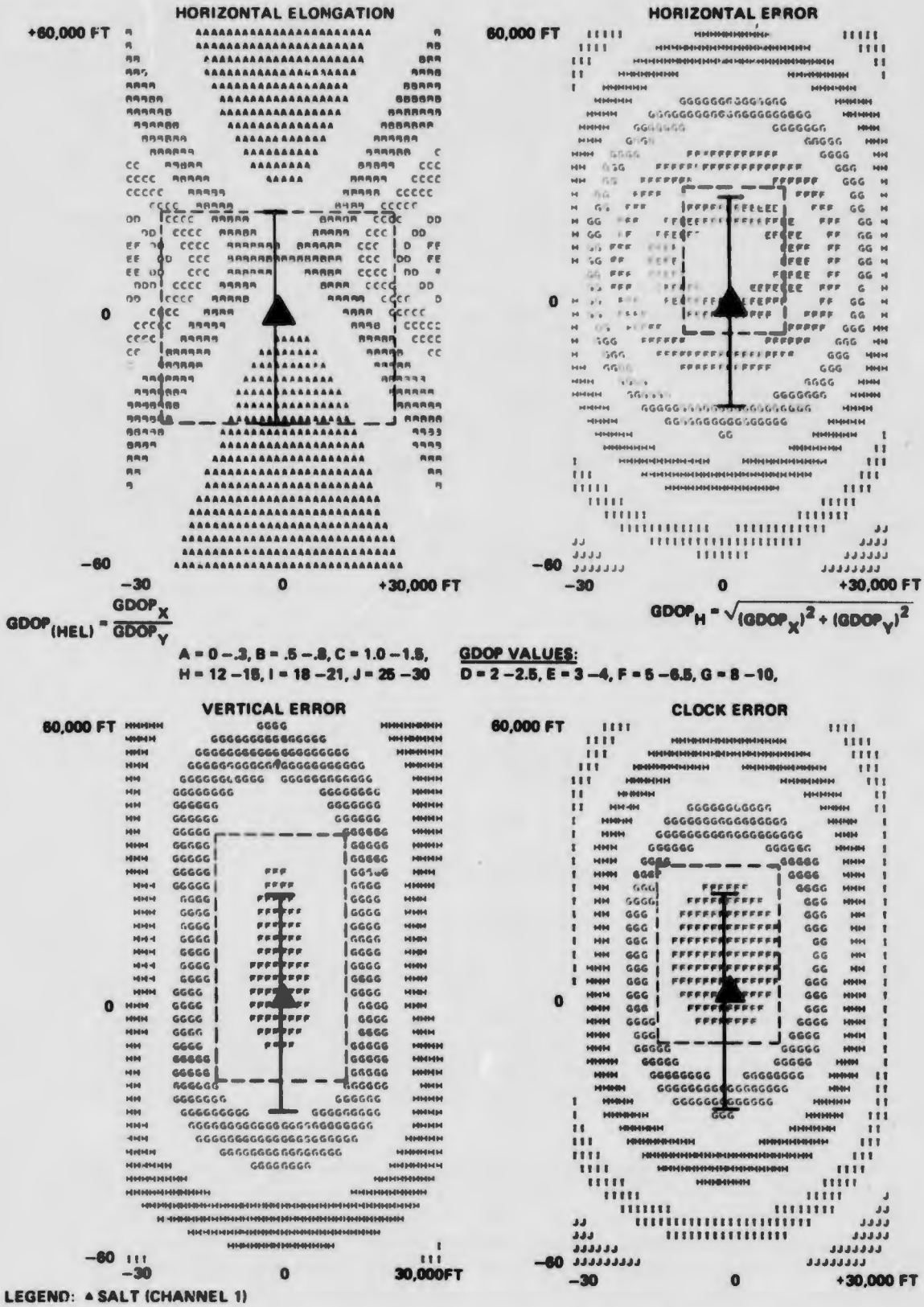

Figure 60 Primary Flight Path Overlaying Zone of Good GDOP Simulation at Altitude of 34, 000 Feet MSL

Areas Of Investigation		IOC	Global
Satellites (Demo & ILS)		Y	Eggbeater
GDOP	Inclination, Deg	20 – 40	
	Eccentricity	0.268 (Typ)	Special Parameters
		Angular Variation ±20 Deg	
		Distance Variation ±4000 N Mi	
		Rate $\dot{R}$ = 1720 Ft/Sec Max $\ddot{R}$ = 0.1 Ft/Sec^2 Max	
	Coverage	3 To 4 Satellites	11 Sats
	Satellite/User Look	±9 Deg	±9
	Power Variation	6 db	____db
	Errors Ionospheric	Function Of Alt & Envir	Same
	Multipath	Sat Grd-User Hi-Alt (500 Ft –50K)	As
	Clock	Free Drift Performance	Y
User (Aircraft)			
Demo	User To Sat. Look ∡	Antenna Coverage f (Lat, Long.)	Best Constellation Selection (Ref Y Global)
	Multipath Errors	Airframe	
	Maneuvers	Attitude Effects	
		Dynamics-Accel, Vibration, Etc.	
	Antenna Installation	Location & Envir Factors	
		Receiver EMI & Envir	Same
	Computer Implementation	Optimum & Min Cost Performance	As Y
ILS	Acquisition	Range & Alt Req'ts (1 Mile)	
	ILS Req't	Cat. I, II, IIIA, B & C	
	Antenna Coverage	Acquisition, Acq Decision Point, Dec Point-Touchdown & Roll-Out	
	Multipath Errors	Airframe	
		Grd Xmtr To A/C Satellite-Grd-Aircraft	
	User To Sat. Look ∡	Selection Of Best Satellite(s)	Best Satellite Selection (Ref Y Global)
	Computer Implementation	Optimum ILS Routine	
Airborne Receiver Demo		Envir: Nominal ✓, Max ✓; Dynamics: Nominal –, Max –	
	Sensitivity		
	Acquisition	✓ – – –	
	Reacq	✓ ✓ – –	
	Loop Tracking	– – ✓ ✓	
	Range Accur	✓ ✓ ✓ ✓	
	Velocity Accur	✓ ✓ ✓ ✓	
	Sequential Channel	Investigate Possible Implementation	Same As Y
ILS	Channel Interference	Investigate Performance	
	Channel Switching	Investigate Performance	
Ground Transmitter (ILS)			
	Location	Accuracy & Acq Range	
	Power	Max Acq Req't	N/A
	Multipath	Transmitter Altitude & Terrain	
		Antenna Pattern	
	Satellite Dependence	Synchronization (Timing)	
	Environment	Multipath Variation, Etc.	

Figure 61 Areas of Possible Investigation Relative to Operational System

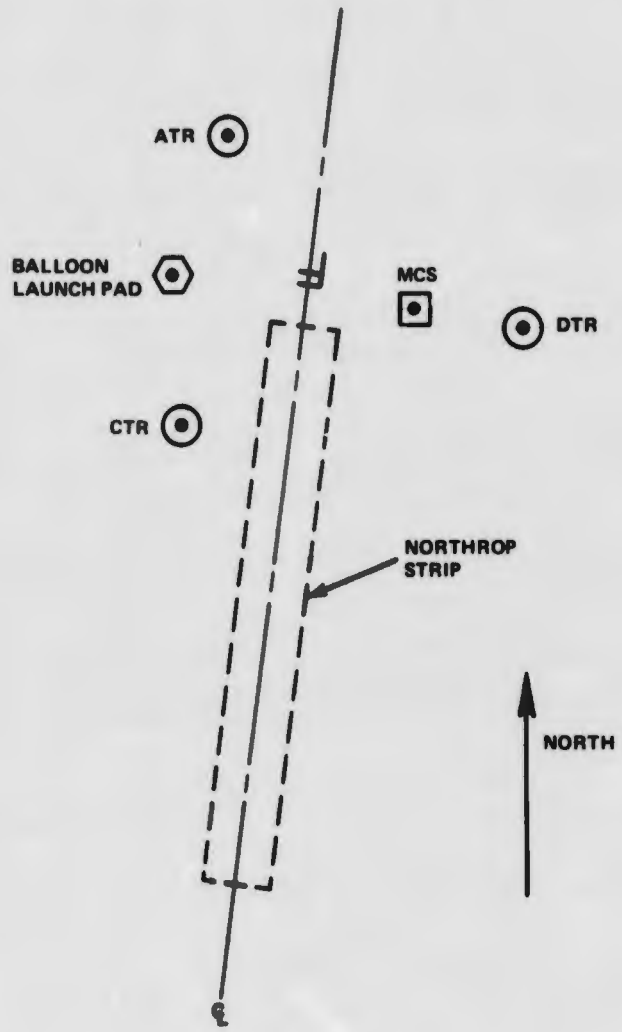

Figure 62 Northrop Strip Site Configuration

traffic. For test aircraft safety during the landing tests, the tethering cable was tagged and an open communications channel kept to the pilot. Second, the test required accurate knowledge of the balloon and aircraft position to evaluate the test results. Locating sufficient instrumentation around an operational airport while maintaining good geometry and line of sight was a formidable problem. At Northrop Strip the terrain is almost perfectly flat with no obstructions and virtually no limitations on placement of suitable optical instrumentation.

One operational question regarding the use of Northrop Strip was the ability of the lake bed to withstand repeated landings of a cargo type aircraft. In the case of 621B, the aircraft was a converted KC-135 cargo airplane. The California Bearing Ratio tests conducted in September 1971 confirmed that such landings were possible, (Ref. 7).

Another problem was the physical difficulty of working in that area. The salt flat and surrounding region are white, providing very good solar reflection. During

the summer months the free air temperature reached 100° to 110°F to which the effect of heat reflection was added. In spite of very primitive working conditions, however, the strip did provide a suitable landing field for the test aircraft. (See Figure 63 for a view of the ILS configuration.)

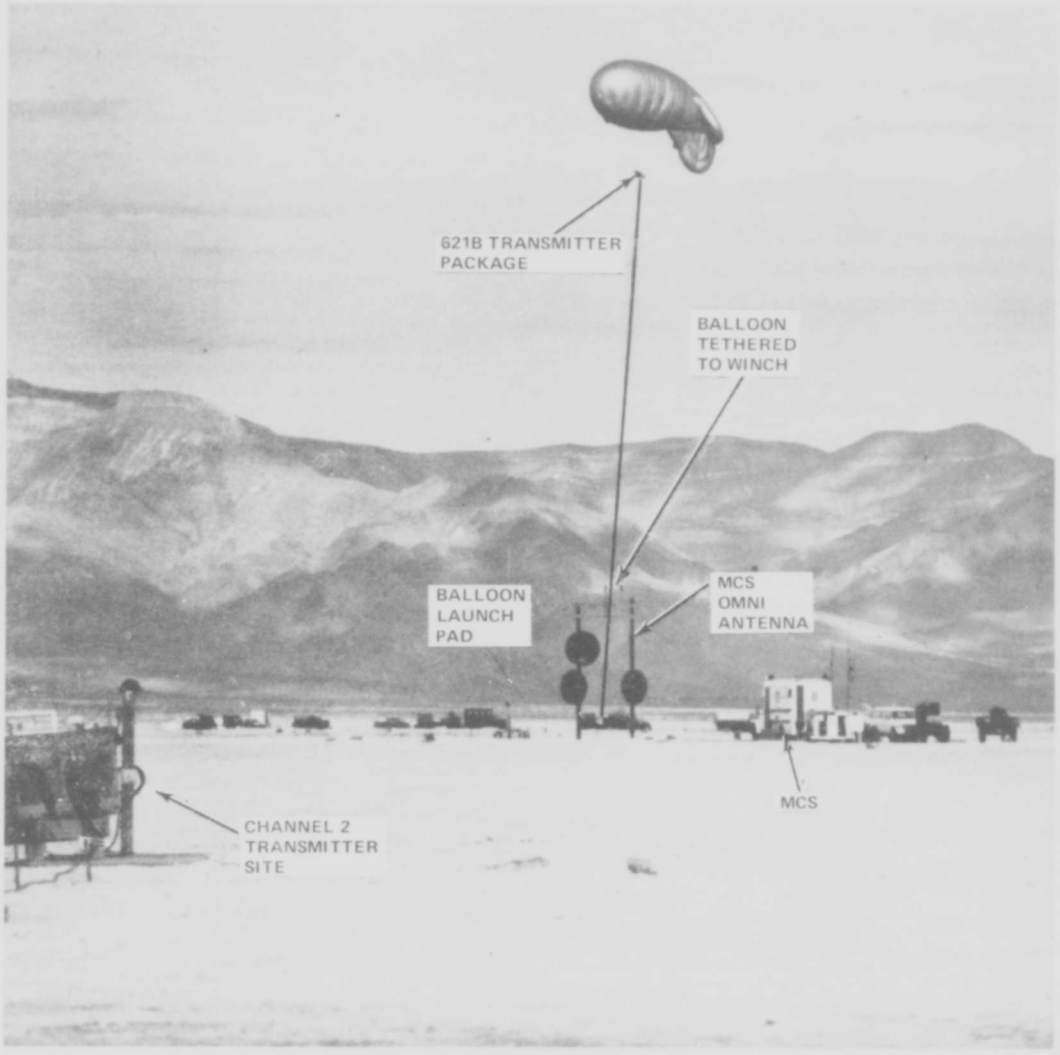

Figure 63 ILS Northrop Strip Configuration

3.2 GROUND EQUIPMENT INSTALLATION

For area navigation tests, equipment installation was done at the five sites previously defined. Each transmitter site was configured similarly. The configuration consisted of transmitter, associated mounting and power connections, a pole which held the antenna at the proper height, and electric power provisions. The equipment

located at Corner Site consisted of the calibration receiver housed in the MCS, electric power provisions, and poles with antennas mounted so that the signals from the transmitters could be received.

The installation period extended from Nov. 1971 to Feb. 1972. While the period was longer than that anticipated (due to changes in equipment availability) it provided for an installation which we felt would withstand the desert environment adequately, provide ease of equipment maintenance as necessary and provide a signal well controlled in both signal level and propagation delay.

3.2.1 Pole And Antenna Installation

On 8 Nov. 1971 the WSMR engineers completed the installation of six power poles at the 621B sites, one pole at each transmitter location and two at the MCS. The power poles were 50 ft long with 7 ft buried below the surface. The 43-ft pole lengths were decided on as a result of a study to eliminate possible multipath due to antenna proximity to the ground (Ref. 19). Installation of pole hardware (antenna mounts, dishes) was finished by 13 Nov. 1971.

Work began on 28 Dec. 1971 to install the uplink antennas with their patterns oriented along the flight profiles as dictated by computer simulations performed earlier. The pattern orientation with respect to antenna mounts was achieved by electro mechanically aligning the antennas at Grumman and locking them into assemblies in such a way that the electrical source was aligned in both azimuth and elevation along a N/S orientation for "A" antenna and along a $43^{o}/223^{o}$, azimuth for the "B" antennas (Ref. 9). These assemblies were shipped to Holloman AFB intact and were installed in the uplink mounts on the poles at the transmitter sites. Great care had been taken in levelling the antenna mounts on the poles, so that when the uplink assemblies were installed they were properly positioned in the elevation plane. An azimuth alignment tool was made that could be attached to the counterweight shaft to serve as a sighting references, Figure 64.

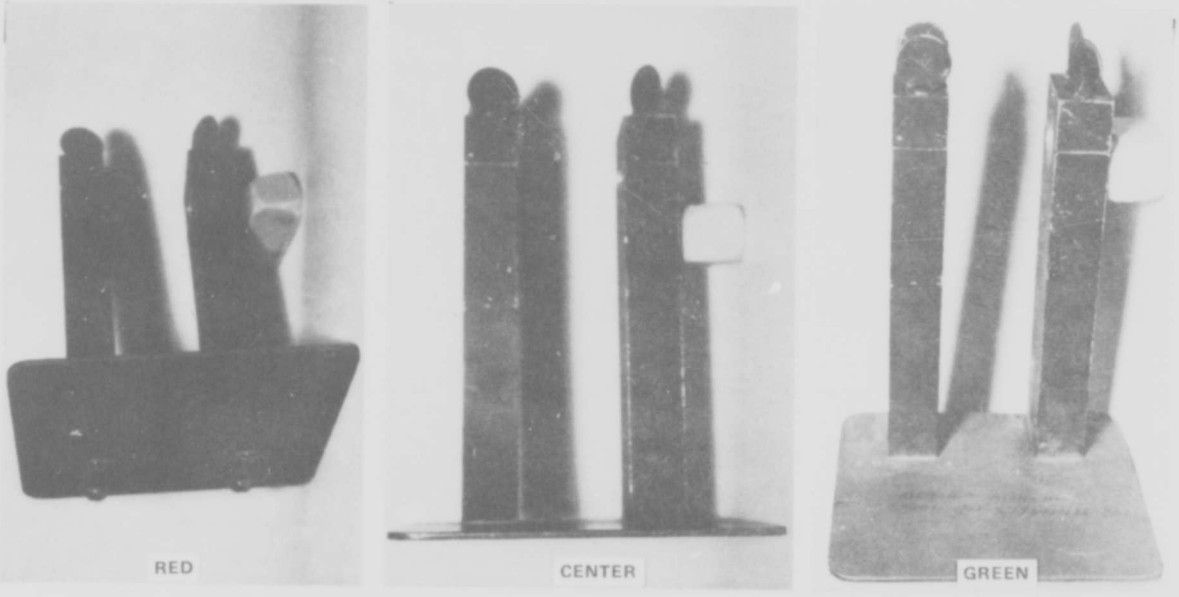

Figure 64 Optical Alignment Tool

The Optical Alignment Tool was attached to the uplink counterweight shaft, while an engineer on the ground would sight over a surveyed True North stake with binoculars and would indicate to the engineer in the cherry picker basket the direction to rotate the uplink assembly - clockwise or counterclockwise, Figure 65. When the ground engineer was satisfied that the optical alignment tool was truly pointing north, the locking bolts were tightened thereby locking the uplink antenna into the proper azimuth and elevation.

For the "B" antennas at WC-50 and EC-50, the ground engineer sighted over a surveyed stake that was 43° east of true north. Salt Site and SC-50 each had one variable positioned uplink antenna. For "A" flights (N/S at 34,000 ft MSL) the variable positioned uplink antenna at Salt and SC-50 is positioned at 0° elevation and 0° azimuth. For "B" flights (43° TN heading at 34,000 ft MSL) two locking pins are pulled, one from the elevation axis shaft and one from the azimuth axis shaft. The Salt antenna is then rotated 43° east of the north in azimuth and 32° down in elevation to the "B" flight configuration. The SC-50 antenna is rotated 43° in azimuth and 10° down in elevation (Ref. 9).

The alignment accuracies achieved with this technique were sufficient since the antenna patterns, while directive, provide adequate angular coverage of the aircraft flight path when the antennas were nominally oriented along the direction of flight.

The MCS required two poles in order to maintain good line-of-sight to the transmitters. The poles were placed approximately 200 ft apart straddling a communications pole line. The MCS was placed between the two poles and underneath the communications lines, Figure 66.

Since plans dictated moving the MCS occasionally for other tests, and the road paralleling the communications lines was frequently used, we decided to bury the antenna lines connecting the MCS with the two poles. This proved to be a poor decision since the lines going to the north pole (facing WC-50 and EC-50) began to exhibit sharply increasing attenuation within a few months. We think this occurred because of ground seepage finding a way into the coaxial cables (Spiroline type with solid aluminum exteriors) and causing internal rf leakage paths; we had to replace these lines. The new ones were not buried but strung overhead from the pole to the MCS. It was inconvenient because they had to be taken down for clearance when trucks used the road, but they did not degrade in any way as had the buried lines.

The parabolic dish antennas at the MCS site were optically boresighted to the transmitter sites by removing the rf feed assembly and placing an alignment tool at the back of the dish. This alignment technique proved to be satisfactory, Figure 67.

3.2.2 Generators

Salt, EC-50 and the Mobile Calibration Station at the Corner Site had to be powered by electric generators. WSMR provided four generators, (one 400 Hz and three 60 Hz) which the project engineers (Grumman and USAF) delivered 65 miles north to the 621B sites. During the period 7 Jan. to 20 June 1972, two generators were replaced and one was sent in for maintenance. The USAF provided one generator as backup, and it was quickly phased in as a primary operating at EC-50. Grumman provided a generator system consisting of a 60 Hz, 400 Hz, and 28 vdc generators powered by a 6-cylinder diesel engine, mounted on a trailer, and towed by the MCS. It was to be utilized as a backup support to the Army generators, but the Grumman system was the primary source of power for the MCS until May 1972.

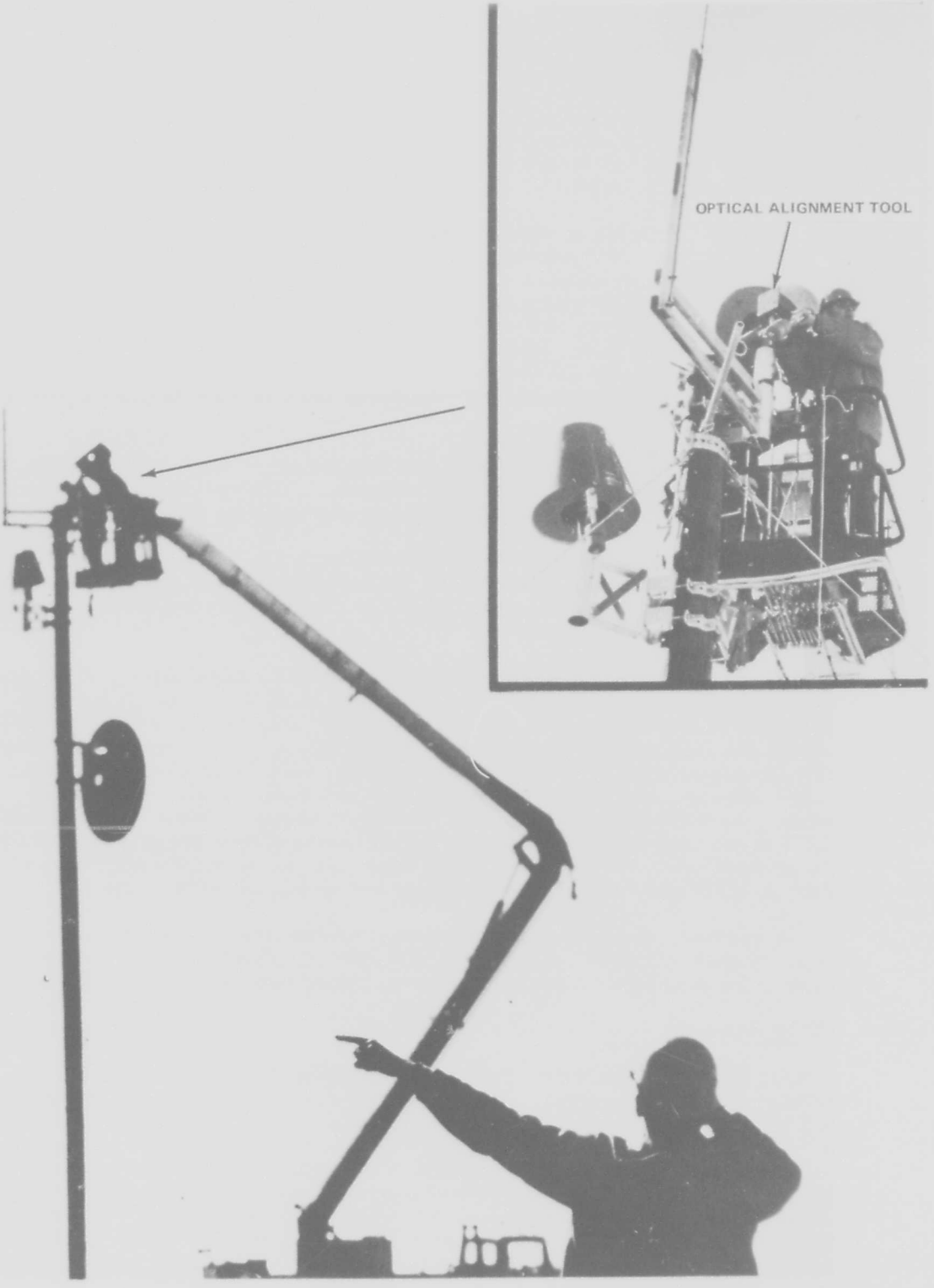

Figure 65 Optical Aligning "A" Uplink

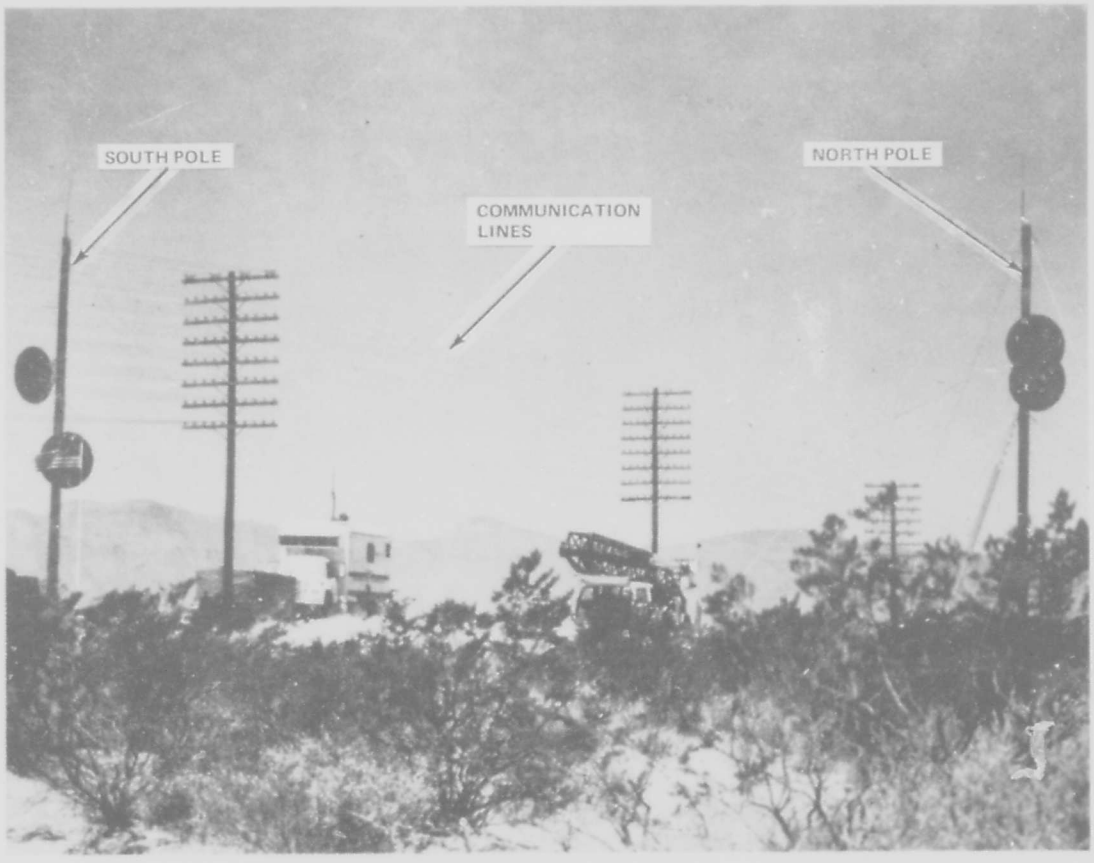

Figure 66 MCS Poles in Relation to Communications Poles

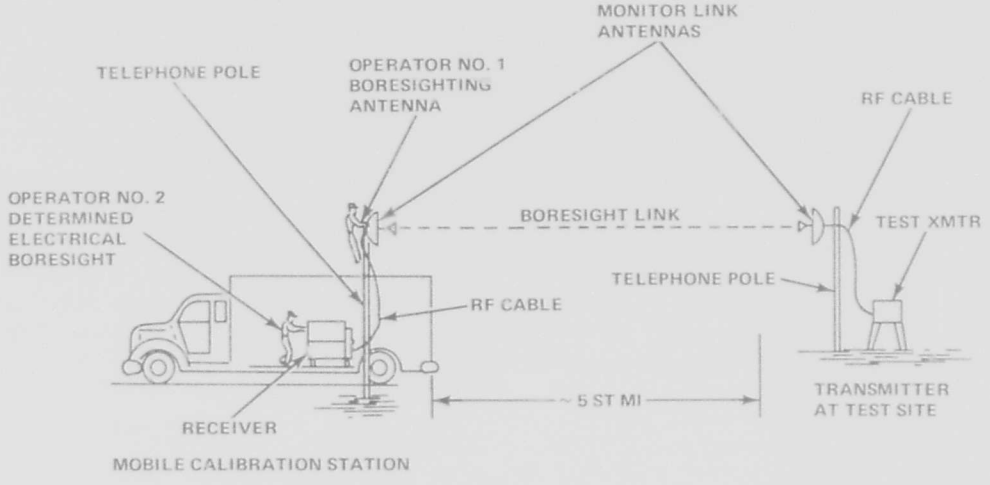

Figure 67 Boresight Test (Monitor Link)

3.2.3 Sites Completed

During the period 29 Jan. to 2 Feb. 1972, the four Hazeltine transmitters were installed on work benches at their respective sites and the calibration receiver was installed at the MCS. See Figure 68 for completed transmitter site and Figure 18 for MCS site.

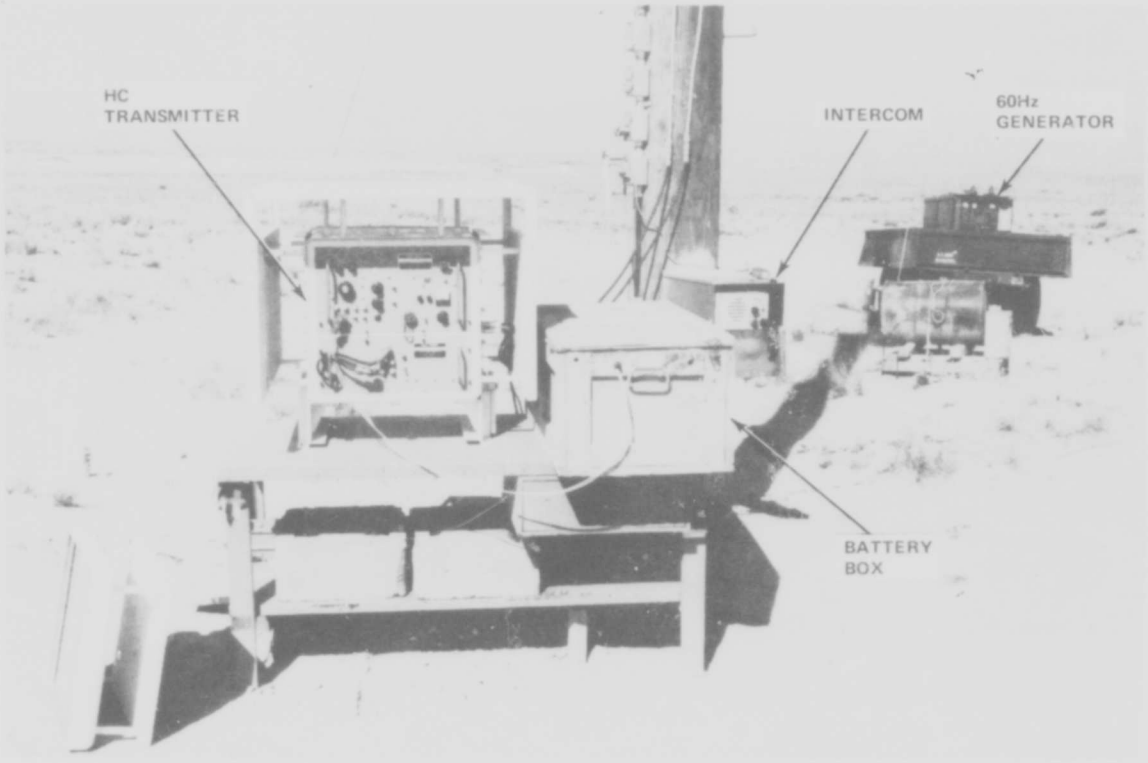

Figure 68 Salt Site Transmitter Installation

3.2.4 ILS Ground Site

The balloon transmitter and MCS sites at Northrop Strip were constructed during May and June of 1972. The transmitter site, comprised of a 4 by 6 ft concrete pad with a wooden 4 ft high antenna pole cemented in the pad, is shown in Figure 69. The 621B transmitter assembly and its external battery box was supported by a wooden bench that rested on the concrete pad. Ac (60 Hz, 115v) power was supplied to each of the three transmitter pads by WSMR-furnished gasoline powered generators. Figure 69, shows the "A" transmitter site; sites "C" and "D" are configured in the same manner.

The balloon launch pad was installed as per 621B Program Introduction 492A0 dated March 19, 1971. Briefly, the balloon pad consisted of seven tie-down anchors used to moor the balloon on non-flight days. Each stainless steel anchor was set in a 5 by 3 ft concrete block buried to a depth of 5 ft allowing the anchor to be at ground level. A 120 ft radius circle about the center anchor was graded and rolled.

The MCS site was constructed as shown in Grumman drawing 477AV10135. Two wooden poles standing 25 ft above the ground were installed, one north, one south of 621B survey point MOS. (See survey section of 3.3.1.6 and Ref. 16 for coordinates.) Three dish and one omni antenna were mounted to the poles as shown in Figure 70. It was found after ground rf surveys that the three dish antennas were not needed, greatly simplifying navigation solution data reduction. The three dish antennas were left mounted during the flight test program at Northrop Strip but were not used. The MCS van, during ILS testing, was parked 35 ft north of the north pole. IRIG B timing was rf-linked from a repeater station on the west mountain range into the MCS van's instrumentation system. The VHF antenna used to receive IRIG B timing is shown in Figure 70. Two WSMR generators, one 60 Hz, 115v and one 400 Hz, 115v were supplied by the range and were used to back up the multiple Grumman generator.

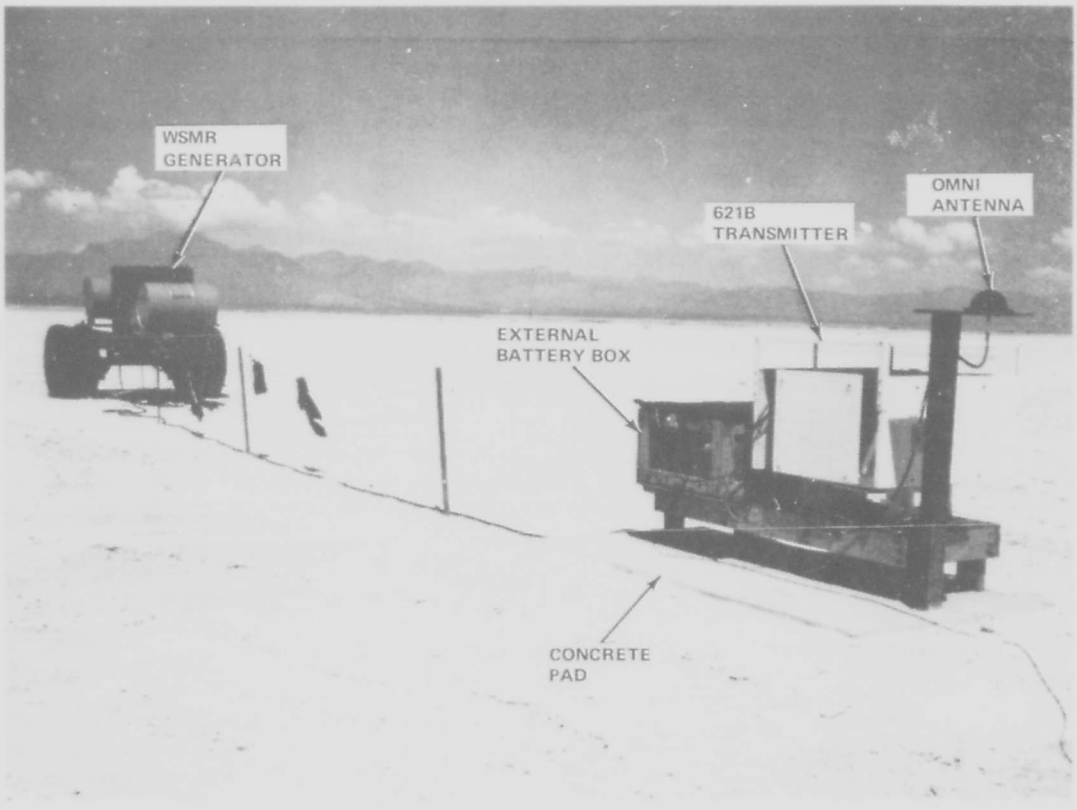

Figure 69 621B Transmitter Site

3.3 SITE MEASUREMENTS

Upon completion of the design portion of the 621B User Equipment Definition and Experiment Program, it was evident that several system measurements, such as cable lengths and signal propagation path length between transmitter and the calibration receiver, could only be made after equipment installation in the field.

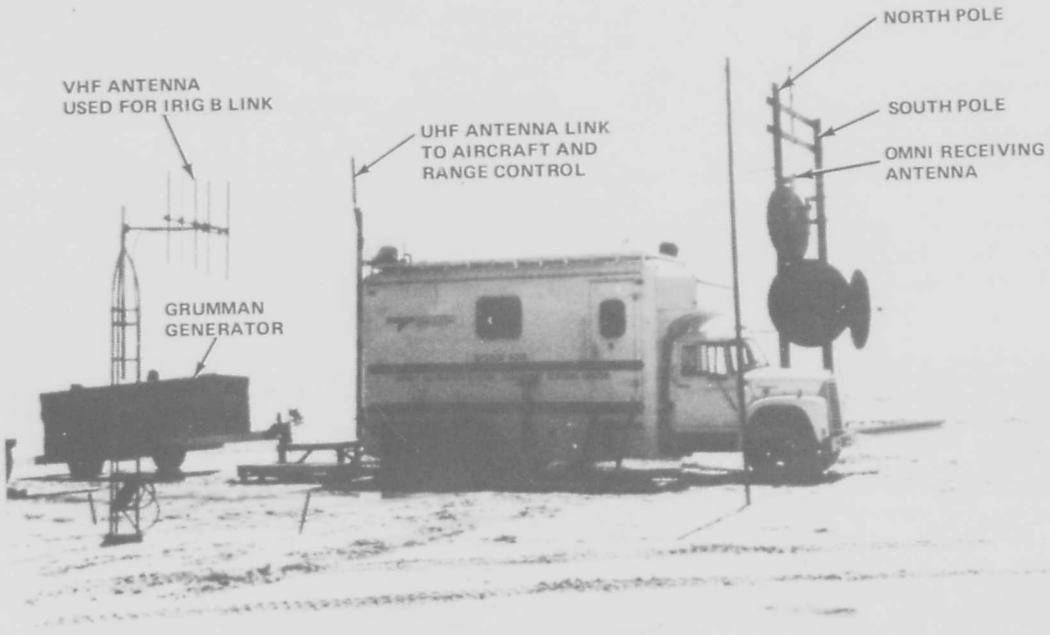

Figure 70 Mobile Calibration Ground Site at Northrop Strip

Three basic kinds of site measurements were performed: (1) determination of the specific location of the transmitting antennas; (2) signal path time of travel measurements, and (3) measurements which insured the integrity of various components. Two of these measurements were necessary elements in the formation of the 621B solution, and the other was necessary to understand certain aspects of the ground system operational characteristics.

As seen in paragraph 1.3.1, the pseudo range from the ith satellite to a user is given by

$$\rho_i = \bar{\epsilon}_i \cdot (\bar{R}_i - \bar{R}_u) + b_u + b_i \qquad i = 1,2,3,4$$

where $\bar{R}_i$ = location of the ith transmitter
ρ_i = pseudo range measurements from the ith transmitter
but b_i = clock bias
$\bar{R}_u$ = user position
$\bar{e}_i$ = ith unit vector

The user position and clock bias are determined by simultaneously solving the four equations given the transmitter locations and four pseudo range measurements. It was therefore necessary to accurately determine the transmitter locations (apparent signal source origin).

The four pseudo-range measurements needed are derived from (see paragraph 1.3.2.)

$$\rho_i = PRK_i - PRU_i$$

where PRK_i = pseudo-range measurements obtained at the calibration receiver which have been referenced to the transmitter locations

PRU_i = pseudo-range measurements obtained at the user receiver

Now, PRK_i are measured at the calibration receiver located at the MCS. In order to reference these measurements to the transmitter locations the time delay which the signal undergoes along the path between the point at which the signal is radiated to the user (apparent signal source orgin) and the point at which the calibration receiver is making the pseudo-range measurement, must be known. Thus the second type of ground site measurement was required before a solution could be obtained.

Finally, a number of measurements were made which do not contribute directly to the solution but are necessary to insure that the ground system operation is satisfactory. These include items such as rf signal line insertion loss, electric power voltage and frequency, and transmitter power output.

These measurements are discussed in detail in the following paragraphs.

3.3.1 Site Survey

3.3.1.1 Area Navigation Survey

The U.S. Army Engineer Topographic Command at White Sands, New Mexico conducted surveys within the 50 mi area of WSMR at the request of the 621B Program (Ref. 8). The purpose of the surveys was to find the geodetic coordinates of each antenna used in the area navigation portion of the flight test program. The aircraft position solution, which is a product of the flight test program, requires the coordinates of each signal source (antenna) be known to ±3 in. For a detailed description of the survey requirements, see Ref. 9.

3.3.1.2 Data Adjustments

As discussed in paragraph 2.2.5, the apparent signal origin within the antenna, is not visible, and it is therefore not possible to survey it. We had to adjust the reported survey data from TOPOCOM (Ref. 10-14) in X, Y and Z to locate the apparent signal origin.

When each antenna was manufactured, the electrical signal origin was located empirically relative to a preselected piece of the antenna mounting hardware. After each assembled antenna was mounted on the WSMR poles, TOPOCOM surveyed in the preselected visible antenna hardware (a bolt, part of the antennas counter weight bracket). (See Figure 71.) The true position of each signal source is the sum of the TOPOCOM surveyed hardware coordinate plus the empirically derived offset to each coordinate. The resulting signal source coordinates are tabulated in Table III A through F for each antenna configuration used in the 621B system demonstration test.

The antenna configurations of Table III A through F coincide with the flight path flown by the NC-135 test bed aircraft. Paragraph 3.5.3.1 describes the ground track covered by each flight path. The B prime antenna configuration was added to the pre-

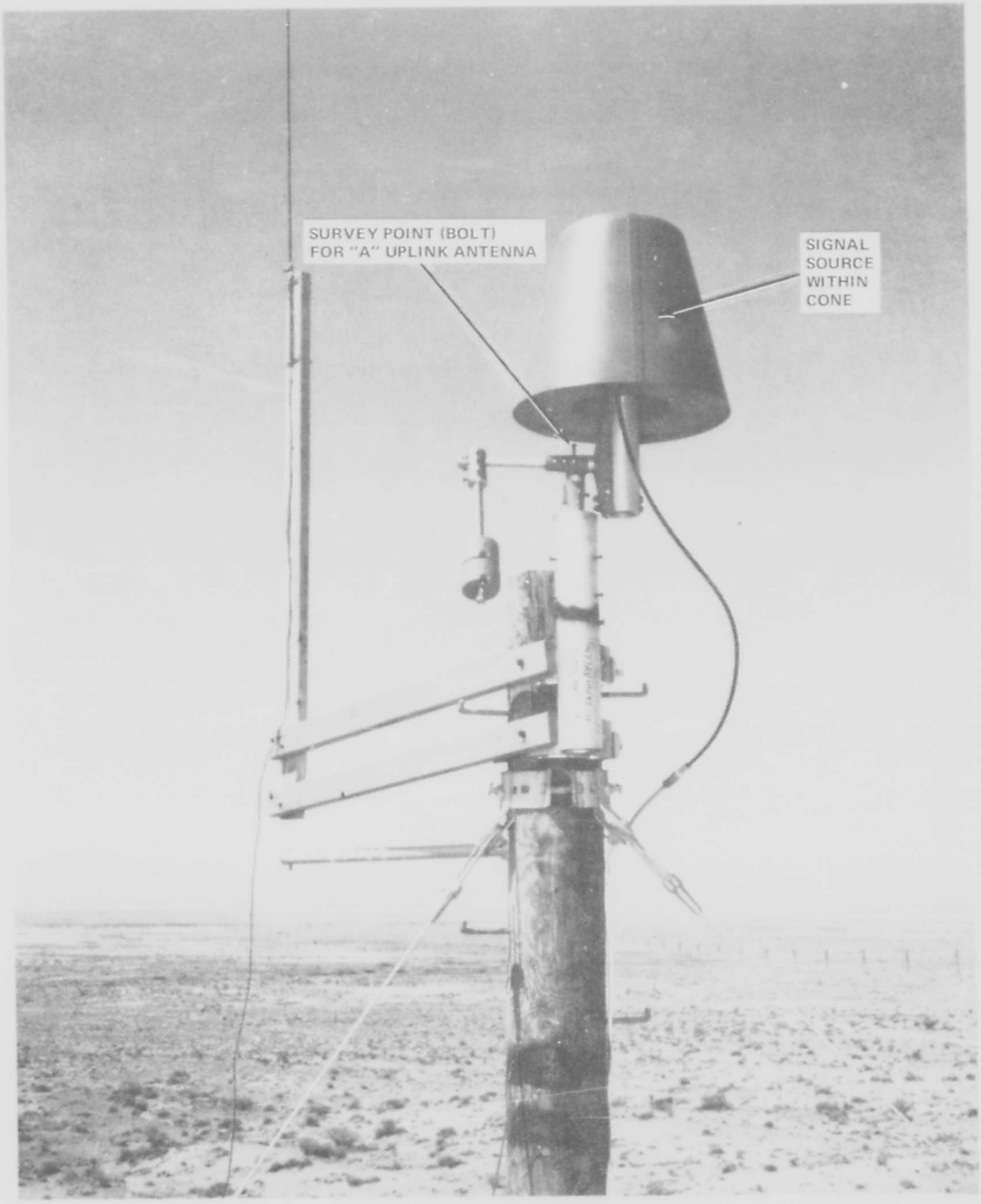

Figure 71 621B "A" Uplink Antenna at Salt Site

Table III 621B Antenna Coordinates for Area Navigation Test

A

A&C Flight Path (North–South)

EC-50	Salt Site	Bomb Site (SC-50)	WC-50
N = 520,213.84	N = 512,481.14	N = 492,989.30	N = 522,490.13
E = 514,457.86	E = 491,284.63	E = 489,198.82	E = 468,094.67
Z = 4,064.72	Z = 4,084.65	Z = 4,025.06	Z = 4,033.75

"B" Flight Path (43° NE, 223° SW)

EC-50	Salt Site	Bomb Site	WC-50
N = 520,212.66	N = 512,480.55	N = 492,939.02	N = 522,489.84
E = 514,461.60	E = 491,285.43	E = 489,199.30	E = 468,095.61
Z = 4,059.56	Z = 4,084.44	Z = 4,025.03	Z = 4,025.88

"B – PRIM" Flight Path

EC-50	Salt Site	Bomb Site	WC-50
N = 520,212.66	N = 512,481.14	N = 492,939.30	N = 522,489.84
E = 514,461.60	E = 491,284.63	E = 489,198.82	E = 468,095.61
Z = 4,059.56	Z = 4,084.65	Z = 4,025.06	Z = 4,025.88

"D" Flight Path (North–South)

EC-50	Salt Site	Bomb Site	WC-50
N = 520,213.25	N = 512,481.14	N = 492,989.30	N = 522,489.91
E = 514,459.15	E = 491,284.63	E = 489,198.30	E = 468,093.21
Z = 4,057.42	Z = 4,084.65	Z = 4,025.06	Z = 4,028.99

621B ANTENNA COORDINATES IN WSCS (DATUM-71)

B

A&C Flight Path

EC-50	Salt Site	Bomb Site (SC-50)	WC-50
Y = 453,708.08	Y = 445,977.06	Y = 426,489.46	Y = 455,983.91
X = 514,454.70	X = 491,286.54	X = 489,201.16	X = 468,101.61
H = 4,079.51	H = 4,090.20	H = 4,029.02	H = 4,070.17

"B" Flight Path

EC-50	Salt Site	Bomb Site (SC-50)	WC-50
Y = 453,708.11	Y = 445,976.47	Y = 426,489.18	Y = 455,983.61
X = 514,455.49	X = 491,287.34	X = 489,201.64	X = 468,102.55
H = 4,074.35	H = 4,089.99	H = 4,028.99	H = 4,062.30

"B – PRIM" Flight Path

EC-50	Salt Site	Bomb Site	WC-50
Y = 453,708.11	Y = 445,977.06	Y = 426,489.46	Y = 455,983.61
X = 514,455.49	X = 491,286.54	X = 489,201.16	X = 468,102.55
H = 4,074.35	H = 4,090.20	H = 4,029.02	H = 4,062.30

"D" Flight Path

EC-50	Salt Site	Bomb Site (SC-50)	WC-50
Y = 453,707.49	Y = 445,977.06	Y = 426,489.46	Y = 455,983.68
X = 514,455.99	X = 491,286.54	X = 489,201.16	X = 468,100.15
H = 4,072.21	H = 4,090.20	H = 4,029.02	H = 4,065.41

621B ANTENNA COORDINATES IN WSTM (DATUM-71)

Table III 621B Antenna Coordinates for Area Navigation Test (Continued)

C

A&C Flight Path (North–South)

EC-50	Salt Site	WC-50	Bomb Site (SC-50)
N = + 7,732.63	N = – 0.07	N = +10,008.92	N = –19,491.91
E = +23,173.76	E = + 0.53	E = –23,189.43	E = – 2,085.28
Z = + 21.05	Z = +40.97	Z = – 9.93	Z = – 18.62

"B" Flight Path (43° NE, 223° SW)

EC-50	Salt Site	WC-50	Bomb Site (SC-50)
N = + 7,731.45	N = – 0.66	N = +10,008.63	N = –19,492.19
E = +23,177.50	E = + 1.33	E = –23,188.49	E = – 2,084.80
Z = + 15.88	Z = +40.76	Z = – 1.75	Z = – 18.65

"B – PRIM" Flight Path

EC-50	Salt Site	WC-50	Bomb Site (SC-50)
N = + 7,731.45	N = – 0.07	N = +10,008.53	N = –19,491.91
E = +23,177.50	E = + 0.53	E = –23,188.49	E = – 2,085.26
Z = + 15.88	Z = +40.97	Z = – 17.75	Z = – 18.62

"D" Flight Path (North–South)

EC-50	Salt Site	WC-50	Bomb Site (SC-50)
N = + 7,732.04	N = – 0.07	N = +10,008.70	N = –19,491.91
E = +23,175.05	E = + 0.53	E = –23,190.89	E = – 2,085.28
Z = + 13.74	Z = +40.97	Z = – 14.69	Z = – 18.62

*The above 621B Antenna coordinates are expressed in 621B Data Reduction Coordinate System. This system has all axes parallel to the corresponding WSCS axes and with the same direction sense, same point of tangency but with an offset to Clark's Spheriod of 1866 such that the reference peg at Salt Site antenna pole is N = 0, E = 0 and Z = 0. All distances are measured in feet.

621B ANTENNA COORDINATES IN 621B DATA REDUCTION COORDINATE SYSTEM*

D

Mobile Calibration Station to "A" Uplink Signal Path Length

Channel 1	Salt Site	7,037.60 Feet
Channel 2	WC-50	31,672.65 Feet
Channel 3	EC-50	17,679.29 Feet*
Channel 4	SC-50	21,891.75 Feet

Mobile Calibration Station to "B" Uplink Signal Path Length

Channel 1	Salt Site	7,036.84 Feet
Channel 2	WC-50	31,671.66 Feet
Channel 3	EC-50	17,682.23 Feet*
Channel 4	SC-50	21,891.81 Feet

Mobile Calibration Station to "D" Uplink Signal Path Length

Channel 1	Salt Site	7,037.60 Feet
Channel 2	WC-50	31,673.97 Feet
Channel 3	EC-50	17,680.23 Feet*
Channel 4	SC-50	21,891.75 Feet

*For Flight 23 and Subsequent EC-50 (Channel 3) Path Lengths Are:

"A" Uplink	17,680.79 Feet
"B" Uplink	17,683.73 Feet
"C" Uplink	17,681.73 Feet

GROUND SIGNAL PATH LENGTH FROM TRANSMITTER SITE UPLINK ANTENNA TO THE MOBILE CALIBRATION STATION ANTENNA

Table III 621B Antenna Coordinates for Area Navigation Test (Concluded)

E

From Mobile Calibration Site Antenna to the Following Ground Site Antenna:

Channel 1	Salt Site	7,039.24 Feet
Channel 2	WC-50	31,675.28 Feet
Channel 3	EC-50	17,681.76 Feet
Channel 4	Bomb Site	21,892.58 Feet

621B GROUND SIGNAL PATH LENGTH FROM MCS MONITOR ANTENNA TO EACH TRANSMITTER SITE MONITOR ANTENNA (GROUND SIGNAL PATH IN AIR)

F

North Pole

Mate For EC-50 (Flights 1 Thru 22)

E = 7,035.77 N = 525.48 Z = 14.09

Mate for WC-50 Site Channel 2

E = 7,024.60 N = 524.88 Z = 10.93

Mate for EC-50

E = 7,034.60 N = 524.42 Z = 14.09 (FLIGHT 23 AND ON)

South Pole

Mate for SC-50 Channel 4

E = 7,024.47 N = 408.81 Z = 11.30

Mate for Salt Site Channel 1

E = 7,020.87 N = 413.71 Z = 1.93

Note: All coordinate values are positive and are in feet.

CALIBRATION DISH ANTENNA FEED TIP LOCATION IN 621B DATA REDUCTION SYSTEM

viously described A and B configurations for convenience in test operations. The B' configuration had the SC-50 (channel 4) and Salt Site (channel 1), antennas in the A position and the EC-50 (channel 3) and WC-50 (channel 2) antennas in the B position. This made it possible to test certain aspects of the B flight path with minimum re-orientation of the antennas.

In addition to antenna position, the ranges from the MCS site antennas (at Corner Site) to each transmitter site antenna was required to be known. This physical distance can be converted to signal delay time which is a parameter required for the navigation solution. This range, called the ground signal path length in air, was calculated using surveyed data. For example, the feed tips of the dish antennas located at both the MCS and transmitter site were selected as the survey point for the dish antennas. The slant range from feed tip to feed tip was only part of the distance travelled by the signal. To this tip-to-tip range, an additional length equal to approximately four times the coaxial shaft length had to be added to account for the true signal path length in air, Figure 72. Both the path length between dishes at the MCS and transmitter sites dish antennas (see Table III E) as well as the ground signal path length between the MCS dish antenna and the transmitter uplink antennas were calculated. For this second configuration, the physical distance changed as a function of the uplink antenna that was being used to project the signal, see Table III D and Figure 73.

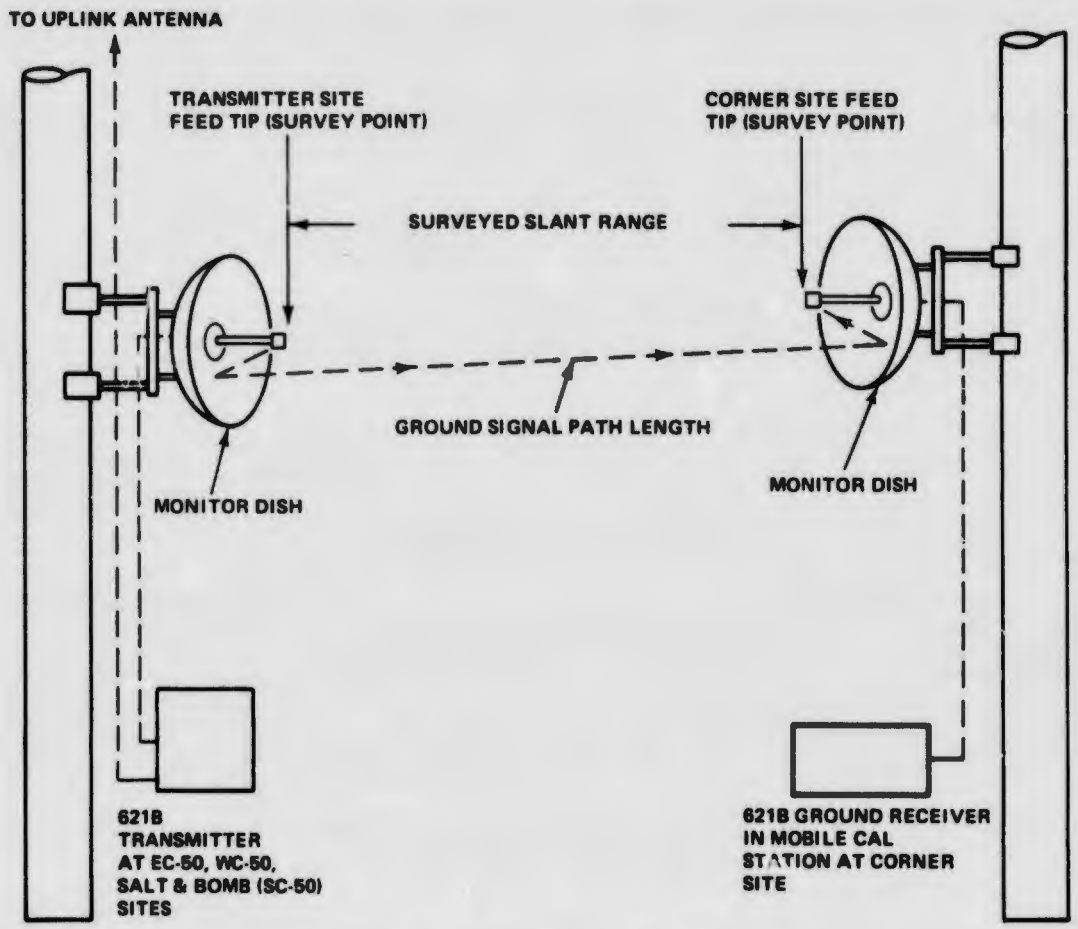

Figure 72 Ground Signal Path Length

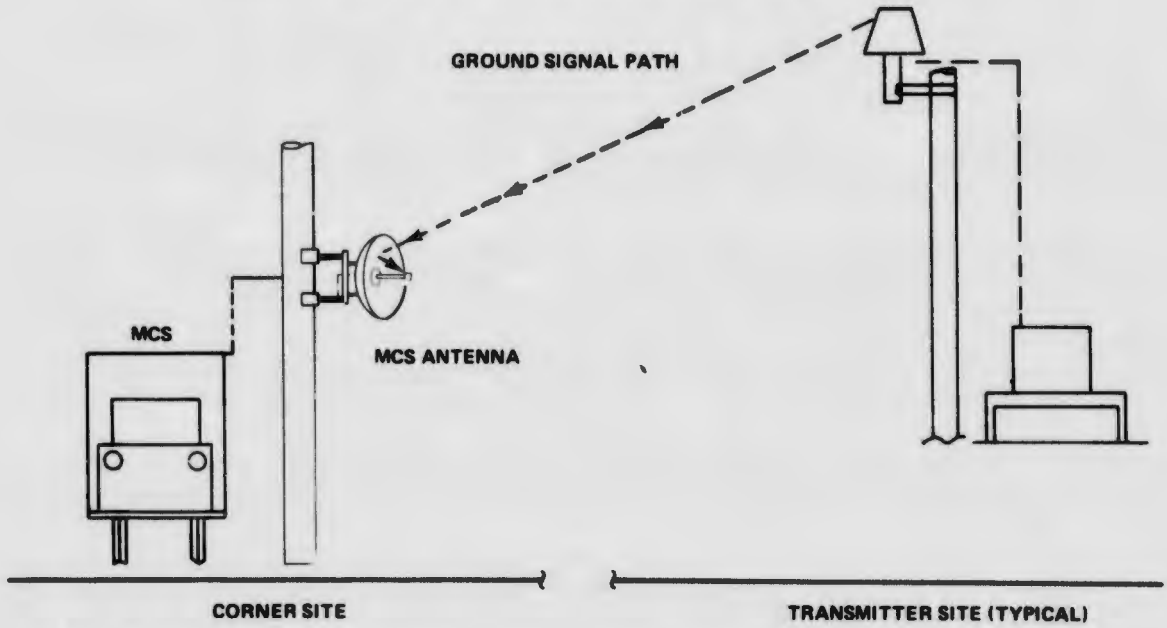

Figure 73 621B Ground Signal Path Length Uplink to MCS Antenna

3.3.1.3 WSCS Coordinate Systems

Table III A lists the coordinates of the 621B antennas in White Sands Cartesian System (WSCS). This coordinate system (Ref. 15) has its origin at a point tangent to Clarke's Spheroid of 1866, 33° 05' latitude north and 106° 20' longitude west. The system is a plane perpendicular to the normal of a point on the surface of the spheriod. All lines north and south are parallel to 106° 20' meridian, while east and west lines run perpendicular to 106° 20' meridian. The system assumes a false easting and northing of 500,000 ft, northing positive to north, easting positive to east from this origin. Elevations are heights above this plane not mean sea level.

All slant range calculations were done using this system (Table III E and D). WSMR cinetheodolite, DOVAP and radar data used for the 50 mi area testing were reported in this coordinate system.

3.3.1.4 Data Reduction System

Table III C and F lists the coordinates of the antennas in the data reduction system. This system is identical to the White Sands Cartesian System except the origin of this system was translated to a reference peg located on the transmitter antenna pole at Salt Site (channel 1). There were no rotations of coordinate systems when converting from WSCS to the data reduction system. This system was created to aid in the reduction of receiver data. The navigation solution and quick look radar data are reported in this system.

3.3.1.5 WSTM System

Table III B lists the coordinates of the antenna in White Sands Transverse Mercator (WSTM) system. This curvilinear system is based on a cylindrical surface passed just below the earths' surface, the projection of the cylinder from the earth's spheroid surface is the grid of the WSTM system. The origin is at latitude 32° 10' north with a false northing of 100,000 ft (Y), and 106° 20' longitude west with a false easting of 500,000 ft (X), and H is the elevation positive above mean sea level. The WSTM system is used for range documentation purposes (Ref. 15).

3.3.1.6 Description of ILS Survey

The ILS survey was divided into two phases. The first phase was to locate, to within 3 ft, all of the transmitter sites, MCS site (MCS site and MOS site are synonymous, see Ref. 17), airstrip boundaries and center line approach markers. The coordinates for these sites were supplied to the WSMR Geodetic Group by Grumman. In this first survey, it was felt that "pinpointing" each site to ± 3 in. was not necessary since concrete pads and poles had to be constructed at these points and finalization of antenna location could not occur until ground testing was finished. The Geodetic Group at WSMR developed traverse stations in the concrete pad at each transmitter site (Figure 74) which created a base network used to measure each antenna position plus cinetheodolite sites involved in the test program at Northrop Strip. It was necessary to "tie" in both antennas and the range instrumentation to the same base so that the BET, derived from the cine data, and the navigation solution, derived from antenna position could be compared to each other to determine system performance. The first survey effort was completed in April 1972. Rhodes Canyon Engineering (part of WSMR) built the ground sites and runway markings in each position defined by the survey. Grumman personnel installed antennas at each pole when construction of the ground sites was completed.

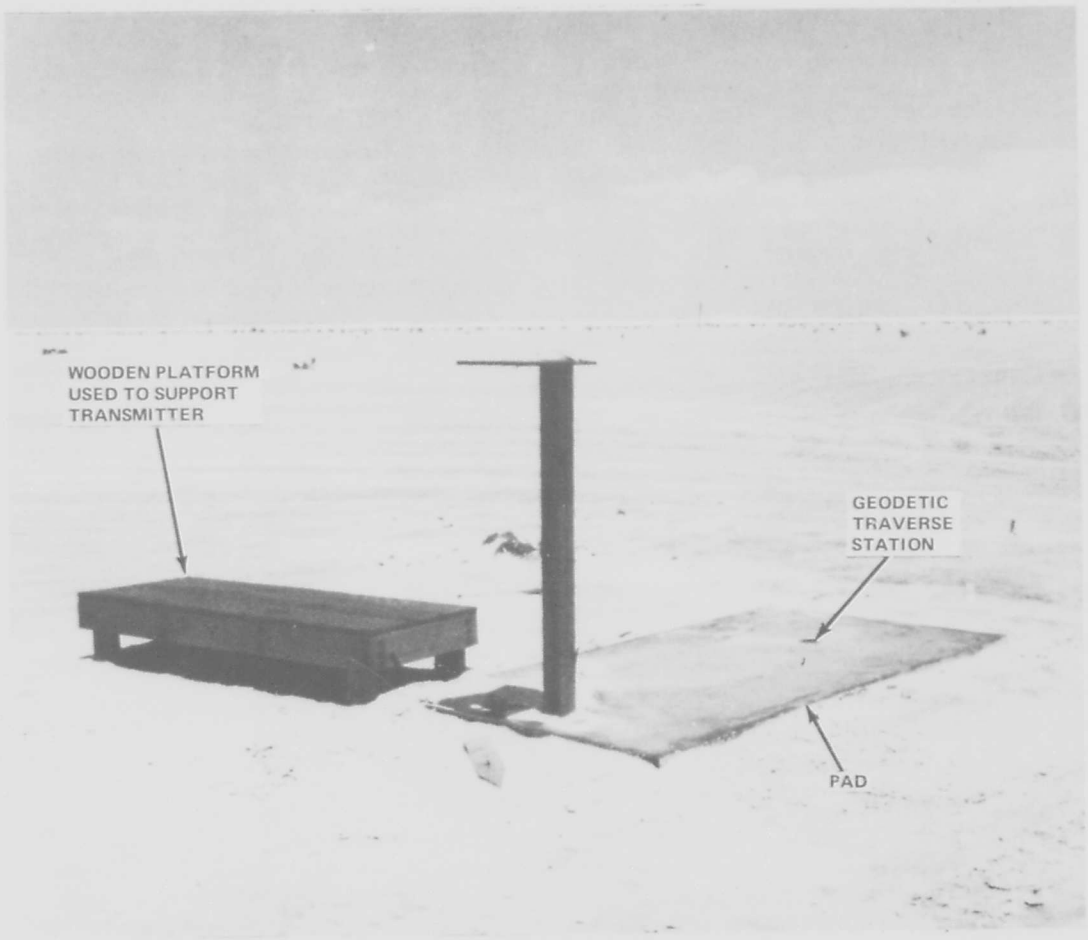

Figure 74 621B Transmitter Site Pad

The second ILS survey located the position, to within ± 3 in. of each antenna and the point called Flare, of the origin of the data reduction coordinate system for ILS tests. The resulting coordinates are reported in Table IV A through D. Table IV A and C is a tabulation of antenna coordinates in the WSCS and WSTM coordinate system. Table IV B lists the antenna coordinates in the ILS data reduction coordinate system (DRCS). For ILS the DRCS is not the same as was used in the 50 mi Area Navigation Test.

The 621B DRCS is a rotation and translation of the WSCS system such that the origin is at ground level position called Flare. This position was located on the runway center line at the point below where the aircraft flares during a normal ILS approach. Easting, in the 621B DRCS, is positive to the southeast at a heading of 97° 15' from WSCS grid north, northing is positive to the northeast at a heading of 07° 15'. Z is positive upward and is parallel to WSCS Z axis. All other coordinate system characteristics are the same as WSCS, Figure 75.

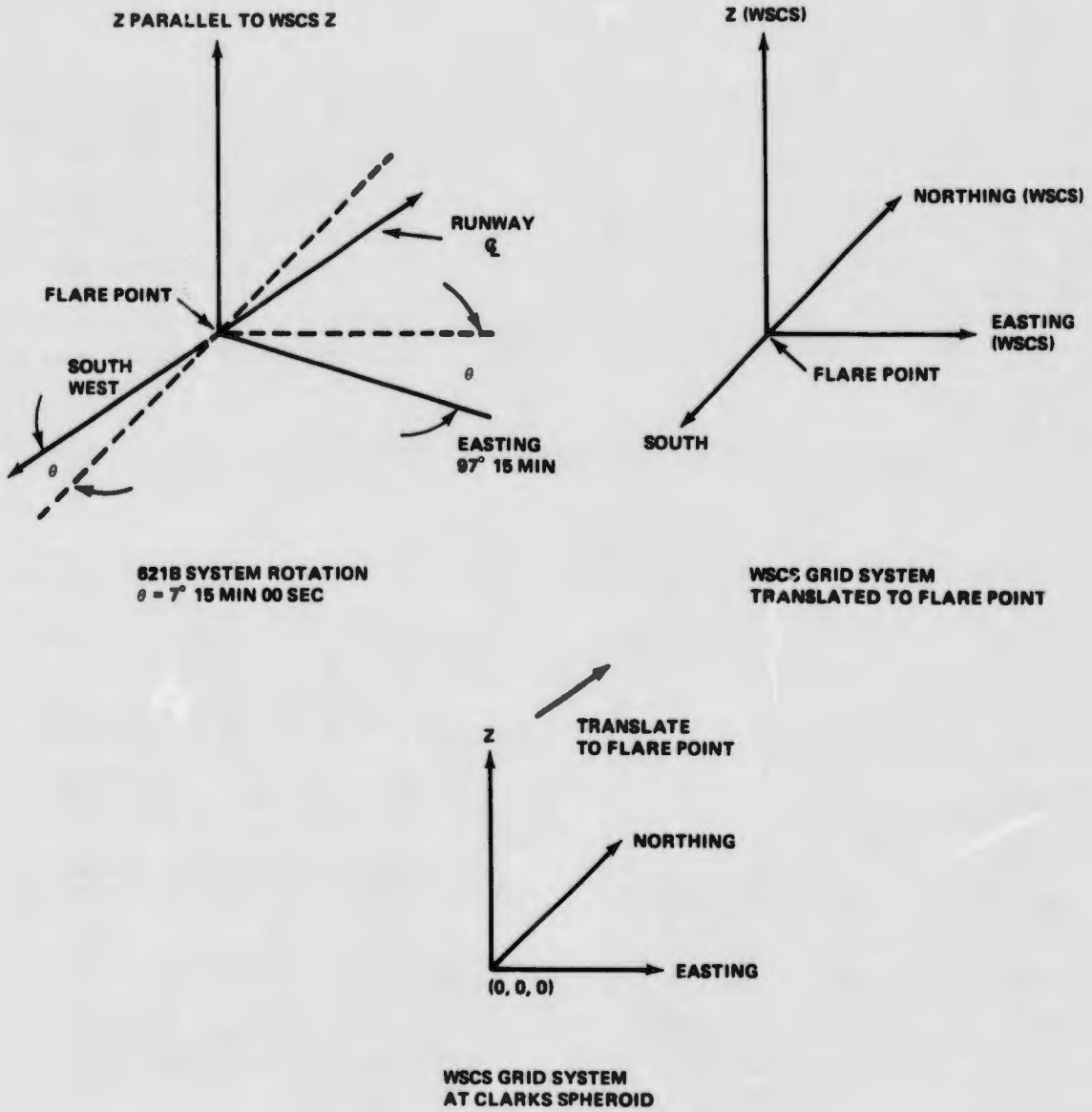

Figure 75 ILS 621B Data Reduction Coordinate System

Table IV D also contains the Calibration Signal Path Length, (Figure 76) which is the physical length (distance) the 621B signal travels from the transmitting omni antenna to the receiving omni antenna at the Mobile Calibration Station. WSCS coordinates were used to calculate this path length.

3.3.2 Resurvey and Installation Accuracy

3.3.2.1 Accuracy and Resurvey of 621B Hardware

The accuracy of the 621B survey data is stated to be within ± 3 in. for X, Y and Z coordinate values. That is, each coordinate value resides in a 6-in. diameter sphere of uncertainty. The Topographic Command Survey group established triangulation stations, in the area of the 621B hardware. These "known" stations were used to develop a base from which the 621B coordinates were derived. The base network is known to much greater accuracy than most other points on the range (1.67×10^{-6}, Ref. 16). The accuracy of the 621B survey data is a function of what base network was used to measure (optically) each antenna point. The WSMR Topographic Command determined what base should be used, what angle should be taken and how the data networks should be developed so as to satisfy the ±3 in. requirement of the 621B program.

Table IV ILS Antenna Coordinates

A

ATR Channel 1	DTR Channel 2	CTR Channel 3
E = 473,858.03	E = 476,618.88	E = 473,427.89
N = 458,975.64	N = 456,911.18	N = 456,601.40
Z = 3,855.57	Z = 3,858.13	Z = 3,850.45

FLARE Point	BTR Channel 4 Mounted On Ballon, Tethered In The Area Of:
E = 474,634.75	E = 473,636.39
N = 457,163.96	N = 457,290.86
Z = 3,851.60	Z = 3,850.49

621B ILS ANTENNA COORDINATES IN WHITE SANDS CARTESIAN SYSTEM (WSCS)

B

DTR Channel 2	Flare Point
E = +1999.82	E = 0.0
N = + .38	N = 0.0
Z = + 6.53	Z = 0.0

ATR Channel 1	Calibration Site Omni Antenna	CTR Channel 3
E = – 996.96	E = +999.01	E = –1000.10
N = +1,699.26	N = + 4.42	N = –1702.35
Z = + 3.97	Z = + 18.06	Z = – 1.15

ILS 621B ANTENNA COORDINATES IN 621B DATA REDUCTION COORDINATE SYSTEM (621B DRCS)

C

ATR Channel 1	DTR Channel 2	CTR Channel 3
X = 473,863.55	X = 476,623.83	X = 473,433.50
Y = 392,482.96	Y = 390,418.94	Y = 389,109.43
H = 3,912.24	H = 3,915.70	H = 3,914.57

FLARE Point	BTR Channel 4 Mounted On Balloon, Tethered In The Area Of:
X = 474,640.11	X = 473,641.95
Y = 390,671.67	Y = 390,798.52
H = 3,910.96	H = 3,910.82

Note: The above channel placement is valid for flights 26 and on. Flight 24 and 25 channels one and four were interchanged.

621B ANTENNA COORDINATES IN WHITE SANDS TRANSVERSE MERCATOR SYSTEM (WSTM)

D

Calibration Signal Path Length

ATR Channel 1 to MCS Antenna 2,620.04 Feet
DTR Channel 2 to MCS Antenna 1,001.19 Feet
CTR Channel 3 to MCS Antenna 2,628.54 Feet

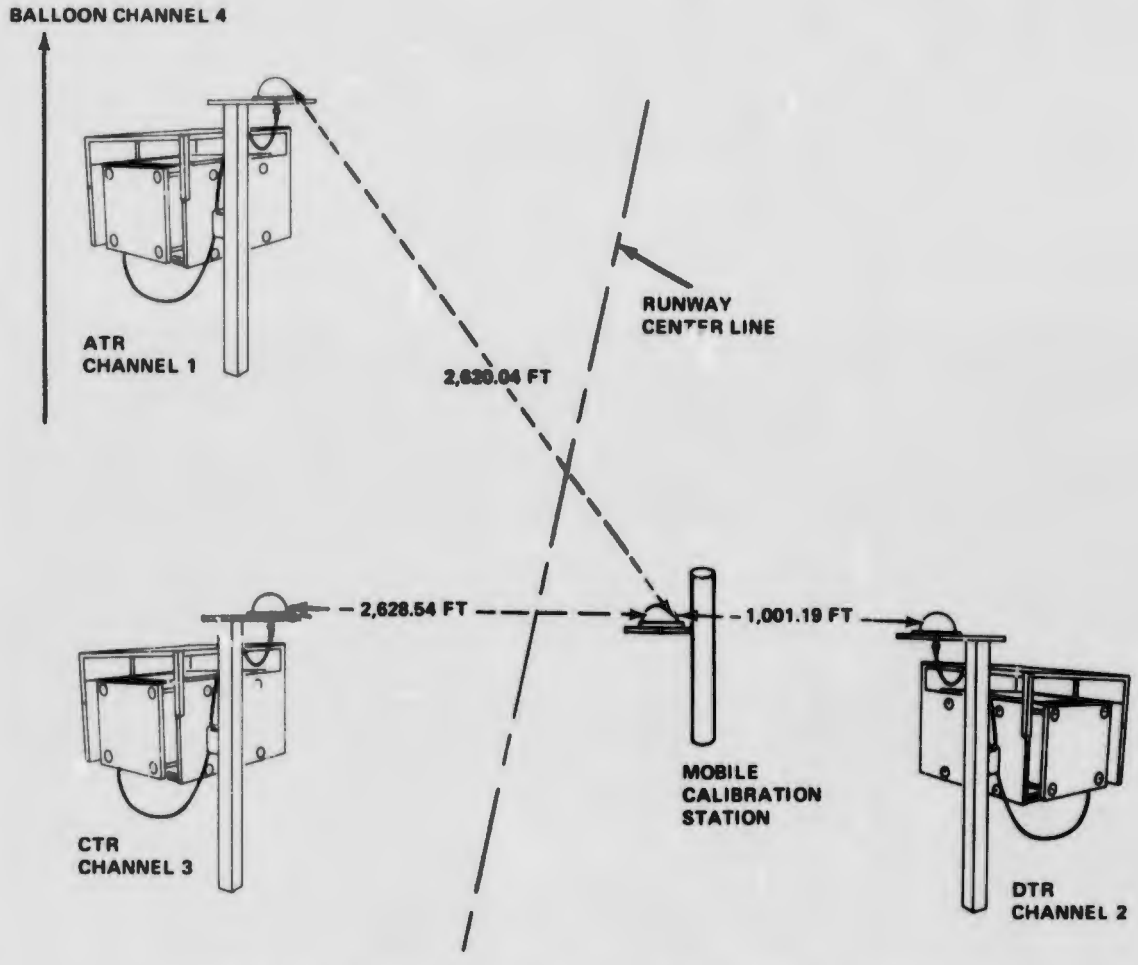

Figure 76 Calibration Signal Path at Northrop Strip (ILS)

During the buildup of the field test, surveys were conducted at various stages. The first survey located the poles at each site before the antennas were installed. This first pole survey (Ref. 10 through 14) aided in the development of the data reduction program and also served as a check on future surveys. When the antenna survey was completed, the surveyed pole positions were used as a gross check on the antenna coordinates. Another useful function of the pole coordinates was to verify slant ranges from antenna to antenna. As a check on one of the slant ranges, we requested TOPOCOM to resurvey the pole to pole distance between the Corner Site south pole and the pole at SC-50 (channel 4) using a technique independent of the previous optical survey. This check was done with a radio device Figure 77 called an Electro Tape made by Cubic Corp. (Ref. 17). The results of the optical technique yielded a slant range of 21,892.43 ft (Ref 12 and 14), while the range measured with the Electro Tape was 21,892.56 ft (Ref. 17), a difference of 0.13 ft, well within the accuracy requirements of the test program.

The same south pole at Corner Site experienced storm damage from a thunderstorm on 12, July 1972. After the damage was repaired, the antennas were resurveyed and found to be within 1.5 in. of their previous position. Another resurvey was requested when we changed mounting hardware on the EC-50 Corner Site

Figure 77 621B Survey Crews Using Electrotape to Measure Slant Range

dish. The switch in hardware was required to meet multipath testing requirements at Northrop Strip. The resurvey (Ref. 18) showed the new mounting hardware held the dish closer to the pole than before thus increasing the slant range between the transmitter site EC-50 dish and Corner Site receiver dish by 1.5 ft. The increased range is shown in Table IV D.

3.3.2.2 Pole Movement Indicator

The pole movement indicator is a 3-ft metal tube mounted perpendicular to the wooden antenna pole with 0.020 in. Monel safety wire tied to one end and allowed to hang freely to ground level, Figure 78. A plumb bob was suspended from the safety wire and allowed to come to rest at ground level. This "rest" position was then marked on the surface of the ground by driving a steel T-pin at the rest point, Figure 78 and 79.

This procedure was followed at the time of the antenna installation on the wooden poles before flight testing began. During the five-month flight testing, the rest position of the plumb bob was checked and found to be within 0.5 in. of its original position (exception below) where movement of $\pm$ 3 in. was felt to be acceptable. This check was done two ways; the first was done as described above by using the plumb bob. The second method, performed by TOPOCOM, used two theodolites to optically "drop" the point at which the wire was tied to the tube to ground level. This optical method confirmed the plumb bob results. Checks using the plumb bob were performed four times at each of the six antenna poles. During the five-month flight testing period, these checks were done during extremely low wind conditions since during windy days, the plumb bob would not stabilize enough to give repeatable results. Figure 79 shows how the plumb bob is deflected by a wind loading on the monel wire suspending the plumb bob. When the wind subsided during this same test, the plumb bob returned to the T-pin rest position.

On the night of 12, July 1972, a storm with winds in excess of 50 kt passed through the 50 mi area of WSMR. Nine telephone poles suspending multiple rows of copper communication wires were sheared off at ground level and thrust over the MCS at Corner Site. The resulting damage to the MCS was small, but the south pole with the dish antennas that look toward SC-50 (channel 4) and Salt Site (channel 1) was tilted when the communications lines fell on the pole guy cable system, Figures 80 and 81. When the damaged communication line poles were removed, the pole movement plumb bob was used to measure the amount of tilt in the pole. The plumb bob came to rest 9-12 in. from its original T-pin rest position. This was considered an unacceptable amount of movement. Civil engineering at Rhodes Canyon returned the south pole to its original position by using the plumb bob/pole movement indicator system as a guide. The pole was returned on 18 July 1972 to within 1 in. as measured by the plumb bob and T-pin match, Figures 82 and 83. This result was verified by a resurvey of both antennas on the south pole by TOPOCOM on 24 July 1972.

3.3.3 Ground System Calibrations

Calibrations of parameters such as signal delay through cables, link delays, insertion loss, and interaction of antennas were obtained in order to provide necessary parameters used in the navigation solution and to isolate possible sources of error. As experience was gained in the test system behavior we found additional calibration necessary to precisely define the ground system characteristics.

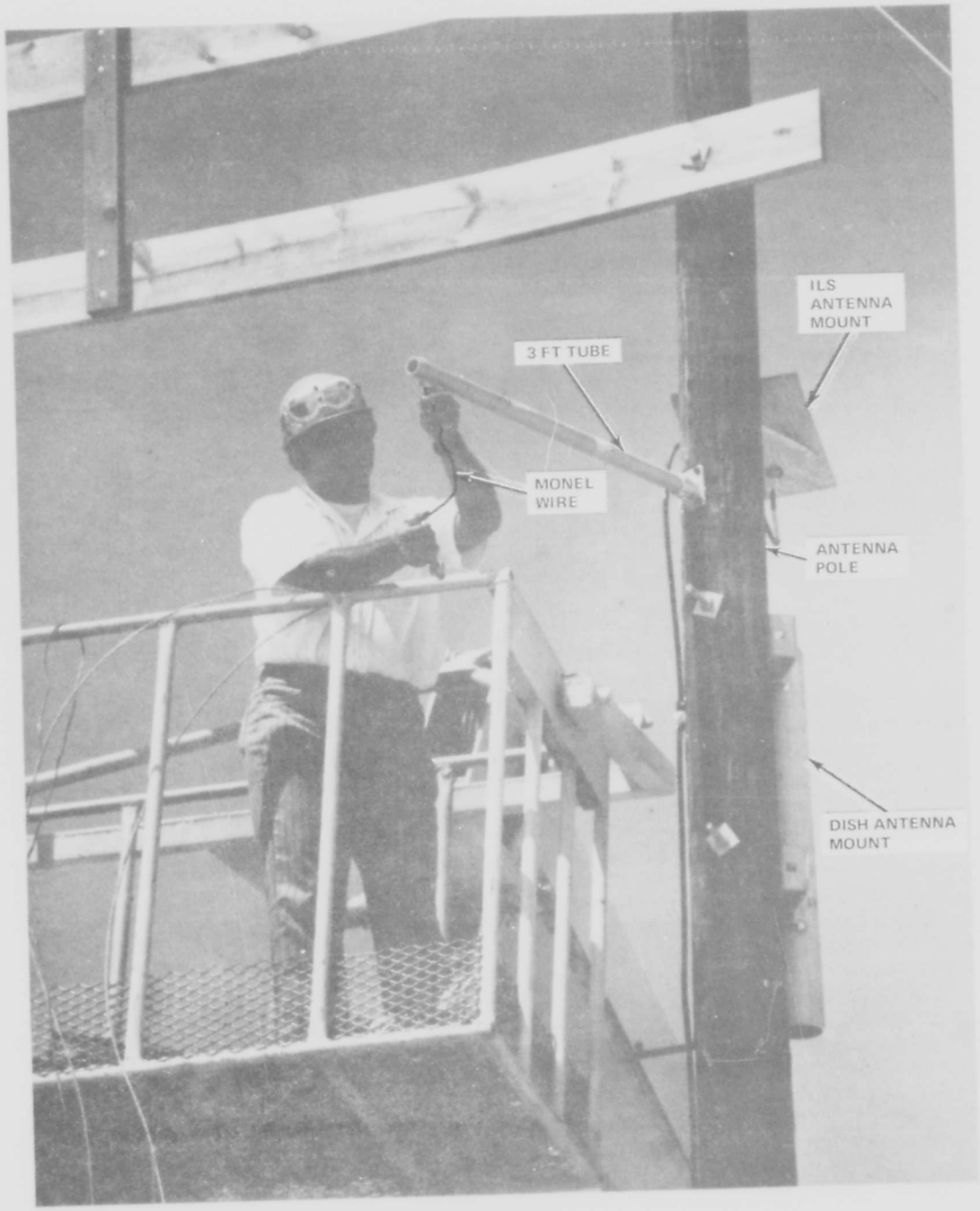

Figure 78 621B Pole Movement Indicator Being Installed on ILS Pole at Northrop Strip White Sands Missile Range

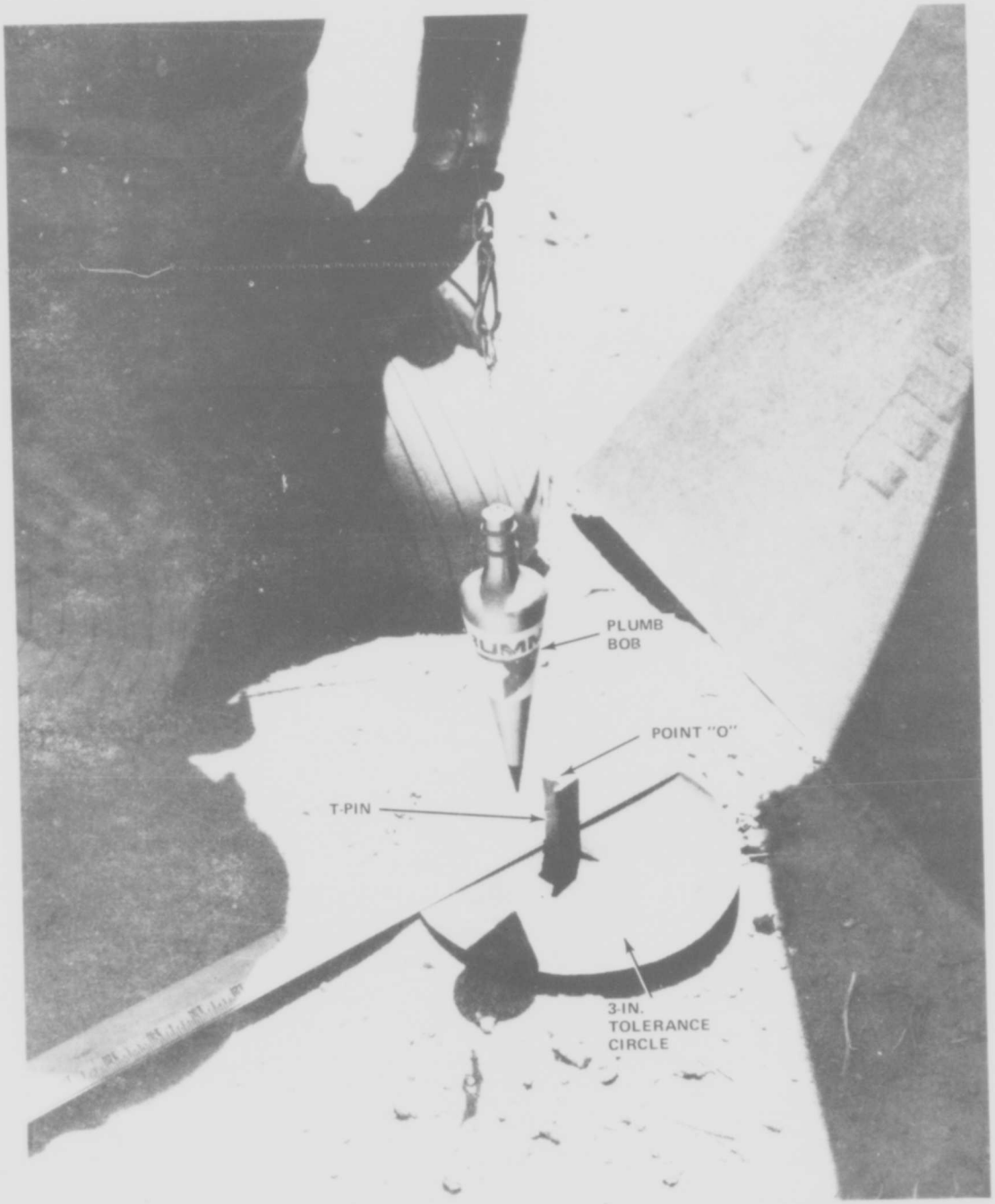

Figure 79 621B Pole Movement Indicator Plumb Bob and T-Pin Check

Figure 80 South Pole Movement as a Result of Wind Damage

Figure 81 Storm Damage

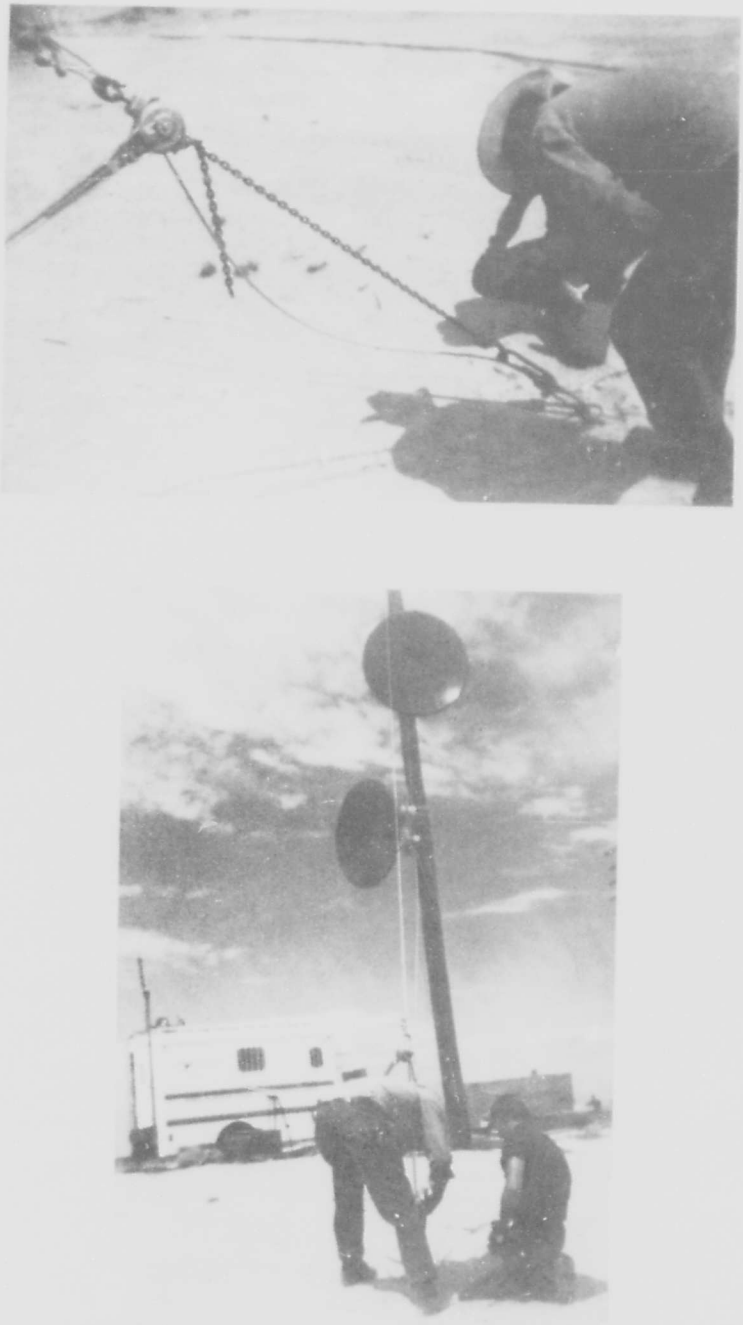

Figure 82 WSMR Engineers Straightening South Pole

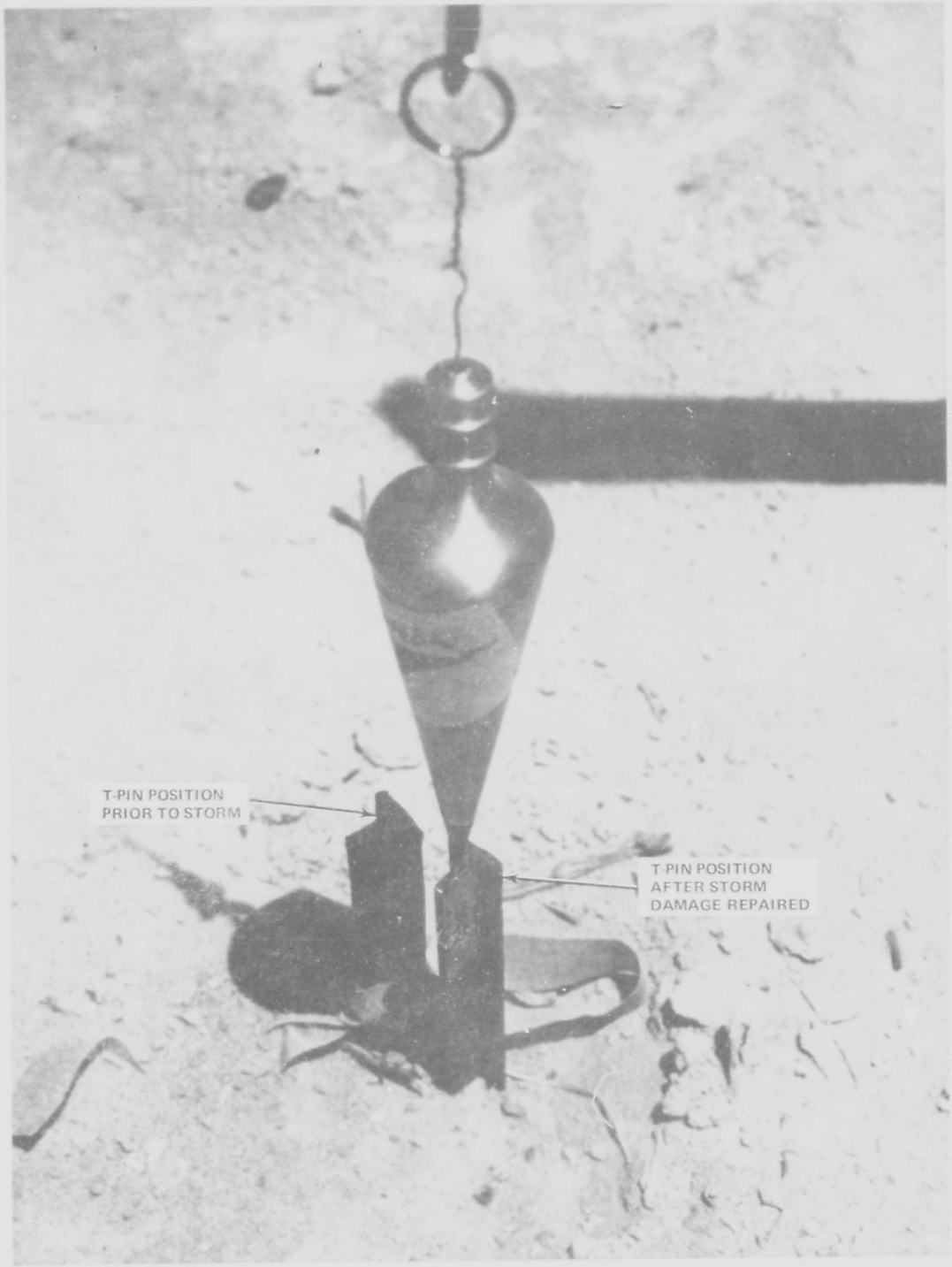

Figure 83 Tip Pin Position for South Pole at MCS Site After Pole Was Straightened

3.3.3.1 Ground System Calibration Summary

A. Calibrations Planned at the Start of Field Operations

Calibration Type	Measurement Techniques
1. Align all ground antennas	Antennas and mounts were mechanically aligned at Bethpage for each site. Antenna assemblies were mounted on site poles and visually aligned with survey markers at WSMR (see paragraph 2.2)
2. Establish satisfactory link power	Transmitter power output checked. Cabling VSWR and insertion loss measured. Appropriate attenuation placed in links so that power levels from the sites were balanced at the user end (aircraft) and at the MCS
3. Determine the signal path time delay from transmitters to the MCS	Measure cable time delays using a test signal and the receiver. Measure link time delays using the stable oscillator technique (described later in this section). Use envelope detector to detect possible multipath on links
4. Insure that signals directed to the aircraft are not interferring with those directed to the calibration receiver at the MCS	This was done by measuring the power level of the two different signal sets at the MCS and then making the proper attenuator adjustments so that interference was minimized

B. Calibration Added After Operational Experience Was Gained

Calibration Type	Measurement Techniques
1. Probe rf field at the MCS to determine if receiving antennas were at suitable locations	A simple dipole antenna was used to probe the vertical field in front of each receiving antenna at the MCS
2. Cable megohm tests to check cable rf integrity	A megger was used to determine if rf shorts were present in the Spiroline cabling due to moisture entering the cable
3. Investigation of possible multipath on Salt link	We observed signal variations at the MCS when vehicles were driven along the road that crosses the Salt rf link. A terrain survey was performed to see if an analytical justification of the observations could be obtained

Calibration Type	Measurement Techniques
4. Investigation of low power on WC-50 link	Cable loss measurements and transmitter power output tests performed. A terrain survey along the link path was performed to analyze possible multipath effects. Signal polarization at the antennas was checked
5. Measurement of transmitter internal delays	The receiver was used to measure the internal delays in the transmitter between the uplink and monitor link outputs
6. Salt uplink antenna orientation	Special flight profiles were used to determine if the Salt uplink antenna pattern was oriented N/S. The aircraft crossed the N/S flight profile at 90° and made signal level measurements
7. Uplink antenna interval delay measurements	The uplink antennas were installed on a specially developed site near the MCS and the calibration receiver was used to measure the apparent signal delay through the antenna as a function of antenna orientation.

The greatest amount of time was spent trying to determine the time delay between transmitters and the calibration receiver. Our goal was to know this time delay within 1 nanosec. As testing progressed, it became obvious that the actual signal path was varying by amounts larger than this amount and in the desert environment, could not be stabilized for measurements of this quality.

We started out by using the envelope detector to determine if multipath existed on a link, and using the stable oscillator technique to measure link delays.

The envelope detector technique is a test method that permits examination of the envelope of the received 621B rf signal. If no multipath is present the phase change notch will be unaffected (that is, it goes practically to zero) as shown in Figure 84. The presence of multipath produces a distorted signal envelope, that is, the notch is filled in or changed in shape. Although the envelope detector does not produce a quantitative measure of multipath conditions, it can verify the absence of multipath. Limited tests indicate that multipath producing as little as 2 nanosec tracking error produces an obvious distortion of the phase change notch.

The envelope detector is shown in Figure 85. The received rf signal is amplified (60 db) to a level sufficient to be displayed on the sampling scope with a signal to noise ratio that permits examination of the phase change notch. The scope is triggered by the boosted envelope which is obtained by the detector and video amplifier. A signal of -50 dbm at the input to the amplifier-filter is the minimum that may be used to keep larger signals within the linear range of the amplifier-filter. A special code plug is required in the transmitter to provide a short code (approximately 320 μs period) because the normal 3.3 second code period does not provide enough data points per second to operate the sampling scope. This increased the transmitters short code rate by 10^{+4} per second.

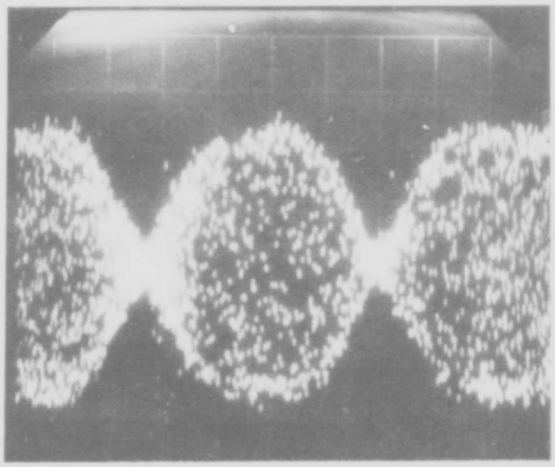

DISPLAYING NO PRESENCE
OF MULTIPATH

DISPLAYING MULTIPATH

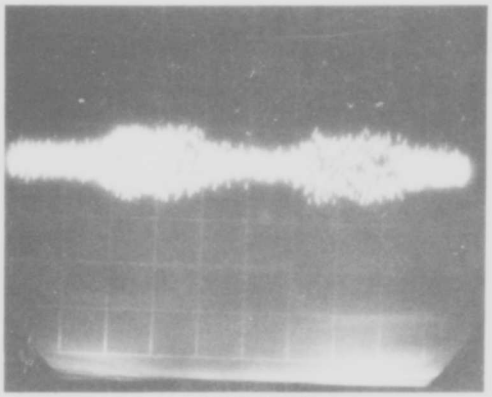

OUT-OF-PHASE

ENVELOPE DETECTOR MULTIPATH
DISPLAYS

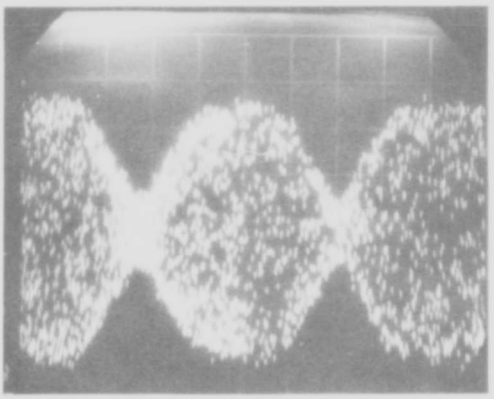

INTERMEDIATE

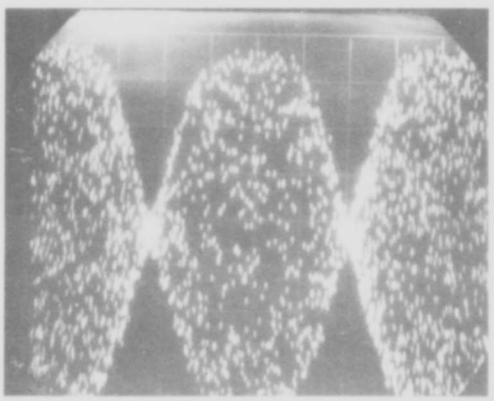

IN PHASE

Figure 84 Envelope Detector Multipath Displays

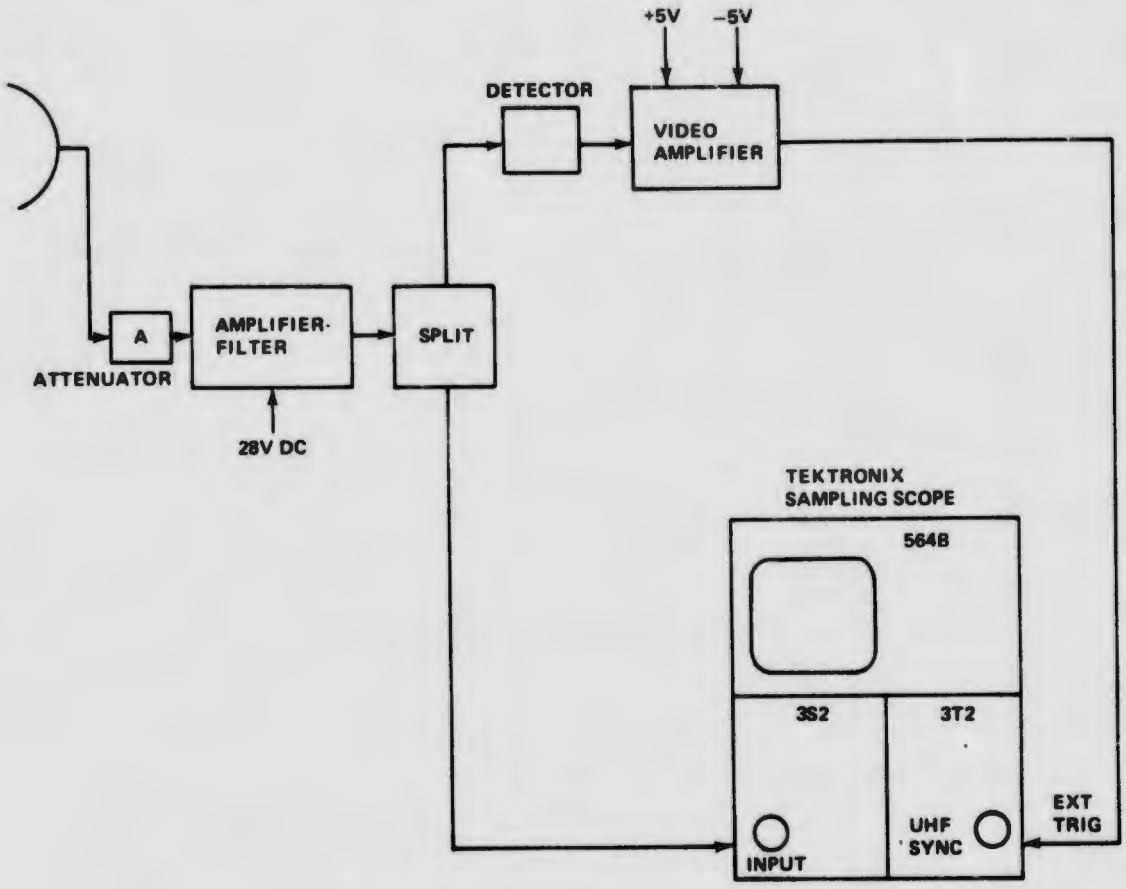

Figure 85 Envelope Detector Setup

The envelope detector was used to detect multipath conditions over the Salt link. The Salt monitor signal level varied as trucks drove by on the road that passes through the Salt link. This variation in power as a function of truck location was also observed in the recorded data. The signal has been observed to dip 15 to 20 db due to passage of a large truck. Therefore, roadguards were stationed at each end of the road to stop traffic from affecting the signal during an aircraft data-taking pass.

3.3.3.2 Delay Measurement Techniques

A method of determining link delay is shown in Figure 86. The delay measurement technique consists of stabilizing a 621B transmitter and the 621B calibration receiver, each with a separate cesium frequency standard. The transmitter and receiver are directly connected to obtain a reference reading. The transmitter and its cesium standard are then transported, while operating continuously, to the other end of the link to be measured and another reading at the calibration receiver is obtained. Basically, the delay in the link is the difference between the two readings. However, because the relative change in the two cesium standards during the time it takes to travel to the far end of the link was significant, it was necessary to correct for this drift. This was accomplished by returning the transmitter/cesium standard to the receiver to obtain another reference reading. The measurement was then corrected by approximating the drift between reference readings by a straight line.

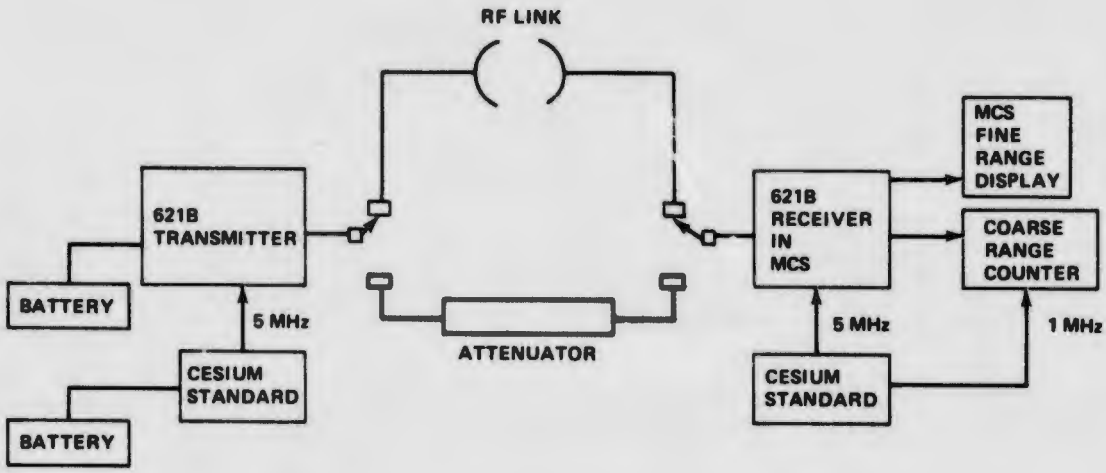

Figure 86 Link Delay Measurement Setup

Cable time delays were measured by two different procedures. The first was to place the calibration receiver in the self test mode. A cable of known length and known delay time was connected to the 621B rf cable at one end and connected to the antenna at the other end. The receiver then locked onto the signal and the fine range was recorded. The known cable was then taken out of the loop, the unknown cable reconnected to the antenna, and the receiver was allowed to lock once more. The second fine range reading was subtracted from the first, with the difference being the delay time of the unknown cable mounted on the pole.

The second method utilized a Hewlett Packard Time Domain Reflectometer. All the 621B cables were remeasured using this instrument and the values measured were compared with the self test method.

Non-repeatability of the cable signal delay measurements could be caused by a low resistance between the conductor and the protective shield of the Spiroline rf cable. Megohm tests indeed revealed such was the case, and it was discovered that hot desert days and cool nights induce condensation inside of the rf cable. This was responsible for the difference in delay measurements occasionally observed or some cables. The solution was to periodically purge the lines with nitrogen gas and then to check each cable with a "megger" to insure that all electrical shorts had been removed.

Another problem was discovered in the monitor link. The monitor link signals (codes) were to be precisely delayed by 200 nanosec relative to the uplink code. This delay was introduced to insure rejection of monitor link signals at the aircraft; however, it was discovered during tests of monitor link versus uplink codes that this delay was not precisely 200 nanosec, and was not stable. This decreased the solution accuracy drastically. When it was discovered that the calibration receiver could lock onto the uplink antennas, the monitor links were discarded and the MCS began receiving the code that the aircraft was seeing.

In studying the agc levels on the initial 621B flights, it was determined that the shaped beam uplink antenna on channel 1 did not give the proper signal level when the aircraft flew a straight north/south pass. On flight 10, runs 8 and 9 were flown perpendicular to the A flight path (north/south-34,000 ft MSL).

The received agc levels indicated that the uplink antenna at Salt Site was electrically misaligned 25° east of north. A crew went to Salt Site rotated the antenna 25° to the west, which aimed the shaped beam toward the aircraft's flight path. Later, examples of signal levels confirmed that this indeed was the correct positioning of the antenna.

The above tests were concerned with the 621B Ground System. Certain tests were conducted on the airborne system which included EMI, VSWR, system air worthiness and uplink antenna pattern verification prior to the start of the formal flight test program. These tests revealed certain minor problems of the test system originating from aircraft related factors. The Hazeltime receiver would occasionally lose lock on self test when the number one engine started. IRIG timing would intermittently lose sync during transfer from external aircraft power to the internal aircraft power generating system. During the ILS Test, the MRL receiver occasionally lost lock when the aircraft touched down and did not regain lock until the succeeding data run. These problems, once accounted for, were either fixed or if the impact of the problem on the test results was negligible, or if impossible to correct, the problem was acknowledged and lived with.

3.4 FLIGHT EQUIPMENT INSTALLATION

The airborne equipment for this test consisted of the MRL 621B receiver, HC 621B receiver, antenna installations, Grumman data interface system, and Air Force instrumentation recording system, Figure 87.

The equipment was installed in the NC-135A (AF 60-371) at KAFB immediately following completion of the System Integration Test conducted at Grumman in Bethpage. Checkout of the aircraft system paralleled ground system buildup during Jan. and Feb. Aircraft system acceptance tests (described in paragraph 4.1.1) were successfully completed before the first data flight.

The equipment was located in the C-135 as shown in Figure 88.

The aircraft is used as an electronic test bed. As a result it is primarily outfitted with standard relay racks for equipment installation and has special environmental controls to handle the heat loads. The actual installation is shown in Figures 89 and 90.

The antenna system was designed to be able to select top or bottom antennas (ILS or Area Navigation Test respectively) and to insert a fixed amount of attenuation in series with the signal. The location of the antennas on the aircraft is shown in Figure 91. A schematic diagram showing the rf connections between the receivers and the antennas is shown in Figure 92. Table V contains measurement data on the rf losses of the aircraft antenna system.

3.5 TEST DESCRIPTION

This section contains a description of the various system evaluation testing accomplished during this effort. Tests can be separated into two groups.

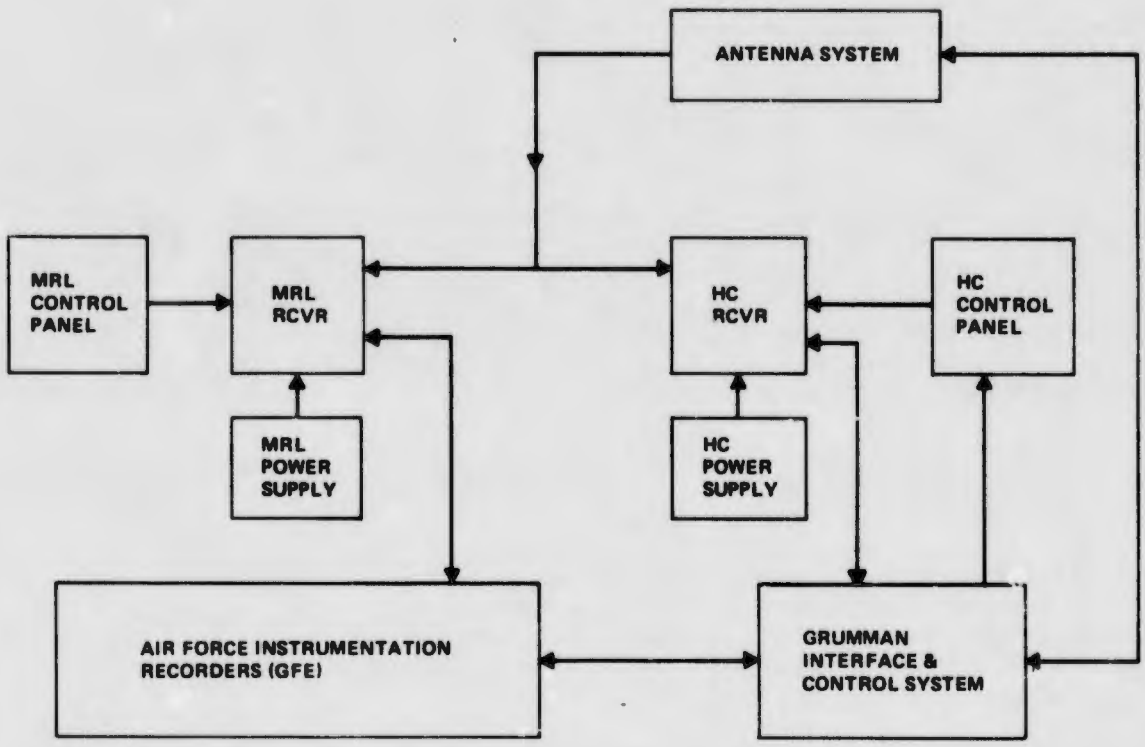

Figure 87 Flight Equipment Block Diagram

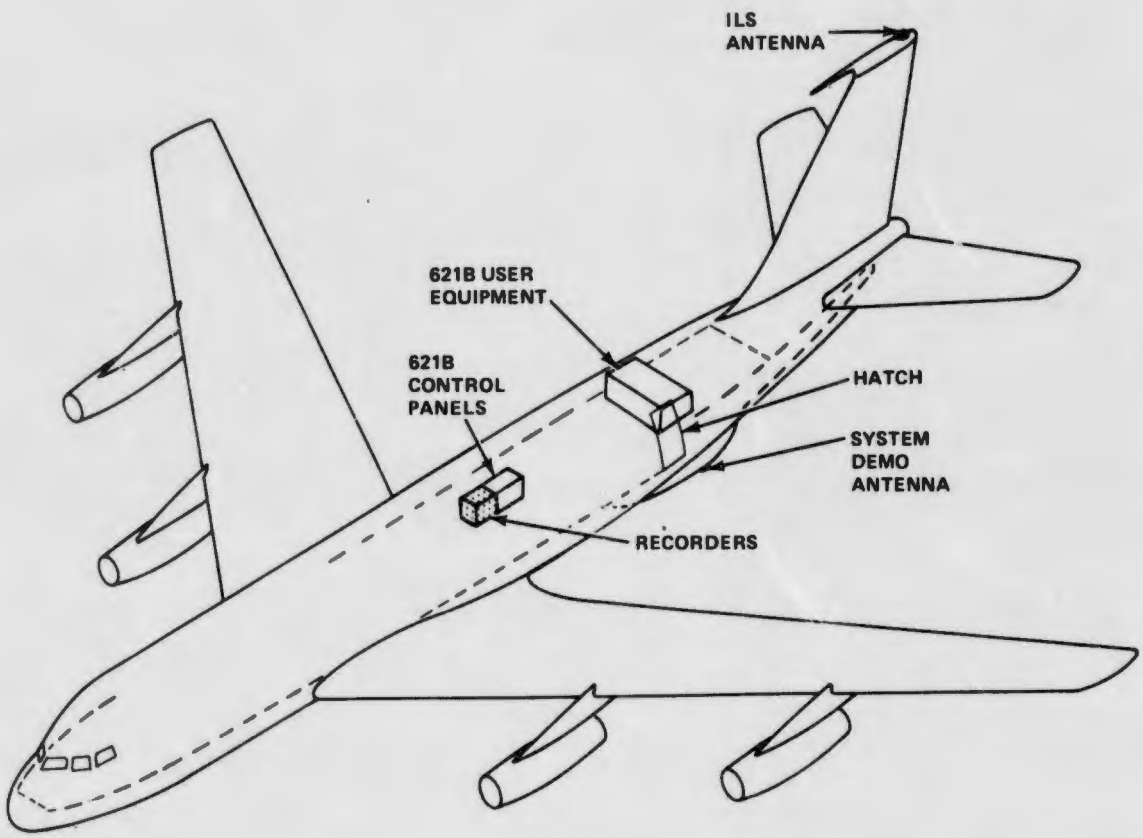

Figure 88 621B Installation Inboard Profile

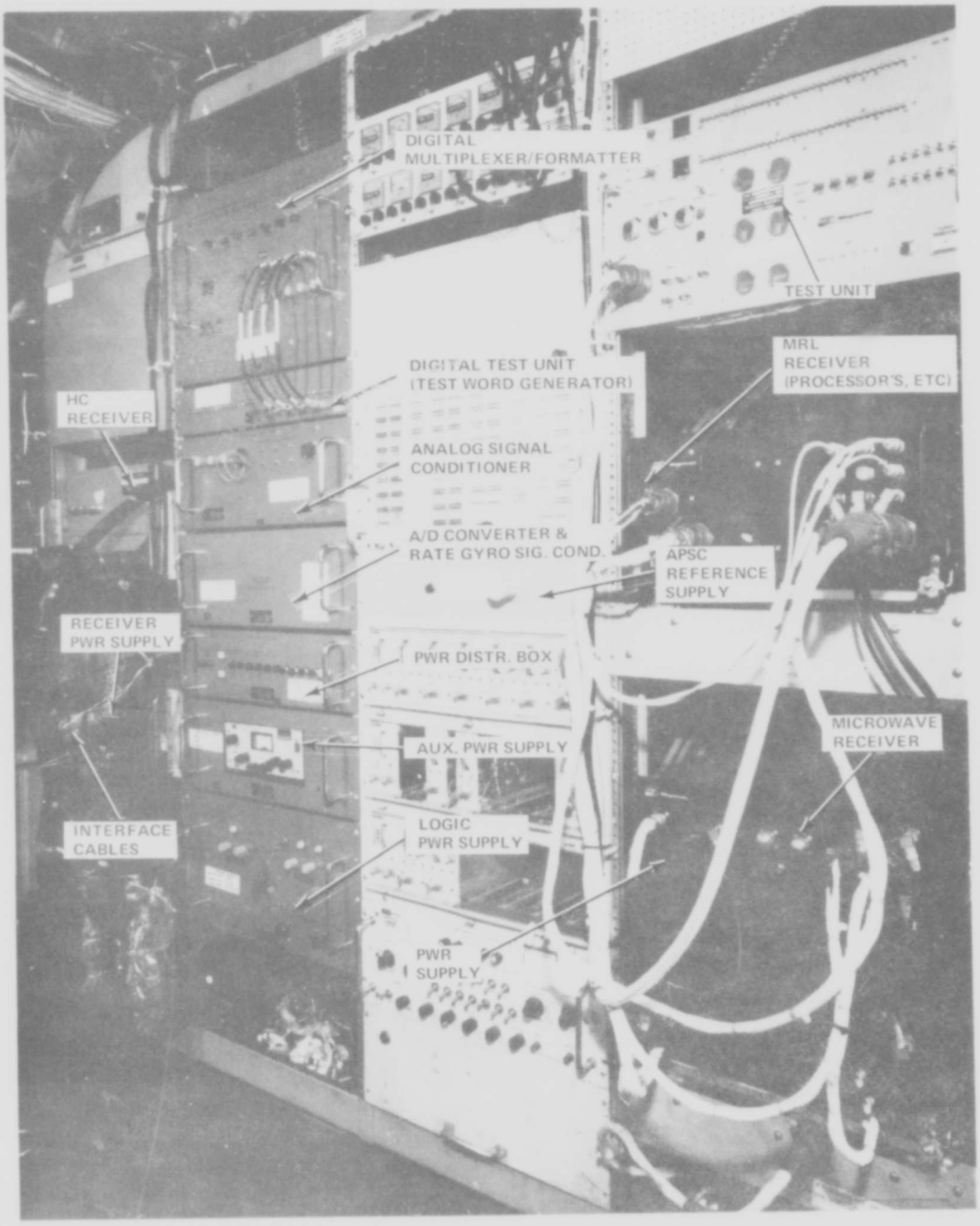

Figure 89 Aircraft Installation of 621B Receivers and Interface Unit

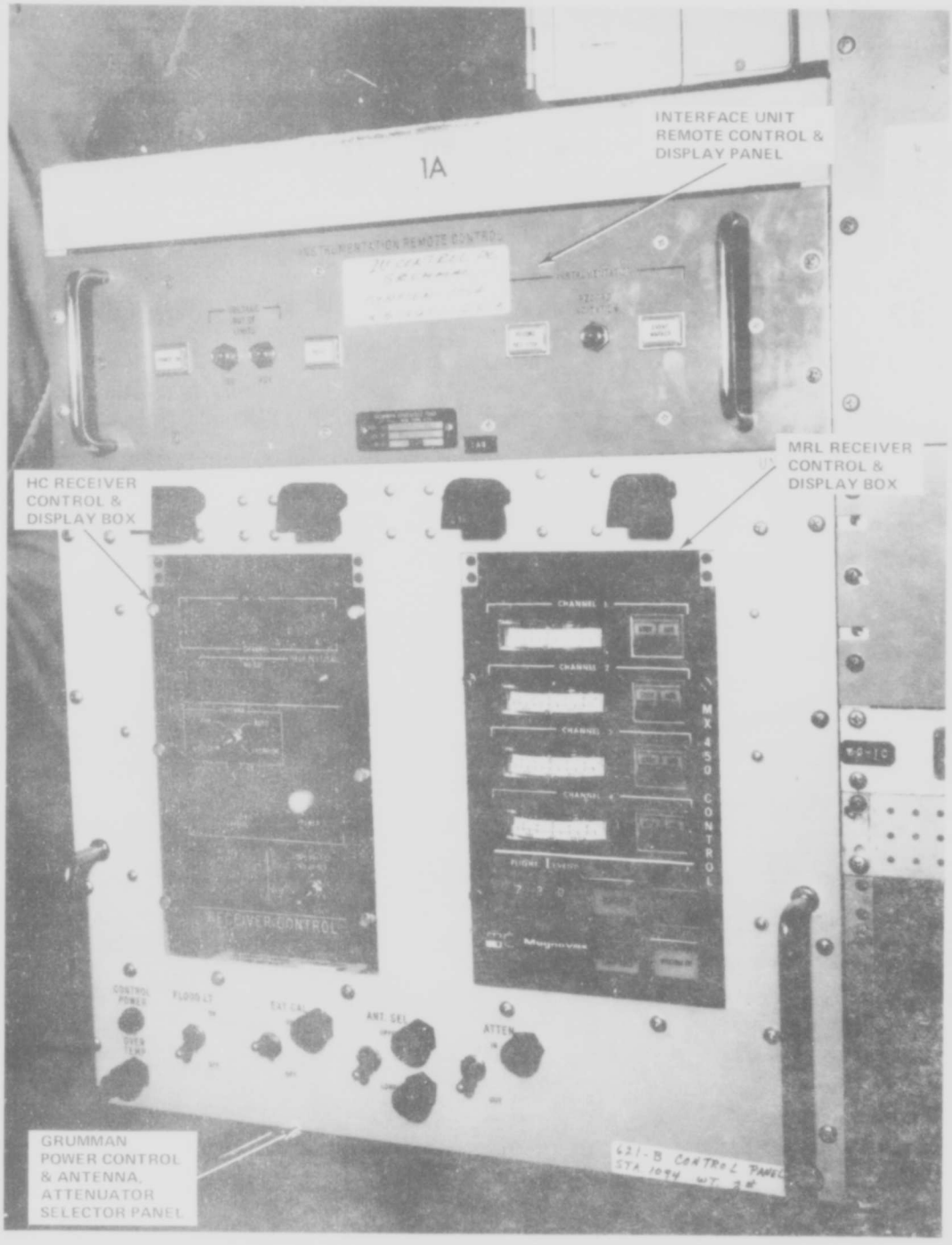

Figure 90 621B Control Panels

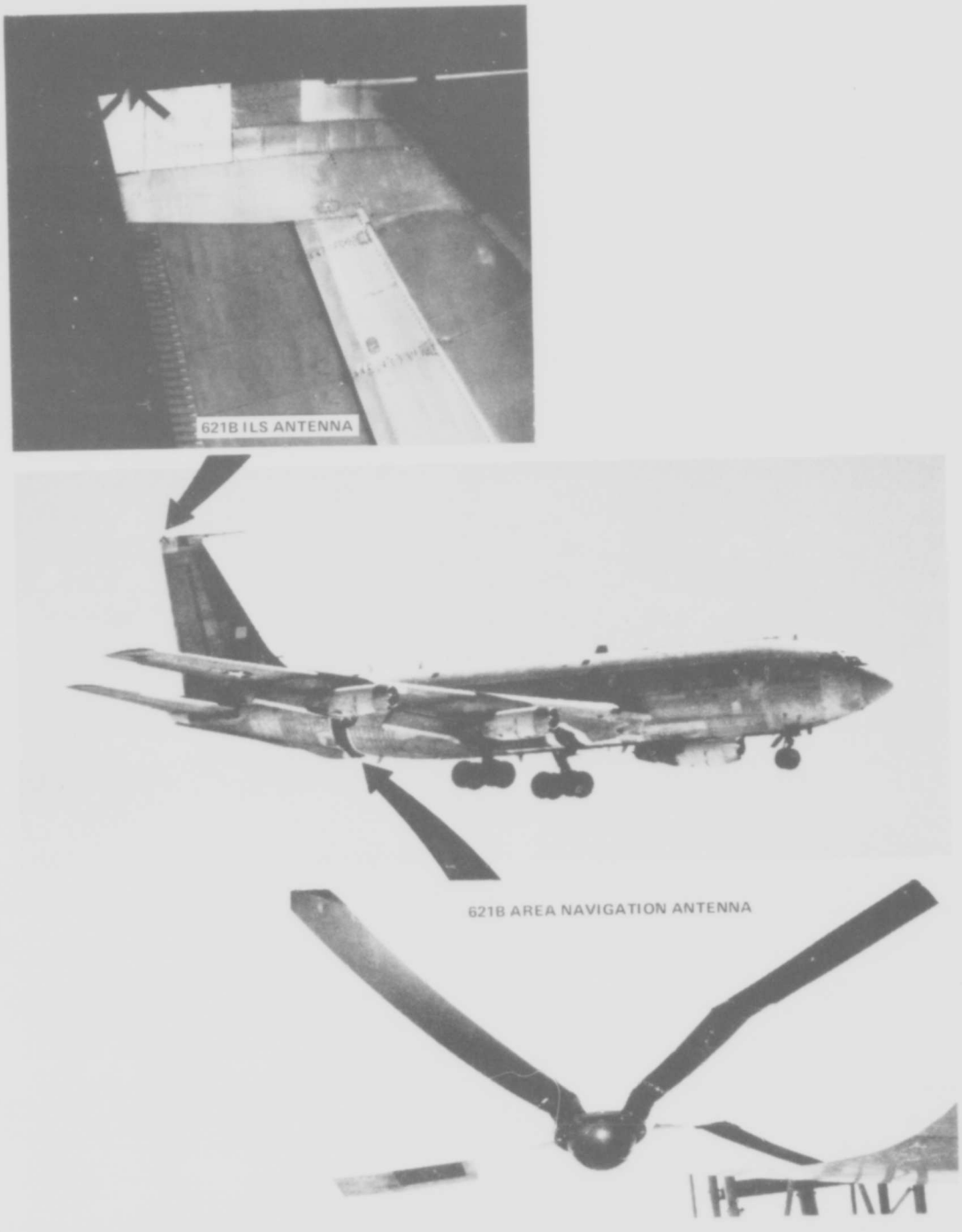

Figure 91 621B Antenna Installation

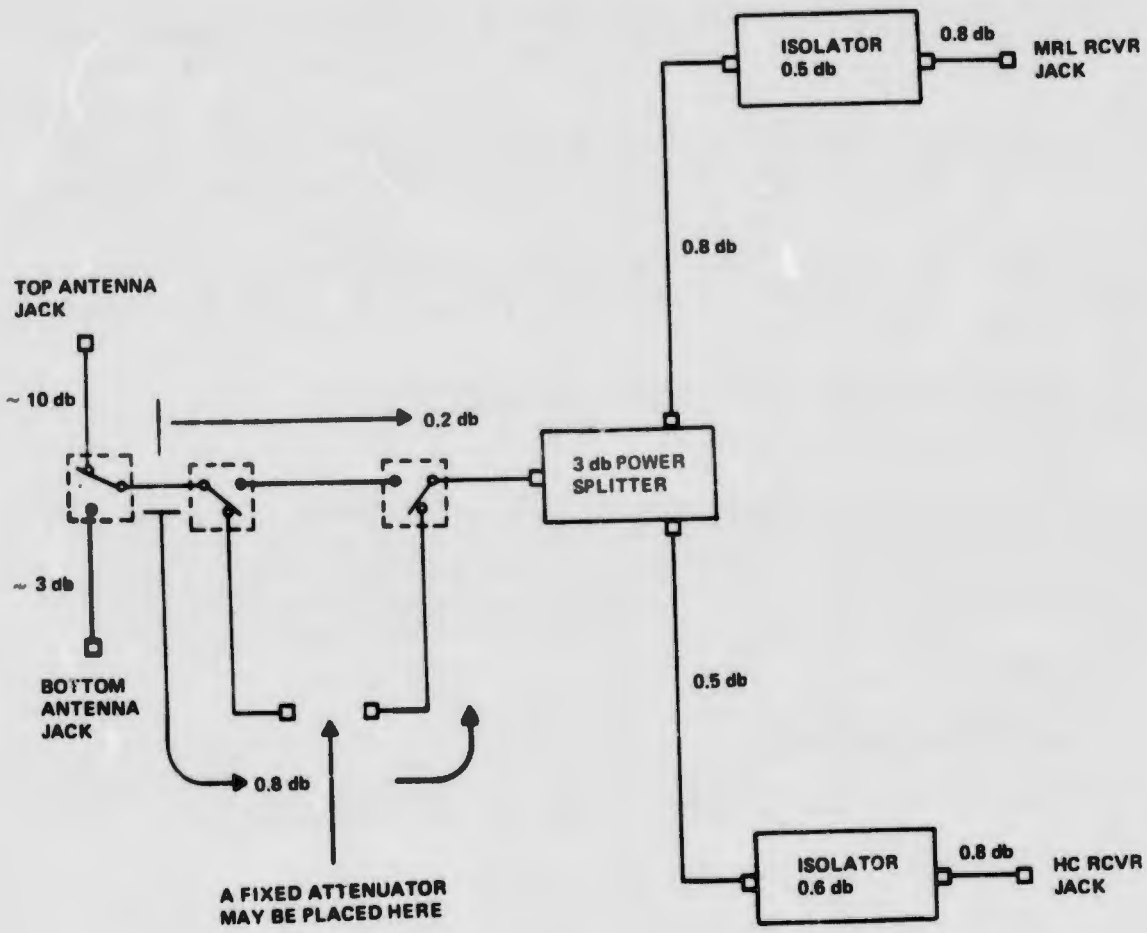

Figure 92 621B Antenna Installation in NC-135A

Table V Total Signal Loss in Antenna System Antenna Jack to Receiver Jack

	Top Antenna		Bottom Antenna	
	Attenuation In	Attenuation Out	Attenuation In	Attenuation Out
HC	16 ± 0.1 db + atten	15.8 ± 0.1 db	8.8 ± 0.1 db + atten	8.1 ± 0.1 db
MRL	16 ± 0.1 db + atten	15.4 ± 0.1 db	9.0 ± 0.1 db + atten	8.4 ± 0.1 db

- Hardware tests which demonstrated individual box and system integrity prior to flight. These include acceptance tests, system integration tests, and preflight readiness tests

- System evaluation tests in simulated operational environments. These include Area Navigation flight tests, ILS type approach and landing navigation flight tests, and ground user multipath tests.

A description of the objectives, methodology, and configurations of these tests is presented to a level sufficient for understanding of test results given in Volume III of this report.

3.5.1 Equipment Test Prior to Flight Evaluation Phase

3.5.1.1 Acceptance Tests

A form of acceptance testing was performed on all the hardware elements in the test system. We called it "readiness" testing to place more emphasis on hardware compatibility of the system and certain aspects of hardware performance thought to be essential to obtaining more valid results than "acceptance" testing normally implies. Test procedures and criteria were developed for the following elements:

- 621B Receivers

- 621B Signal Transmitters

- Controls and Displays for both aircraft and ground equipments

- 621B data interface and control boxes

- Antennas, including those used for aircraft, uplink, and monitor links

- Aircraft and ground mechanical installation kits

- Mobile Calibration Station installation.

The readiness tests were completed for the transmitters, HC ground receiver, MRL receiver, interface and controls, and antennas prior to start of the System Integration Test in December 1971. These tests included:

- For all equipments: Temperature cycling, vibration, functional tests of all controls, mechanical integrity, and EMI.

- For receivers: Signal acquisition, range and range rate measurement accuracy under various signal conditions, and anti-jamming margins

- For transmitters: Signal level output, signal spectral purity, and signal coding composition

- For interface units: Calibrations of analog environment sensors and compatability of data formats to instrumentation recorded

- For antennas: Antenna VSWR, coupling levels between test probe and antenna (where applicable), and antenna radiation patterns.

The HC airborne receiver initially exhibited a deficiency in channel sensitivity to received signal strength, but was found acceptable to waived requirements after modifications were completed. This subject will be discussed in more detail relative to its impact on overall test results in Volume III.

Although the most important figure of merit considered before shipping equipment to the field was how well the system would perform together in a bench environment, it is worth reviewing the pertinent performance characteristics of the receivers alone since they are the heart of the test system. (The bench system behavior will be discussed in paragraph 3.5.2.) Each receiver was required to comply with the following criteria as established during the test program definition phase:

- Maximum Dynamics(1)

	MRL for Measurement Accuracy	HC for Measurement Bias Error
$\dot{R}$ =	7000 ft/sec	3500 ft/sec
$\ddot{R}$ =	175 ft/sec^2	88 ft/sec^2
$\dddot{R}$ =	0 ft/sec^3	0 ft/sec^3

- Maximum dynamics for tracking, $\dddot{R}$ = 320 ft/sec^3
- Measurement accuracies at -140 dbm to -80 dbm
  - Standard deviation: 1σ
  - Pseudo range (each channel): 5 ft
  - Pseudo doppler (each channel): .05 ft/sec
- Measurement Bias Error at -135 dbm to -106 dbm
  - Pseudo range (each channel referenced to channel 4) ± 3ft(max) for HC waived requirement) and ± 0.5 ft (max) for MRL
- Antijam margin for input signal at -130 dbm: 45 db (min)
- Acquisition at -123 dbm
  - Minimum 0.7 probability of lock-on on first try with $\dot{R}$ Zero and 1405 ft/sec
- Maintain Lock
  - Down to -143 dbm with zero dynamics for 1 minute
  - Down to -140 dbm with $\dddot{R}$ = 320 ft/sec^3 for 10 test cycles

(1) Specified limits of $\dot{R}$, $\ddot{R}$, and $\dddot{R}$ are upper limits; none may be exceeded when measurements are required.

- Digitizer Characteristics
  - Pseudo-range resolution (per channel): 0.5 ft
  - Pseudo-range resolution (per channel) counted over 0.1 sec nominal: 0.05 ft/sec
- Output Characteristics
  - Five sets of measurements (i.e., time, pseudo ranges, pseudo range rates) per second.

3.5.1.2 System Integration Test

The System Integration Test (SIT) was designed to demonstrate the system in the laboratory. The test utilized the four transmitters, the airborne system, the MCS, and the software. In addition, the envelope detector (multipath detector) and the stable oscillator delay measurement techniques (used to calibrate ground system), were demonstrated.

The four transmitters were hardwired to the airborne and MCS receivers via cables where the cable rf signal delays were selected to simulate a known position. Airborne and MCS data were recorded, using two different airborne received signal levels, and processed using the software (data flights 47, 48, and 49.) In addition, loss of lock on one channel was demonstrated on data flight 50. The hardwired set-up block diagram is presented in Figure 93 with the coupling control shown in detail in Figure 94.

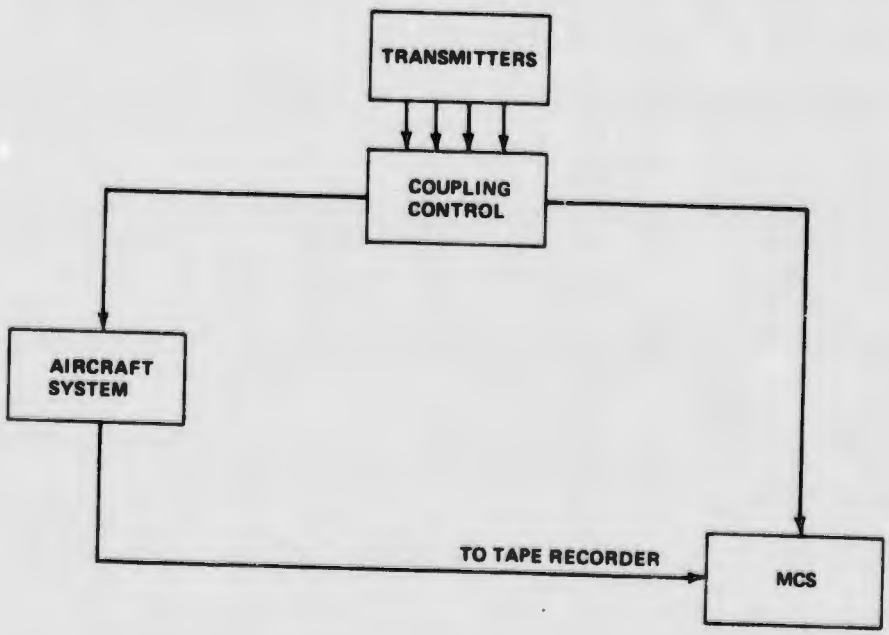

Figure 93 Hardwired Block Diagram

Diagram Symbol	Quantity	Description	Comments
A, $D_1 - D_4$	5	Fixed Attenuator, 60 db	Similar to NARDA #771
A	1	Fixed Attenuator, 40 db	Similar to NARDA #771
A,F	2	Fixed Attenuator, 20 db	Similar to NARDA #771
A,F	2	Fixed Attenuator, 10 db	Similar to NARDA #771
A,F,K,H	4	Fixed Attenuator, 6 db	Similar to NARDA #771
A,F,E,H,L	4	Fixed Attenuator, 3 db	Similar to NARDA #771
A,F,H	6	Fixed Attenuator, 1 db	Similar to NARDA #771
G	1	Line stretcher, 50 ohms	
$C_1 - C_5$	5	Power splitter	
$B_1 - B_2$	2	Hybrid (4 inputs, 1 output)	
J	1	Hybrid (2 inputs, 1 output)	

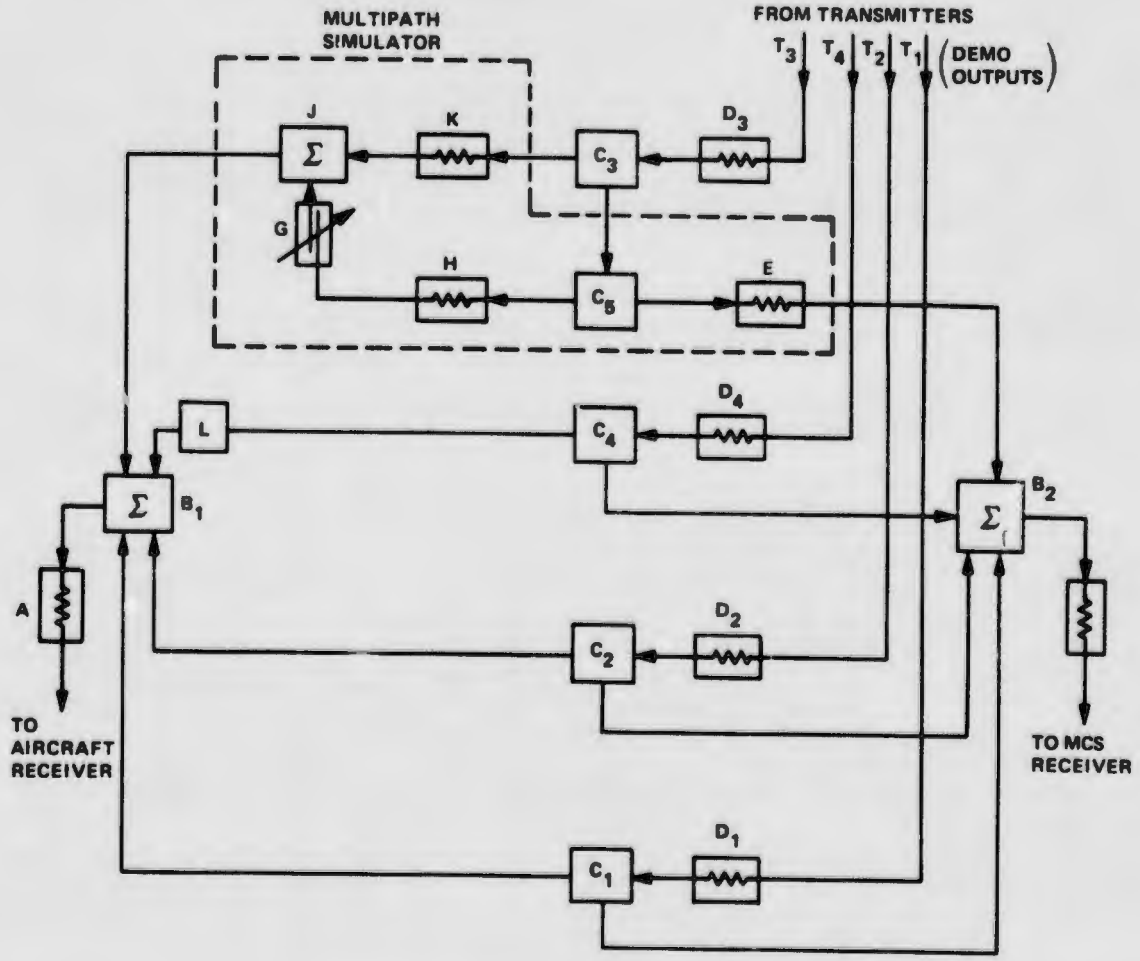

Figure 94 Coupling Control

The hardwired set-up also contained a multipath simulator in the signal path from one transmitter (Figure 94). Three differential delays were set-up and data recorded and processed (data flights 51, 52, and 53). The envelope detector was demonstrated using the multipath simulator. The results indicate that multipath producing as little as 2 nanoseconds tracking error can be detected.

In the radiated test, Figure 95, a radiation link was introduced in place of the hardwired link for one transmitter and system performance evaluated under these conditions (data flight 54).

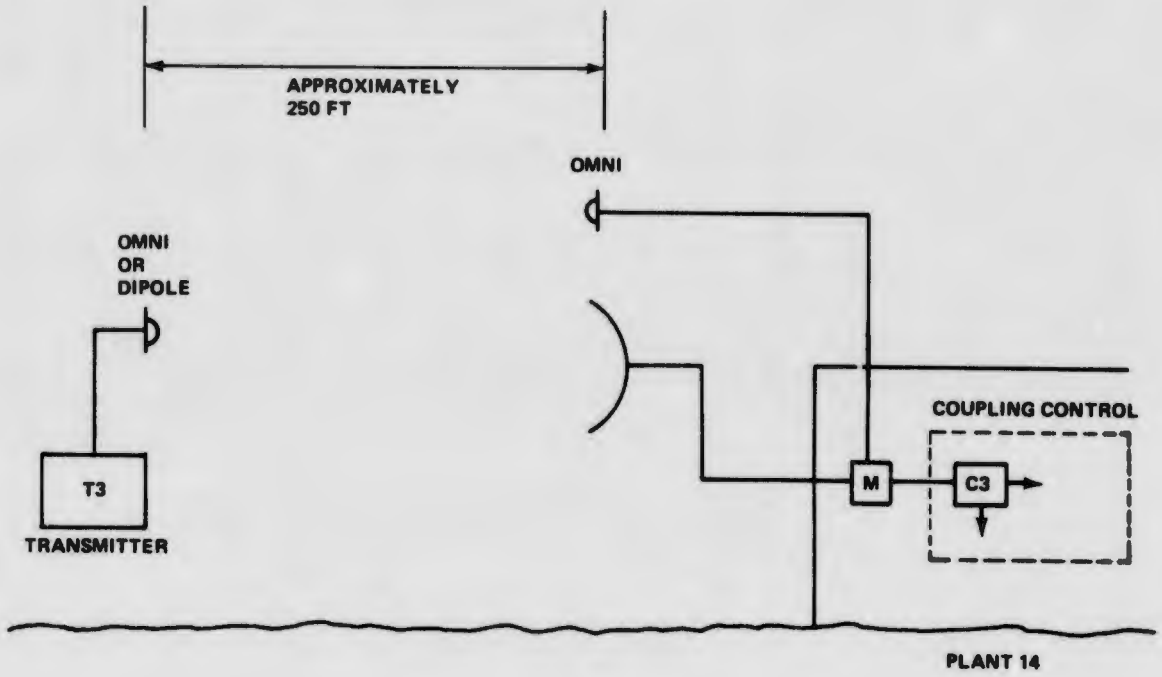

Figure 95 Radiation Link

The envelope detector and stable oscillator delay measurement techniques were demonstrated on the radiation link. The envelope detector was used to observe the multipath effects as one antenna was changed in height. The stable oscillator technique was used to measure the signal delay on the radiated link. The measured value was 181 nanosec while the calculated value was 177 nanosec. (Later in the program the measurement technique was modified to include corrections for cesium drift.)

The primary result of the SIT was a demonstration of the system's ability to work together, produce the appropriate data tapes, and produce a navigation solution with the developed software within a predicted error band. The SIT configuration differed from the eventual WSMR configuration in the following areas:

- Hardwired rf links instead of the transmitter to calibration receiver and transmitter to aircraft WSMR links
- No simulation of aircraft dynamics was attempted
- The software utilized was not completely finalized although the basic solution routines were representative of the final configuration

- The transmitters were driven off a common oscillator instead of using individual oscillators as at WSMR (see below for reason why this was necessary)

- Simultaneous recording of "aircraft" receiver data with calibration receiver data was not possible since only one recording system was available. This meant that the calibration receiver data had to be extrapolated ahead many minutes while the recorder was transferred to the "aircraft" receiver. We decided to use a single oscillator to drive the four transmitters to simplify the data processing and error analysis.

The results of the various SIT tests presented in Table VI show the SIT data to be within the predicted error bands. We were very encouraged by this since the test had some built-in problems and was difficult to conduct. For instance, the solution point was very sensitive to the hardware cable lengths. The cable lengths had been chosen to simulate the aircraft position nominally at X, Y = O and Z = 56 ft using a symmetrical Y transmitter grid. Since the dimensions were so small, minor cable length errors caused large changes in the computed position, or worse, no solution point at all due to physically unrealizable geometry.

3.5.1.3 Flight Readiness Test

To demonstrate an adequate level of system performance before beginning tests to assess system accuracy, a flight readiness test plan was created which defined test procedures and pass/fail criteria. The flight readiness test was considered a major milestone and had to be passed in a specified time period after the start of field testing. These readiness tests were actually separated into three parts:

- Preflight ground system readiness

- Preflight aircraft system readiness

- In-flight system readiness

The preflight ground system readiness consisted of physical completion of site installations, functional tests of equipment in place at the sites, and calibration of appropriate equipment, cabling, and signal paths. The ground readiness test was conducted on Feb. 14 and 15 with the following results.

- Sites were essentially completed with the exception of the dc battery supplies. The battery box installations were in process at the time. The sites were considered satisfactory from an installation standpoint

- Functional checkout of the sites went according to the procedure for the most part. An inability of the receiver to lock on channel A was noted - this was later determined to be the result of misadjustment in the acquisition circuitry which allowed lockup on channel B but not channel A and was not considered a test failure since the receiver only needed to function on one of the channels with the other serving as a backup

- Ground calibrations were not done with the exception of transmitter power output which was satisfactory. Calibrations of signal path length over the ground link by cesium beam techniques (paragraph 3.3.3), envelope detector tests, and cable insertion loss and VSWR checks were yet to be accomplished.

Table VI System Integration Test Summary

Test Description		Criteria for Acceptable Results							Actual Test Results						
			X	Y	Z	$\dot{X}$	$\dot{Y}$	$\dot{Z}$		X	Y	Z	$\dot{X}$	$\dot{Y}$	$\dot{Z}$
Test #1	• Airborne receiver, −123 dbm • MCS receiver, −106 dbm using RF-IF A	μ	0±8ft	0±8	56±12	0±0.1 fps	0±0.1	0±0.1	μ	-3ft	5.2	59	-0.1	0	-0.7
		1σ	2ft	2	5	0.2 fps	0.2	0.5	1σ	1ft	1	3	0.1	0.15	0.8
Test #2	• Airborne receiver, −123 dbm • MCS receiver, −106 dbm using RF-IF B	μ	0±8	0±8	56±12	0±0.1	0±0.1	0±0.1	μ	-3.5	5	60	0	-0.08	-0.3
		1σ	2	2	5	0.2	0.2	0.5	1σ	1	1	3	0.03	0.05	0.2
Test #3	• Airborne receiver, −123 dbm using Channel B, MCS receiver, −106 dbm using RF-IF A	μ	0±8	0±8	56±12	0±0.1	0±0.1	0±0.1	Test only applies to HC airborne receiver and was not attempted due to scheduling constraints						
		1σ	2	2	5	0.2	0.2	0.5							
Test #4	• Airborne receiver, −140 dbm • MCS receiver, −106 dbm using RF-IF A	Not specified for −140 dbm, results should only be consistent with test setup							μ	-7	9	70	0	0.2	-0.9
									1σ	4	4	10	0.4	0.4	0.8
Test #5	• Airborne receiver, −123 dbm • MCS receiver, −106 dbm using RF-IF A	Channel #1 signal is interrupted for 30 sec. Data processing system shall recognize this, give the proper messages, and not attempt a solution													
Test #6	• Airborne receiver, −123 dbm • MCS receiver, −106 dbm • Simulated multipath on Ch. 3, ζ = −0.99 and differential path length = 1 nsec	μ	0±8	-0.3±8	56±12	0±0.1	0±0.1	0±0.1	μ	-3	6.5	60	0	-0.2	-1.0
		1σ	2	2	5	0.2	0.2	0.5	1σ	1	1	3	0.1	0.2	0.5

Test #5

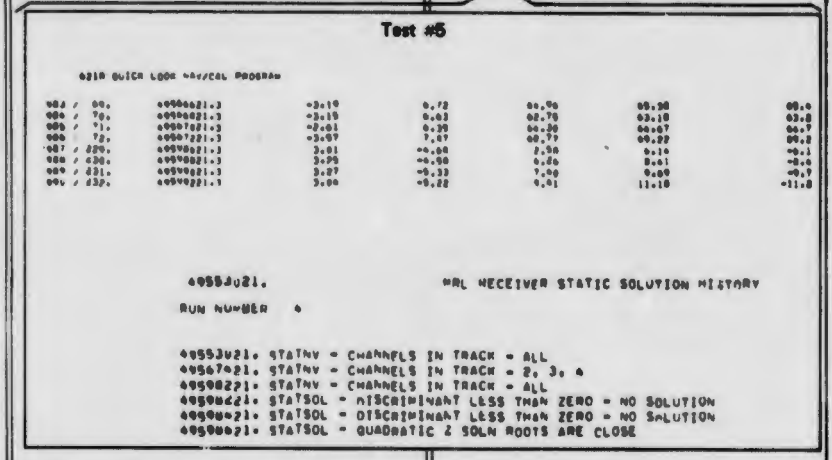

Table VI System Integration Test Summary (Concluded)

Test Description		Criteria for Acceptable Results							Actual Test Results						
			X	Y	Z	$\dot{X}$	$\dot{Y}$	$\dot{Z}$		X	Y	Z	$\dot{X}$	$\dot{Y}$	$\dot{Z}$
Test #7	• Airborne receiver, −140 dbm • MCS receiver, −106 dbm using RF-IF A • Simulated multipath on Ch. 3, ζ = −0.99 and differential path length = 1 nsec	μ	No quantitative criteria for −140 dbm, software shall print appropriate messages indicating correct processing of data						μ	−8	11	70	0	0	1.0
		1σ							1σ	3	3	10	0.3	0.3	1.0
Test #8	• Airborne receiver, −123 dbm • MCS receiver, −106 dbm • Simulated multipath on Ch. 3, ζ = 0.3 and differential path length = 30 nsec	μ	0±8	-6±8	50±12	0±0.1	0±0.1	0±0.1	μ	−3	11	52	0	0.2	-1.0
		1σ	2	2	5	0.2	0.2	0.5	1σ	1	1	2	0.2	0.1	0.5
Test #9	• Airborne receiver, −140 dbm • MCS receiver, −106 dbm • Simulated multipath on Ch. 3, ζ = 0.3 and differential path length = 30 nsec	μ	See comments for Test #7						μ	-9	15	62	-0.2	0	1.7
		1σ							1σ	4	5	11	0.2	0.3	0.5
Test #10	• Airborne receiver, −123 dbm • MCS receiver, −106 dbm • Simulated multipath on Ch. 3, ζ = 0.3 and differential path length = 75 nsec	μ	0±8	-15±8	42±12	0±0.1	0±0.1	0±0.1	μ	-3	16	46	-0.05	-0.14	1.0
		1σ	2	2	5	0.2	0.2	0.5	1σ	1.5	1	2	0.1	0.05	0.4
Test #11	• Airborne receiver, −140 dbm • MCS receiver, −106 dbm • Simulated multipath on Ch. 3, ζ = 0.3 and differential path length = 75 nsec	μ	See comments for Test #7						μ	-6	19	46	0	0.2	-0.2
		1σ							1σ	3	5	6	0.2	0.3	0.8
Test #12	• Airborne receiver, −123 dbm • MCS receiver, −106 dbm • RF link used on Ch. 3 similar to field set up using field antennas	μ	0±8	0±8	56±12	0±0.1	0±0.1	0±0.1	μ	-3	17.8	43	0	0	-0.2
		1σ	2	2	5	0.2	0.2	0.5	1σ	1.5	1	3	0.1	0.3	0.9

Due to the lead time involved in making some of these measurements it was decided to proceed and make the measurements at the earliest possible time. They were accomplished in March before the in-flight readiness decision was made.

The preflight aircraft system readiness test consisted of completion of the aircraft installation, functional test of equipments and quantitative evaluation of receiver accuracy while operating in the self test mode. The test was very straight-forward with both receivers passing during March. A typical output from the quantitative accuracy portion is shown in Figure 96. The passing criteria was range 1σ less than 5 ft and velocity 1σ less than 0.5 fps. The bottom portion of the output indicates the percentage of data points exceeding these limits.

```
                                        FLIGHT NO,  81   03/04/7
                                        DATA PROCESSED  03/06/72

          MAGNAVOX 9218 READINESS TEST
  2  MRL PRE-FLIGHT READINESS TEST

      **********************************
      *                                *
      *  RECEIVER HAS PASSED THIS TEST *
      *                                *
      **********************************

  STATISTICS FROM  808 DATA POINTS

  STANDARD DEVIATIONS ESTIMATED FROM 2ND DIFFERENCES

                          ----------CHANNELS----------
                             1       2       3       4
  RANGE      ( FT )       .693    .560    .519    .664
  VELOCITY (FT/SEC)       .150    .153    .152    .155

  PERCENTAGES OF DIFFERENCES GREATER THAN LIMITS

                          ----------CHANNELS----------
                             1       2       3       4
  RANGE      ( FT )      0.000   0.000   0.000   0.000
  VELOCITY (FT/SEC)      0.000   0.000   0.000   0.000
```

Figure 96 Preflight Readiness Test Results

The in-flight readiness test was accomplished during flight 3, 28 March 1972. The criteria for this readiness test was that the system performance be such that meaningful data analysis could be accomplished. Thus erratic system behavior, unreliable hardware operation, improper control functioning, and other similar phenomena were to have been eliminated prior to passing in-flight readiness. A quantitative measure of performance was arrived at which stated that comparison of the navigation solution trajectory with WSMR derived trajectory should show X and Y coordinates to be within 110 ft and Z coordinates to be within 275 ft. Flight 3 demonstrated this performance. A detailed discussion of these flight results is found in Volume III, paragraph 3.

3.5.2 Flight Test History

In the course of the flight test program 31 flights were recorded. (For a detailed breakdown of these 31 flights see Table VII.) For the purpose of this discussion flights that have similar characteristics are grouped in the following manner in Table VIII.

Flights 1-3 are called shakedown flights because their successful completion was a precondition of the inauguration of the formal flight test program. Equipment was checked out, antenna patterns verified, and test concepts were justified.

Flights 4-15 are called monitor link flights because we used the monitor link dish antennas to complete the ground rf link between the transmitter sites and the MCS. It was discovered that the calibration receiver was able to lockup on the rf signal emanating from the uplink antennas. After looking at the data provided by flights 4-15, it was determined that trajectory accuracy would be enhanced if the monitor links to the MCS were eliminated.

Consequently, flights 17-23 were conducted with the calibration receiver locked on to the uplink antennas. After flight 23 it was determined that the quantity and quality of the trajectory data were sufficient for analysis, and the ground system was reconfigured at Northrop Strip to begin ILS flights. On 2 Aug. 1972 the MCS was installed at Northrop Strip and the ILS test configuration was completed.

Flights 24-27 were low altitude passes over the runway. The equipment was the same as the Area Navigation Tests but new antenna patterns and test concepts were verified by these initial aircraft passes. Permission for the NC-135A to land on the Salt Flats was given, and flights 28-31 simulate most closely a true ILS trajectory. During the latter ILS flights the test system was exercised during aircraft sink, flare, touchdown, and roll out; these are the critical parameters necessary to evaluate 621B as a possible instrumented landing system.

3.5.3 Area Navigation Tests

The environment for these tests was chosen to simulate a typical user performing area navigation. Within the limitations of the test environment, such as lack of realistic satellite emphermeris errors and ionospheric signal disturbances (see paragraph 3.1), the system concept has been verified using real hardware, and system performance has been established for the test configuration.

Flt. No.	Date	OD No.	Flight Profiles	Data Runs	Non-Data Runs	Receiver Status (MRL, HAZ, CAL)	Recorder Status (GFE)	XMTTR Status (HC)	IU Status (GAC)
1.	3/7/72	04	A,C,Descent	0	9	CAL NO-GO	LTN-51 Recorder No-Go	Okay	A/D Converter Malfunctioned
2.	3/21/72	04	A,C,Descent	0	6	MRL,HAZ. NO-Go*	*MRL,HAZ Recorders No-Go	Okay	Okay
3.	3/28/72	04	A,C,Descent	11	1	MRL GO HAZ GO* CAL GO	*HAZ Recorder No-Go	Okay	Okay
4.	4/5/72	04	A,C,Descent	9	0	MRL GO HAZ NO-GO	Okay	Okay	Okay
5.	4/7/72	02	A,B,C,Descent	0	9	MRL GO HAZ GO CAL GO*	*CAL MAG Tape Ruined	Okay	Okay
6.	4/12/72	07	A,C,D,Ascent	0	7	CAL No-Go	LTN Recorder No-Go	Okay	Okay
7.	4/13/72	01	A,B',C,Descent, Orbit	4	5	CAL (No-Go Runs 5-9)	Okay	Okay	Okay
8.	4/27/72	02	A,B',C,Descent	12	0	MRL GO HAZ GO (HAZ In MCS) CAL No-Go	Analog No-Go	Okay	Okay
9.	5/1/72	04	A,C,Descent	9	0	MRL GO HAZ NO-GO CAL GO	Okay	Okay	Okay
10.	5/4/72	04	A,C,Descent Runs 8&9 Ran Perpendicular to A path	9	0	Okay	Okay	Okay	Okay
11.	5/9/72	08	D,Ascent	5	1	Okay	Okay	Okay	Okay
12.	5/10/72	08	C,Ascent	0	8	MRL GO CAL-No-Go HAZ GO*	*HAZ Recorder No-Go	Okay	Okay
13.	5/13/72	06	Cloverleaf, 90 degree turns	8	0	MRL GO HAZ-No-Go CAL GO	Okay	Okay	Okay
14.	5/17/72	03	A, B, C, Ascent	12	1	MRL GO HAZ-No-Go CAL GO	Okay	Okay	Okay
15.	5/19/72	05	B; Clouds forced A/C to fly at 24K' MSL. (This was a deviation)	13	0	Okay	Okay	Okay	Okay
16.	6/7/72	04	A/C Did Not Take-Off	0	0	–	–	–	–
17.	6/14/72	08	A,B'	2	5	CAL-No-Go	Okay	Okay	Okay

*Recorder failure

–Flights resulting in no data

**Flight 16 is a mismomer, the mission was cancelled just prior to takeoff

***Flights producing good quality 621B data, but satisfying duplicate test points

Table VII Detailed Flight Breakdown

Data Runs	Non-Data Runs	Receiver Status (MRL, HAZ, CAL)	Recorder Status (GFE)	XMTTR Status (HC)	IU Status (GAC)	Sensors Used In BET (WSMR)	Quality of BETS (WSMR)	Test Points Fulfilled
0	9	CAL NO-GO	LTN-51 Recorder No-Go	Okay	A/D Converter Malfunctioned	N/A	–	1,2,3,6,7
0	6	MRL,HAZ. NO-Go*	*MRL,HAZ Recorders No-Go	Okay	Okay	N/A	–	–
11	1	MRL GO HAZ GO* CAL GO	*HAZ Recorder No-Go	Okay	Okay	Optics, Radar	Poor- (Tgt. Uncertain)	4,9,10
9	0	MRL GO HAZ NO-GO	Okay	Okay	Okay	Optics, DOVAP, LTN-51	Poor (Tgt. Uncertain)	***
0	9	MRL GO HAZ GO CAL GO*	*CAL MAG Tape Ruined	Okay	Okay	–	–	8***
0	7	CAL No-Go	LTN Recorder No-Go	Okay	Okay	–	–	–
4	5	CAL (No-Go Runs 5-9)	Okay	Okay	Okay	DOVAP, LTN-51	Fair	5
12	0	MRL GO HAZ GO (HAZ In MCS) CAL No-Go	Analog No-Go	Okay	Okay	Optics, DOVAP LTN-51	Good	***
9	0	MRL GO HAZ NO-GO CAL GO	Okay	Okay	Okay	DOVAP, LTN-51	Fair	14,19,20,15, 16,21,22
9	0	Okay	Okay	Okay	Okay	Optics, DOVAP, LTN-51, Radar	Good	55,56,72,73, 57,58
5	1	Okay	Okay	Okay	Okay	Optics, DOVAP	Poor (Low Altitude)	35,36,77,41
0	8	MRL GO CAL-No-Go HAZ GO*	*HAZ Recorder No-Go	Okay	Okay	–	–	–
8	0	MRL GO HAZ-No-Go CAL GO	Okay	Okay	Okay	Optics, DOVAP	Good	76,63,61,62 89,88
12	1	MRL GO HAZ-No-Go CAL GO	Okay	Okay	Okay	DOVAP, LTN-51	Fair	66,67,42,29, 30,27,33,17, 18,23,24
13	0	Okay	Okay	Okay	Okay	Optics, LTN-51 Radar	Fair	***
0	0	–	–	–	–	–	–	–
2	5	CAL-No-Go	Okay	Okay	Okay	DOVAP LTN-51	Fair	92,93

rior to takeoff
duplicate test points

Flt. No.	Date	OD No.	Flight Profiles	Data Runs	Non-Data Runs	Receiver Status	Recorder Status (GFE)	XMTTR Status	IU Status	Sensors in BET
18.	6/20/72	04	A,C	7	0	Okay	Okay	Okay	Okay	Optics, D LTN-51
19.	6/22/72	04	A,Descent	7	1	Okay	Okay	Okay	Okay	Optics, D LTN-51
20.	6/26/72	04	A	12	0	CAL GO MRL-No-Go (CH2) HAZ GO	Okay	Okay	Okay	Optics, D LTN-51
21.	6/28/72	03	D(A/C Hit Buzzard and Aborted Mission)	0	1	–	–	–	–	–
22.	7/27/72	05	B	12	2	Okay	Okay	Okay	Okay	Optics, D LTN-51
23.	8/1/72	07	D	4	5	MRL GO HAZ GO CAL (No-Go, Runs 7-9)	Okay	Okay	Okay	Optics, D LTN-51
24.	8/16/72	09	ILS/Fly By	0	5	MRL GO HAZ (In MCS) GO	Okay	Okay	Okay	–
25.	8/18/72	09	ILS/Fly By	8	2	Okay	*HAZ Primary No-Go, HAZ Secondary OK	Okay	Okay	Optics
26.	9/20/72	09	ILS/Fly By	0	4	HAZ&MRL Could Not Lock. CAL did lock	Okay	CH 2 No-Go	Okay	–
27.	9/25/72	09	ILS/Fly By	8	4	MRL Go Haz-No-Go	Okay	Okay	Okay	Optics
28.	9/27/72	09	ILS/Touchdown	0	12	MRL GO HAZ-No-Go CAL GO	*MRL-Recorder No-Go	Okay	Okay	–
29.	9/28/72	09	ILS/Touchdown	6	0	MRL GO HAZ-No-Go CAL GO	Okay	Okay	Okay	Optics
	9/29/72	09	ILS/Touchdown	2	1	Okay	Okay	CH 4 Battery Depleted	Okay	Optics
31.	9/30/72	09	ILS/Touchdown	7	1	MRL GO HAZ GO* CAL Power Supply Malfunctioned After Run 7	*HAZ-Recorder Malfunction (No HAZ Secondary Recorder)	Okay	Okay	Optics

NOTES:

*Recorder failure

–Flights resulting in no data

***Flights producing good quality 621B data, but satisfying duplicate test points

Table VII Detailed Flight Breakdown (Concluded)

Data Runs	Non-Data Runs	Receiver Status	Recorder Status (GFE)	XMTTR Status	IU Status	Sensors Used in BET	Optimum BETS	Test Points Fulfilled
7	0	Okay	Okay	Okay	Okay	Optics, DOVAP, LTN-51	Good	•••
7	1	Okay	Okay	Okay	Okay	Optics, DOVAP, LTN-51	Good	13,26,65,69, 43,83
12	0	CAL GO MRL-No-Go (CH2) HAZ GO	Okay	Okay	Okay	Optics, DOVAP, LTN-51	Good	31,32,64
0	1	–	–	–	–	–	–	–
12	2	Okay	Okay	Okay	Okay	Optics, DOVAP, LTN-51	Poor (Bad Optics)	59,75,96,68, 100,101,38,60
4	5	MRL GO HAZ GO CAL (No-Go, Runs 7-9)	Okay	Okay	Okay	Optics, DOVAP, LTN-51	Poor (Bad Optics Low Altitude)	28,51,80
0	5	MRL GO HAZ (In MCS) GO	Okay	Okay	Okay	–	–	–
8	2	Okay	*HAZ Primary No-Go, HAZ Secondary OK	Okay	Okay	Optics	Good	1,4,5,3 (ILS)
0	4	HAZ&MRL Could Not Lock. CAL did lock	Okay	CH 2 No-Go	Okay	–	–	–
8	4	MRL Go Haz-No-Go	Okay	Okay	Okay	Optics	Poor	•••
0	12	MRL GO HAZ-No-Go CAL GO	*MRL-Recorder No-Go	Okay	Okay	–	–	–
6	0	MRL GO HAZ-No-Go CAL GO	Okay	Okay	Okay	Optics	Poor	6,7,8,9 (ILS)
2	1	Okay	Okay	CH 4 Battery Depleted	Okay	Optics	Poor	10 (ILS)
7	1	MRL GO HAZ GO* CAL Power Supply Malfunctioned After Run 7	*HAZ-Recorder Malfunction (No HAZ Secondary Recorder)	Okay	Okay	Optics	Good	11,15,16 (ILS)

t satisfying duplicate test points

Table VIII Flight Categories

Flight Type	Flight No.
Shakedown	1 – 3
Area Nav on Monitor Link	4 – 15
**	
Area Nav on Uplink	17 – 23
ILS Fly By	24 – 27
ILS Touchdown	28 – 31

**Flight 16 is not included in the above categorization because of an aircraft abort.

3.5.3.1 Flight Profiles

The specific objectives of the Area Navigation Test were:

- Establish the range and range-rate accuracy of a four-channel receiver in an airborne environment
- Determine the effects of the aircraft flight environment on the receiver and airborne antenna performance
- Determine the effects of various aircraft-to-simulated satellite transmitter geometries on system performance including acquisition
- Evaluate the effects of different signal power levels on system performance.

To achieve the test objectives, a series of flight profiles along with various test procedures were established. Individual tests (called test points) were defined and a comprehensive flight test program evolved to accomplish all the test points. The flight profiles described here were used for a majority of the flights. In addition, special tests were added in order to resolve questions about the ground antenna pointing angles, and to gather additional data on alterations of the ground equipment configuration.

Table IX shows the major features of the Area Navigation Test compared to area navigation in the operational system.

The Area Navigation Test utilized four basic flight profiles for a majority of the tests. The four flight paths are summarized below:

Flight Path A

The A flight path, simulating a rotating 30^{o} satellite configuration as seen from the equator, covers a ground track over Salt Site with a heading of 0^{o} True North or 180^{o} True North, at an altitude of 34,000 ft MSL straight and level. The 20 mi flight path has the following terminal points:

Table IX System Demonstration Test Configuration Characteristics

Parameters	Range of Values Expected in Actual System Configuration	Range of Values Which Were Tested in Simulation Configuration
Signal Power Level	−120 dbm to −135 dbm	−100 dbm to −140 dbm
Satellite/User Dynamics		
$\dot{R}$, ft/sec	± 4000	± 700
$\ddot{R}$, ft/sec^2	± 200	± 1640
$\dddot{R}$, ft/sec^3	± 300	± 3300
Satellite Configuration and Orbit Parameters	Y, Eggbeater	Y, Eggbeater
Satellite/User LOS (worst case)	10° (Demo) 40° (ILS)	10° (Demo) 40° (ILS)
GDOP	1 to 6	1.5 to 13

WSTM X = 491,000 and X = 491,000
Y = 508,000 Y = 388,000

Flight Path B

The B flight path simulating a rotating 30° Y satellite configuration as seen from the continental United States, covers a ground track east of the transmitter Y configuration. The ground track is 5260 ft southeast of EC-50 and Bomb (SC-50) sites, heading of 43° True North and 223° True North flown in both directions at an altitude of 34,000 ft MSL. The 20 mi flight path has the following terminal points:

WSTM X = 549,500 to X = 446,500
Y = 484,500 Y = 395,000

The center of the flight path is located at:

X = 508,000
Y = 440,000

Flight Path C

The C flight path covers the same ground track as that of the A flight path but at an altitude of 22,000 ft MSL. The 20 mi flight path has the same terminal points as the A flight path. This flight path represents the GDOP and power profile of an "Eggbeater" satellite configuration.

Flight Path D

The D flight path covers the same ground tract as that of the A flight path but at an altitude of 7000 ft MSL. The 20 mi flight path has the same terminal points

and headings as the A flight path. This flight path objective is to exercise dynamics of the system in R, $\dot{R}$, $\ddot{R}$ and $\dddot{R}$. One version of the D flight path is to fly over one channel at 300 ft AGL on the A ground track to measure $\dot{R}$ lock-up capabilities. Figure 97 shows a typical flight profile diagram.

3.5.2.3 Test Techniques

Area navigation testing was accomplished during flights 1-23. Two major configurations were used. The first configuration used both the monitor and uplink outputs of the transmitter (Figure 54) during flights 1-15, and the second configuration used only the transmitter uplink output (Figure 55) during flights 17-23. Flights 17-23 repeated many of the tests conducted earlier to gain comparison data on the second configuration.

In general, a test flight lasted two hours and collected 20 minutes of test data on each receiver. A view of the emphasis placed on various aspects of the test can be seen in Figure 98. Primary emphasis was on obtaining data in good geometry regions at signal levels of -123 dbm. Each number represents a test condition specified in the test point table. These conditions were established by changing flight profiles and equipment operating modes. A single data run, approximately three minutes, was used to meet a single test condition. The circled numbers show test conditions which were accomplished during the field tests.

In order to stabilize the equipment oscillators, each oscillator was turned on a day prior to the test. On the average, this meant the oscillators were operating from 12 to 20 hours before collecting test data. In addition, preflight activity started a minimum of four hours prior to the test insuring that equipment had ample time to warm up.

A typical flight test was conducted in the following sequence:

- Preflight
  - Briefings to WSMR, contractor and flight personnel beginning a day prior to the test
  - Preflight checkout of WSMR instrumentation, ground system, and aircraft systems beginning four hours prior to test
  - Equipment status checks and decisions to go ahead with test approximately one hour before test
- Flight
  - Aircraft penetrates range airspace within five minutes of start of assigned test time block
  - All status checks completed at one minute prior to first run (and all subsequent runs) with a decision to proceed with test or hold
  - Receiver acquisition is expected on all channels within ten seconds of the start of a run. Some flight profiles were worse in this respect due to antenna coverage. In all cases acquisition was achieved before the aircraft reached the good geometry regions

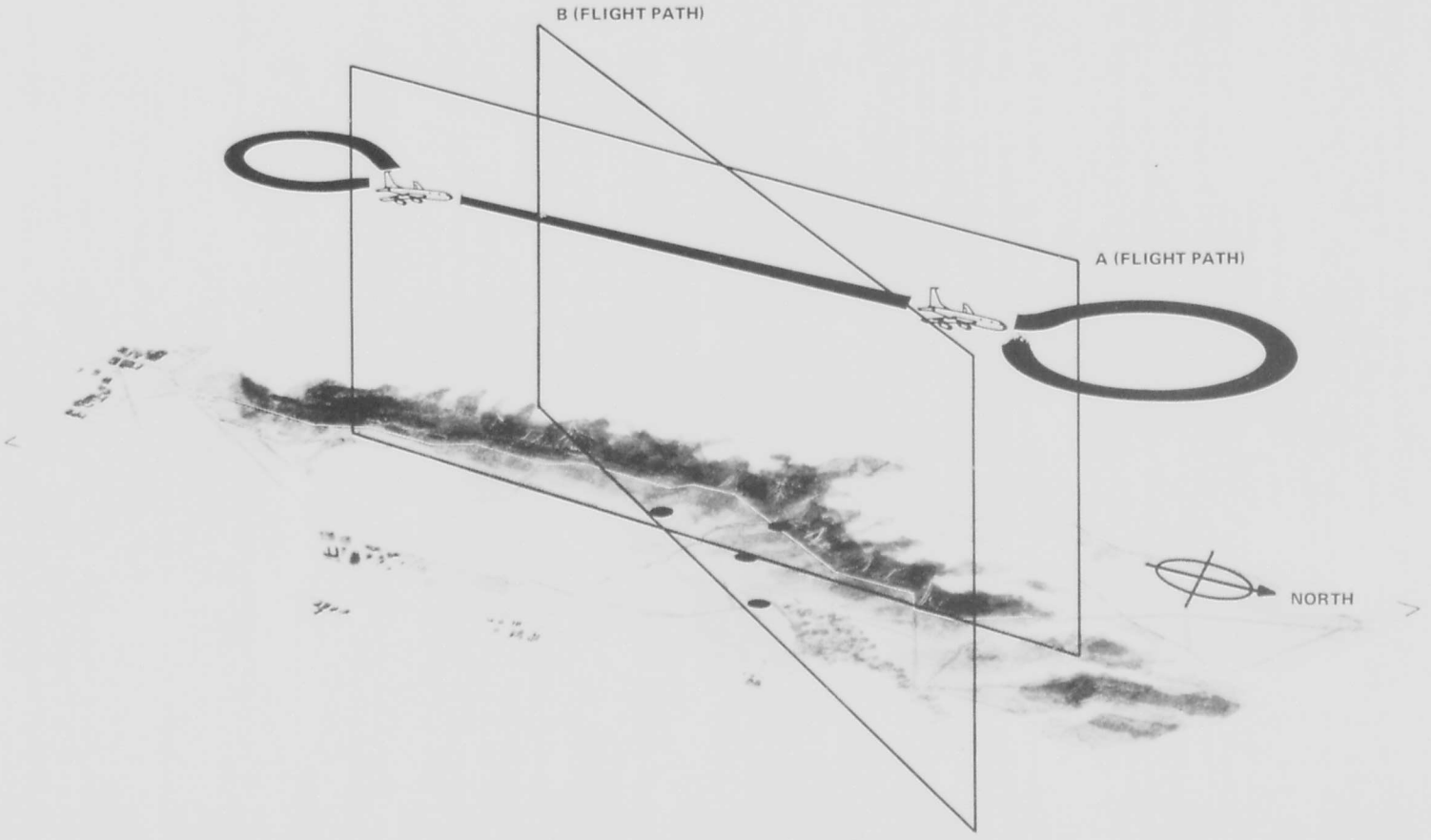

Figure 97 Typical Flight Profiles Centered at Salt

Flight Geometry	Test Points @ −123 dbm	Test Points @ −133 dbm	Test Points @ −136 dbm	Test Points with Other Special Conditions
Type A Profile	(1) (2) (3) (4) (5) (9) (10) (13) (14) (19) (20) (38) (39) (55) (56) (72) (73) 90, (92) (93)	(26) (29) (30) (31) (32) (64) (65) (69) 81, 82	(27) (33) 70, 71, 84, 98, 99	25, 47, 48, 49, 50
Type B Profile	(8) (17) (18) (23) (24) (59) (60) (75) (96) 97	(68)	(100) (101)	
Type C Profile	(6) (7) (15) (16) (21) (22) (57) (58) 74, 91, 94, 95	(66) (67) 83	85	
Type D Profile	(28) (36) (77) (80)	34, 53, 86, 87	37, 54	(51) 52
Other Than Above Type Profile	11, 12, 35, 40, (41) 46, (61) (62) (63) (76) 78, 79, (88) (89)	(42) 44	(43) 45	

(○) INDICATES SUCCESSFUL COMPLETION OF TEST POINT

REFER TO TEST POINT LIST IN GENERAL TEST PLAN FOR DETAILED EXPLANATION OF TEST POINTS

Figure 98 Planned Flight Geometry Vs Power Level

- If low signal level was desired, the aircraft attenuator was switched into the antenna line after acquisition
- WSMR tracking instrumentation starts approximately ten seconds prior to good geometry region and is off at the other end of the good region. For area navigation tests this amounts to data collection + 5 n mi of grid center or 90 seconds of time correlated test system and WSMR data
- Aircraft completes testing within five minutes of the end of the assigned test block

• Post-Flight

- Debriefings held within three hours of flight
- Data processing requests are generated and processing is begun within six hours of flight
- Data reviews of flight accomplishments and equipment performance, debriefing information, and recorded measurements (if possible) are accomplished and plans for the next flight, and associated equipment maintenance and preparation are completed

The internal calibration features of each receiver were used on every flight. The procedure used was:

- Hazeltine airborne receiver - self test cycle recorded before each data run
- Hazeltine calibration receiver - self test cycle recorded at least three times during the flight
- MRL airborne receiver - self test cycle recorded before the first data run.

The calibration cycle data established receiver performance for each flight on channel delay mismatch data and on channel signal level monitoring devices. This information was used in the data reduction phase to correct navigation measurements.

Aircraft flight trajectory was coordinated from the gound. A flight controller provided radar vectors to the aircraft based on the flight profiles scheduled for the mission. The flight controller together with the WSMR tracking instrumentation controller and a representative from the test program formed the test coordination nucleus. Communications channels connecting this group with the aircraft and the ground system personnel at the MCS provided for effective test control.

During the course of the program many modifications were made to the basic approach. We started out with our ground preflight six hours before flight time and were able to shorten this to four hours. Similarly the aircraft preflight was shortened from four to two hours. We were able to identify the types of failures which could be handled in a preflight. These included items such as:

- Inoperative transmitter - generally resolved as loose internal connections, or bad battery power supply
- Missing data from the receivers - generally caused by poor connections, sometimes shorts were found in subminiature coax connectors and temporary fixes accomplished.

Certain items were identified which could not be fixed in preflight:

- Failed oscillators or elements in frequency generation circuitry - this type of failure could not be fixed in the field and had to be returned to the factory
- Bad supply voltages from receiver supplies
- Inability of a processor to lock onto self test signals - occasionally this problem could be fixed in preflight, but generally required the equipment to be removed and fixed in the lab.

The weather was a factor due to our requirement to have optical tracking. Much of our flying was done at 34,000 ft MSL and high cloud layers would cause real trouble for the WSMR optical trackers. The weather forecast would often look much worse than what actually occurred during the flight. There was great temptation to cancel some flights due to poor weather, but waiting the situation out usually proved to be the right decision.

General improvements in the test operation occurred. Initially, it was difficult to obtain decent data. Problems occurred in all equipments from the receivers to data recorders, and occassionally even aircraft problems. However, this situation gradually improved as the test installations became better understood. Unfortunately, much data was lost due to failures in equipment areas not specifically being evaluated, for example loose connections, faulty environmental control equipment (a blower failed), and recorder equipment failures. These failures were most frustrating since finding causes and making the appropriate fix did not contribute to the understanding of the system being evaluated.

3.5.4 ILS Tests

Eight simulated ILS missions were performed at Northrop Strip, White Sands Missile Range, New Mexico to determine the navigation system performance for use in an all-weather ILS landing system.

Two missions were flown to evaluate antenna coverage and transmitter-receiver functions. The remaining six ILS profiles flown included touchdowns and roll out runs measuring the system performance under actual ILS approach conditions. The flight testing closely followed the flight test plan for ILS (Ref. 20). The eight missions, numbers 24 through 31, that were flown at Northrop Strip, started 16 Aug. 1972 and ended 30 Sept. 1972.

3.5.4.1 Flight Profile and Limitations

The airstrip, approach, balloon and ground transmitters were established as shown in Figures 56 and 99. The airstrip and approach markings simulated an instrument (IFR) runway configuration for United States Civil Airports (Ref. 21 and 22). Certain elements of the approach differed from that of a Category II approach for no electronic marker system was used. The differences are as follows:

- No inner marker, middle marker or outer marker beacons were used; visual aids along the glide slope ground path (Figure 100) were substituted
- No localizer beacon was used; runway edge markings were substituted
- No threshold or decision lights were used; approach markings, threshold and end of runway markings were used
- No glide slope transmitter was used; an optical landing aid and theodolite were substituted

The configuration parameters that were kept the same were:

- 1000 ft cleared before and after the runway
- Distance from flare to touchdown held to 1914 ft as per Ref. 23 (Figure 101)
- Position of middle and outer marker same as Category II
- 2.5^{o} glide slope projected to aircraft via use of Fresnel lens optical landing aid and by use of manned theodolite

Figure 99 ILS Flight Profiles

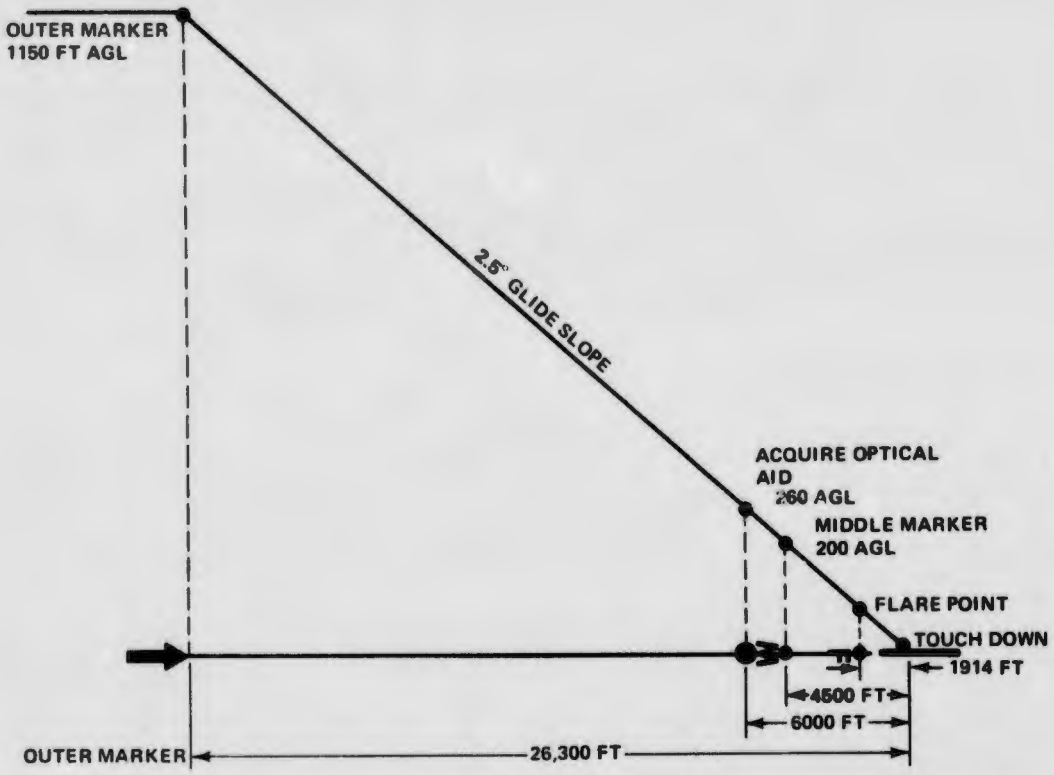

Figure 100 Glide Slope and Approach Markings at Northrop Strip WSMR

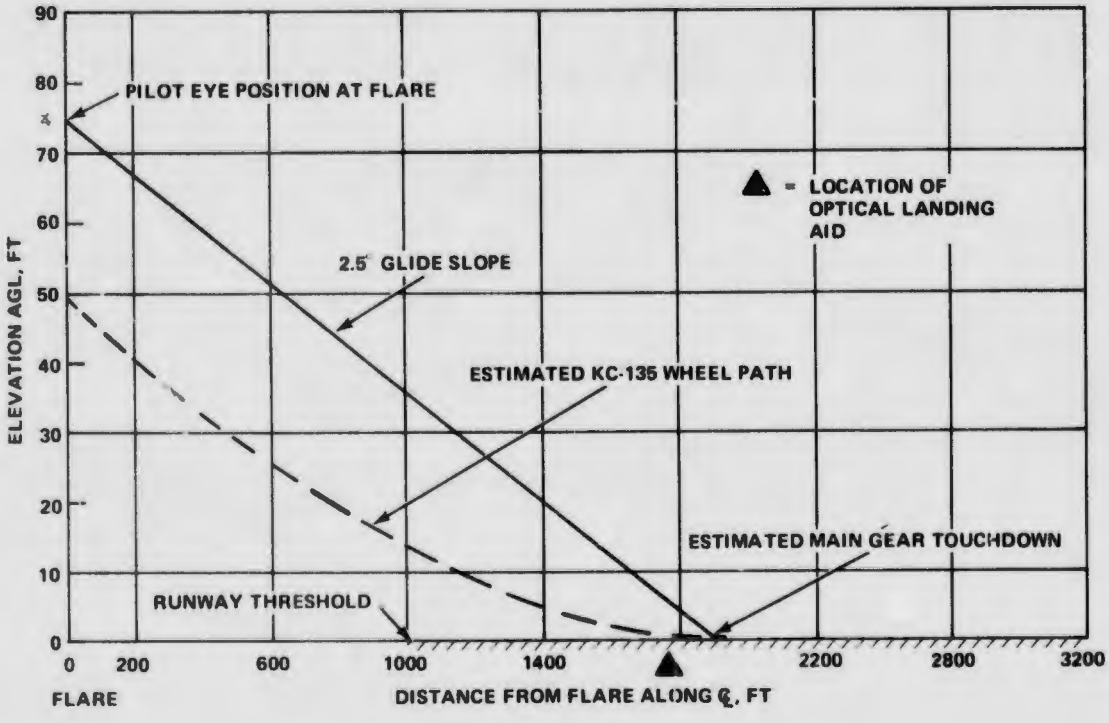

Figure 101 621B Flare to Touchdown Geometry for KC-135 Aircraft on Category II Landing

Runway and approach marking consisted of; an outer marker made from plywood painted red, shaped into an arrow 24 ft long; middle marker made to look like the letter "M" 24 ft high drawn with black road surfacing oil; optical landing aid marker, a circle 24 ft in diameter drawn with black oil; flare point, marked with the letter "F" in black oil; threshold marker and end of runway marker, a strip of black oil across the 150 ft runway noting the formal runway terminal points; runway edge markers, 7 ft wide strips of black oil 50 ft long running on both sides of the runway for 10,000 ft. The runway surface was prepared for the mission by grading and rolling the 12,000 ft airstrip surface before flights 24 and 26. It was necessary to grade the runway twice because of heavy rains experienced at Northrop Strip during the period between flights 24 and 26. Figures 102 and 103 show the flooding caused by heavy rains that delayed the ILS portion of the flight test program.

Figure 102 Flooded Northrop Strip Access Roads

Figure 103 Flooded Balloon Launch Pad and Northrop Strip

3.5.4.2 Balloon Operations

The ILS test performed at Northrop Strip utilized a transmitter suspended from a 45,000 cu ft, helium filled balloon. The purpose of raising a transmitter 5000 ft AGL and placing it in a specific orientation with relation to the rest of the transmitters was to optimize the geometry (GDOP) in the Z (the elevation) axis about the flare point (see paragraph 3.1).

The launching, maintenance and operation of the balloon was the responsibility of the AF Cambridge Research Lab (AFCRL). In Jan. 1972 a test inflation and flight of the balloon and transmitter was performed. The transmitter, balloon control package and radar transponder was suspended from the balloon load bar and flown at 2500 ft AGL. The electronics were removed from within the transmitter case for this first flight and replaced with lead plates having the same mass. This checkout flight proved the equipment was satisfactory for ILS mission.

ILS missions were flown from Aug. 1972 to Sept. 1972. During that time of year, weather played an important role in balloon operations. Inflation and launch could not be accomplished if:

- Surface winds exceeded 10 kt for inflation, 20 kt for launch
- Poor weather forecast, i.e., wind and/or rain
- Air space not cleared by the range
- Not enough daylight hours to complete effort-approximately two hours.

Thunder storms in the area of Northrop Strip were troublesome. The balloon launch pad was covered with water as a result of unusually heavy rains on one occasion, which caused the launch to be delayed. Lightning struck the balloon during a storm which destroyed the balloon telemetry package and tore 3-in. holes in the balloon fabric while the balloon was moored at 500 ft AGL. Storms in that area were unpredictable and grew very rapidly.

Under normal conditions the balloon was inflated and launched in about two hours. Once the load bar and telemetry package were installed, the transmitter and radar transponder was mounted and checked out. The balloon was then transferred from its mooring line to the motorized winch and raised to its desired altitude. The winch was positioned so that the balloon's ground projection was about 1000 ft west of the runway centerline, for safety of flight reasons, and in the area of transmitter pad BTR to keep it in line with the flare point. Communications with the balloon ground crew was accomplished by land line intercoms between the balloon van and MCS van. The transmitter was commanded on and off at the request of test personnel. At the conclusion of the mission the balloon was reeled down, transmitter and transponder removed and the balloon was transferred back to its mooring line. The balloon was deflated only if schedule holds of more than a few days were predicted. It was felt that the balloon should be moored at 500 ft AGL on a separate mooring cable, for the cable used by the winch was light, so as to increase the payload carrying capacity of the balloon at high altitudes. The mooring line was quite heavy, increasing the safety margin over that of the winch cable line at low altitudes. The 621B equipment was removed at the end of each mission to minimize possible damage from lightning or other natural disasters.

3.5.4.3 Test Techniques

The test techniques employed strived to simulate a realistic ILS environment and collect all the necessary data required to evaluate the system performance. Accurate aircraft position data were required from about 4000 ft before the flare point to approximately 6000 ft beyond. The position data collected by the system was then compared to the position data collected by WSMR instrumentation - the BET. WSMR utilized cinetheodolites to derive the BET for ILS. The following techniques were employed to develop an aircraft approach that was both predictable and repeatable:

- The airstrip and approach markings were constructed so as to guide the pilot down a nominal 2.5° glide slope
- An approach plate integrating the airstrip approach markings and glide slope was given to each pilot at preflight briefings, Figure 104

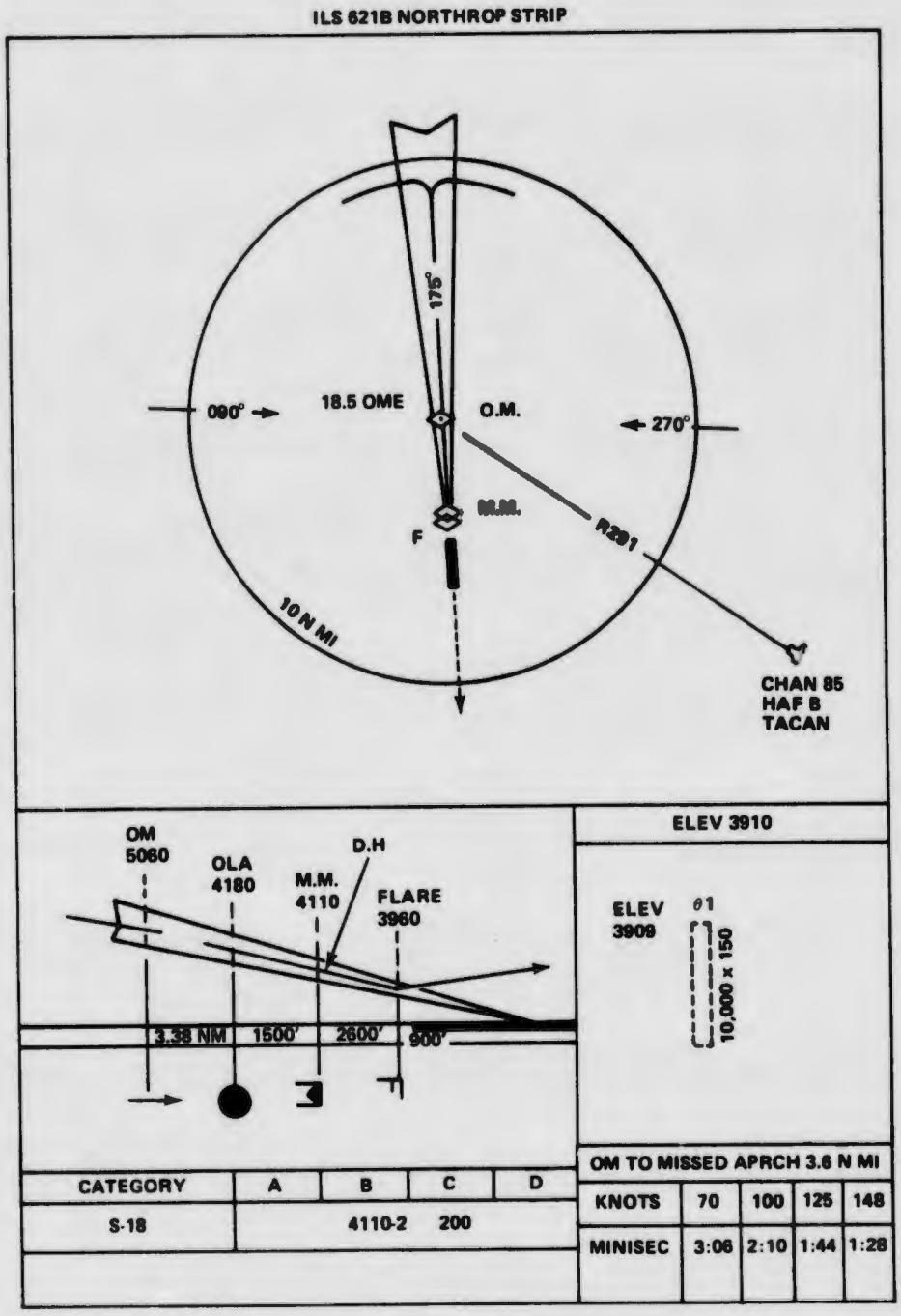

Figure 104 Approach Plate for Northrop Strip

- An optical landing aid (OLA) and manned theodolite were employed to aid the pilot down the glide slope

- Touchdown target markings were constructed on the side of the airstrip at the request of the pilots, to aid in the last few seconds of the aircraft's approach.

The OLA was positioned as shown in Figure 56. The purpose of the OLA was to guide the pilot down the 2.5° glide slope, (Figure 99) for the last 6000 ft of the 26,300 ft approach glide path allowing 20 seconds for pilot correction. (See Ref. 23 for a detailed description.) It was found that the 2.5° projected beam was not visible on bright days for the full 20 seconds, Figure 105. After flight 24 and flight 25 it was decided to supplement the aid with a surveyors theodolite. The theodolite position, next to the OLA and set to 2.5° elevation, was manned during the aircraft's approach. The ground observer would talk the aircraft onto the 2.5° glide slope via a UHF radio link between aircraft and the ground observer, Figure 106. This method was utilized for flights 26 through 31 for it was found to improve the aircrafts position during the approach and touchdown. The OLA, theodolite, aircraft radar altimeter and approach markings were all used to keep the aircraft on the theoretical glide scope.

The aircraft flew down the glide slope, flared, then passed over the airstrip at a constant 100 ft AGL, for all of the flight legs of flights 24, 25, 26 and 27. The aircraft touched down on flights 28, 29, 30 and 31, rolled out and took off. Each time the aircraft touched down the impression left by the landing gear tires was marked. At the end of each flight, the impressions were surveyed by WSMR geodetics to within one foot accuracy. The touchdown was documeted by:

- A high speed mobile telescope (T-619)

- Five cinetheodolites

- Onboard the aircraft, two accelerometers mounted; one in the IU, the second, in the HC receiver recorded changes in "g" forces during the flight

- Three auto pilot gyros (pitch, roll and yaw) outputs were integrated

- The operators onboard the aircraft activated the "event" marker on the IU at touchdown

The above data were utilized to record the position of the aircraft and IRIG B time at the instant of touchdown.

The comparison of surveyed position data to BETs and navigation solution trajectory data served as a check on the position solution accuracy, Figure 107.

3.5.5 Ground User Multipath Test

3.5.5.1 Test Scope and Resulting Sites

The scope of the multipath tests was to examine the test receiver ranging performance in selected multipath environments typical of those encountered by a ground user. Parameters associated with terrain, atmospheric conditions, time, signal strength, attenuator settings, test antenna height, polarization and fine range difference were recorded so that multipath errors could be examined.

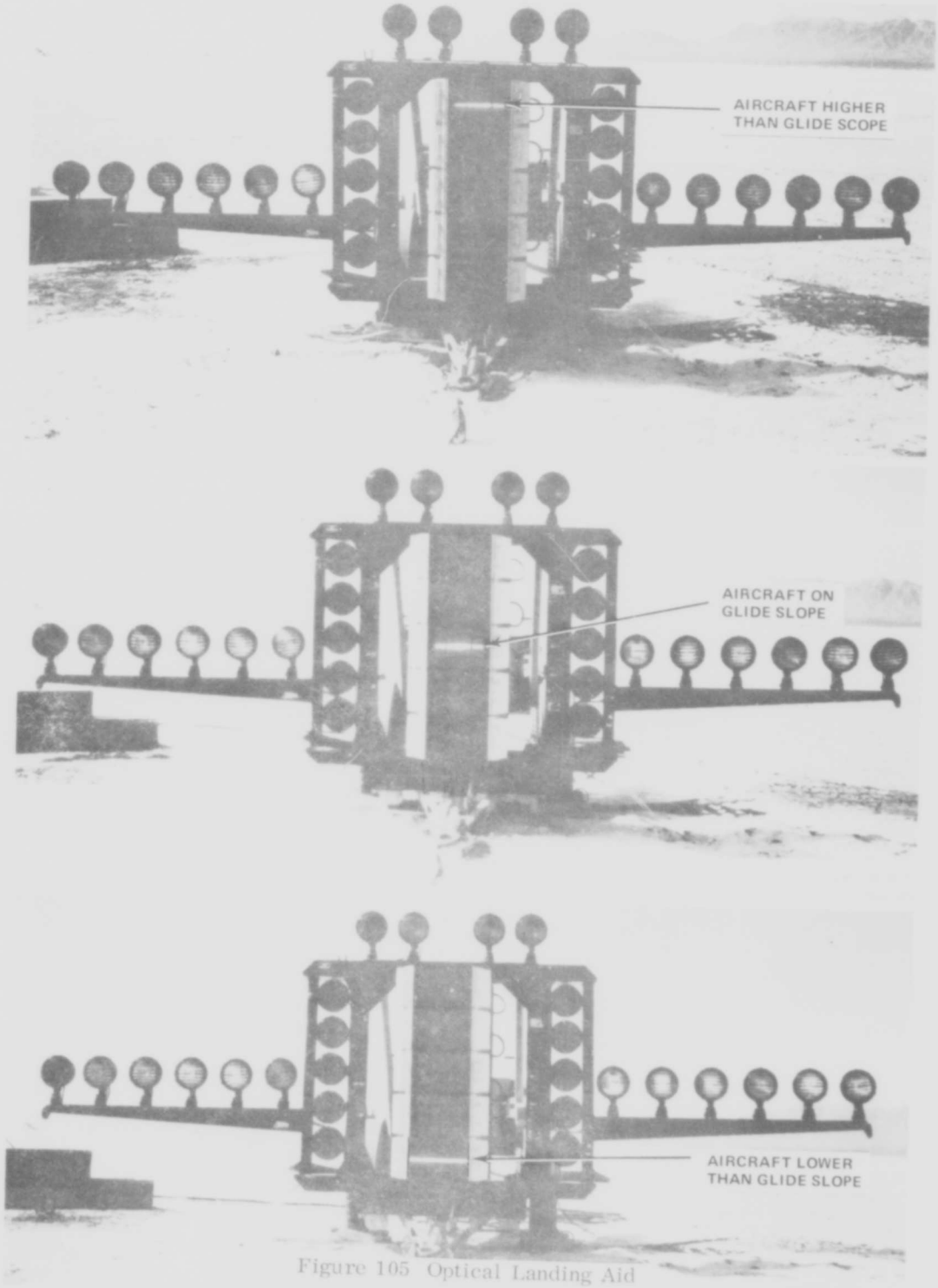

Figure 105 Optical Landing Aid

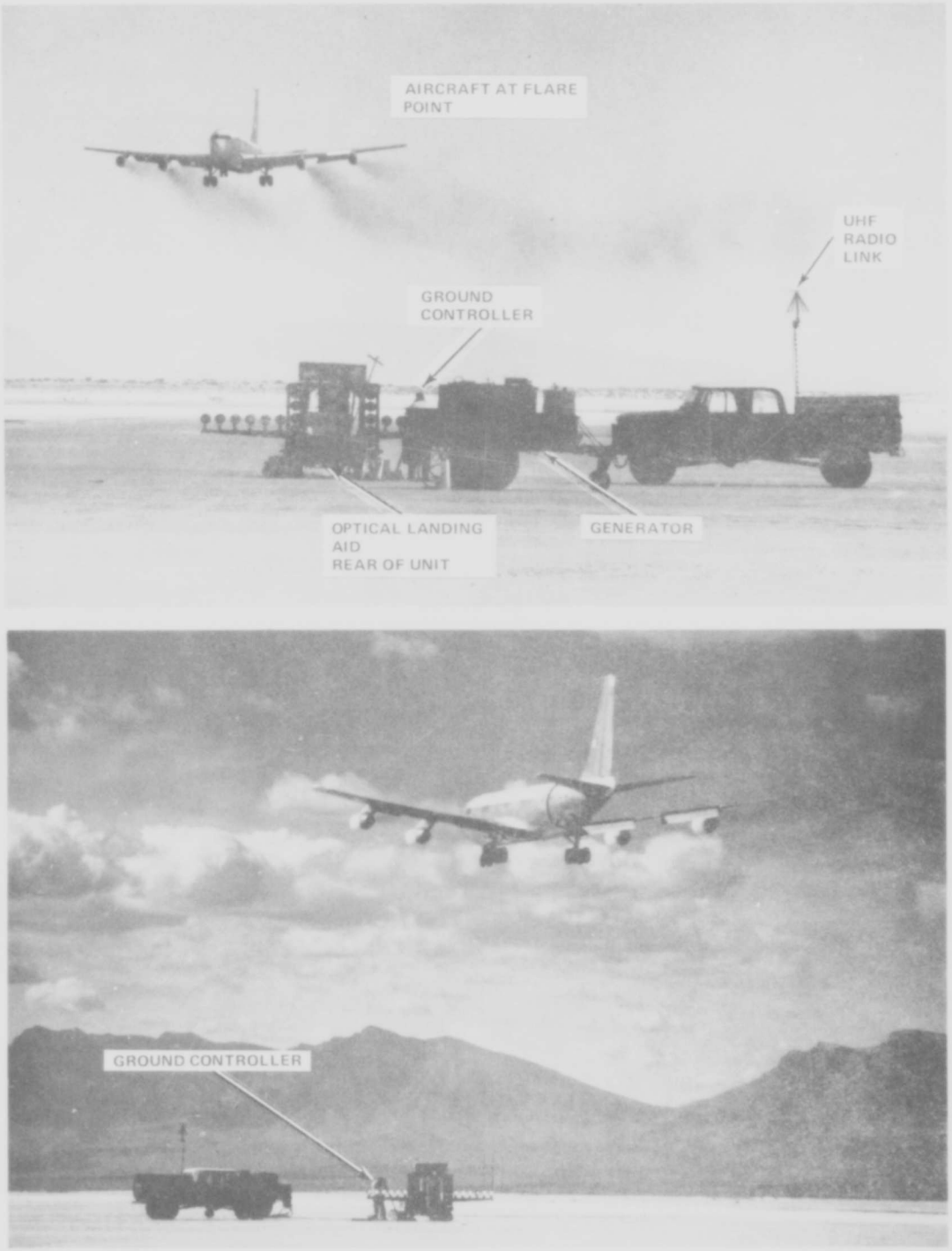

Figure 106 Optical Landing Aid and Thedolite

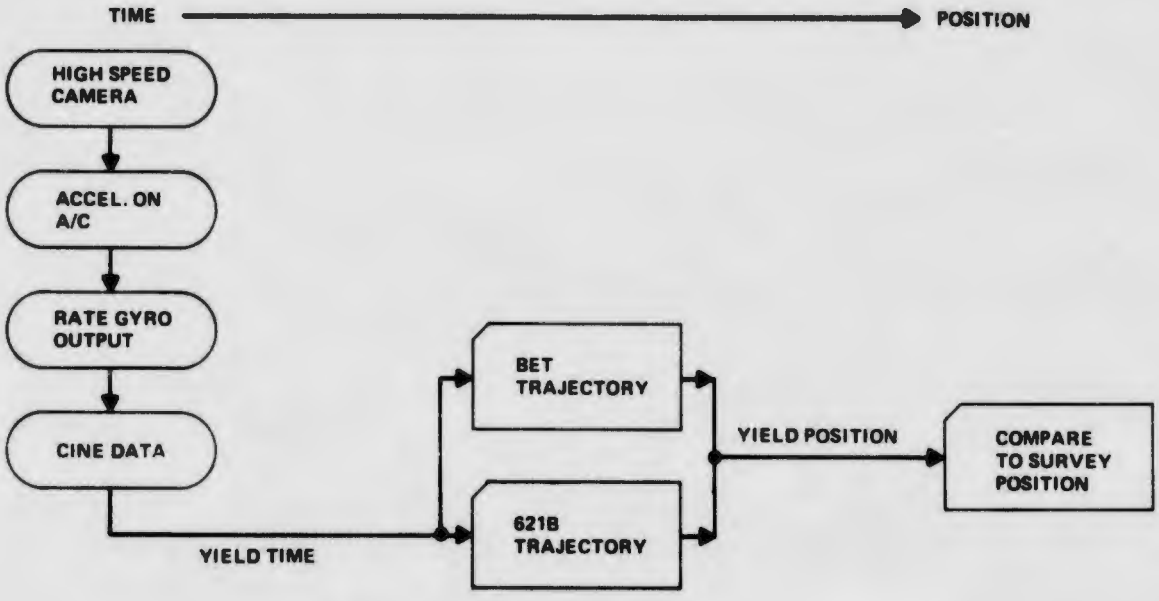

Figure 107 Implementation for Checking 621 B Position Solution Accuracy

Suitable test environments were found at WSMR to simulate conditions of smooth earth, rocky terrain, undulating hills, and high density vehicular traffic.

Tula Peak was selected because of its height and the large rocks scattered along the side of the hill. Dead Man's Canyon was selected for the height and the intense vehicular traffice associated with a road construction crew operation.

Two locations were utilized in the Northrop Strip area. One was the strip itself; it was used for smooth earth tests. The other was centered in the sand dunes adjacent to the strip. These dunes roughly 25 to 40 ft high, were used to simulate hills (rough earth).

3.5.5.2 Test Techniques

Preliminary Multipath Test Check-Out

Due to the delays in checkout of the HC receivers and transmitters and system tests during Dec. 1971, a complete initial checkout could not be performed at our plant. A preliminary checkout was performed using a HC transmitter on cw and the Polarad receiver installed inside the MCS. Readings were taken first through the dish antenna and then through the omni antenna which was mounted on the MCS mast. It was originally planned to use two receivers and a dual channel recorder to gather data; time did not permit it. This checkout served as a training exercise on the available equipment. As a consequence of this exercise, supporting struts were added to the dish antenna trailer. A diagram of the test set-up is shown in Figure 108.

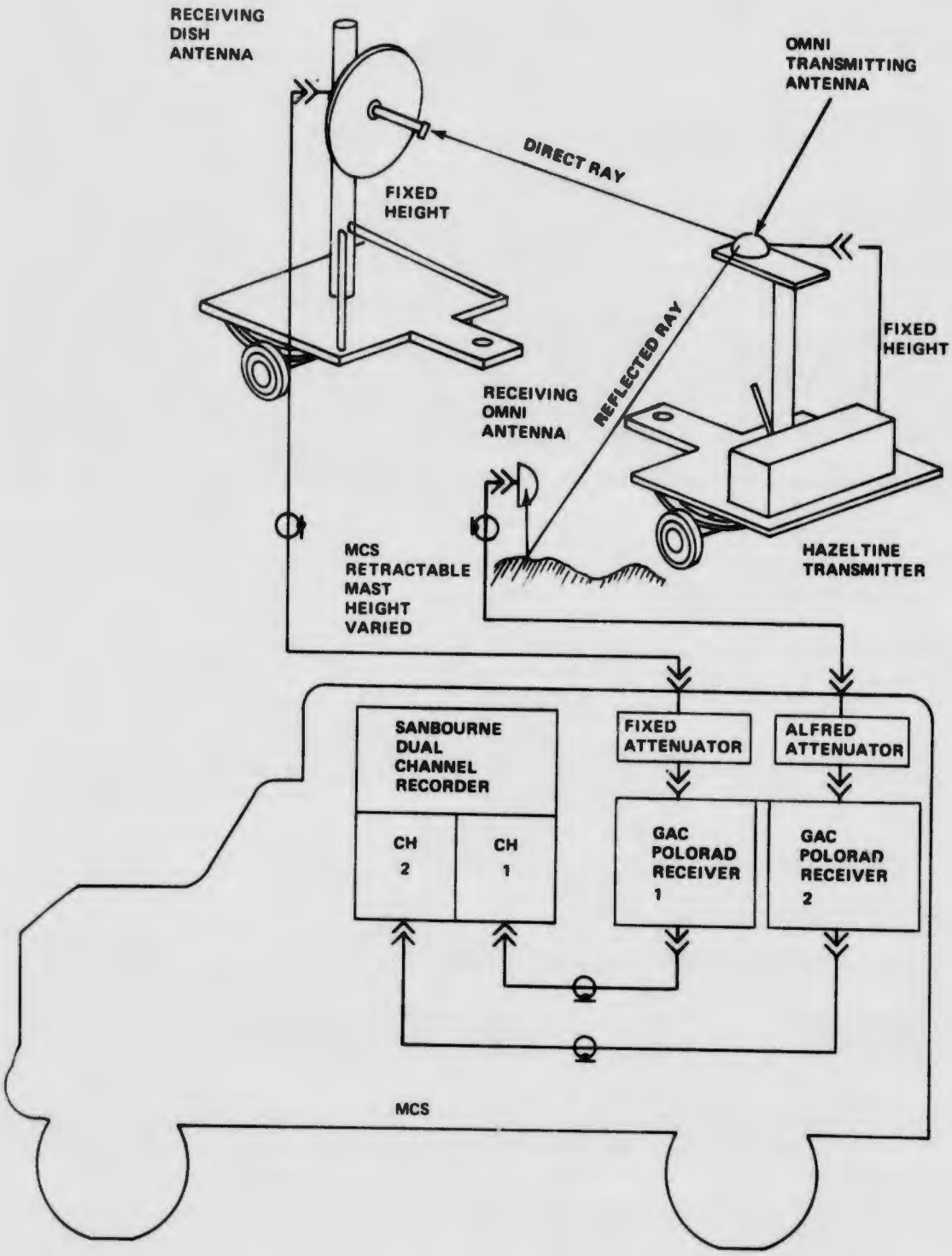

Figure 108 Multipath Preliminary Checkout in Bethpage, N.Y., Dec. 1971

Sequence of Events Prior to Multipath Testing

Eight dish antennas were purchased for the field test program. Four of the antennas were mounted at the MCS Site and one at each of the transmitter sites in the 50 mi area. The dish antenna mounting brackets at each of the transmitter sites permitted $\pm 10^{o}$ tilt while the mounting brackets at the MCS permitted -5 to $+50^{o}$ tilt. Since the dish antennas at the transmitter sites were not required for flights 17-23, an antenna was available for use on the dish antenna multipath trailer. The trailer, however, required the use of the -5^{o} to $+50^{o}$ tilt mounting brackets in order to provide the coverage for the multipath tests. It was decided to pull the dish antenna and mounting bracket from EC-50 and swap it for the EC-50 directed dish and mounting bracket at the MCS north pole. The swap was accomplished on 27 July 1972. On 4 Aug. 1972, the dish antenna was installed on the multipath trailer and taken out to the MCS Site at Northrup Strip. Prior to 4 Aug. 1972, the multipath sites had been located, inspected and dispositioned. On 17 July 1972, a road was bladed smooth from the balloon launch pad to all the sites to be used in the Northrup Strip smooth earth and White Sands Dune Rough Earth Multipath Tests. The bladed road was required for transport of the balloon winch truck, the MCS and the multipath trailer.

Decision to Use MCS Mast in Place of Field Probe to Support the Omni Antenna

In order to obtain the necessary geometry changes during the multipath tests, the omni antenna height was to be varied approximately 30 ft. An erectable mast of sufficient height, the rf field probe, Figures 109 and 110, was planned for this purpose. The MCS was to be configured as shown in Figure 111 and the field probe height varied until a satisfactory height in terms of time delay changes and signal strength was obtained. This test set up was required at each multipath site. After the initial checkout at the first site at Northrop Strip, it was decided to use the MCS 35 ft retractable mast for the multipath tests instead of the field probe. Originally it was felt that the dust conditions would cause extreme wear on the MCS mast seals. However, the set-up was much simpler with the MCS retractable mast and satisfactory multipath performance was obtained, so the rf field probe was abandoned.

Fine Range Difference as Multipath Indicator

The fine range difference from the receiver was investigated as a measurement of multipath effects on the receiver. The test set-up is shown in Figure 111. The receiver fine range outputs were observed on a duel trace scope. By observing the behavior of fine range output derived from the channel connected to the omni receiving antenna with respect to the behavior of the fine range output derived from the channel connected to the dish receiving antenna while different multipath conditions were created, we were able to determine that the fine range outputs would provide a suitable multipath measurement point. For this and subsequent tests, it was decided that channel 4 would be the reference channel (direct channel connected to the dish antenna) and that channel 1 or 3 would be compared to it with the convention shown in Figure 112. Further testing showed that channel 1 and channel 3 fine range outputs behaved identically as multipath conditions were changed. Channel 2 was not used since the receiver mechanization causes this signal output to have an inherent range displacement from channel 4. This made it very difficult to display on the oscilloscope without introducing an ambiguous reading.

Figure 109 Installation of Field Probe

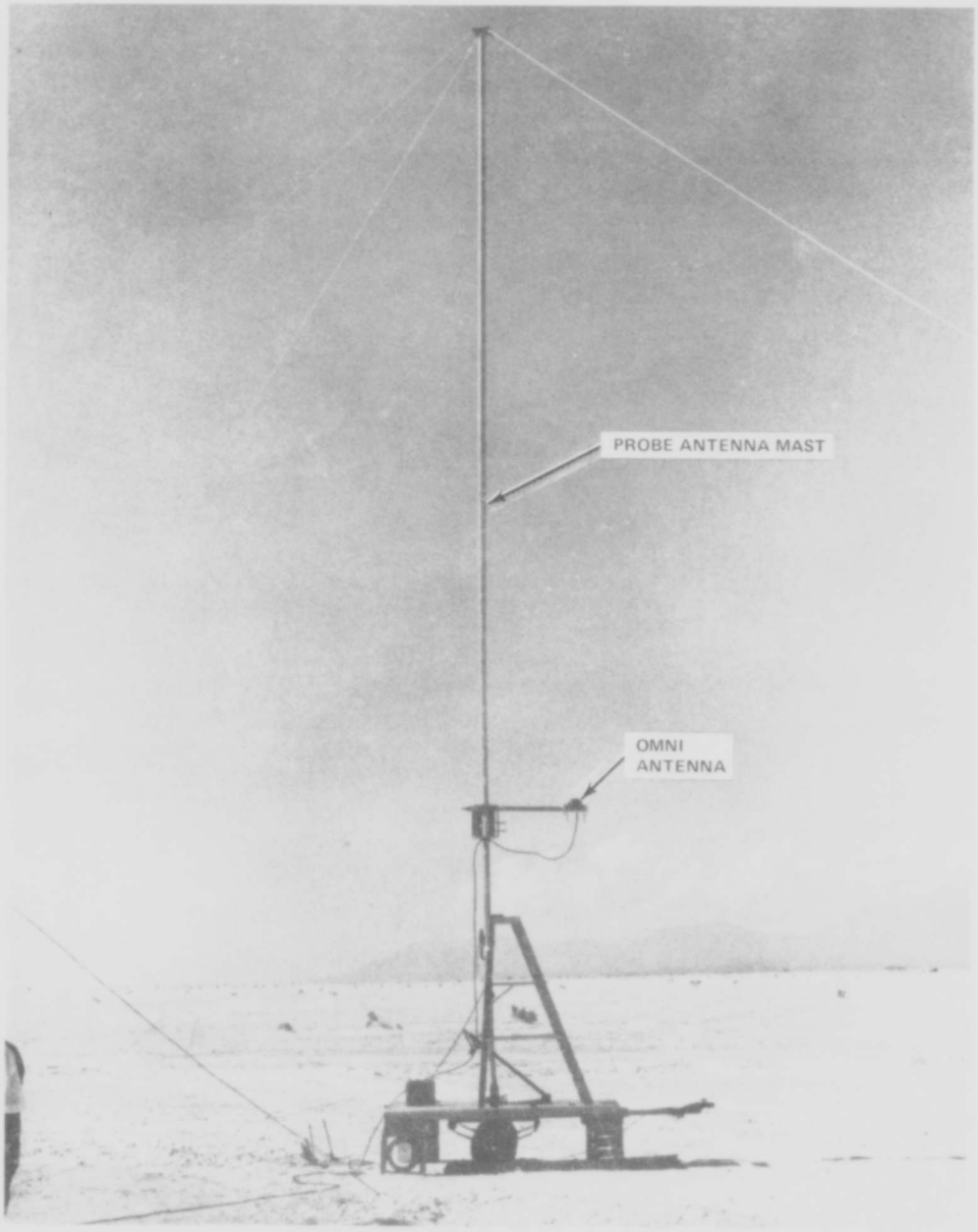

Figure 110 Field Probe Installed at Northrop Strip

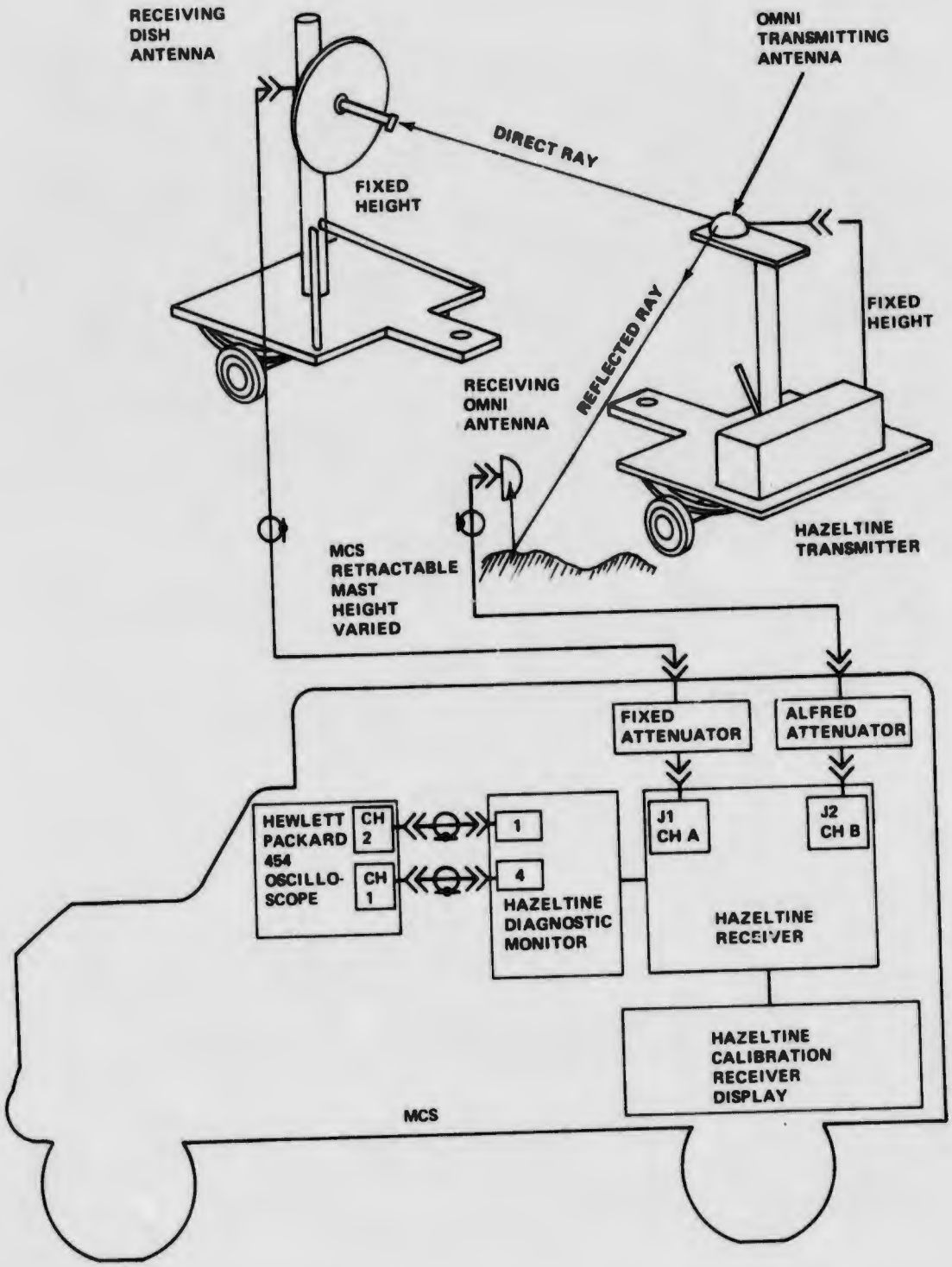

Figure 111 Multipath

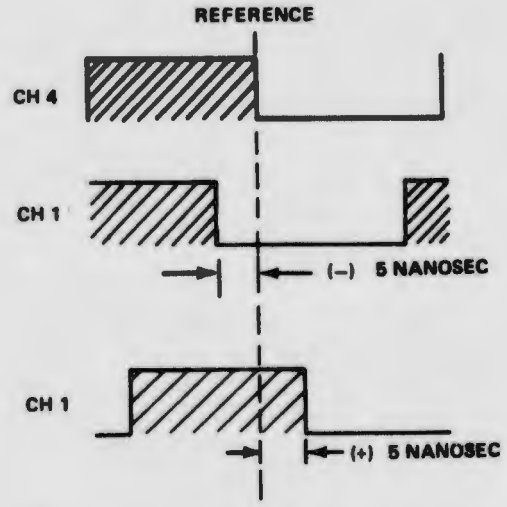

Figure 112 Fine Range Reading Convention (Sync to Channel 4)

Receiver Calibration of Fine Range Differences

An inherent requirement of multipath testing was to use two distinct signals (direct and reflected). This required the use of two RF/IF sections in the receiver. To determine if these RF/IF's were identical, a test was performed.

For this test, the equipment was set up as shown in Figure 111 with the calibration receiver control switches sequenced and the antenna cables connected as indicated in Table X. The fine range difference observed for these configurations is noted in Table X.

Table X Fine Range Difference Receiver Calibration

	Antenna Connection		Calibration Receiver Control Switch Positions			Fine Range Difference		
Test	Dish To	Omni To	Channel A/B	Multiple Test	2nd/3rd Order	1:4	2:4	3:4
1	J1 Ch A	J2 Ch B	A	Off	3rd	–2	–19	–2
1	J1 Ch A	J2 Ch B	A	On	3rd	+1	–17	+1
1	J2 Ch B	J1 Ch A	B	Off	3rd	0	–17	0
1	J2 Ch B	J1 Ch A	B	On	3rd	FORBIDDEN OPERATION		
2	J1 Ch A	J2 Ch B	A	Off	3rd	–3	–20	–3
2	J1 Ch A	J2 Ch B	A	On	3rd	–5	–20	–5
2	J2 Ch B	J1 Ch A	B	Off	3rd	–1	–18	–1
2	J2 Ch B	J1 Ch A	B	On	3rd	FORBIDDEN OPERATION		

Considering that the transmitter was suspended from a balloon experiencing wind gusts during this calibration and the inherent jitter of the system (± 3 nanosec), the fine range difference between the two receiver RF/IF channels remained essentially constant for the various receiver configurations.

It was decided that no substantial errors existed between the two receiver RF/IF channels.

Calibration of Receiver Signal Level Display

The receiver signal level display meters were calibrated by taking the self test signal and feeding it into channel A of the receiver via a variable attenuator. A set of attenuator values versus calibration receiver display readings was obtained for processor channels 1, 2, 3 and 4. This calibration was repeated for channel B. A plot of these data, referenced to the receiver input power, is shown in Figure 113.

Induced Multipath Test

To determine credibility in the multipath test set-up, the bench test shown in Figure 114 was performed.

The self test signal emerging from self test jack J3 was fed to a splitter, one output of which went directly to channel B of the receiver while the other went to channel A via a trombone in series with an attenuator. The fine range difference was observed when the trombone was displaced at increments up to a wavelength while the attenuator was adjusted so that the receiver signal level display reading remained constant. As anticipated, the fine range difference was observed to change indicating that induced multipath was present. The fine range was observed to change consistently with trombone settings, and was quite readable. We concluded that this method of recording the data would be satisfactory.

Minimization of Multipath Signal in Dish (Reference) Antanna

A sighting tube was clamped to the bottom of the dish parallel to the feed horn. The dish was first mechanically and then electrically boresighted to the transmitting antenna, and the angle (A_1) between a line parallel to the ground (a datum) and the sighting tube was noted. The dish was then elevated until minimum signal was observed. This angle between the datum and the tube was noted as A2. The critical reflection region was determined empirically by walking on a straight line between the Dish and transmitting antennas and observing by means of an inclinometer the angles between the ground and both antennas. The critical reflection point is located at the point where the angles between both antennas are equal and noted as A3. The antenna was then tilted below the datum to an angle equal to $A_3 + A_1 - A_2$. At this point, minimum multipath entered the dish (reference) antenna.

Multipath Procedure

1. The equipment was set up as shown in Figure 111 at the preselected sites.

2. The transmitting trailer with onmi antenna was pointed to the MCS and leveled by means of cinder blocks and scrap wood so that it was stable. If required, the trailer was tied down. The transmitter was turned on.

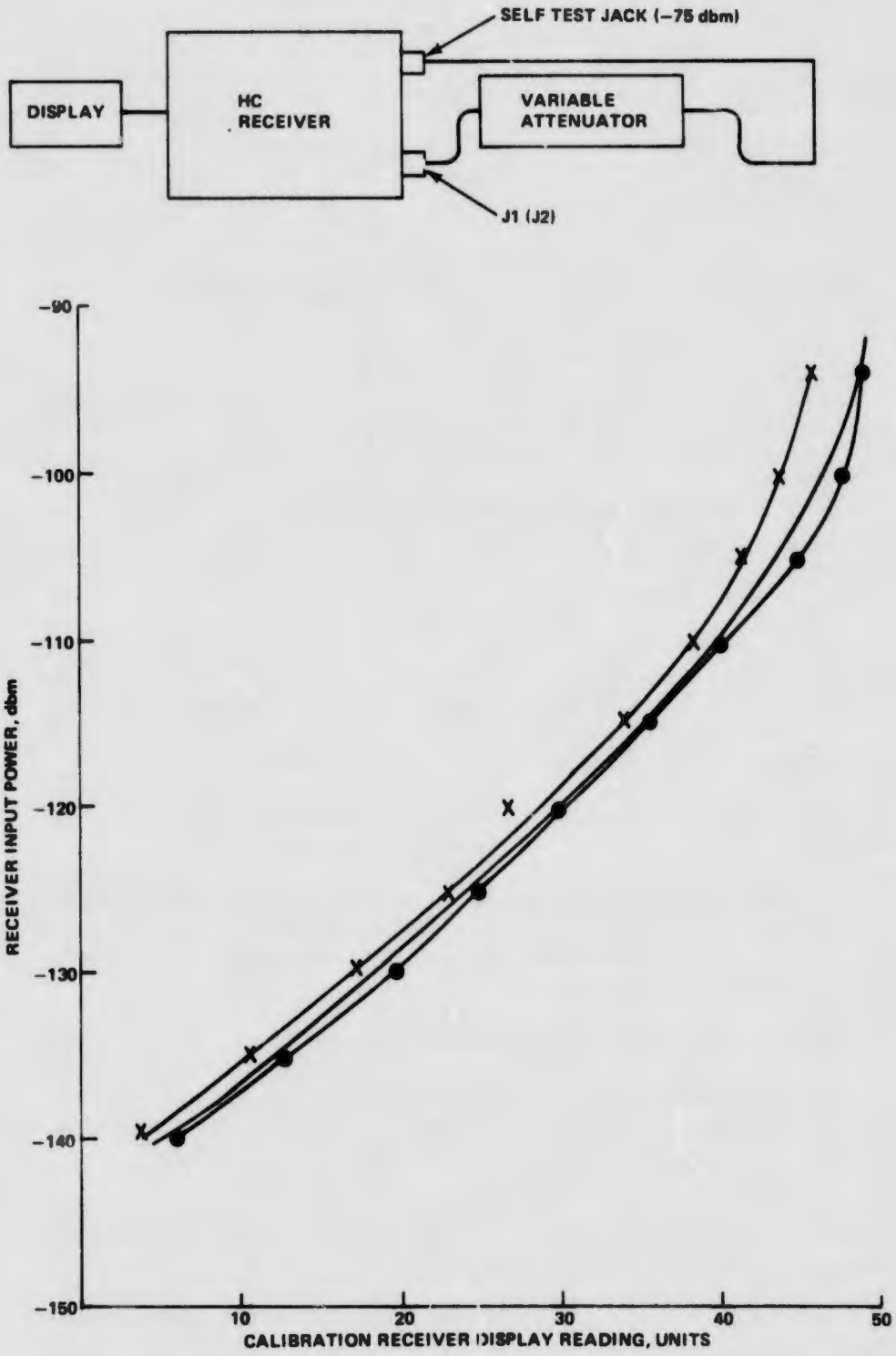

Figure 113 Calibration of Receiver Display

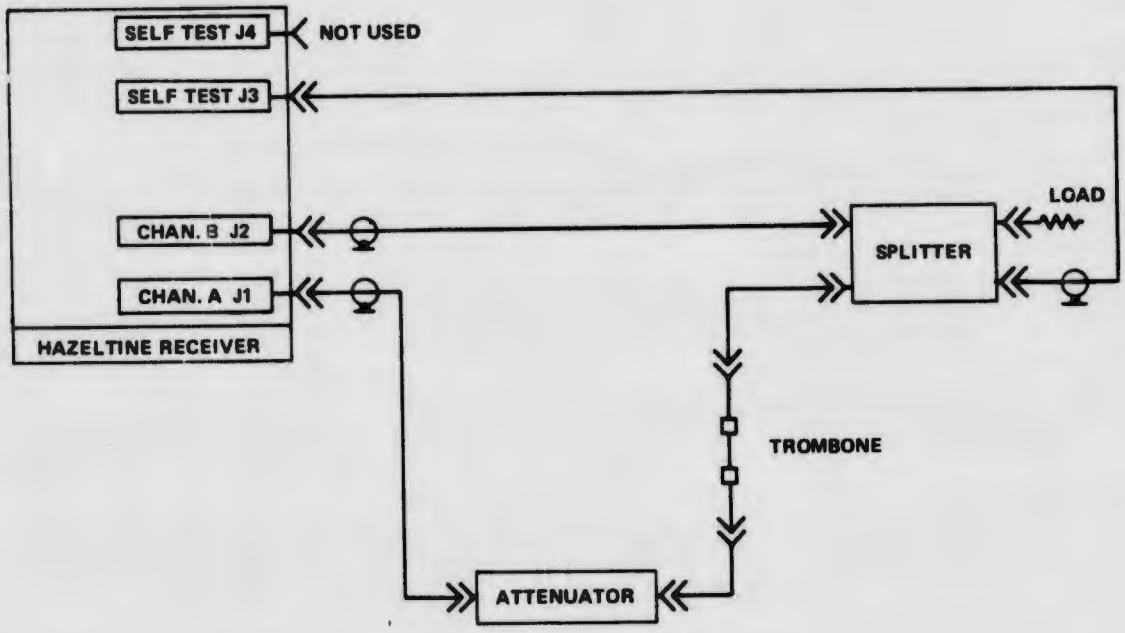

Figure 114 Induced Multipath Test

3. The receiving dish antenna trailer was positioned, leveled and tied down. The dish antenna was adjusted so that its multipath was minimized.

4. The geometry of the site was measured and recorded.

5. Meteorological data recording was initiated and continued throughout the test period.

6. The MCS omni antenna was mounted on the MCS mast and a steel measuring tape was taped to the antenna cable. A datum line was affixed 5 ft above ground. Mast height was read directly off the tape with the 5 ft added giving antenna height above ground.

7. The MCS IRIG "B" time generator was set to local time.

8. The MCS receiver was set on self test for channel A and the time and processor outputs were recorded by hand and on tape.

9. Same as above for channel B.

10. The MCS receiver was placed in normal with the dish antenna connected to channel A. The fixed attenuators were adjusted so that the calibration receiver display read approximately 30 on each channel. The value of the fixed attenuators was recorded. The time and processor outputs were recorded by hand and on tape.

11. The dish antenna cable and fixed attenuator was removed from channel A. The omni antenna cable was connected via the Alfred Attenuator to channel A. The Alfred Attenuator was adjusted until all channels read approximately 30 on the calibration receiver display. The setting of the Alfred Attenuator was recorded. The time and processor outputs were recorded by hand and on tape.

12. Step 11 was repeated for channel B.

13. Step 10 was repeated for channel B.

14. The receiver multipath test On-Off switch was placed in n position. This connects channel A to processors 1, 2 and 3 and channel B to processor 4. The dish (direct) antenna was connected to channel B and the omni antenna was connected to channel A. The time and processor outputs were recorded on tape.

15. Step 14 was repeated with antenna cables at the receiver interchanged.

16. The MCS mast supporting the omni antenna was raised to its maximum height (31 ft) and time, processor 4 calibration receiver display reading and fine range difference between processors 1 and 4 were recorded by hand. Time, all processor outputs and fine range differences were recorded on tape.

17. Step 16 was repeated using test antenna (dipole) in vertical position.

18. Step 16 was repeated using test antenna (dipole) in horizontal position.

19. Calibrate receiver display versus input power for both channels.

20. Measure antenna rf cables for insertion loss and time delay using the procedure shown in Figure 115.

Multipath Procedure Comments

The above procedure evolved from the tests performed at WSMR. The procedure was modified at some sites due to the slightly differing requirements of each site. To perform these tests, a minimum of three men were required for setup. If the rf field probe on the transmitter trailer had been used, a total of five men would have been required for setup.

3.5.5.3 Tula Peak Multipath Test

Tula Peak is located on the eastern border of WSMR and is approximately 260 ft higher than its surrounding terrain; its top had been flattened to form a plateau 200 ft square to support WSMR test facility. The 621B transmitter was set atop the plateau with its omni antenna facing down Tula Peak's east slope. The MCS was positioned in two places 1550 ft and 1000 ft down the slope with its dish and omni antenna looking west up the Tula's east slope at the 621B transmitter omni (Figure 116). This site provided a multipath environment containing medium size rocks (~1-2 ft diameter) and small desert bushes.

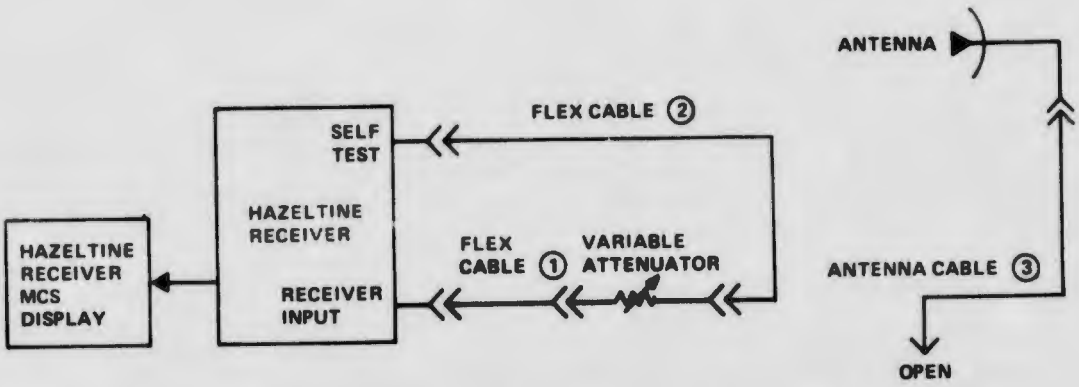

CALIBRATION: ADJUST VARIABLE ATTENUATOR UNTIL MCS DISPLAY READS 30. NOTE VARIABLE ATTENUATOR VALUE AND FINE RANGE DISPLAY READING AND THEN CONFIGURE CABLING AS SHOWN BELOW.

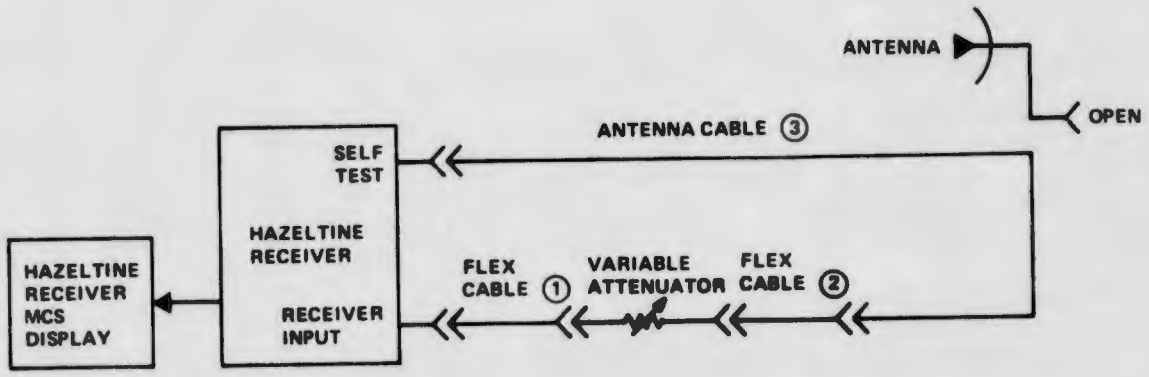

MEASUREMENT:

INSERTION LOSS: ADJUST VARIABLE ATTENUATOR UNTIL MCS DISPLAY READS 30. NOTE VARIABLE ATTENUATOR VALUE. SUBTRACT THIS VALUE FROM THE ONE OBTAINED ABOVE. DIFFERENCE IS INSERTION LOSS.

TIME DELAY: READ FINE RANGE DISPLAY, SUBTRACT THIS VALUE FROM THE ONE OBTAINED ABOVE. DIFFERENCE IS TIME DELAY.

Figure 115 RF Cable Time Delay and Insertion Loss, MCS Receiver Self Test Method

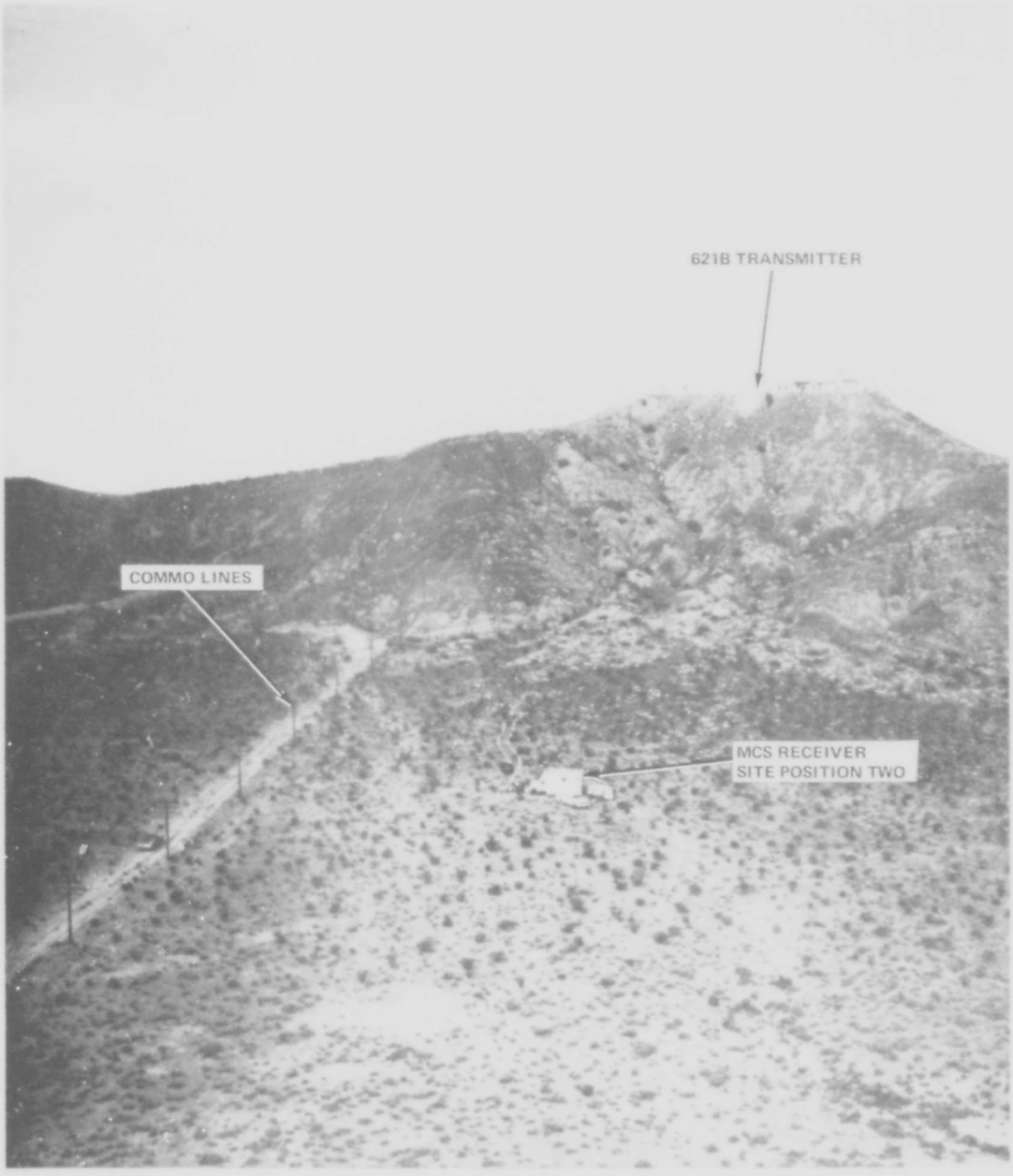

Figure 116 Tula Peak Looking West

3.5.5.4 Dead Man Canyon Test

The Dead Man Canyon Multipath Test was run on the west boundary of WSMR at the base of the San Andres Mountains in a gravel quarry located within Dead Man Canyon, Figure 117. The canyon contained small salt bush brush, a gravel pile, two water tanks, a cliff drop-off resulting from the removal of soil used to construct road beds, heavy construction equipment traveling in and out such as trucks, dozers, buckets and stationary gravel processing equipment. During the multipath testing, trucks and bucket loaders ran at random through the field of view of the receiving antennas.

3.5.5.5 Smooth Earth Test at Northrop Strip

The smooth earth multipath test was conducted on the Salt Flats in the area southeast of Northrop Strip on WSMR, Figure 118. This test utilized a balloon-borne transmitter. The balloon was launched carrying the transmitter aloft to 2000 ft AGL. The position of the MCS receiving site was moved along a constant 145^{o} azimuth (TN) to presurveyed sites to form look angles of approximately 60^{o}, 40^{o}, 30^{o}, 20^{o}, and 10^{o} from receiving to transmitting antennas. The ground surface between receiver and transmitter antennas was extremely flat, dry, and hard consisting of gypsum, sand and a high degree of salt.

3.5.5.6 Rough Earth Test at White Sands Dune Area

An area of sand dunes southeast of the WSMR Salt Flats was selected to run the rough earth multipath testing. Dunes ranging from 10 to 60 ft high spaced 100 to 200 ft peak to peak, formed the rough earth test area. The sand, salt and gypsum surface was relatively soft and granular for about 3 to 6 in. in depth. Dust storms, blowing fine sand, are common to this area. Unlike beach sand, the dune's sand was very small in grain size. Three sites in the dunes area with look angles to the balloon of 30^{o}, 40^{o}, and 60^{o} were utilized. Figure 119 shows a typical setup in the dunes area.

A more detailed description of the factors at each site affecting the multipath measurements is presented in Volume III along with the test results.

VIEW TO RECEIVING SITE FROM TRANSMITTER POSITION NO. 1

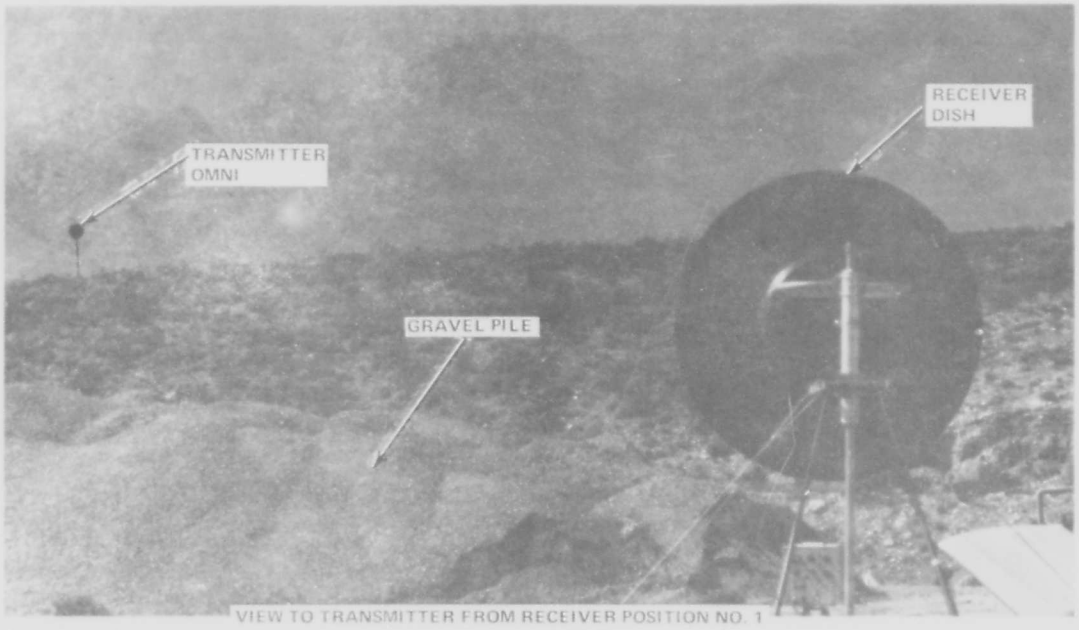

VIEW TO TRANSMITTER FROM RECEIVER POSITION NO. 1

Figure 117 Dead Man Canyon Multipath Test

Figure 118 Smooth Earth Multipath Test Position 2, $\theta = 40^{\circ}$

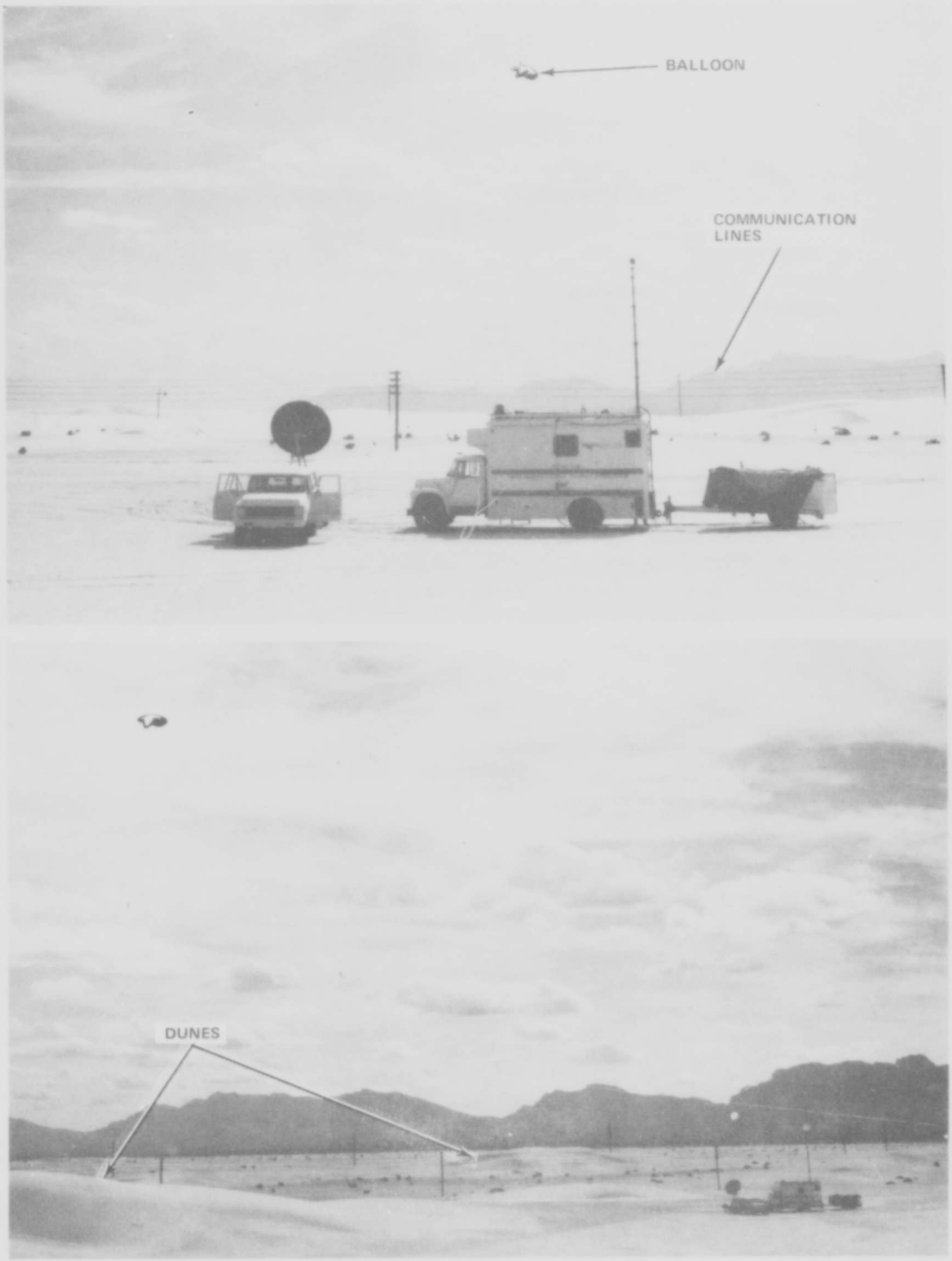

Figure 119 Rough Earth Multipath Test Position, No. 8, $\theta = 30^{\circ}$

SECTION IV

DATA PROCESSING

This section describes the main flow of data from the raw measurement tapes to the final output. In this discussion we will go to a level of detail commensurate with the results presented in Volume III. A complete discussion of the various software elements of this process can be found in Ref. 25, 621B Software Documentation Library.

4.1 OVERALL DATA CONCEPTS

The data collection, reduction and analysis processes of the flight tests is separated into seven distinct parts:

- Three independent instrumentation systems collect time-tagged data for each of the three receivers and direct it to separate magnetic tapes
- The engineering units/validation program (EUVAL) simultaneously reads the three raw data tapes, reformats the tapes for computer compatibility, validates the time data and writes a single, chronologically ordered output tape
- The navigation and calibration program (NAVCAL) forms the total user pseudo-range quantities from ground and airborne measurements, performs the deterministic navigation solution and supports, in part, the field data analysis effort by estimating system random errors in the navigation solution
- The filter program (FILTER) implements the two-state clock bias filter in order to reduce the random error component of the static trajectory (i.e., from static to dynamic GDOP sensitivities)
- The trajectory merge program (MERGE) lays the foundation for complete data analysis by computing system versus reference trajectory residuals (that is, estimates of navigation solution errors) and plotting them versus time and other system parameters on a per-run basis
- The trajectory residual characterization program (INQUIRE) statistically analyzes short time series of MERGE residuals (data slices within a run) for bias, random and periodic content
- The cross plot analysis program (CORLATE) supports the overall data analysis function by plotting the INQUIRE error statistics against system state parameters taken over the ensemble of runs and flights.

Thus the data system takes the data engineer/analyst from raw receiver measurements to plots which display system error quantities as a function of system state.

Our discussion of this data system starts with a brief account of data logistics and flow, then proceeds to the detailed descriptions of each of the major system

components. We shall then mention the numerous additional programs which were developed in conjunction with the 621B tests but were not a part of the major flow of data, and complete the section with a discussion of the reference data trajectory generation program from White Sands Missile Range.

4.2 DATA HANDLING

The acquisition of data during a flight test occurs at each of the three receivers simultaneously through three independent instrumentation systems. There are relatively few measurements:

- Four channels of pseudo-range information
- Four channels of pseudo-doppler measurements
- Four channels of received signal level data
- Receiver status discrete data including receiver mode and channel lock status
- Instrumentation status data including tape ID, antenna select and airborne attenuator select
- Instrumentation time of data sample.

Time Correlation

While descriptions of the instrumentation systems are contained in Section 2, time correlation of the data sources is of particular interest in the discussion of the data system.

A fundamental problem in the test data configuration is the manner in which the data recorded at the calibration site, on board the aircraft, and at WSMR aircraft tracking devices are correlated to time of day. The timing system was designed to accommodate time correlation errors likely to be encountered as the results of aircraft dynamics associated with a high speed aircraft (i.e., RF-4C). Since the flight test bed was an NC-135A, the aircraft dynamics involved in the tests were small, and the data sources need only be correlated in time to about 1 ms. At aircraft speeds of 800 fps, a 1 ms timing error between the data recorded on-board the aircraft and the WSMR reference trajectory results in a 0.8 ft position error. This is the worst case and is considered an acceptable value considering the accuracy obtainable from the WSMR reference trajectories. In order to achieve the 1 ms time correlation, the following technique was utilized:

White Sands Missile Range supplies accurate time of day information to all range users via microwave and hardwire links. Thus the calibration site and WSMR reference trajectory system were synchronized by this network. The aircraft data system contained, as GFE, an IRIG modulated B format time code generator which was aligned to the WSMR time before each flight. Misalignment measurements were made before and after each flight by simultaneously recording WSMR and aircraft time on an oscillograph. The misalignment data allowed us to make offset and drift estimates and the data were subsequently corrected during data processing for time misalignment. Typical aircraft-WSMR offsets were 0.5 to 1.5 ms, and the drifts so small (typically 1.5 ms over a 3-hour flight) that the mean offset was used as the correction factor in the software.

Test Data Flow

After each flight the data tapes were collected and transmitted to the data processing personnel. The CDC 6600 computer at Kirtland AFB served as the data reduction center for the field programs, and, referring to the overall data flow diagram on Figure 120, the three tapes were transmitted from HAFB to KAFB via a microwave data link. The engineering units and validation program (EUVAL) was then executed. This program selects time slices of data for processing, reformats and validates the raw data and combines the three source input data on a single chronologically ordered E.U. tape. The program also produces tabular listings of the measurement parameters which were used by field analysis personnel to isolate and analyze data anomalies. Immediately following EUVAL processing the navigation and calibration program, NAVCAL, was executed. This program contains a major portion of the system navigation algorithms, namely the deterministic navigation solution, plus a certain amount of data analysis capability. Files of diagnostic information about receiver and navigation solution status are provided in chronological order along with random error estimates based on variate differences and polynomial fits. Unfortunately, by necessity, the NAVCAL program cannot produce estimates of system bias errors. This analysis must be deferred until a reference trajectory is available.

In the case of an ILS flight, a cinetheodolite-derived balloon trajectory is incorporated into the ephemeris subroutine of NAVCAL. This tape was supplied by WSMR and interpolated to the 621B time.

After the EUVAL and NAVCAL processing produced acceptable results, the deterministic trajectory data (also called the static trajectory) was forwarded to Grumman personnel on the East Coast. Here the data were filtered using a two-state Kalman filter (the clock bias filter) to produce the navigation solution best estimate of trajectory (BET). The two-state filtered data were reformatted in accordance with SAMSO requests and transmitted to the Air Force as an official data submittal. After this submittal, the trajectory reference data from the tracking range were supplied to Grumman for system analysis purposes. These analyses start with a computation of trajectory residuals by the MERGE program, which interpolates the WSMR data to 621B time, forms the residual error estimates, derives a predicted error band for the random components of the test system data and WSMR data and plots time-histories and cross plots of these data. The MERGE output plots proved invaluable in the detection and identification of predominant system errors. Further, these plots vividly demonstrate the absolute accuracy of the test system with respect to the WSMR references.

Two steps remain in the complete analysis of system errors: the formation of error statistics, and the presentation of these statistics taken over the ensemble of data flights. Data processing programs INQUIRE and CORLATE perform these two steps.

The statistics program, INQUIRE, considers manually selected time slices of ten-second duration. These slices generally start after the first 621B-WSMR time match and continue, 50 points at a time, until the end of the run. The manual override in slice selection is provided to preclude any wild or blunder points which may have occurred in either the test system or reference trajectories. INQUIRE then computes a variety of statistical quantities from the 50-point data slice. Average errors of the position and velocity residuals as well as estimates of the average error in the test system channel range measurements are computed. Random errors are characterized by moments and ordered statistics of the data. Finally, frequency content of the data is determined by a power spectrum analysis and by computing the autocorrelation.

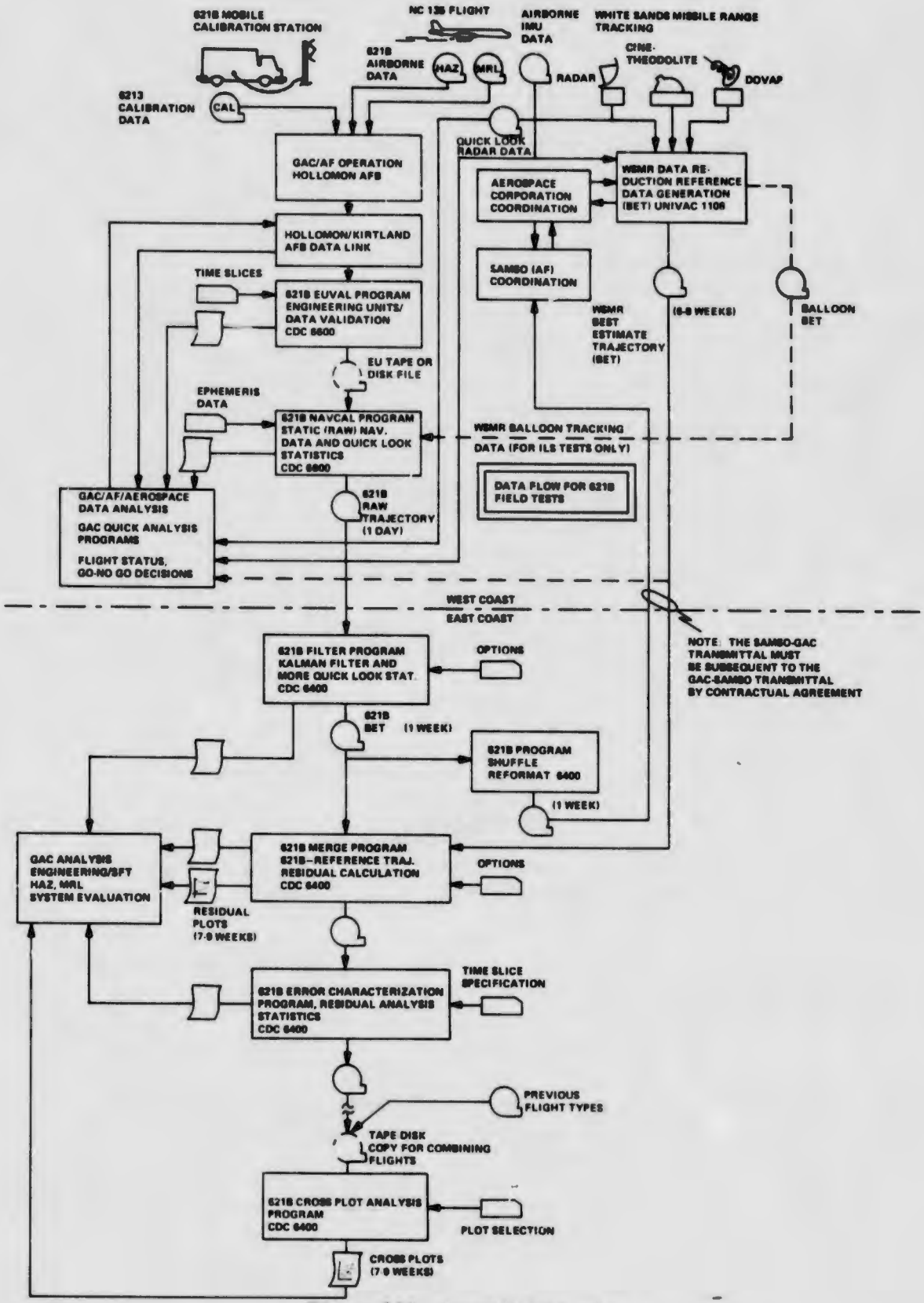

Figure 120 Overall Data Flow

Program CORLATE reads the INQUIRE tape(s) and produces cross correlation scatter diagrams of the residual statistics vs various system parameters. For example, interchannel bias errors (i.e., mean of range 2 minus range 1 residuals) may be plotted against received signal level in channel 1 or, say, elevation look angle from channel 2. These plots represent the final output of the data system and are used to reveal error dependencies not obvious in the per-run data.

4.3 621B DATA PROCESSING PROGRAMS

Each major program in the mainstream data flow (Figure 120) is discussed in the following paragraphs in sufficient detail to show the primary computational content. Interested readers are directed to Ref. 25 for a more thorough treatment of the individual programs.

These programs were specifically developed for the WSMR field test, and, as such, contain features which are peculiar to flight testing. These features, such as diagnostic files and quick look statistics, would not become a part of the normal data flow in an operational system. They serve the purpose of alerting analysis personnel to data inconsistencies, but also obscure such operational studies as computer sizing and timing allotments.

Although the software was, for the most part, perpetually changing to accommodate unseen analyses and debug, the underlying technical approach did not radically change from the outset. Therefore, we will not dwell upon the system theoretical formulations but rather on the way the test data is actually handled. The details of the system theoretical foundation can be found in the Phase I Final Report (Ref. 1).

The programs are described in sequence of use in the data flow. See paragraph 4.2 for an overview of the data flow.

4.3.1 EUVAL, The Engineering Units and Validation Program

Program EUVAL is the first program to be executed in the data system. Its purpose is threefold: (1) to decode and reformat the raw receiver data tapes from its hardware-oriented word structure to a software-oriented one; (2) to check data for hardware validity (such as record length, sync word pattern, etc.); and (3) to output tabular and tape files of computer compatible engineering units data. The EUVAL data flow is shown in Figure 121.

EUVAL accepts inputs of time slice specification cards (one run per slice) and the three raw data tapes. The three data sources are assigned alpha and numeric indicators as follows:

Source	Alpha	Numeric (INDIC)
HC ground calibration receiver	CAL	1
HC airborne user receiver	HAZ	2
MRL airborne user receiver	MRL	3

Each data source (receiver data tape) is processed for the time slice specification. The data are ordered in the computer by record and tagged with the appropriate INDIC value.

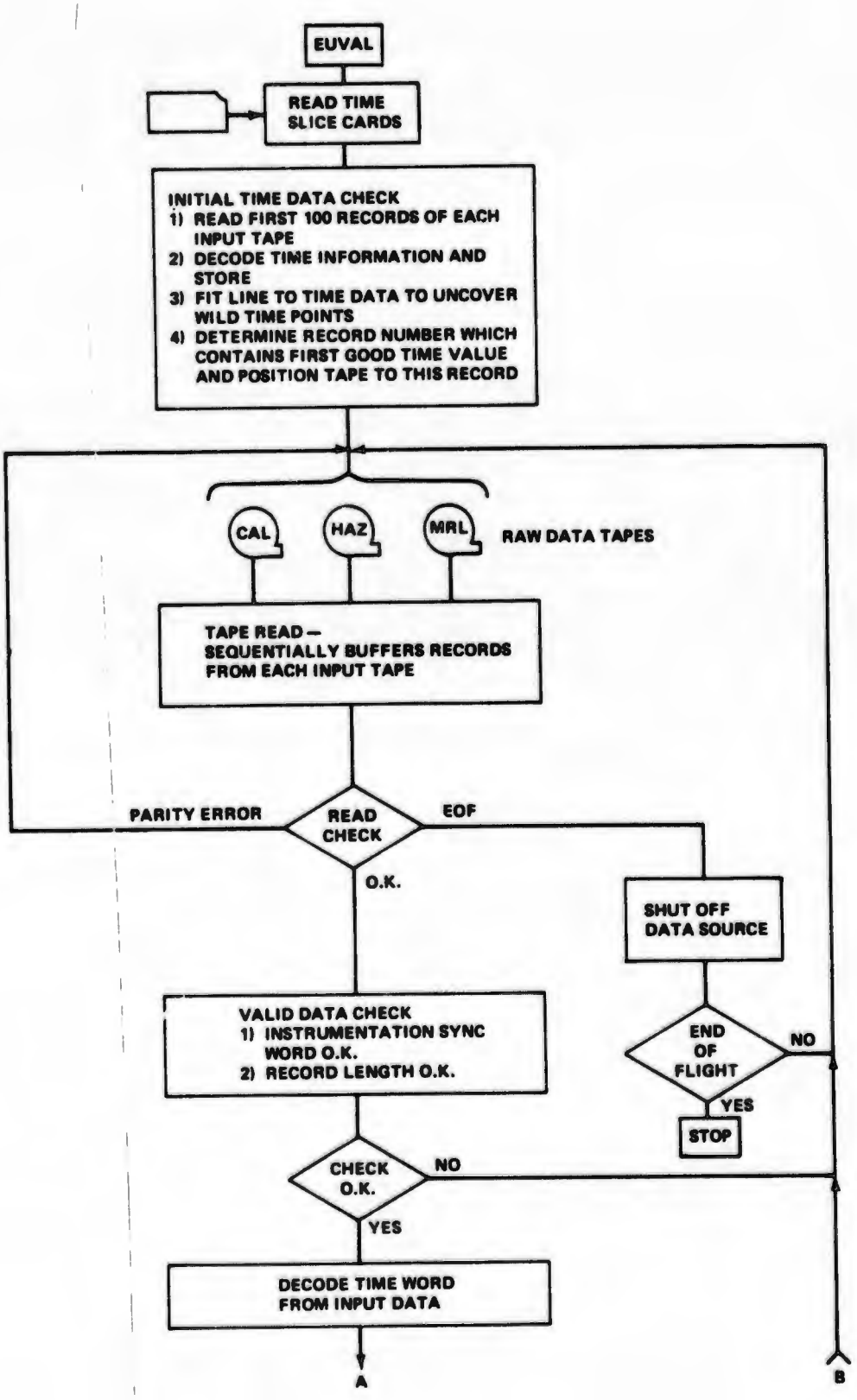

Figure 121 Engineering Units Validation Program Flow

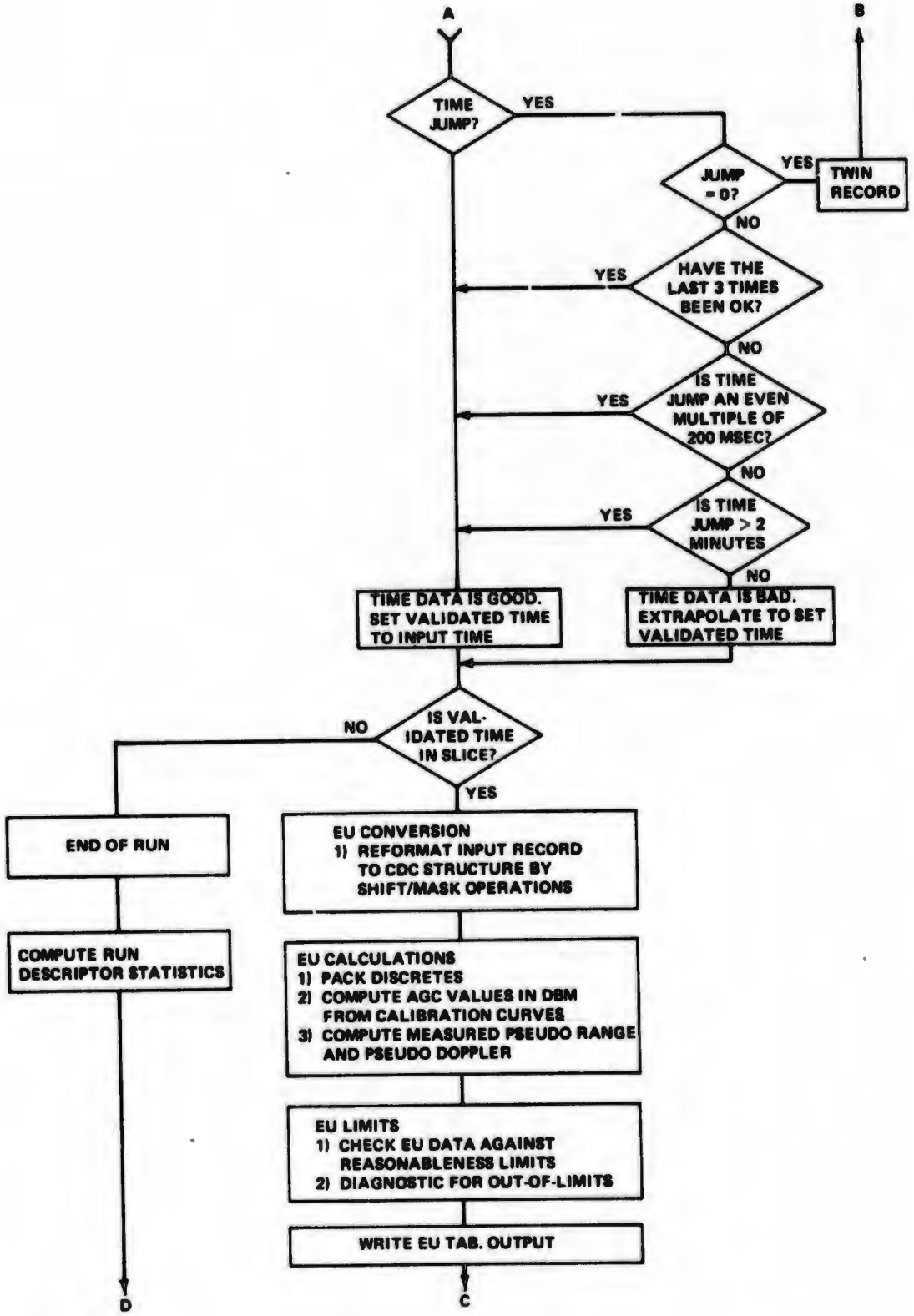

Figure 121 Engineering Units Validation Program Flow (Continued)

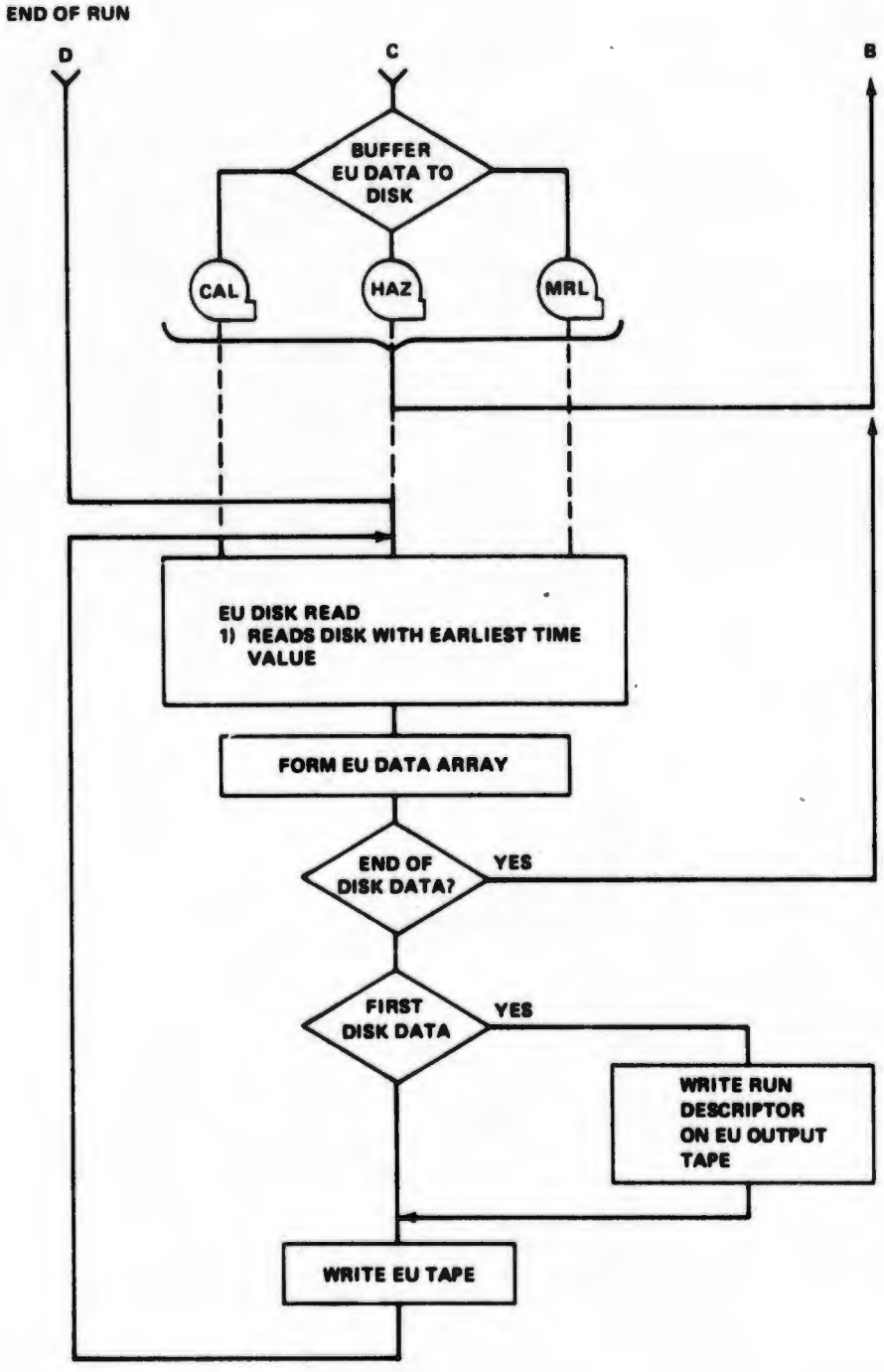

Figure 121 Engineering Units Validation Program Flow (Concluded)

The validation of time data is of primary importance in the EUVAL program since wild time points or constant time offsets seriously affect results in computation of the navigation solution. Therefore a time validation scheme was devised. The data flow is summarized below:

- A check of the time data must be made to determine where the first good time exists on the data tape in order to initiate the time validation process. This is done by a probabilistic method which considers the first 100 data records on the source tapes. The first 100 records are examined as a set of points in which the time data between successive samples should be the inverse of the sampling rate. Lines are fitted to the data and wild points eliminated so that the first good time on the tape may be determined. The input tape is then positioned to the first good record and probabilistic statements about the success of the analysis are made based on the ratio of good to bad points.

- During the mainstream program execution checks are made on the input time data for proper increase since the last validated time point. If a time discontinuity occurs the logic must determine its validity. A jump is assumed valid if: (1) the jump is a positive even multiple of 200 ms: (2) the time jump is greater than two minutes; or (3) the last three data points after an assumed bad time jump have increased by the proper 200 ms interval. The time jump is assumed to be a defect if it shows no time change since the last record or does not satisfy any of the three criteria above.

While this timing logic is certainly not flawless, it has proven very effective in the EUVAL program. However, the consequences of invalid time data are so severe (especially when only subtle discrepancies result) future instrumentation systems should incorporate a low accuracy redundant time source (such as a free-running binary counter) so that an exact decision can be made by the time validation logic.

After the time of sample has been validated it is checked against the time slice specification. Within the slice limits the following processes occur:

- EU conversion of the raw binary tape data parameters to CDC 6600 binary word structure (60-bit word)

- Calculations involving EU parameters such as agc calibration assignments, pseudo range, doppler calculations and packing of discrete information

- Limit checks for data reasonableness

- Storage of pertinent data statistics for run summary information (e.g. antenna switch position, in sync etc.)

- Generation of the EU tabular data listings

- Buffering of all EU parameters to intermediate storage disk files.

When the end of the time slice is encountered on all three data sources, the second section of the program completes the per-run processing by calculating statistics for tabular and tape output and writing a chronologically ordered EU tape from the disk file data.

4.3.2 NAVCAL, The Navigation and Calibration Program

The Quick Look Navigation/Calibration Program is executed immediately after the Engineering Units/Validation Program. The NAVCAL Program reads the engineering units tape, performs a static navigation solution and generates first-cut statistics describing system random errors. Program output consists of tabular listings and a magnetic tape.

The primary source of input data for the NAVCAL program is the engineering units tape. Other data required for NAVCAL processing (transmitter locations, indicators, etc.) are input on cards or exist in resident tables except for the ILS test flights when the coordinates of one transmitter are determined by interpolation of the balloon trajectory tape supplied by WSMR (transmitter 4 position for ILS).

Data flow in the NAVCAL Program occurs in three major phases per run:

- Reading the EU (and balloon) tapes and performing the static navigation solution. The solution outputs are directed to disk files
- Writing a tabular and tape output of navigation solution data.
- Performing statistical analysis on disk file data

The detailed data flow in the program is described by Figure 122. Referring to this figure the first part of the NAVCAL flow sets up the data required by the static (or deterministic) navigation solution. The EU run description statistics are read from the EU tape and run suitability determined by considering channel in-lock percentages. If the run is suitable for navigation processing, a record of EU data is read, the ephemeris data (transmitter position) established by table look-up for the run's geometry and, if necessary, the balloon tape is time aligned and interpolated for the extraction of transmitter 4 trajectory data. The static navigation subroutines are then called and a static solution produced. The trajectory is stored on disk for subsequent statistical processing and pertinent data output to tabular and tape files.

Quick look statistics for the deterministic trajectory are generated by variate differences and polynomial fits taken over short data slices. The slices are arranged to have approximately stationary statistical qualities by initiating a new slice when:

- The static GDOP's change by more than a factor of 1.4
- The number of points in the slice exceed 250
- A time jump occurs in the data.

The quick look statistics do not warrant further discussion here, but the interested reader is directed to Ref. 26 which details the method, its derivation and simulation results.

4.3.2.1 The Static Navigation Algorithms

The deterministic solution of the four pseudo-ranging equations (the Static Navigation Solution) forms a major part of the NAVCAL program. It is composed of several subroutines which: (1) construct the total user pseudo range from airborne

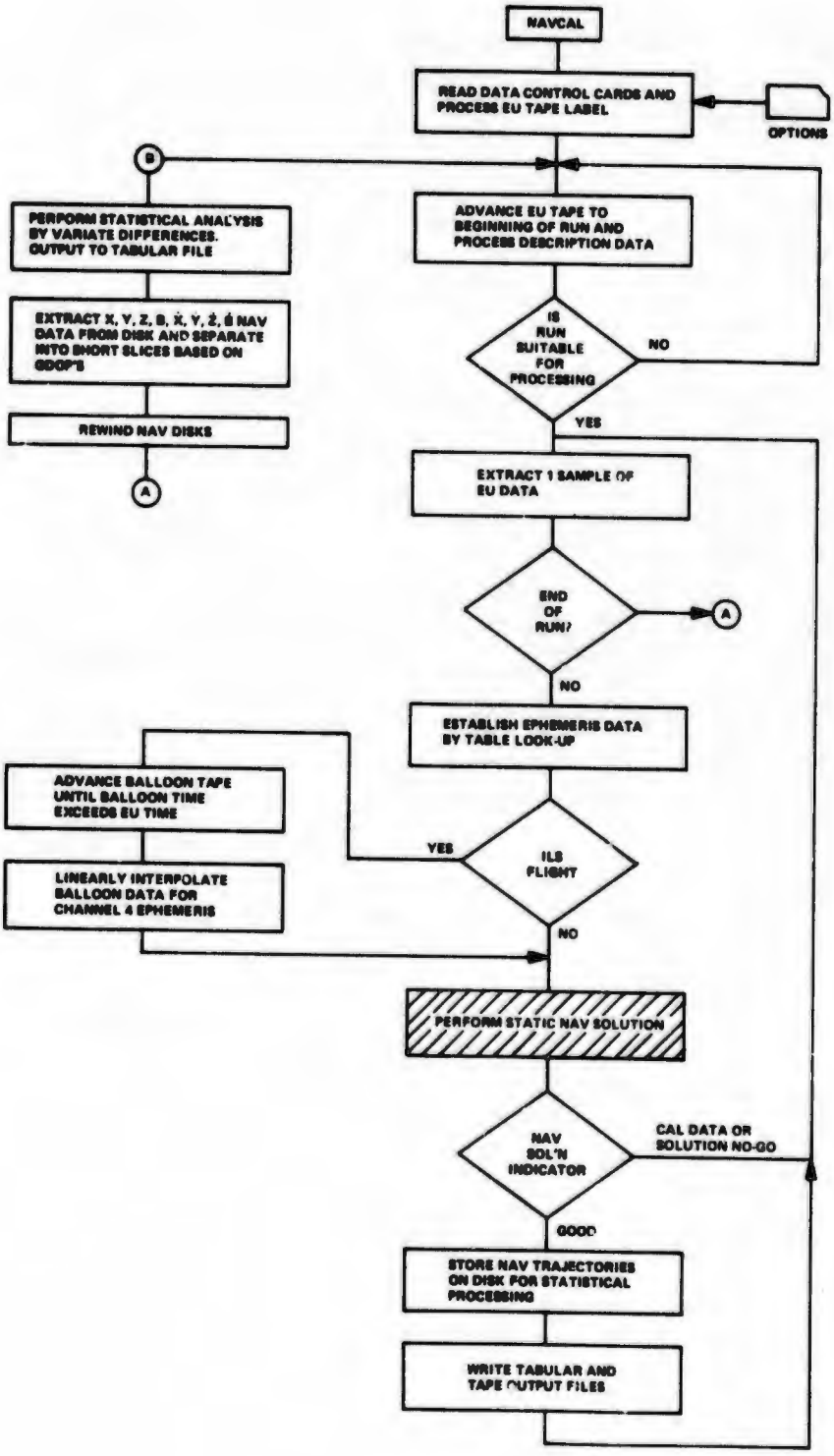

Figure 122 NAVCAL Flow

and ground measurements; (2) correct the pseudo ranges for interchannel delays and tropospheric refraction, and (3) solve the navigation algorithm (quadratic in Z) for the user's rectilinear position and velocity plus measured clock bias and bias rate. Paragraph 1.3 gives the mathematical formulation for the solution.

The Static Navigation Solution data flow is presented in Figure 123. It consists of an executive subroutine (STATNV) and subordinate subroutines. The executive subroutine screens the data for diagnostic information and routes it according to data source and receiver status. The major functions are performed in the subordinate subroutines as follows:

- CHANDEL - computes instantaneous and filtered values of channel delay mismatch for the Hazeltine calibration and user receivers
- CALROUT - computes calibration site and transmitter geometry and the calibration information for the pseudo-ranging algorithms
- HAZROUT - computes Hazeltine user receiver information for the pseudo-ranging algorithms
- CALUSE - computes the total pseudo-ranges and pseudo-range rates for both users by combining the calibration and user pseudo-ranging information
- STATSOL - performs the deterministic pseudo-range and pseudo-doppler position and velocity navigation solution and calculates related quantities including linear error analysis terms and tropospheric refraction corrections.

The scope of this volume does not permit the complete discussion of each algorithm presented in Figure 123, but a few items of interest are pertinent to the interpretation of the NAVCAL program and the data in general are described below.

4.3.2.2 Recycling Ambiguities

Since the test system pseudo random noise (PRN) code is not of infinite duration, the measured values of received pseudo range must recycle as the code recycles. The software must, then, remove the ambiguity which results when a single channel recycles independently of the others and when the combination of ground and airborne pseudo-range components result in ambiguous total pseudo ranges. For the Hazeltine equipment this procedure is executed at three separate points in the logic: (1) after the correction for channel delay mismatch; (2) after the formation of the received pseudo range by the differencing of replica and reference clocks, and (3) after the combination of ground and user measurements. The Magnavox equipment performs the first two functions above within the receiver itself. The third function, however, is not as obvious in this case due to the short MRL ambiguity interval (4096 chips). For the MRL data the ground and user measurements are combined as usual but the subsequent ambiguity check must consider all four channels simultaneously to ascertain resolution. Channel 1 is taken as reference and the other three adjusted to be within 4096 chips.

4.3.2.3 The Deterministic Navigation Solution

The deterministic solution of the four pseudo-range and pseudo-doppler equations, along with related calculations, are performed in subroutine STATSOL. The quadratic pseudo-range position solution is used so that one of the Z roots must be discarded.

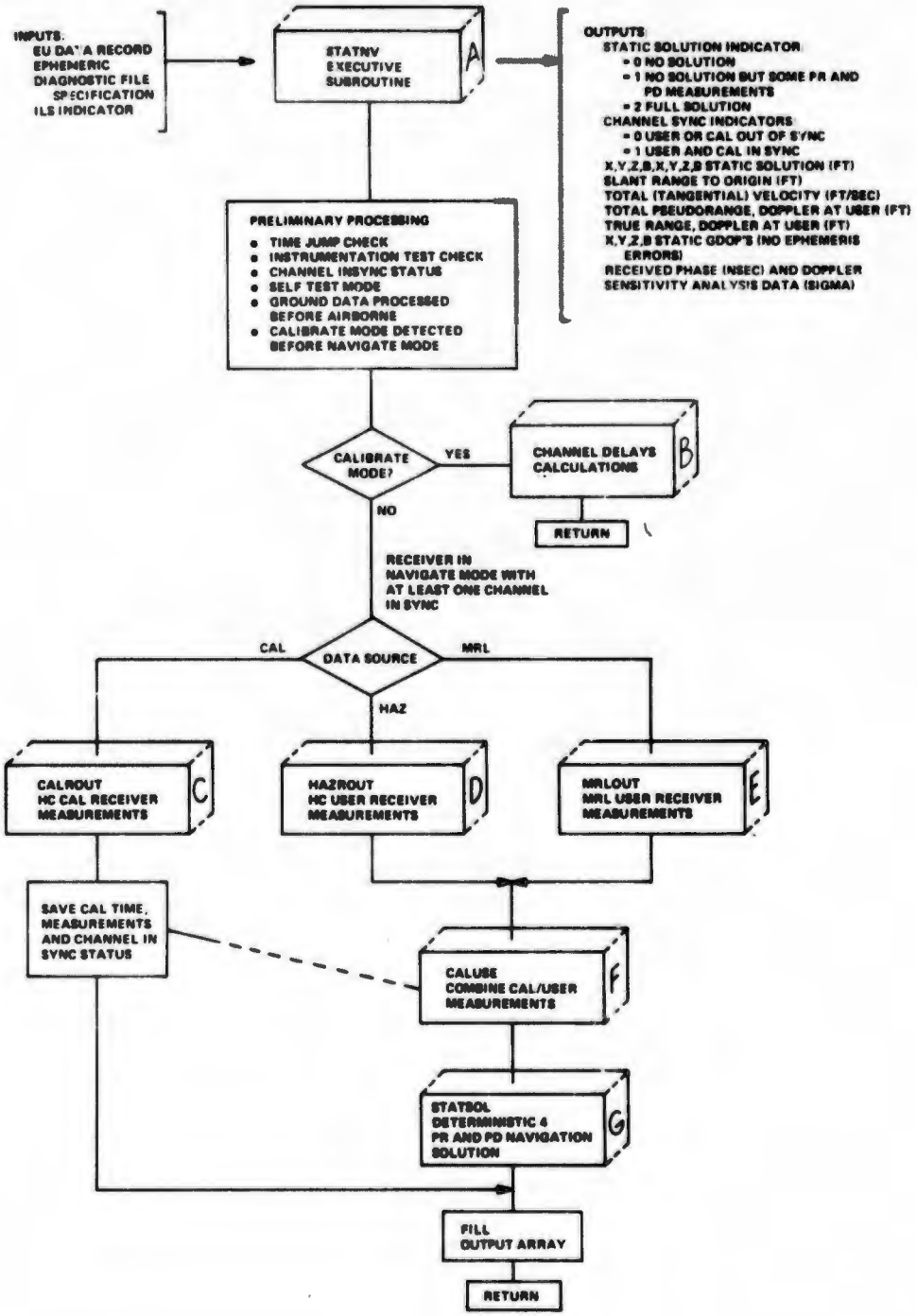

Figure 123 Static Navigation Solution Data Flow, Executive Subroutine

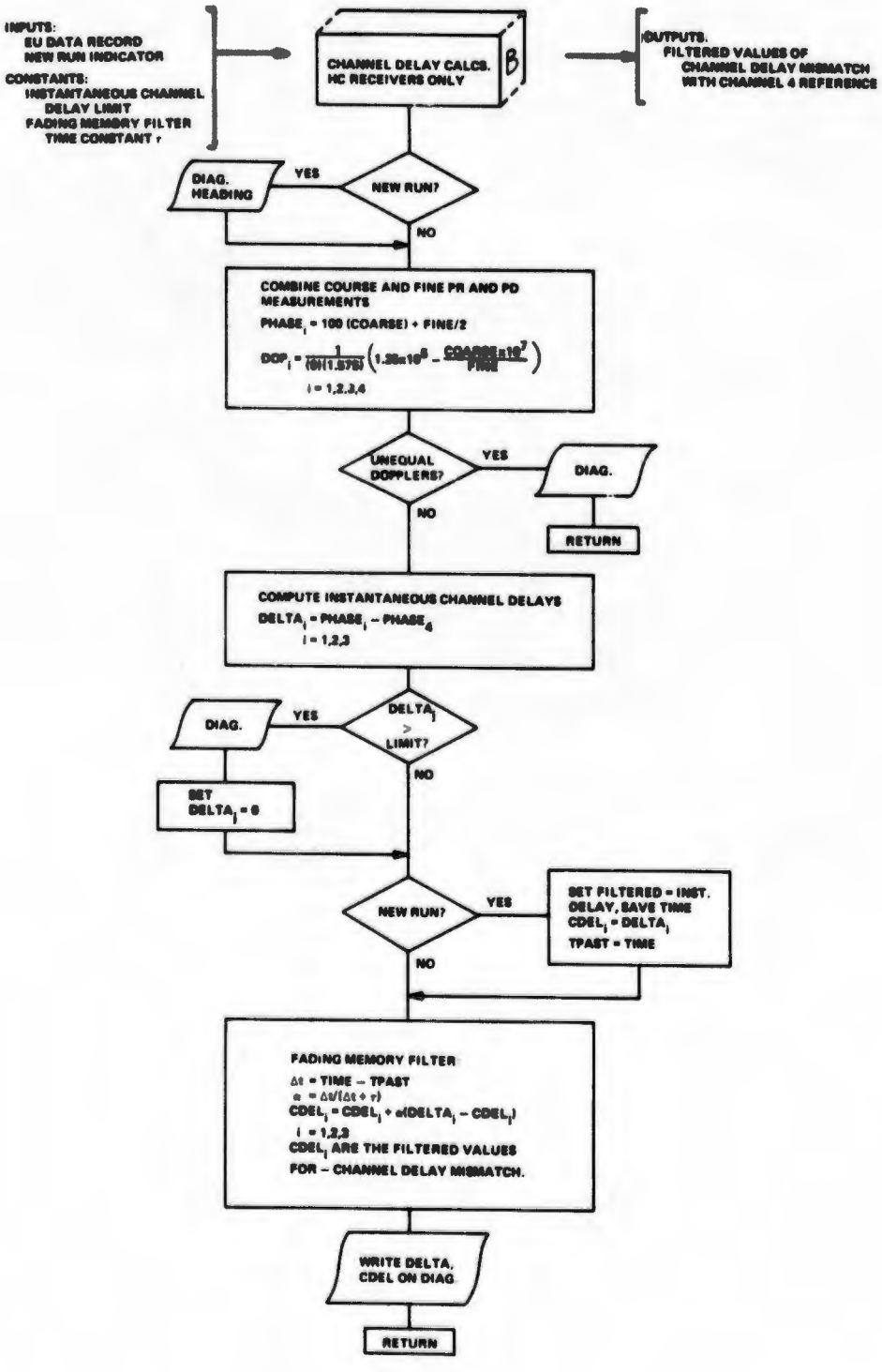

Figure 123 Static Navigation Solution Data Flow, Channel Delay Mismatch Calculations (Continued)

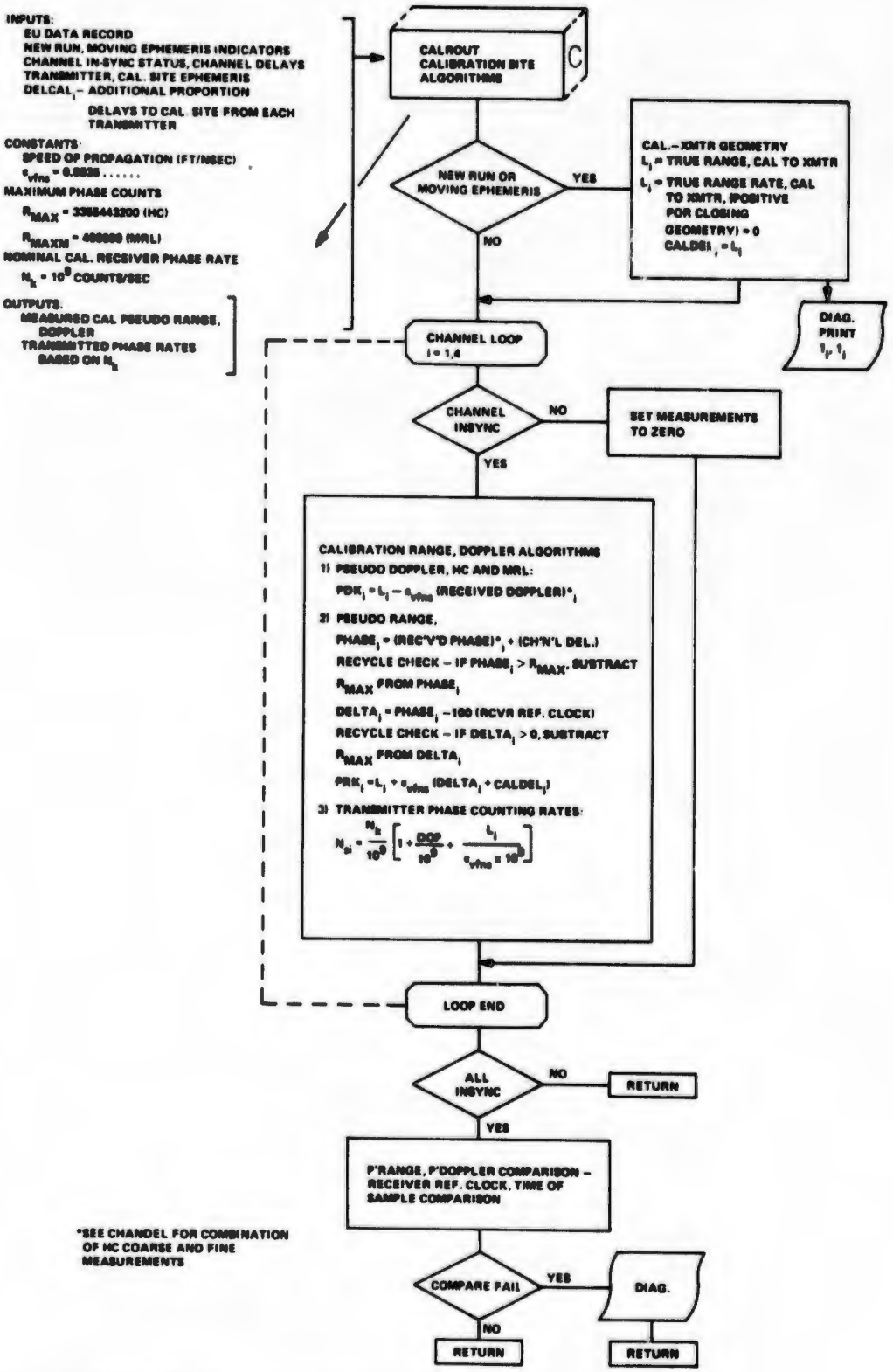

Figure 123 Static Navigation Solution Data Flow, Calibration Algorithms (Continued)

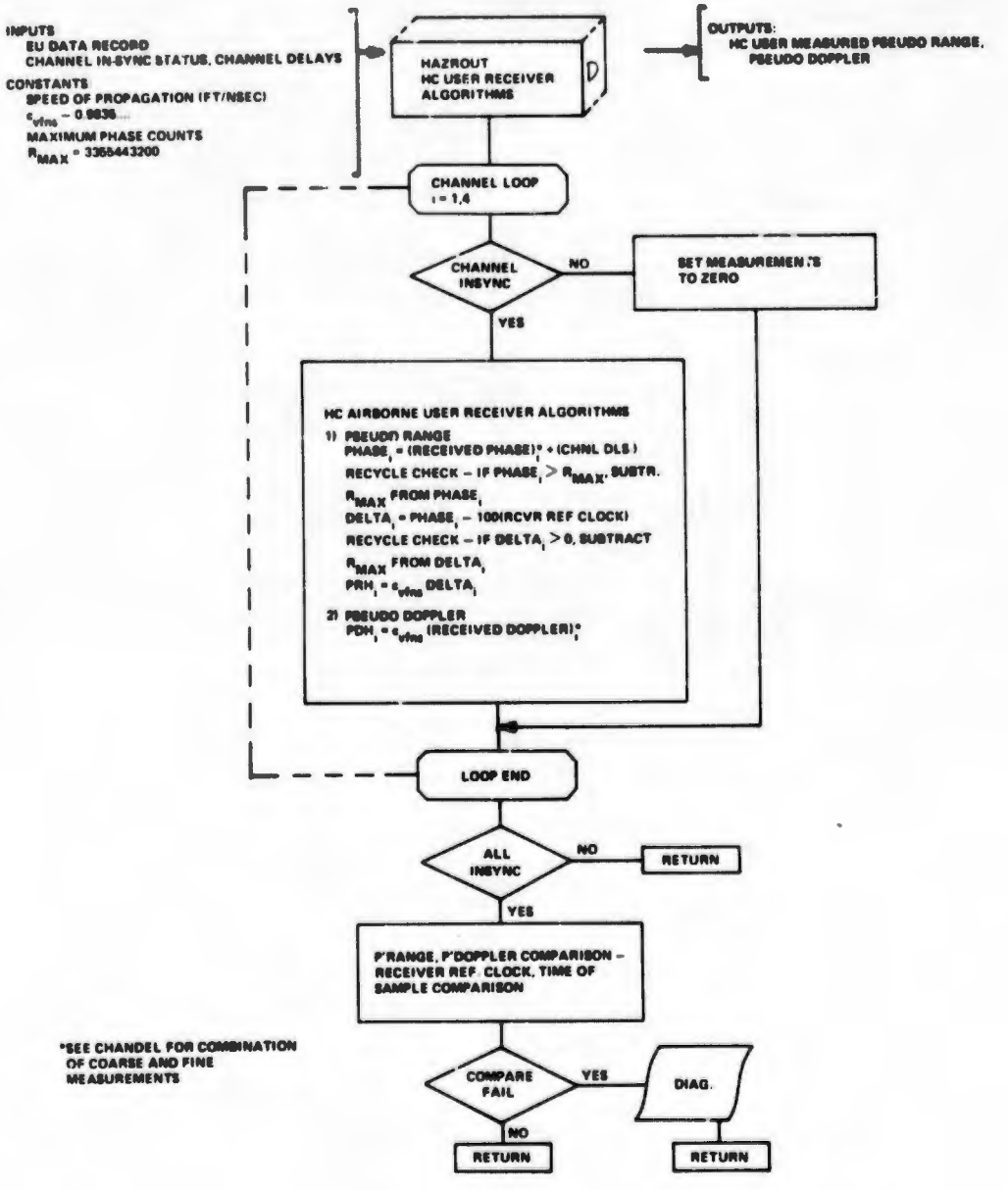

Figure 123 Static Navigation Solution Data Flow, Hazeltine Receiver Algorithms (Continued)

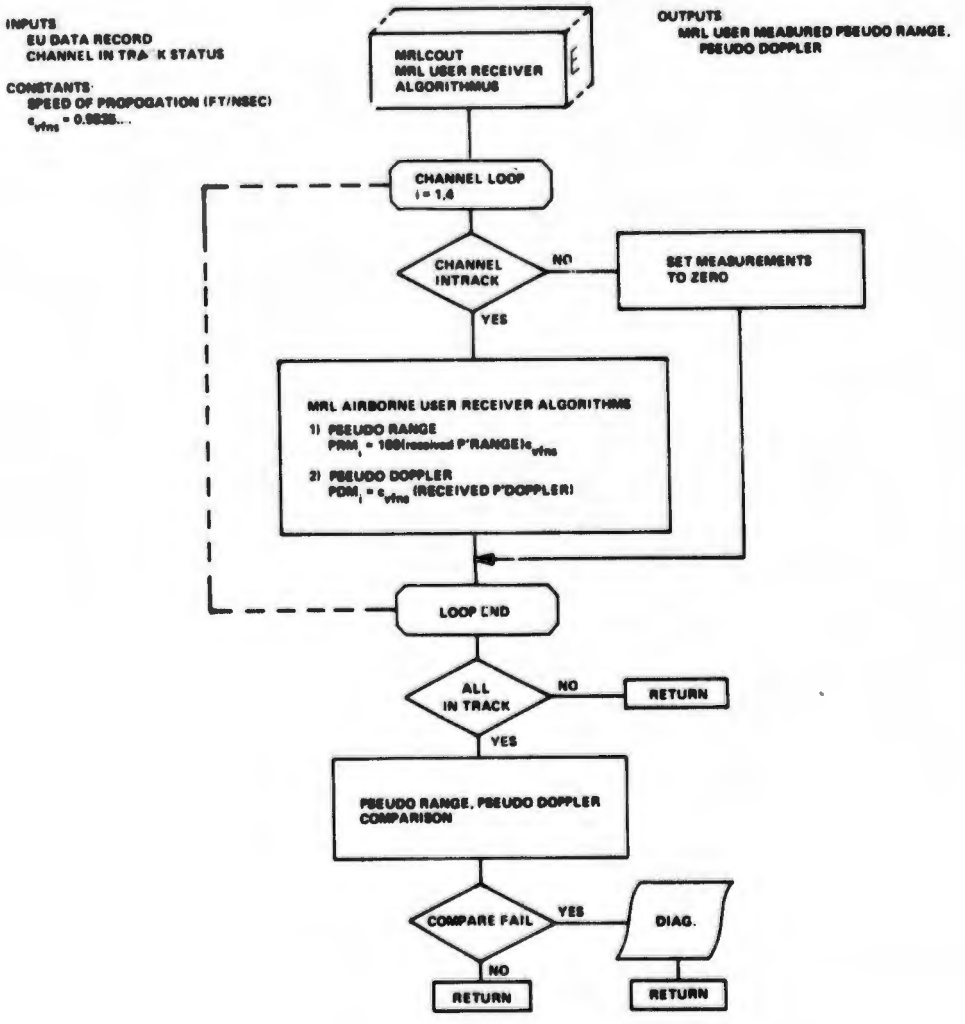

Figure 123 Static Navigation Solution Data Flow, MRL Receiver Algorithms (Continued)

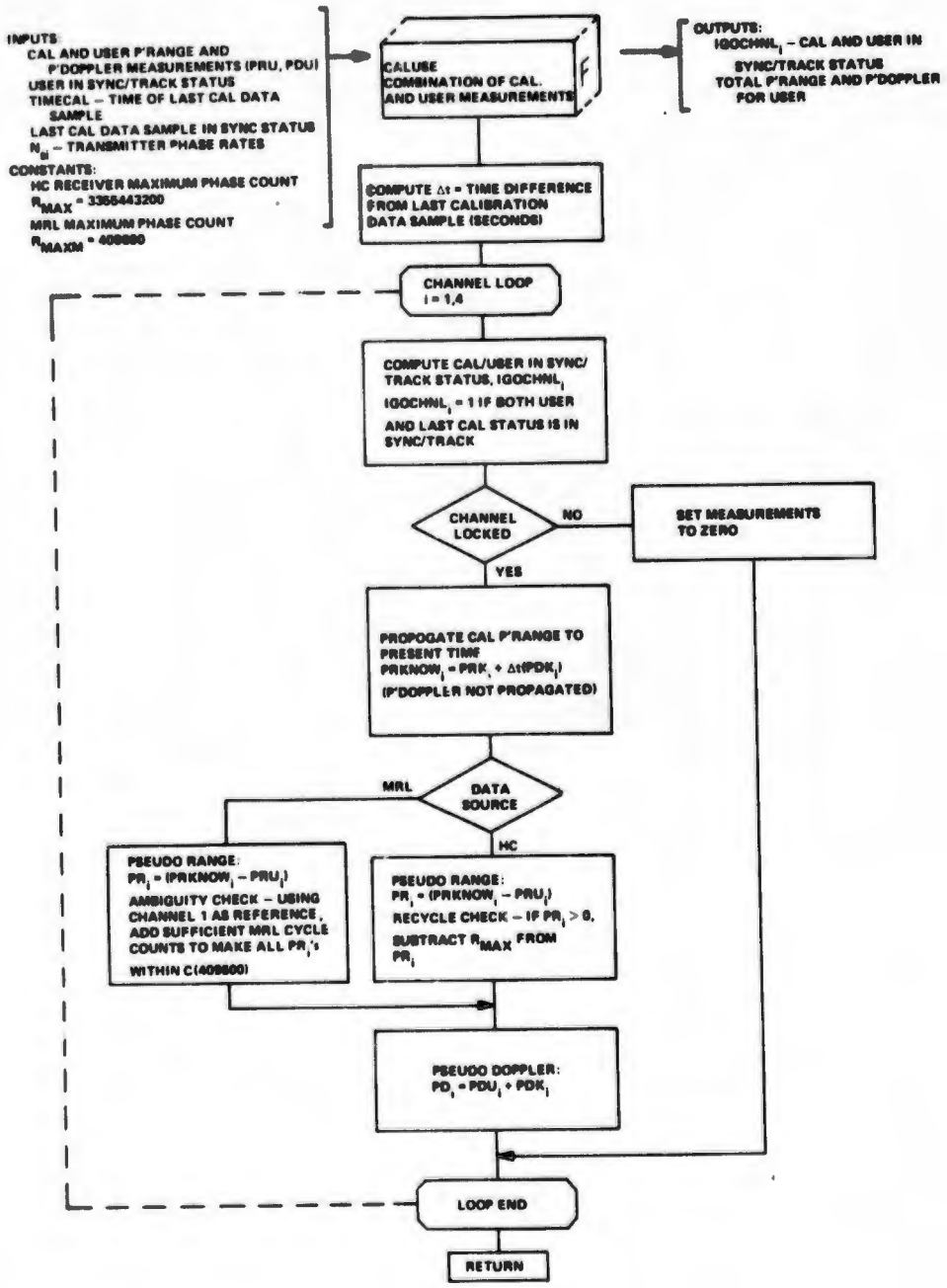

Figure 123 Static Navigation Solution Data Flow, Combination of Cal and User Measurements (Continued)

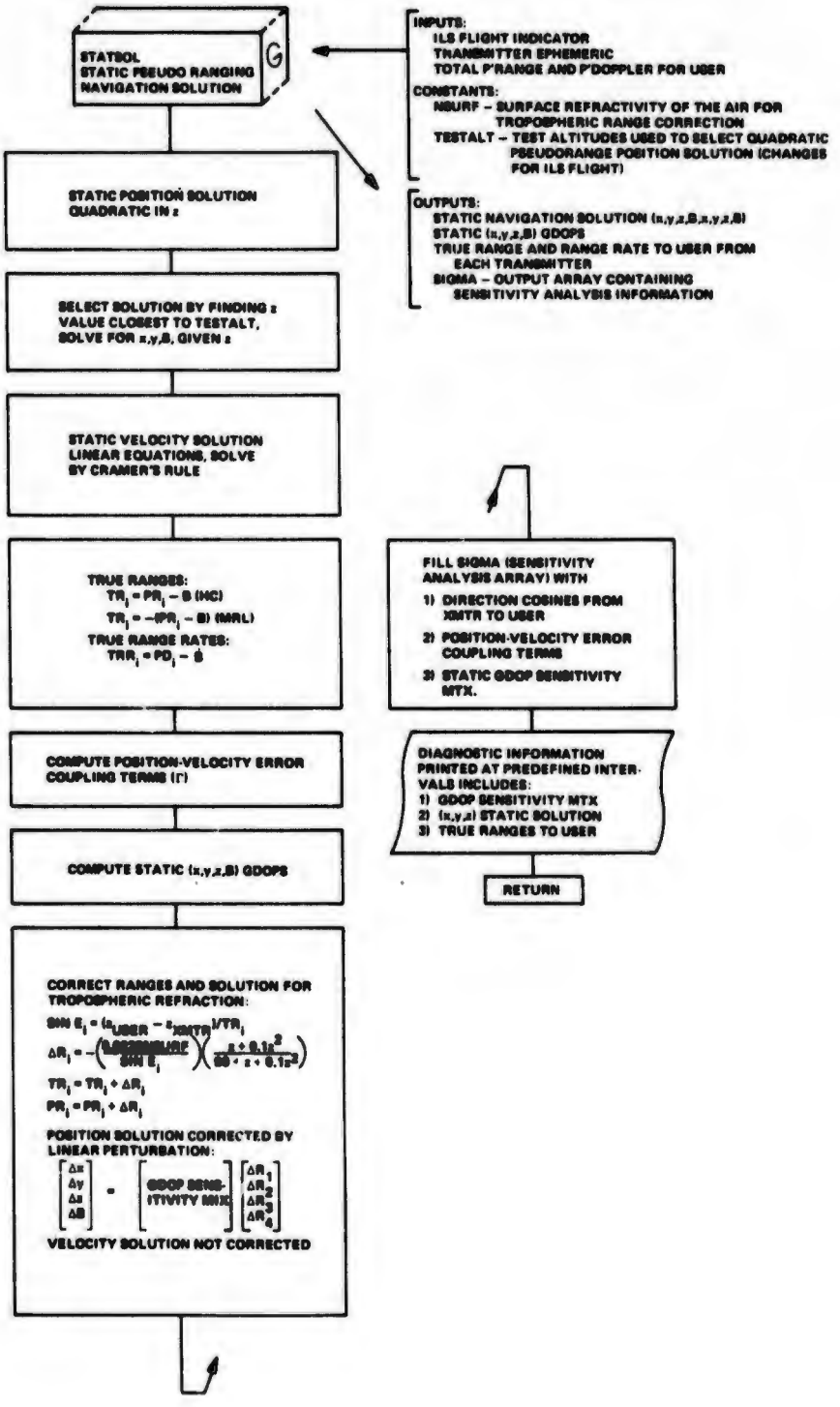

Figure 123 Static Navigation Solution Data Flow, Solution of Navigation Equations (Concluded)

This is done by comparing both Z roots to a test value, and selecting the root which is closest. The test values are: 10,000 ft for the area navigation tests, and 250 ft for the instrument landing system tests. The linear velocity equations are solved by Cramer's rule. The GDOP sensitivity matrix, which is identical to the velocity solution matrix, is saved for output along with other error analysis terms.

4.3.3 FILTER, The Two-State Bias Filter Program

After the static navigation solution has been determined by the NAVCAL program, a simple two-state Kalman filter is used to demonstrate one of the advantages of pseudo ranging over range differencing - the well behaved clock bias.

While the range differencing equations have a computational advantage over the pseudo-ranging equations, the formation of range differences causes a loss of information about the bias between the user reference oscillator and the overall system time reference. This term, usually expressed in feet, is called the pseudo-range bias and it relates the measured pseudo-range quantities to the user's true range from each of the 621B transmitters:

$$r_i = R_i - B$$

where r_i are the true ranges, R_i the (measured) pseudo ranges and B is the pseudo-range bias.

The pseudo-range bias is, ideally, a function of user and ground timing only, and is therefore well behaved. In fact, with no oscillator drift, the pseudo range is a straight line in time.

When the pseudo-ranging concept is applied to the measured doppler signals, a similar bias term evolves. This bias, usually expressed in feet per second, relates the frequency of the user and ground oscillators and is called the pseudo-doppler bias. The true and pseudo-range rates are related by the pseudo-doppler bias, $\dot{B}$/ft sec:

$$\dot{r}_i = \dot{R}_i - \dot{B}$$

where $\dot{r}_i$ and $\dot{R}_i$ are true and pseudo measurements respectively and B is the pseudo-doppler bias.

Further, to first order:

$$\dot{B} = \frac{dB}{dt}$$

Since both biases B and $\dot{B}$ are will behaved and are strongly related to each other, they are especially adapted for filtering. By rendering the error in estimating the value of these biases insignificant, we may realize four true measurements from the four available pseudo measurements and thus reduce the random errors in the user trajectory. Program FILTER implements this concept.

4.3.3.1 Two State Filter Design

The filter states are bias and bias rate:

$$\bar{X} = \begin{bmatrix} B \\ \dot{B} \end{bmatrix}$$

and the state covariance is derived from the sensitivity analysis of the pseudo-ranging equations:

$$(\bar{Y}_c - \bar{X}_i)\cdot(\bar{Y}_c - \bar{X}_i) = (R_i - B_c)^2$$

$$\frac{(\bar{X}_c - \bar{X}_i)}{R_i - B_c}(\bar{V}_c - \bar{X}_i) = \dot{R}_i - \dot{B}_c$$

where $\bar{Y_c}$, B_c, $\bar{V_c}$ and $\dot{B_c}$ are the deterministic position and velocity navigation solution and $\bar{X_i}$ and $\bar{\dot{X}_i}$ are the location and velocities of the four transmitters similar to a true satellite rotating Y configuration. The sensitivity analysis gives state covariance from predicted pseudo measurement errors. The state transition matrix uses the first order approximation.

$$\phi = \begin{bmatrix} 1 & \Delta t \\ 0 & 1 \end{bmatrix}$$

where Δt is the elapsed time between samples. The plant noise matrix models bias acceleration ($\dot{B}$, oscillator drift rate) as a zero mean normal radom variable. The filter is initialized by the deterministic navigation solution and subsequently accepts inputs of: (1) the predicted pseudo range and pseudo-doppler measurement errors; (2) the predicted bias acceleration variance, and (3) the measured static biases B_c and $\dot{B}_c$.

Once the filtered values of the biases are available, this added information is applied to the coordinate trajectory. This is accomplished by forming four true ranges and range rates:

$$r_{fi} = R_i - B_f$$

$$\dot{r}_{fi} = \dot{R}_i - \dot{B}_f$$

where the f subscript indicates the filtered value. These four true measurements are used in a least squares solution for the coordinate position and velocity. The least squares solution is realized by the pseudo-inverse technique. The resulting decrease in random errors in the user trajectory is summarized by the filter improvement factor, defined:

$$fif = \sqrt{\frac{\sigma_x^2 + \sigma_y^2 + \sigma_z^2}{\sigma_{xf}^2 + \sigma_{yf}^2 + \sigma_{zf}^2}}$$

where the f subscript indicates the filtered error predictions. For the 621B Area Navigation Tests typical improvement factor values are

fif $\approx$ 1 at the beginning of the run, (60,000 ft down range)
fif $\approx$ 3 over the center transmitter
fif $\approx$ 2.5 at the end of the run

This filter scheme tends to change the shape of the random error distribution from highly elongated in Z to approximately spherical.

4.3.3.2 Modes of Filter Operation

Under normal conditions the filter program operates in the (two-state) filter mode. Two degraded modes are available: (1) the secondary three-measurement mode, and (2) the tertiary extrapolate (or dead reckon) mode.

The three-measurement mode is invoked when one channel produces bad measurements and at least one previous acceptable navigation point is available for bias extrapolation. The three-measurement navigation solution is derived in Ref. 27.

When there is no deterministic navigation solution available and/or the primary and secondary modes have failed, the full extrapolation mode is used in an attempt to fill the gap in the data. This highly degraded mode is not used for more than two consecutive seconds and requires at least five seconds of previous data to operate. The extrapolation is performed on the trajectory coordinates independently by least-squared residual polynominal fits. A linear curve is fitted to the velocity data and is subsequently integrated for position extrapolation. The constant of integration is determined by fitting the integrated velocity curve to the position data by least-squared residuals.

The filter program selects its operating mode in accordance with the logic shown in Figure 124. The channel-locked discretes from the user and ground calibration station are checked first. If all four channels show good locks, the deterministic navigation solution is then checked for feasibility. In the present program configuration this feasibility check is based on deterministic geometry, error predictions and a comparison of the raw pseudo-range and pseudo-doppler data. If a bad static navigation solution is indicated, it may be due to a single bad measurement. This one-bad-channel possibility is checked by comparing the first difference of the four pseudo dopplers to the second difference of the four pseudo ranges.

When all three program modes fail to produce a meaningful trajectory, the lost data results in time jumps in the output.

4.3.3.3 Filter Models

The two state bias filter requires two externally derived parameters:

- The predicted variance of bias acceleration is estimated from system oscillator statistics and refined through examination of flight data. It is used in Q matrix computation.

$$\text{Var}\,(\ddot{B}) = 0.0005\ (\text{ft/sec}^2)^2$$

This value is admittedly very conservative. The clock stability is good, and, if it were the only unmodelled error, the Q matrix could probably be set to zero. Unfortunately, unmodelled measurement bias errors have forced the insertion of a large filter Q so that the filter does not diverge from the static solution. This is done at the expense of the filter improvement factor (reduction of random error content). This situation could be corrected by implementing a higher state filter which would model measurement bias errors.

- The predicted variance of pseudo-range and pseudo-doppler errors is used to obtain the predicted state covariance. These errors are predominantly thermal noise and are modelled such:

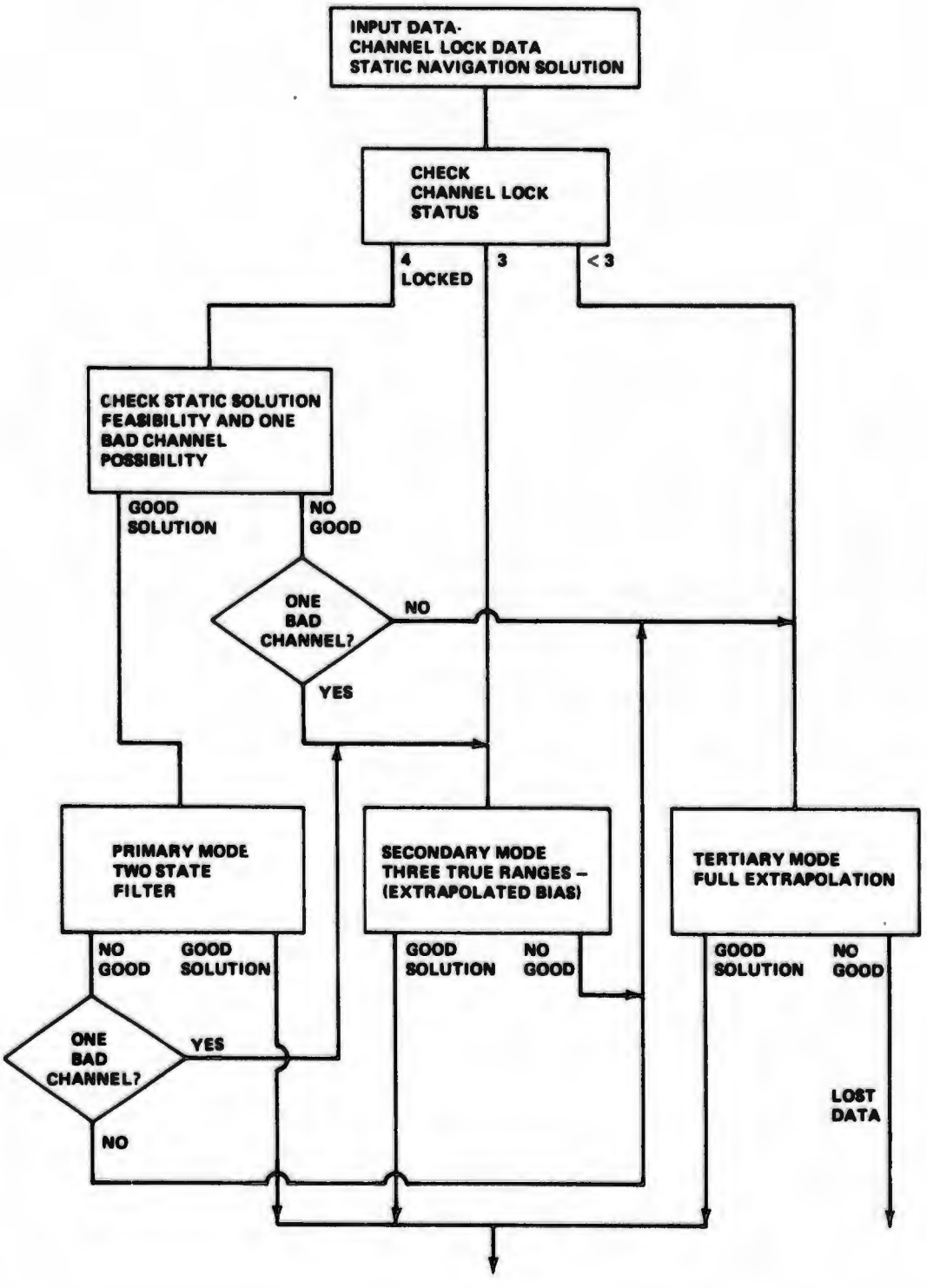

Figure 124 Filter Mode Selection

Received power watts is

$$PW = 10^{[(Pdbm - 30)/10]}$$

Defining constants

$$K_{code} = \frac{cT_c\sqrt{BW_{code}\ 10^{No/10}}}{2}$$

$$K_{carr} = \frac{\sqrt{BW_{carr}\ 10^{No/10}}}{T_{DOP}(2\ \pi f_{carr})}$$

where

c = speed of signal propagation (ft/nanosec)

T_c = phase chip length (nanosec)

BW_{code} = two sided noise bandwidth of code loop (Hz)

BW_{carr} = two sided noise bandwidth of carrier loop (Hz)

N_o = noise density (dbw/Hz)

T_{DOP} = doppler counting time (sec)

f_{carr} = carrier frequency (GHz)

then

$$\sigma_R = K_{code}/\sqrt{PW}$$

$$\sigma_{\dot{R}} = K_{carr}/\sqrt{PW}$$

where :

$T_c = 100$

$BW_{code} = 5.6$

$BW_{carr} = 43.6$

$T_{DOP} = 0.1$

$f_{carr} = 1.575$

Other sources of measurement error have been lumped into a single contribution. These errors have been empirically assigned as:

$\sigma_R^2 = (2)^2$ for HC

$\sigma_R^2 = (1)^2$ for MRL

$\sigma_{\dot{R}}^2 = (0.25)^2$ for both receivers

4.3.3.4 Computer Implementation

The two-state 621B bias filter has been implemented on the CDC 6400 computer with emphasis on producing a maximum amount of useful flight testing information. Overall flow charts of the executive program and major subroutines appear in Figure 125.

The executive program reads the deterministic navigation solution information from the NAVCAL program output tape. It then checks data status, selects the filter mode and calls the corresponding subroutine. A separate subroutine is used for tape and tabular output.

4.3.4 MERGE, BET Residual Calculation and Presentation Program

After the BET has been transmitted to SAMSO, a reference trajectory from WSMR is made available to us for comparison purposes. The MERGE program calculates trajectory residuals and presents them graphically.

Figure 126 shows the MERGE flow. Transmitter positions are extracted from the Run Descriptor Record (except in ILS tests where the balloon position is contained in the data record) and reference range and range rate trajectories calculated from them. Both WSMR and Aerospace Corporation BET's are accepted. Linear interpolation of the reference data to 621B time is performed. Trajectory acceleration and jerk are computed from the reference data by differentiation of the velocity information.

The trajectory residuals calculated are:

- X, Y, Z position and velocity
- Range and range rate from each of the transmitters to the user.

These residuals are estimates of the system error (if the reference BET were perfect, the residuals would be the system errors) and are plotted, according to card input options, versus time or other system parameters.

On the time history plots a second curve may be added. This is the predicted error band for the random error in the residuals. It is calculated as the 3-sigma point of the root sum of squares (RSS) value of the test data and reference BET predicted errors. Since, in general, the reference position trajectory is much smoother than the FILTER trajectory, the error band is almost completely due to the test system contribution. (In the velocity trajectory the opposite is true and the error bands are almost completely due to the reference BET.) The purpose of the error band is to alert the data analyst to unmodelled errors. If the residuals fall outside the band more than (approximately) 99% of the time, an unmodelled source of error has become significant.

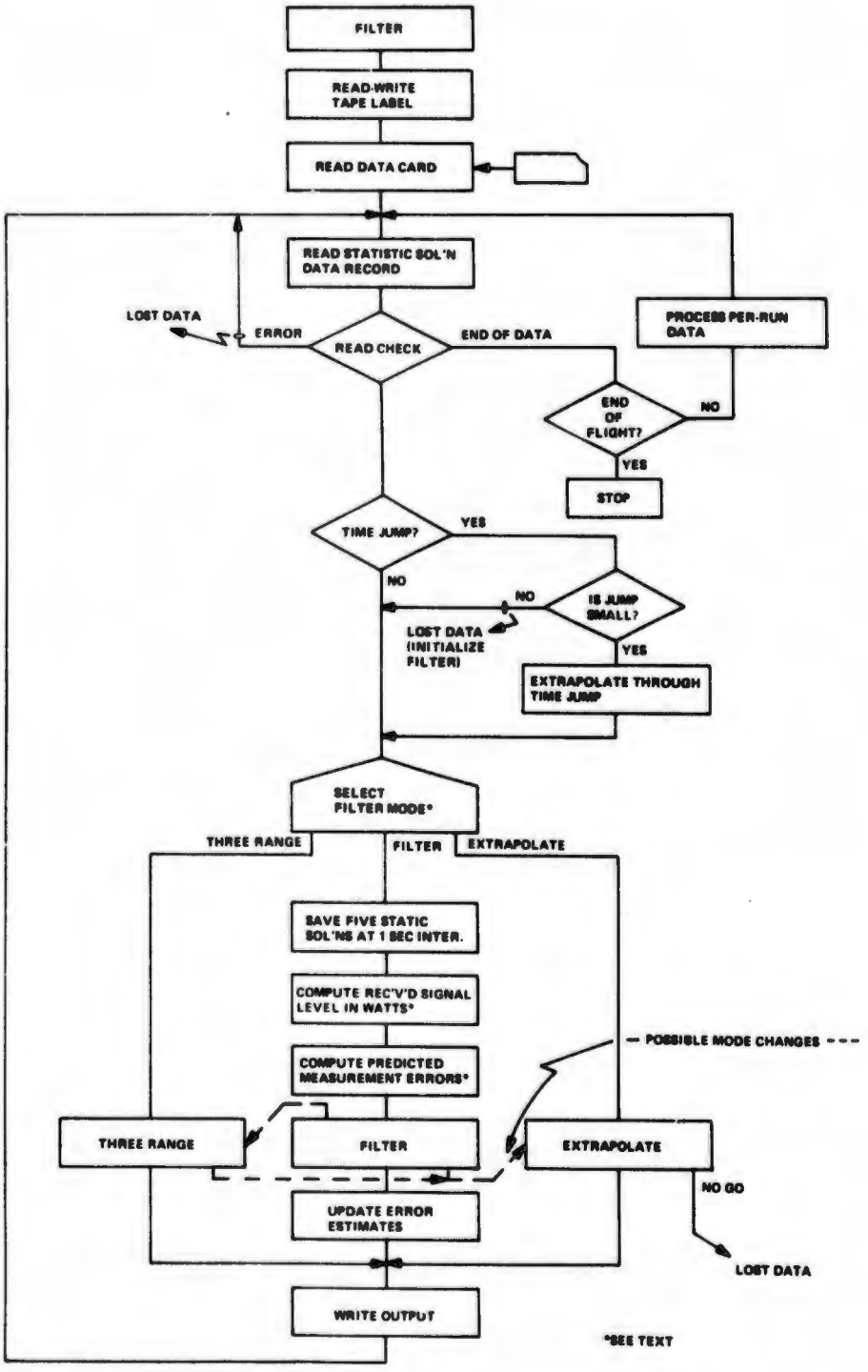

Figure 125 Two-State Bias Filter Implementation, Executive Flow

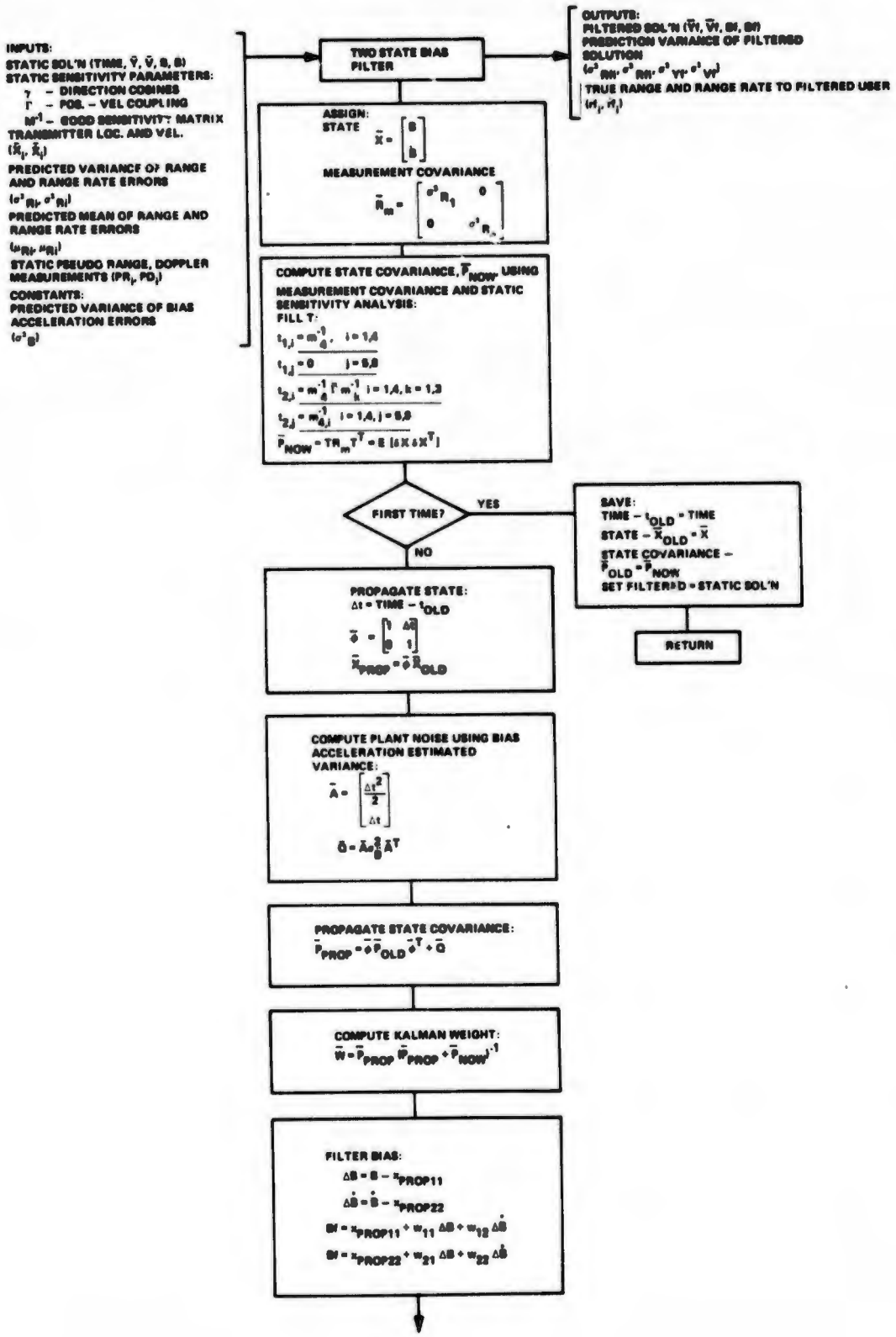

Figure 125 Two-State Filter Flow, Filter Algorithms (Continued)

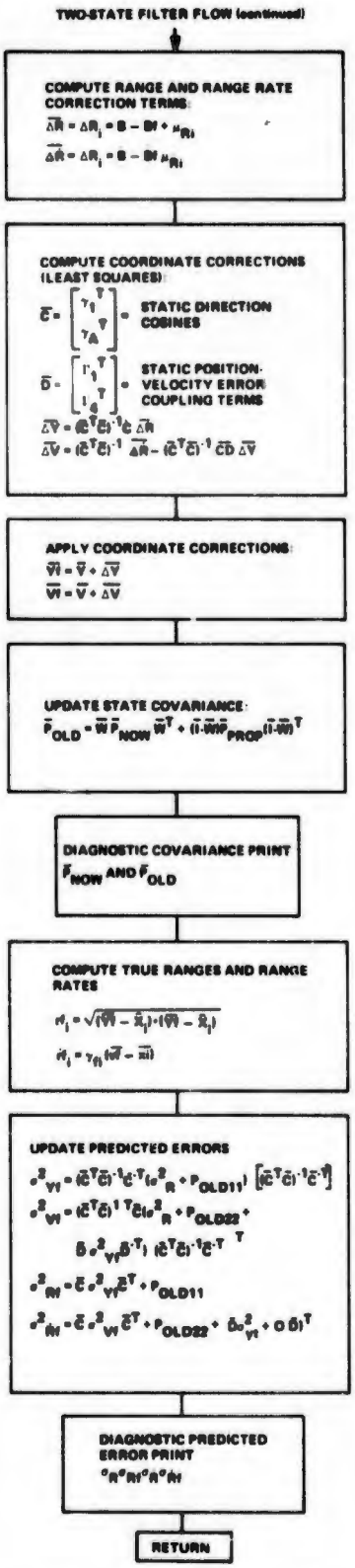

Figure 125 Two-State Bias Filter Data Flow, Filter Algorithms (Continued)

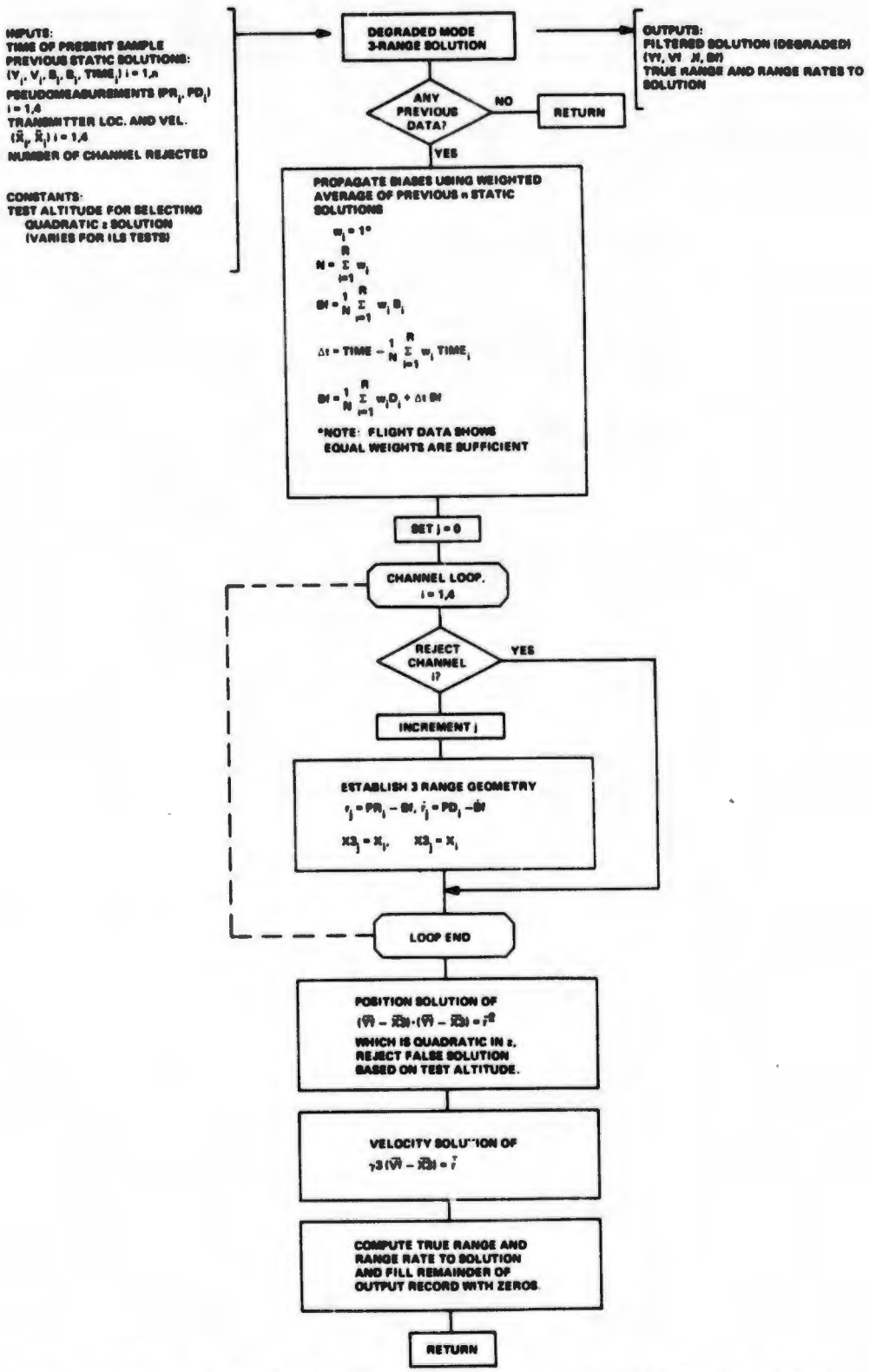

Figure 125 Two-State Bias Filter Data Flow, 3-Range Navigation (Continued)

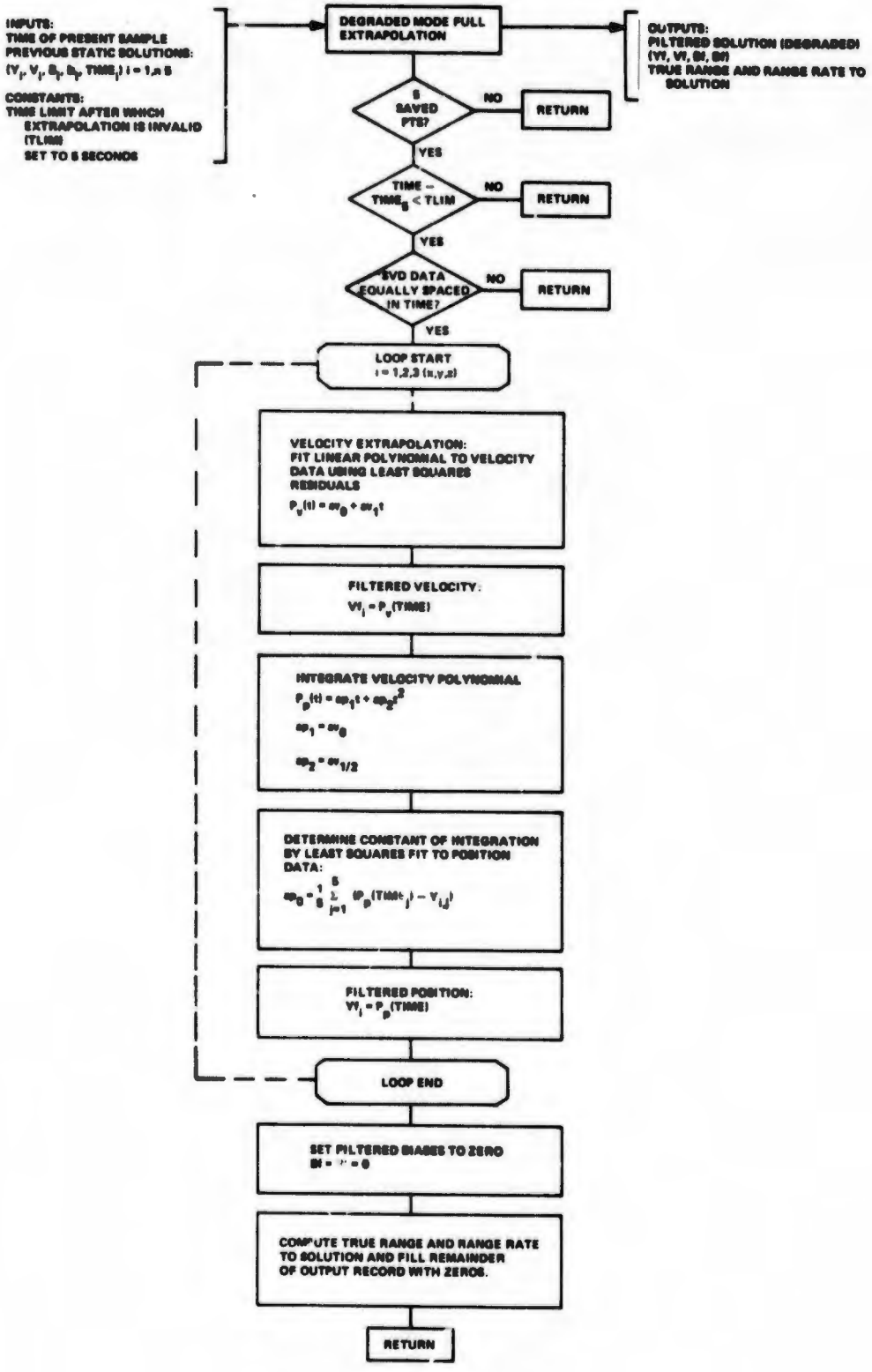

Figure 125 Two-State Filter Flow, Dead-Reckon Navigation (Concluded)

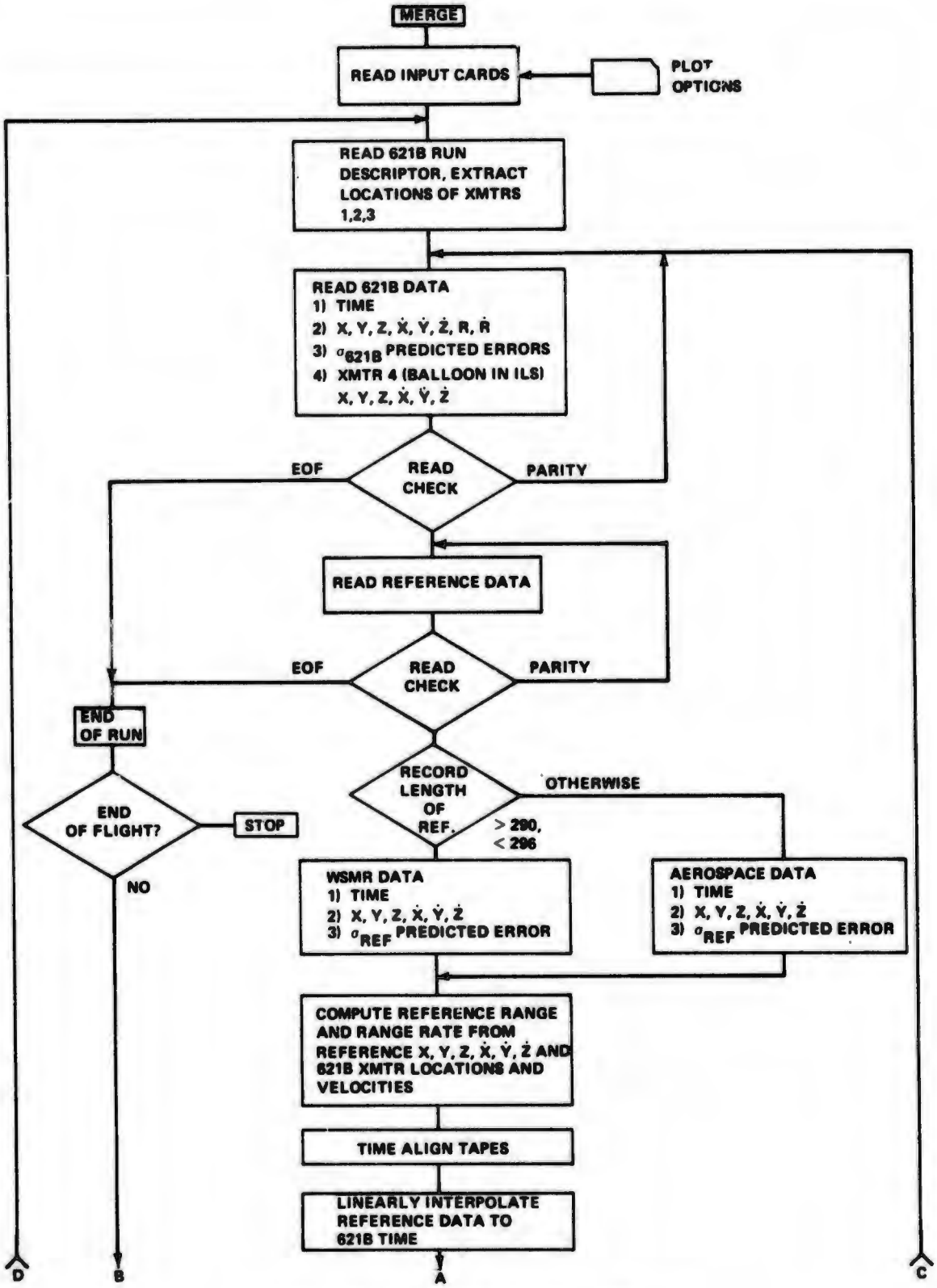

Figure 126 MERGE Program Flow

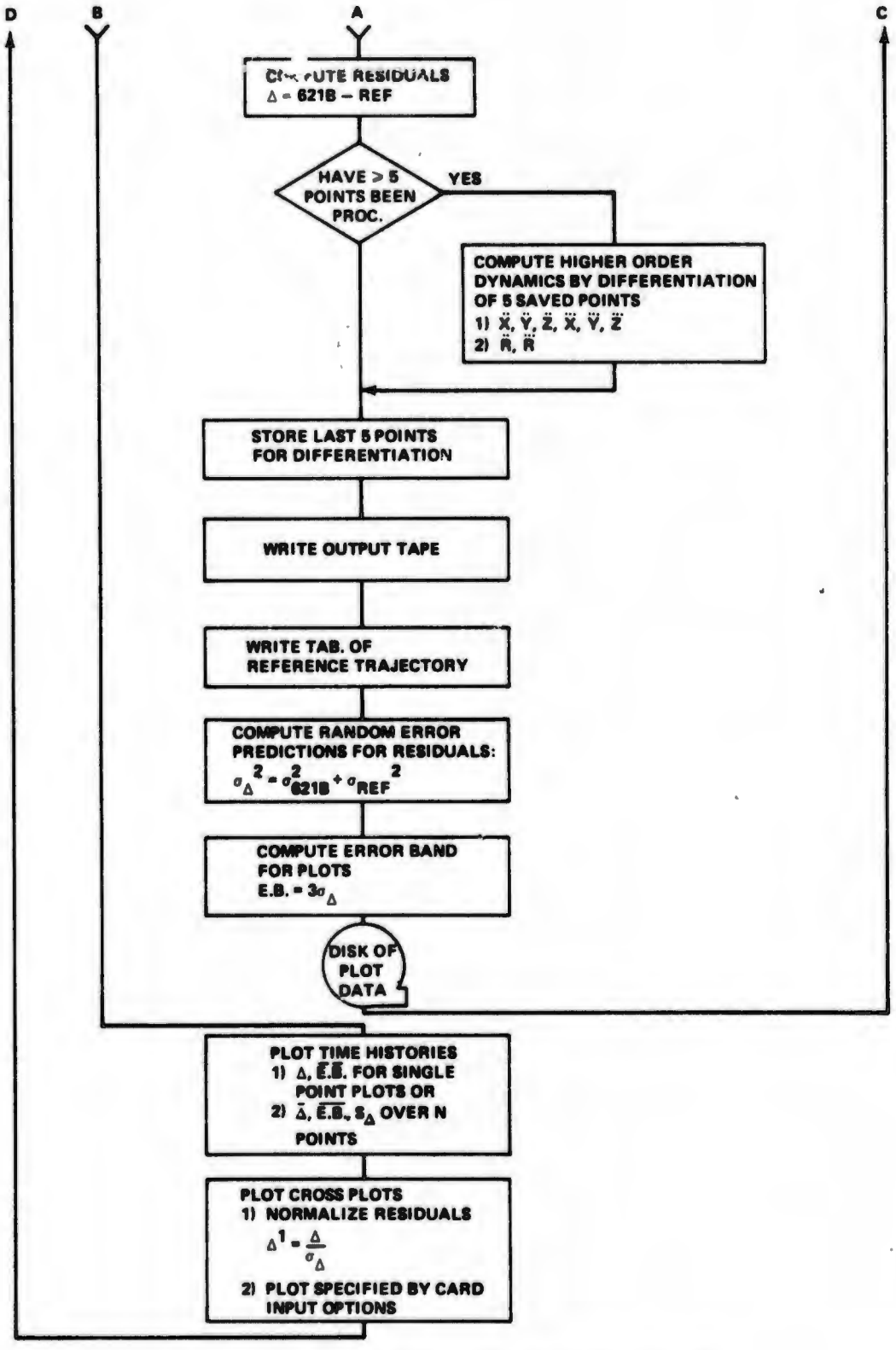

Figure 126 MERGE Program Flow (Concluded)

4.3.5 INQUIRE, The Trajectory Residual Characterization Program

While the MERGE output plots graphically present each trajectory residual, they cannot fully characterize the properties of system errors. We must draw on mathematical statistics for this task. Program INQUIRE forms statistics for the MERGE residuals.

The program considers manually specified time slices of the data. Manual slice selection allows wild point editing before statistical analysis. Each slice is defined to be 10 seconds (50 data points) in length and is assumed to have stationary statistics (inspection of the MERGE plots shows this to be a valid assumption, especially in the good GDOP regions). Statistics related to deterministic, random and periodic analyses are calculated:

- Deterministic error characterization
  - Sample mean
  - Least squared residuals linear fit with sample number, slope and intercept, residual standard deviation
  - Difference sign test statistic for whiteness test against trend (number of times that the series increases)
- Random error characterization (for the data)
  - Second through fourth central moments
  - Unbiased estimate of standard deviation
- Random error characterization (for the linear fit residuals)
  - Residual range
  - Residual median
  - Residual percentage points (1, 5, 10, 50, 90, 95, 99%)
- Periodic error characterization (for linear fit residuals)
  - Turning points test statistic for whiteness test against periodicity (number of turning points in data)
  - First 20 serial correlation coefficients (correlogram through lag 20)
  - Power spectral density to one-half Nyquist frequency
  - Two-term Yule autoregressive coefficients
  - Frequency of maximum power spectral density.

These statistics are calculated by a general purpose subroutine EXAMINE. Of particular importance to our discussion are: (1) the sample mean which estimates system bias errors; (2) the sample standard deviation which estimates system random error; (3) the turning point test statistic which determines if the errors are

white noise or contain some low frequency component(s), and (4) the frequency of maximum power spectrum. The software is implemented so that the maximum spectrum frequency is ignored unless it is significant.

Program INQUIRE calculates all of the above statistics for both the rectilinear coordinate residuals (X, Y, Z, $\dot{X}$, $\dot{Y}$, $\dot{Z}$) as well as the interchannel residuals:

$$\Delta R_{j-i} = (PR_j - PR_i)_{621B} - (R_j - R_i)_{Reference}$$

$$(j,i) = \{(2,1), (3,1), (4,1), (3,2), (4,2), (4,3)\}$$

where j and i are channel number, PR_k the pseudo ranges (or pseudo dopplers), and R_k the reference trajectory true ranges (or dopplers) from user to transmitter. The interchannel residuals are of particular importance because, unlike the X, Y, Z errors, they are independent of geometry. Caution must be exercised, however, in interpreting interchannel results because the statistics contain effects from both channels. This is the unfortunate consequence of not having any accurate knowledge of the true value of the clock biases.

While the system error statistics are important, ultimately we wish to uncover any dependencies between the errors and other external parameters. Program INQUIRE, to this end, characterizes the 50 point time slice over which the residual statistics were taken by evaluating the average values of:

- The user's rectilinear position on range
- The user's velocity vector in polar coordinates
- The user's rectilinear acceleration and jerk
- The true range and range rates from user to transmitters
- The azimuth and elevation look angles from transmitters to user
- The true range accelerations and jerks
- The received signal level at the user
- The elapsed time into run from initial receiver lock-up
- The GDOP sensitivity and direction cosine matrices.

A sample output of Program INQUIRE is shown in Figure 127.

4.3.6 CORLATE, The Cross Plot Analysis Program

The magnetic tape output of program INQUIRE contains residual and system characterization parameters taken over short time slices. By combining the INQUIRE outputs from multiple flights by tape copy operations, program CORLATE presents cross plots of these parameters taken over the ensemble of flights, runs and test points. These plots are used to show consistencies (or the lack of consistencies) in the data from flight to flight and run to run. One-hundred eight pertinent parameters are available for cross plotting, resulting in over 10,000 possible combinations. Of

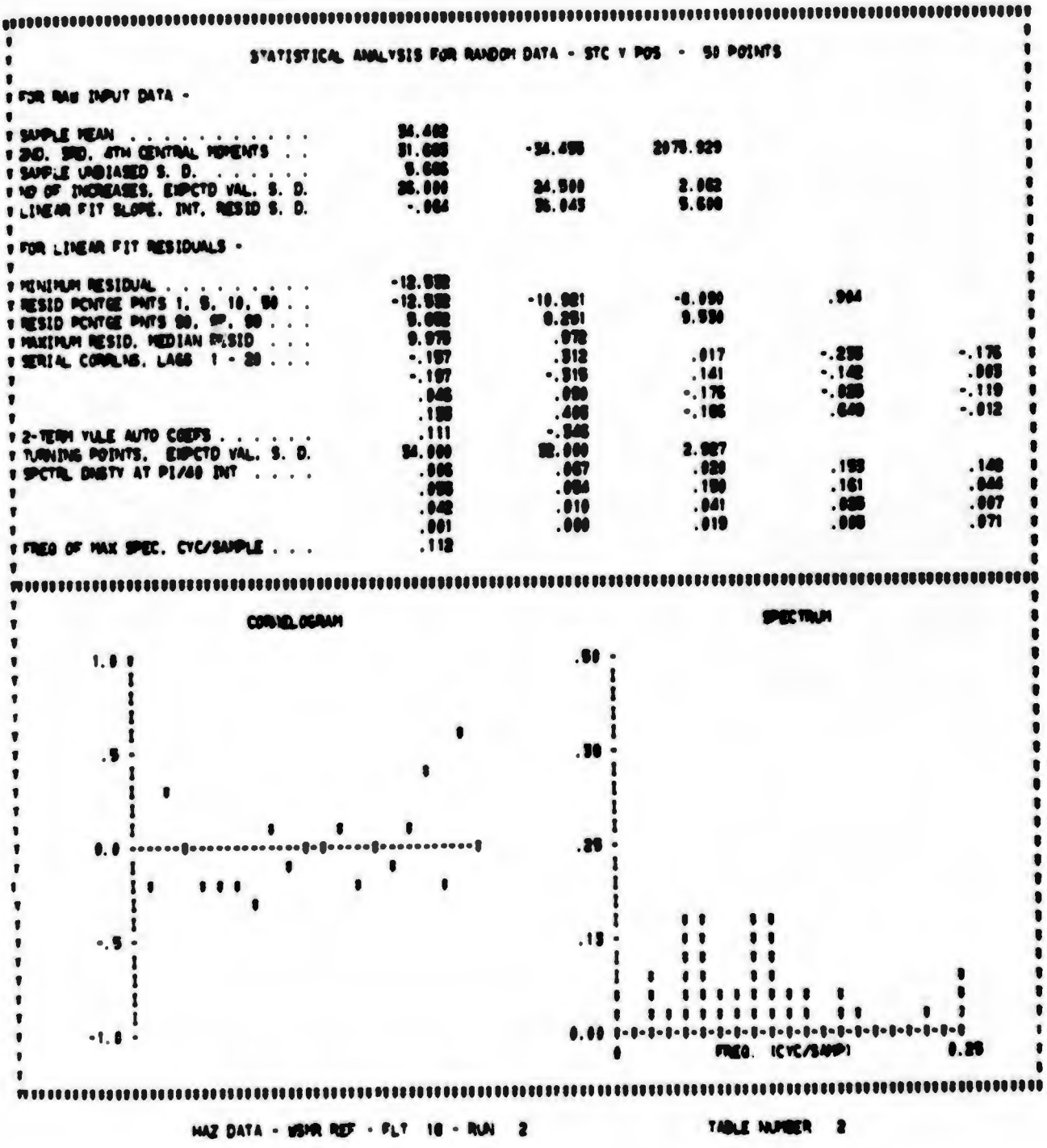

Figure 127 Sample Output from Program INQUIRE

SLICE CHARACTERIZATION PARAMETERS

	X (EAST)	Y (NORTH)	Z (UP)	
AVERAGE POSITION	-2405.49	-11985.60	31496.69	FT
PREDICTED REF TRAJ STAND DEV	5.47	5.41	1.72	FT
PREDICTED STATIC TRAJ STAND DEV	2.65	5.96	9.90	FT
PREDICTED FILTRD TRAJ STAND DEV	5.32	5.35	1.44	FT
AVERAGE VELOCITY	-15.59	700.52	-2.03	FT/SEC
PREDICTED REF TRAJ STAND DEV	.42	.47	.25	FT/SEC
PREDICTED STATIC TRAJ STAND DEV	.57	.70	1.60	FT/SEC
PREDICTED FILTRD TRAJ STAND DEV	.40	.46	.22	FT/SEC
AVERAGE ACCELERATION	-.00	.01	-.00	FT/SEC2
AVERAGE JERK	-.00	-.00	.00	FT/SEC3

	XMTR 1	XMTR 2	XMTR 3	XMTR 4	
AVERAGE RANGE	53012.43	43809.70	49184.93	38469.92	FT
PREDICTED REF TRAJ STAND DEV	2.02	2.00	2.75	1.05	FT
PREDICTED STATIC TRAJ STAND DEV	1.40	2.12	1.60	1.11	FT
PREDICTED FILTRD TRAJ STAND DEV	1.01	2.93	2.99	1.61	FT
AVERAGE RANGE RATE	240.31	309.95	289.02	-199.54	FT/SEC
PREDICTED REF TRAJ STAND DEV	.29	.35	.35	.27	FT/SEC
PREDICTED STATIC TRAJ STAND DEV	.26	.27	.26	.25	FT/SEC
PREDICTED FILTRD TRAJ STAND DEV	.27	.34	.34	.25	FT/SEC
AVERAGE ELEVATION ANGLE (POS UP)	60.60	46.21	44.19	76.11	DEGREES
AVERAGE AZIMUTH ANGLE (CW FM N)	-160.22	156.53	-127.46	-5.04	DEGREES
AVERAGE RECEIVED SIGNAL LEVEL	-126.45	-132.10	-129.31	-120.20	DBM

STATIC GDOP SENSITIVITY MATRIX

I	-.26	1.01	-.00	.15 I
I	-2.00	.05	.27	1.76 I
I	5.54	-2.15	-2.40	-.00 I
I	-4.95	2.10	2.36	1.47 I

STATIC DIRECTION COSINE MATRIX

I	-.074	-.000	.001 I
I	.474	-.000	.700 I
I	-.000	-.430	.007 I
I	-.012	.201	.071 I

ELAPSED TIME INTO RUN	32.1 SEC				
OVERALL RCVD SIGNAL LEVEL	-127.0 DBM				
SGNL LVL DIFFERENCES (2-1...4-1) .	-0.7	-2.9	6.2 DBM		
TOTAL AIRCRAFT VELOCITY	700.7 F/S				
LOS VECTOR AZIM, ELEV	-1.1	-1.1 DEG			
AVG RNGE ACCEL	-15.1600	-0.4672	-0.2260	-14.0960	F/S2
AVG RNGE JERK	-.4167	-.2417	-.3020	.1427	F/S3

Figure 127 Sample Output from Program INQUIRE (Concluded)

these, about 200 are considered noteworthy and are included in the program as a standard plot set. They are separated into four categories:

- Overall characterization plots
  - Flight number and time of day data
  - Power level variations with geometry
  - Range vector geometries attained
- Pseudo-range bias error analysis plots
  - Interchannel mean error vs:
    - o Range vector geometry in three-space
    - o Range dynamics (velocity, acceleration, jerk)
    - o Signal level
    - o Time of day, flight number variations
    - o User velocity vector heading
- Random error analysis plots
  - Interchannel error standard deviation vs:
    - o Elevation look angles from transmitter to user
    - o Signal level
    - o North-South position on range
    - o User velocity vector heading
  - Rectilinear error standard deviation vs:
    - o Signal level
    - o Time of day
    - o Interchannel frequency content
- Pseudo-range, pseudo-doppler periodicities plots
  - Pseudo range, doppler frequency content vs:
    - o Elevation look angles from transmitter to user
    - o Signal level
    - o North-South position on range

- o User velocity vector heading

The plots are generated using an elaborate auto-scaling technique with different plot symbols identifying each flight. The plot parameters are screened for reasonableness by limit checking before they are placed on the grid. See Volume III for plots which show significant results.

4.4 ADDITIONAL SOFTWARE

The data processing programs described in the preceding section accounted for the major software development effort for the field test. However, numerous special purpose routines were developed which did not fit into the mainstream processing but produced important results. In this section we briefly describe these subordinate programs.

4.4.1 Reformatting Programs SHUFFLE, MEASURE and ARRANGE

Two reformatting tasks were of particular importance. Program SHUFFLE was written to simplify the format of the navigation solution FILTER tape for transmittal to SAMSO. The normal FILTER output tape contains label and run descriptor records as well as peripheral test data information such as signal level, channel lock status and GDOP sensitivities. SHUFFLE strips out the pertinent trajectory information and writes an output tape compatible with SAMSO requests.

Program MEASURE was written to simplify the EU tape format for use in ground user multipath tests and other analyses. It, as an option, writes an IBM compatible binary tape.

A third reformatting program, ARRANGE, was written to enable MERGE processing on the static navigation solution. This program reads a NAVCAL output tape and reformats it to a FILTER tape, with the static navigation solution replacing the filtered quantities. This program was used extensively in ILS processing since the FILTER program only produced valid output in the (small) regions of good GDOP. As an option, ARRANGE also reformats a cinetheodolite trajectory tape from WSMR, which allows processing to residuals of cine-BET trajectories.

4.4.2 Field Analysis Software, READY, SWIFT and DELAY

Receiver readiness tests require a means of estimating channel noise under bench test conditions when a navigation solution is not produced. Program READY applies the variate difference method to the pseudo-range data on an EU tape to obtain these estimates. The program produces a separate set of standard deviation estimates for each file on the EU tape.

Other bench tests, used to investigate interchannel effects, require the computation of statistics on the differences of the pseudo-range measurements among the channels. One channel is taken as "common", and the difference between its measurement and that of the other channels is computed at each sample time. Program SWIFT performs these computations from EU data, allowing the selection of the common channel and of wild point edit limits. The differences are printed along with the sample time, and means and standard deviations of the differences are computed for each file of data.

The programs discussed above all operate without using external reference data. However, once a reference trajectory is available some addition calculations can be made on a quick-look basis for field diagnosis of problems. Program DELAY was written to perform a set of calculations especially useful for this purpose. DELAY compares a reference trajectory to the computed solution and calculates the error in each computed range. One range error, arbitratily designated as the "common", is subtracted from the others. The resulting differences are useful because they are not directly dependent upon the GDOP factor and because error components common to both ranges are canceled. Exact agreement with the reference trajectory can be achieved only when all of the differences are zero.

DELAY also calculates statistics on the error differences for each successive intervals of specified length. Usually, 25-second slices were specified. To increase computer efficiency, DELAY operated on reformatted versions of the reference and 621B solution tapes. An option allows the generation of a tape with error differences, so that they may be plotted at the KAFB/Holloman computer facility.

The field analysis software described above was supplemented by a number of minor programs used to edit, reformat, and plot the data. These routines, together with the 6585th Test Group supplied trajectory comparisons, satisfied the field analysis software requirements of the program.

4.4.3 Tabular Listing Program, REVEAL

Program REVEAL generates a tabular listing of data on the NAVCAL tape. It was used to present, in an easily read format, the contents of the static navigation solution tape to facilitate debugging of subsequent programs. Time slices, output parameters and sampling rates are manually selectable. A tabular plot of the static trajectory is produced in the X, Y, Z dimensions.

4.4.2 Random Error Analysis Program, RANDOM

Throughout the analysis of the data (or any other passive user navigation data), we are constantly troubled by the absence of a complete reference data set. That is, there is no reference "trajectory" for the oscillator bias terms. This forces the analyst to use inter-channel quantities for his data base or to make some broad assumptions about the clock biases.

In the case of random error analysis we may use our knowledge of the relative smoothness of the true aircraft trajectory to supplement the data characterization by statistics. Namely, we may apply the method of variate differences to obtain variance estimates for the random error components in each channel independently. Program RANDOM implements this concept.

The program selects 50 point data slices for analysis. The slice is rejected if it contains a time jump or produces a GDOP factor greater than 50. The statistical analysis, performed on a per-slice basis, consists of a whiteness noise test by turning points (a 3-sigma limit is used) on the range-doppler comparison data and variate difference variance analysis on the per-channel and interchannel pseudo ranges and pseudo-range rates. Estimates of the covariance terms are made by combining the variance estimates from the per and inter-channel data. The variance estimates are sorted by power level and user Y position and are directed to tabular output for manual analysis.

4.4.5 The Trajectory Accuracy Summary Program, SUMMARY

While the measurement accuracy is of prime importance to the data analyst, the overall system accuracy claim must ultimately be made in the navigation domain. That is, we must answer the question, "How well can we navigate"? Program SUMMARY was written to answer this question through data presentation by three separate techniques. The program reads a MERGE tape and produces, for HC and MRL static and (two state) filtered trajectories:

- XY and YZ trajectory plots on a per-run basis which show the WSMR reference trajectory and magnified 621B errors
- Scatter diagrams of X and Y user errors for the ensemble of 621B flights
- Histograms, sorted by power level, of X, Y, Z horizontal and total 621B errors for the ensemble of flights

The SUMMARY results are used in a limited manner for data analysis and as the primary data presentation in the Executive Summary Volume.

4.5 GROUND USER MULTIPATH DATA HANDLING

The software supporting ground user multipath analysis is divided into three parts; namely, a data reduction program, data analysis program and a prediction program.

The data reduction program processes the data recorded during the tests from MEASURE tapes and card inputs. The program time slices the data and takes sample means and variances over the available sample size at a rate of once per second. The data available for analysis consists of the channel delay calibration points representing relative channel delay mismatches, cable length calibration, and relative power levels recorded from test data sheets.

The reduction program removes the effects of channel delay and cable differences and computes statistics on the observed differential delay due to multipath.

A simulation program utilizes mathematical models of the surface, the electromagnetic wave propagation and the system characteristics to compute the multipath error predictions for a given geometry and test configuration. The predicted errors are then compared to the measured errors. Differences in these errors are analyzed and presented in summary form in tabulated outputs.

4.6 WSMR REFERENCE TRAJECTORY DATA GENERATION

One area of primary importance in the analysis of 621B trajectory residuals is the generation of the WSMR reference trajectory, or BET. If one assumes that the WSMR BET is perfect, he may be led far astray from the truth about the field test system errors. On the other hand, advertised accuracies (sigmas) of the WSMR BET are quite a bit smaller than those of our test data (about a factor of 3 to 5) and, for random errors at least, the assumption has merit. BET biases are not quite as firmly understood as the random components, but they are probably adequate to give good confidence to statements about pseudo-range bias errors.

We present here an abridged discussion of WSMR BET generation with emphasis on trajectory and measurement modelling. The full document, Ref. 24, was prepared by William S. Agee and Robert H. Turner of the Analysis and Computation Division, White Sands Missile Range. (See Figure 128 for WSMR BET data flow.)

4.6.1 Trajectory Modelling

One of the primary reasons for developing a BET at WSMR is to provide a single estimate of position, velocity, and acceleration through the combination of all available range measurements. Any technique developed for this application must apply to most of the flight test programs at WSMR for which there are data reduction requirements. Obviously, this requires the use of a rather general dynamic model of the flight test trajectory.

One model which meets this requirement is the second order polynominal model presently used in the data reduction process. In state variable from this model is

$$
\begin{aligned}
x_1 &= x \\
x_2 &= y \\
x_3 &= z \\
x_4 &= \dot{x} \\
x_5 &= \dot{y} \\
x_6 &= \dot{z} \\
x_7 &= \ddot{x} \\
x_8 &= \ddot{y} \\
x_9 &= \ddot{z}
\end{aligned}
\qquad
\dot{x} = f(x) = \begin{bmatrix} x_4 \\ x_5 \\ x_6 \\ x_7 \\ x_8 \\ x_9 \\ 0 \\ 0 \\ 0 \end{bmatrix}
$$

This very simple model has been used with some success in stiuations where dynamics of the progess are not too severe such as aircraft tracking and free flight missile trajectories.

WSMR has had much more success with a dynamic model which, rather than $\ddot{X}$, $\ddot{Y}$, and $\ddot{Z}$ as states, uses acceleration components close to "where the action is" namely tangent and normal to the trajectory. Let A_T (tangential acceleration) be tangent to the trajectory, A_N (normal acceleration) be normal to A_T and lie in the vertical plane, and A_L be normal to the A_T and A_N directions and complete right-handed system, Figure 129.

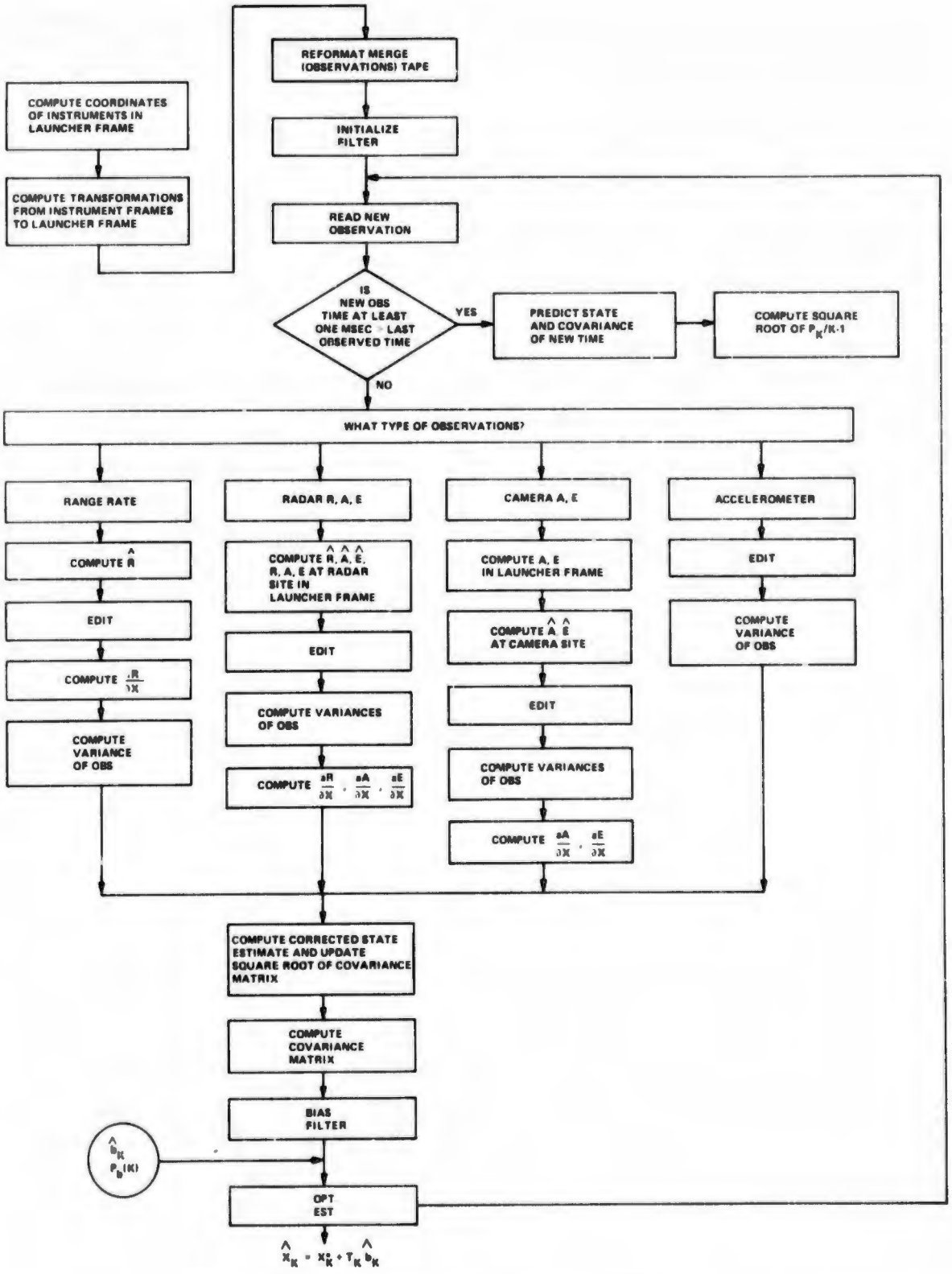

Figure 128 Functional Flow of WSMR Bet

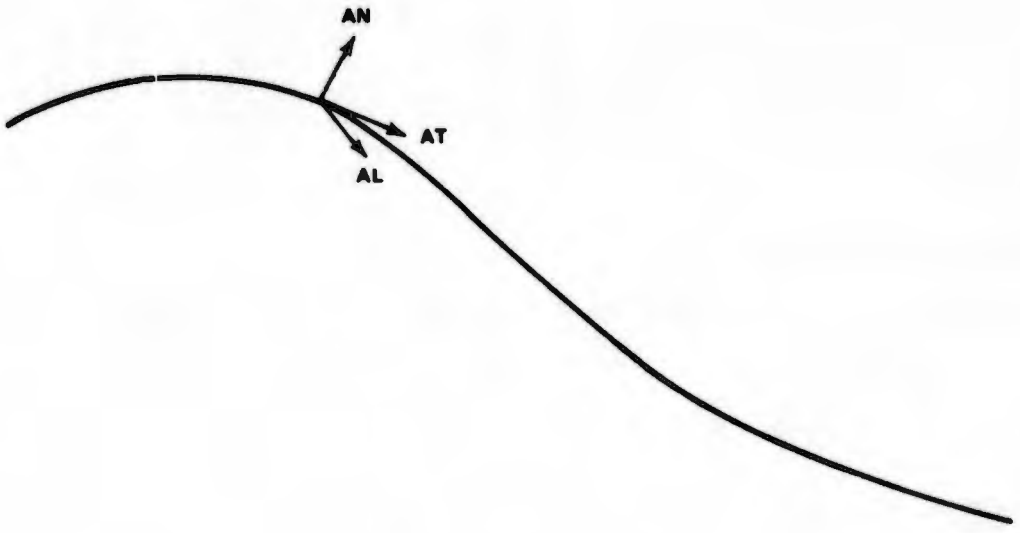

Figure 129 Acceleration Components

It is assumed that these acceleration components do not contain the effect of gravity. Using these accelerations we define the following dynamic material.

$$
\begin{aligned}
x_1 &= x \\
x_2 &= y \\
x_3 &= z \\
x_4 &= \dot{x} \\
x_5 &= \dot{y} \\
x_6 &= \dot{z} \\
x_7 &= A_T \\
x_8 &= A_N \\
x_9 &= A_L
\end{aligned}
\qquad
\dot{x} = f(x) =
\begin{bmatrix}
x_4 \\
x_5 \\
x_6 \\
\dfrac{x_4x_7}{V} - \dfrac{x_4x_6x_8}{V_G V} + \dfrac{x_5x_9}{V} \\
\dfrac{x_5x_7}{V} - \dfrac{x_5x_6x_8}{V_G V} + \dfrac{x_5x_9}{V} \\
\dfrac{x_6x_7}{V} + \dfrac{x_8V_G}{V} + g \\
0 \\
0 \\
0
\end{bmatrix}
$$

where

$$V_G = (x_4^2+x_5^2)^{1/2}$$

$$V = (x_4^2+x_5^2+x_6^2)^{1/2}$$

This is the model which is presently in the BET program. Note that White Sands is still using a constant acceleration assumption as in the quadratic model but that the present model is nonlinear. One reason that this model is considerably more useful is that acceleration measurements, which are made aboard the test vehicle, are usually much easier to model in terms of tangential, normal, and lateral accelerations.

4.6.2 Measurement Modelling

Besides modelling the trajectory, the measurement must also be modelled in terms of the trajectory state variables. Thus, for each measurement WSMR specifies a nonlinear measurement function h(x) which relates the ideal measurement to the trajectory state. It is assumed that the position and velocity state variables (x_1, x_2, x_3, x_4, x_5, x_6) of the trajectory are with respect to a coordinate system which is called the launch system.

4.6.2.1 Radar Measurements

Radar observations are usually from the FPS-16 instrumentation radars. These radars measure range, aizmuth, and elevation of a target in a local radar Cartesian coordinate system. Some of the radars also measure the range rate of the target. The observed range, azimuth, and elevation (RAE) are first corrected for calibration and refraction. Direction cosines are computed from these corrected observations and then related to the launch coordinate system where azimuth and elevation angles are recomputed. In terms of the trajectory state variables which are in the launch coordinate system the radar measurement functions are:

Range

$$h_1(x) = [(x_1-x_I)^2+(x_2-y_I)^2+(x_3-z_I)^2]^{1/2}$$

Azimuth

$$h_2(x) = \tan^{-1} \frac{x_1-x_I}{x_2-y_I}$$

Elevation

$$h_3(x) = \tan^{-1} \frac{x_3-z_I}{[(x_1-x_I)^2+(x_2-y_I)^2]^{1/2}}$$

where (x_I, y_I, z_I) are the coordinates of radar in the launch coordinate system.

Range Rate

$$h_4(x) = \frac{x_4(x_1-x_I)+x_5(x_2-y_I)+x_6(x_3-z_I)}{h_1(x)}$$

4.6.2.2 Optical Measurements

The fixed cameras and tracking cameras measure aizmuth and elevation of the line-of-sight to the target. The observed angles are corrected for calibrations and refractions. The measurement functions for the cameras are the same as for the radar azimuth and elevation measurements.

$$h_2(x) = \tan^{-1} \frac{x_1 - x_I}{x_2 - y_I}$$

$$h_3(x) = \tan^{-1} \frac{x_3 - z_I}{[(x_1 - x_I)^2 + (x_2 - y_I)^2]^{1/2}}$$

where (x_I, y_I, z_I) are coordinates of camera station in the launch coordinate system.

4.6.2.3 DOVAP Measurements

The DOVAP measuring system is a two-way doppler system. The basic digitized measurement is the doppler cycle count over the sampling interval (t_1, t_2), which when properly scaled yields the change in loop range from transmitter to target to receiver. If an addition the measurement is divided by $(t_2 - t_1)$, the result is the average loop range rate over the interval which approximates the instantaneous loop range rate at

$$\frac{t_1 + t_2}{2}$$

Following this procedure WSMR represents the DOVAP observation by the measurement function

$$h_5(x) = x_4\left(\frac{x_1 - x_T}{R_T} + \frac{x_1 - x_R}{R_R}\right) + x_5\left(\frac{x_2 - y_T}{R_T} + \frac{x_2 - y_R}{R_R}\right) + x_6\left(\frac{x_3 - z_T}{R_T} + \frac{x_3 - z_R}{R_R}\right)$$

where (x_T, y_T, z_T) and (x_R, y_R, z_R) are the coordinates of the DOVAP transmitter and receiver. The quantities R_T and R_R are

$$R_T = [(x_1 - x_T)^2 + (x_2 - y_T)^2 + (x_3 - z_T)^2]^{1/2}$$

$$R_R = [(x_1 - x_R)^2 + (x_2 - y_R)^2 + (x_3 - z_R)^2]^{1/2}$$

4.6.2.4 Inertial Measurement Unit

An important class of acceleration measurements comes from inertial measurement units (IMU). This is the type of measurements on the 621B Navigational Satellite Tests. There are many configurations for the IMU measurements. Some IMU's make acceleration measurements in a coordinate system slaved to the local vertical, some in an inertial coordinate system set up at a launch point, etc. In addition to acceleration measurements, attitude measurements of the body with respect to the reference coordinate system are also available.

One simple type of IMU measurements which have been processed with the BET

program came from a purely inertial system. In this case the inertial system was aligned with the aircraft at a specified time. The future accelerations were then measured in this coordinate system. This measurement configuration is shown in Figure 130.

Although inertial platform misalignments and drifts, accelerometer scale factor errors, and accelerometer zero set errors must be modeled and estimated, it is assumed that these are zero for the present discussion. In absence of these errors, the acceleration measurements may be modelled in terms of the trajectory accelerations as

$$\begin{bmatrix} A_1 \\ A_2 \\ A_3 \end{bmatrix} = \underset{3\times3}{M_{Ie}} \; \underset{3\times3}{M_{et}} \begin{bmatrix} A_T \\ A_N \\ A_L \end{bmatrix}$$

Where M_{Ie} is the rotation matrix from the earth fixed launch coordinate system to the inertial system and M_{et} is the velocity dependent rotation matrix from the trajectory coordinate system to the launch coordinate system. In any case the scalar acceleration measurements are linear functions of the trajectory accelerations.

$$h_{10}(x) = \underset{1\times3}{M^T} \begin{bmatrix} A_T \\ A_N \\ A_L \end{bmatrix}$$

where the vector M = M(x) is state dependent.

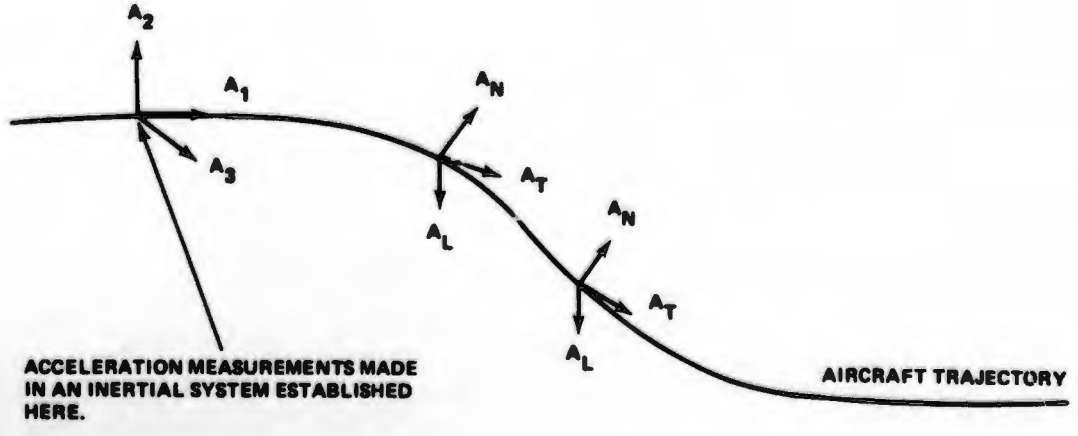

Figure 130 IMU Measurement Configuration

4.6.2.5 Extended Kalman Filter

The White Sands BET program is basically an extended Kalman filter. For the case of systems whose dynamics are linear, the measurement functions are linear and all uncertanties have Gaussian statistics, the Kalman filter is known to provide the optimal recursive estimate of the state. For nonlinear systems the extended Kalman filter obtained by linearizing the nonlinear functions about the current estimate of the state has become a popular and highly useful estimation procedure for nonlinear systems.

For our extended Kalman filter we assume the dynamic trajectory model

$$\dot{x} = f(x) + w$$

where f(x) was previously given and w is a white noise term with zero mean and covariance Q. The presence of the state noise w or rather its covariance is used to compensate the filter gains for the errors made in modelling, in particular for the errors in the trajectory model due to the constant acceleration assumption.

Observations z(K) are available, at discrete instants of time t_K. It is assumed that the z(K)'s are statistically independent scalar observations. The processing of scalar observations provides a numerically efficient as well as intutively appealing method of processing the observations. The assumption of statistical independence of the observations can be removed if necessary. The scalar observations are represented as

$$Z(K) = h(x(K))+v(K)$$

where v(K) is a measurement noise term assumed to have zero mean and variance r^2 (K).

Let $x^*(K/K-1)$ denote the filtered estimate at time t_K after processing all observations through t_{K-1}, and $x^*(K)$ the filtered estimate at t_K after processing all observations through t_K. Assuming that the state estimate $x^*(K-1)$ has been computed, the predicted state estimate for the next measurement time t_K is computed by numerically integrating the trajectory model $\dot{x} = f(x)$ using a second order Taylor series integration procedure

$$x^*(K|K-1) = x^*(K-1)+f(x^*(K-1))\Delta t_K+J(x^*(K-1))f(x^*(K-1))(\frac{\Delta t}{2}_K)^2$$

where

$$\Delta t_K = t_K - t_{K-1}$$

and

$$J(x^*(K-1)) = \left[\frac{\partial f}{\partial x}\right]_{x^*(K-1)}$$

9×9

The covariance matrix of the predicted state estimate, which satisfies a matrix Ricatti differential equation between t_{K-1} and t_K, is computed by using a trapezoidal integration procedure. Let P^*_{K-1} denote the covariance of $x^*(K-1)$ and $P^*_{K/K-1}$ the covariance matrix of $x^*(K/K-1)$. Then we compute $P^*_{K/K-1}$ by

$$P^*_{K|K-1} = \Phi_K(P^*_{K-1}+.5Q\Delta t_K)\Phi_K^T+.5Q\Delta t_K$$

where

$$\Phi_K = I+J(x^*(K-1))\Delta t_K+J^2(x^*(K-1))\frac{(\Delta t_K)^2}{2}$$

and Q is the covariance of the additive state noise w.

The extended Kalman filter employs a matrix square root formulation of the covariance equations, see Ref. 1. WSMR has found that the square root formulation not only provides a numerically stable estimation procedure but it is computationally efficient as well. For the predicted covariance matrix $P^*_{K/K-1}$ computed above, the matrix square root $L_{K/K-1}$ such that

$$P^*_{K|K-1} = L_{K|K-1}L^T_{K|K-1}$$

is computed by means of Choleski decomposition:

For each scalar observation occurring at the new time t_K an updated state estimate and an updated square root of the covariance matrix are computed. Let $x^{*(i)}(K)$ denote the state estimate after processing the i^{th} scalar observation at t_K and let $L^{(i)}_K$ denote the square root of the covariance of $x^{*(i)}(K)$. These quantities are computed from

$$x^{*(i)}_{(K)} = x^{*(i-1)}_{(K)} + \frac{L^{(i-1)}_K L^{T(i-1)}_K H_i}{r_i^2(K)+H_i L^{(i-1)}_K L^{T(i-1)}_K H_i^T}\left(Z_i(K)-h_i(x^{*(i-1)}_{(K)})\right)$$

$$x^{*(0)}_{(K)} = x^*(K|K-1)$$

$i = 1, m = \#$ of observations at t_K

$$H_i = \left[\frac{\partial h_i(x)}{\partial x}\right] x^{*(i-1)}_{(k)} \qquad 1\times 9$$

$$L^{(i)}_K = L^{(i-1)}_K\left(I-\Theta_i L^{(i-1)}_K H_i^T H_i L^{(i-1)T}_K\right)$$

$$L^{(0)}_K = L_{K|K-1}$$

$$\theta i = \left[1 + \frac{r_i(K)}{(r_i^2(K)+H_i L_K^{(i-1)} L_K^{T(i-1)} H_i^T)^{1/2}}\right] \Bigg/ H_i L_K^{(i-1)} L_K^{T(i-1)} H_1^T$$

4.6.2.6 Measurement Bias Estimation

So far one of the most important considerations in the development of a BET program has not been discussed, namely, to account for the inconsistencies produced by bias errors in the measurements. There is a natural way of including bias terms in the extended Kalman filter; one merely adds an additional state variable for each bias term to be considered and forms the optimal estimate of the biases in the same way as for the trajectory state variables. This technique is fine for cases where there are only a few bias terms to be estimated. However, a typical application of the BET program has a large number of measurements involved. For example, a LANCE flight test might have two radars, 28 DOAVP receivers, eight fixed cameras, and eight cinetheodolites. Considering only one bias term per measurement this results in 66 additional state variables to be estimated. With a trajectory state dimension of nine we then would have to compute estimates for 75 state variables. An ordinary Kalman filtering program using 75 dimensional state vector is computationally prohibitive at the present time. Fortunately, Friedland has developed a decomposition technique for Kalman filters which WSMR was able to adapt and extend to the measurement bias estimation problem. The application of this decomposition procedure has resulted in a computationally feasible BET program which includes estimation of measurement biases.

The filter described previously will be called the zero bias filter and the estimates $x^*_{(K)}$ obtained from this filter the zero bias estimates. Let b denote a p-vector of bias terms. The previous measurement model is revised to include these terms.

$$z_i(K) = h_i(x(K)) + g_{i_{1xp}}^T(x(K))b + v_i(K)$$

Thus, one allows the bias of each measurement to be a linear function of several bias variables. For example, a model for the bias of a radar azimuth measurement might be

$$\Delta A = g^T b = b_1 + b_2 \tan E_0 \sin A_0 + b_3 \tan E_0 \cos A_0 + b_4 \tan E_0 + b_5 \sec E_0 + b_6 A_0$$

It is assumed that the constant dynamic model for the bias

$$b(K+1) = b(K)$$

Note that a state noise term is not included in the bias dynamics to account for the possible misassumption that the biases are constant. The reason for not including a state noise term will become evident later.

Now let the bias state vector b, be adjoined to the trajectory state x to form the augmented state vector y

$$y = \begin{bmatrix} x \\ b \end{bmatrix}_{(p+9)\times 1}$$

One could proceed directly and obtain a new extended Kalman filter giving the state estimate

$$\hat{y} = \begin{bmatrix} \hat{x} \\ \hat{b} \end{bmatrix}$$

However, as previously mentioned this is computationally prohibitive for large p. Instead the filter decomposition procedure developed by Friedland (Ref. 29) is employed. This procedure attempts to write the optimal estimate x, which includes the effect of biases, as

$$\hat{x}(K) = x^*(K) + T(K)\hat{b}(K)$$

where $x^*(K)$ is the zero-bias estimate already obtained and $T(K)$ is a $9 \times p$ matrix to be determined. Upon examination it is found that the decomposition holds if the filter satisfies certain restrictive conditions. The details of the derivation are tedious and will not be presented. The restriction imposed by the decomposition procedure is merely an assumption that has been already made:

The bias dynamics must not include a state noise term. This may not seem like much of a restriction since it was assumed to begin with, but this was hindsight. Indeed, this is a very severe restriction since the state noise covariance is used as an adjustable filter parameter to account for mismodelling errors. Fortunately, there is another way of accounting for mismodelling errors in the bias dynamics for which the decomposition does hold. Specifically, WSMR has been able to extend the decomposition (Ref. 30) procedure to the case of a failing memory Kalman filter in which deweighting of past observations is accomplished by exponentially weighting past residuals. We use small fading factors to account for bias mismodelling errors and use the state noise covariance of the zero-bias filter to account for trajectory mismodelling errors.

The form of the bias filter is almost identical to the zero bias filter with the residuals from the zero-bias filter forming the observations. Again square root formulation for the filter is employed. At a new observation time one has the prediction equations

$$\hat{b}(K|K-1) = \hat{b}(K-1)$$

$$C_b(K|K-1) = C_b(K-1)$$

$$T(K|K-1) = \Phi_K T(K-1)$$

where $C_b(K)$ is the square root of the covariance of $b(K)$, Φ_K is the transmition matrix from the zero-bias filter and $T(K)$ is the combining matrix of the decomposition (Ref. 31). For each observation $Z_i(K)$ at the new observation time new bias estimates $b^i(K)$ and the square root of its covariance $C_b^{(i)}(K)$ are computed from

$$\hat{b}^{(i)}(K) = \hat{b}^{(i-1)}_{(K)} + w_b^{(i)}(K)\left(r_i^*(K) - s_i^T(K) b^{(i-1)}_{(K)}\right)$$

where

$$r_i^*(K) = z_i(K) - h\left(x^{*(i-1)}_{(K)}\right) = \text{residual from zero bias filter}$$

and $w_b^{(i)}(K)$ is the vector Kalman gain given by

$$w_b^{(i)}(K) = \frac{C_b^{(i-1)}(K) C_b^{T(i-1)}(K) s_i(K)}{a_i^2(K) + s_i^T C_b^{(i-1)}(K) C_b^{T(i-1)}(K) s_i}$$

$$a_i^2(K) = r_i^2(K) + H_i L_K^{(i-1)} L_K^{T(i-1)} H_i^T = \text{variance of residual}$$

$$s_i^T = g_i^T\left(x^{*(i-1)}_{(K)}\right) + H_i T_{i-1}(K)$$

$i = 1$, $m = \#$ observations at T_K

The square root of the covariance matrix is updated at an observation by

$$C_b^{(i)}(K) = C_b^{(i-1)}(K)\left(I - \theta_i C_b^{(i-1)}(K) s_i(K) s_i^T(K) C_b^{(i-1)}(K)\right)$$

$$\theta_i = \left[1 + \frac{a_i}{\left(a_i^2 + s_i^T C_b^{(i-1)}(k) C_b^{T(i-1)}(K) s_i(K)\right)^{1/2}}\right] \Bigg/ s_i^T(K) C_b^{(i-1)}(K) C_b^{T(i-1)}(K) s_i(K)$$

For each measurement the combining matrix is updated according to

$$T_i(K) = T_{i-1}(K) - w_b^{(i)} s_i^T(K)$$

$$T(K) = T_m(K)$$

$$T_0(K) = T(K|K-1)$$

Where $w_b^{(i)}(K)$ is the vector gain from the zero-bias filter.

The optimal state estimate $\hat{x}^{(i)}(K)$ is computed as

$$\hat{x}^{(i)}(K) = x^{*(i)}(K) + T_i(K)\hat{b}^{(i)}(K)$$

To modify the above equations for the fading memory filter, first choose a fading factor $\alpha_K \geq 1$. The above equations are then replaced by

$$C_b(K|K-1) = \alpha_K C_b(K-1)$$

$$P^*(K|K-1) = \Phi_K(\alpha_K{}^2 P^*(K-1)+.5Q\Delta T_K)\Phi_K^T+.5Q\Delta T_K$$

Where $w^{*(1)}(K)$ is the vector gain from the zero-bias filter.

The optimal state estimate $\hat{X}^{(1)}(K)$ is computed as

To modify the above equations for the fading memory filter, first choose a fading factor $\alpha_K \geq 1$. The above equations are then replaced by

4.6.2.7 Computation of Observation Variances

For each of the scalar measurements Zi(K) a measurement noise variance $ri^2(K)$ must be available for use by the Kalman filter. Several possibilities exist for supplying the variance. An immediately obvious method is use the variance values given in specifications of the instrument or to use variance values computed from past performance history of the instrument. These methods are most useful when the measurement variance is stable from day to day and mission to mission. Another method which is often used is to compute variances from measurement residuals

$$p_i(K) = r_i^*(K)-a_i^T(K)\hat{b}_i(K-1)$$

produced in the BET program. A method for computing variances from the residuals which is economical in both computing time and storage is the fading memory variance estimate defined by the following equations

$$\bar{p}_i(n) = \bar{p}_i(n-1) + \frac{\left(p_i(n)-\bar{p}_i(n-1)\right)}{P_n}$$

$$P_n = 1 + wP_{n-1},\ P_1 = 1$$

$$S_i(n) = wS_i(n-1)+\left(1-\frac{1}{P_n}\right)(p_i(n)-\bar{p}_i(n-1))^2$$

$$F_n = P_n-H_n/P_n$$

$$H_n = 1+w^2H_{n-1},\ H_1 = 1$$

$$\theta_i{}^2(n) = \frac{S_i(n)}{F_n}$$

In the above $\bar{p}_i(n)$ is the estimate of the residual mean, w, $0 \leq w \leq 1$ is a fading factor, and $\hat{\sigma}_i^2(n)$ is the variance estimate for the i^{th} measurement.

An optional approach to the estimation of the measurement variance is the fading memory variable difference technique, see Ref. 3. Let $y_i(n)$ be the k^{th} backward difference of the observation Z_i. If one assumes the mean of the K^{th} differences are zero the following equations define the fading memory variate difference method

$$S_i(n) = wS_i(n-1)+y_i^2(n)$$

$$F_n = wF_{n-1}+\binom{2K}{K}$$

$$\theta_i^2(n) = \frac{S_i(n)}{F_n}$$

SECTION V

REFERENCES

1. Final Report, 621B User Equipment Definition and Experiment Program Phase I, Vol. IV, SAMSO TR 70-440, Dec. 1970.

2. Ackerman, R., Hraban, S., and Kadar, I., "An Annotated Description of the System 621B Navigation Algorithms and the Two State Kalman Filter", Grumman IOM Number 621B-181, Feb. 28, 1972.

3. Technical Report, SAMSO-TR-72-213, Dec. 1972.

4. Operating and Maintenance Manuals for 621B Experimental Equipment, Vol. II, III and IV.

5. Operating and Maintenance Manuals for 621B Experimental Equipment, Vol. V and VI.

6. Introduction to White Sands Missile Range, White Sands Missile Range, New Mexico 88002, Apr. 1, 1968.

7. California Bearing Ratio Tests, Conducted at Northrop Strip, 1972, and Report No. AFWL-TR-66-148, Landing Site Evaluations, Appendix 1, Site 81, White Sands, N. M., L. M Womack and J. T. Lewis, Feb. 1967.

8. Operation Requirement 621B User Equipment Tests and Demonstrations 49201 through 49208,

9. 621B Ground Transmitter Site Survey Requirements for System Demonstration Tests, 621B-158, M. Neglia.

10. 621B Program Antenna Points for Salt Site, Survey No. 189-72, Mr. Beckett/ SY/3718, Feb. 24, 1972.

11. 621B Program Antenna Points for EC-50 Site, Survey No. 116-72, Mr. Beckett/ SY/3718, Feb. 24, 1972.

12. 621B Program Antenna Points for Bomb Site, Survey No. 190-72, Mr. Beckett/ SY/3718, Feb. 24, 1972.

13. 621B Program Antenna Points for WC-50 Site, Survey No. 185-72, Mr. Beckett/ SY/3718, March 6, 1972.

14. 621B Program Antenna Points for Corner Site, Survey No. 184-72, Mr. Beckett/ SY/3718, Feb. 24, 1972.

15. Coordinate Systems Related to WSMR, Data Reduction Division, WSMR New Mexico, July 1964.

16. Comprehensive Survey Report for 621B, No. 700-72, Mr. Beckett/SY 3718, September 15, 1972.

17. Survey Data for 621B Program, Survey No. 829-72, Mr. Beckett/SY/3718, Oct. 20, 1972.

18. Re-Survey of 621B Program Antenna Points, Survey No. 610-72, Mr. Beckett/SY/3718, August 15, 1972.

19. Antenna Height Selection for the Calibration Links, GAC IOM - 621B-73 Apr. 20, 1971 Kadar, I.

20. General Test Plan, 621B, June 11, 1971.

21. Cox, James M. Dayton Municipal Airport ILS RWY6L CAT II Approach Plate Dayton, Ohio.

22. Fried, W.R. and Kayton, M., "Avionics Navigation Systems", Chapter 14, 1969 John Wiley & Sons Inc.

23. 621B Utilization of an Optical Landing System for Repeatable Glide Slope Trajectories, 621B-61 March 23 1971, M.S. Moore.

24. The WSMR Best Estimate of Trajectory - An Overview, Internal Memorandum No. 129, January 1972, prepared by Data Reduction Division, Math Services Branch, White Sands Missile Range, New Mexico, 88002.

25. 621B Software Documentation Library, Grumman IOM Number FAD-07-711-IOM-72-12, April 26, 1972, Richards, P. et al.

26. Richards, P., "The Variate Difference Method of Variance Estimation with Application to 621B Trajectory Data", Grumman Systems Flight Test Technical Report Number SFT-TCR-71-4, October 8 1971.

27. "Richards, P., "Two State Bias Filter Implementation for 621B Flight Test Program", Grumman Systems Flight Test Technical Report Number SFT-TCR-72-2.

28. Agee, Wm. S., "Matrix Square Root Formulation of the Kalman Filter Covariance Equations", The Office of the Chief of Research and Development, Durham, N.C., ARO-D Report 70-1.

29. Fridland, Bernard "Treatment of Bias in Recursive Equations", IEEE Transactions on Control, Oct. 68.

30. Agee, Wm. S., "Exponentially Weighted Variate Differences (A Technique for Real Time Variance Estimator)", WSMR, NM, STEWS-NR-AM, 27 Aug. 70. Technical Report No. 16.

31. Martinez, R. S., Peters, G., Wilkinson, J. H., "Symmetric Decomposition of Positive Definite Matrix", Numerische Mathematik, Bund 7, p. 362-383, 1965.

32. Kadar, I. and Richards P. "621B Best Estimate Trajectory Errors", Grumman Inter-Office Memorandum Number 621B-188 dated June 7, 1972.

33. P. Richards, "Deterministic Navigation Software for System 621B Field Tests", FAD-SFT-TN-71-1, 29 February 1972.

34. I. Kadar, "A Note on the 621B Navigation Algorithm", GAC IOM 621B-176, 2 February 1972.

35. I. Kadar, "Bias Shift Sensitivity of Navigator Position", GAC IOM 621B-184, 20 April 1972.

36. Theory and Applications of Kalman Filtering, AGARDograph 139, Edited by C. T. Leondes, February 1970.

37. I. Kadar, "General Signal Design and Systems Considerations for Navigation Satellites and Links", RFR, 1972.

38. P. Beckmann and A. Spizzichino, The Scattering of Electromagnetic Waves from Rough Surfaces, Pergamon Press 1963.

39. Christensen, R., Capt USAF (Staff Met.), "Index of Refraction Variability at White Sands Missile Range, New Mexico, in Support of Project 621B", 6585th Test Group, Holloman Air Force Base, N. M. July 1, 1972.

40. U. S. Army Manual, CCTM 105-50, Part 3.

41. K. Bullington, "Radio Propagation Fundamentals", Bell Laboratories Report, 1956.

42. A. Papoulis, Systems and Transforms With Applications in Optics, McGraw Hill, 1965.

43. A. G. Longley and P. L. Rice, "Prediction of Tropospheric Radio Transmission Loss Over Irregular Terrain", ESSA, ERL 79-ITS67, July 1968.

44. I. Kadar, "Ground User Multipath Test Procedure for 621B Experiment Program", GAC Report 621B-TP-5, July 1971.

45. J. R. Lundien, "Terrain Analysis by Electromagnetic Means", Technical Report No. 3-693, U. S. Army Material Command, Sept. 1966.

46. Final Report - System 621B User Equipment Definition and Equipment Program, Phase I, Vols. I, II, III, & IV, SAMSO TR70-440, Dec. 1970.

47. R. H. Ott and G. A. Schlak, "Backscattering from Rough Terrain", ESSA RL 60-ITS 57, Sept. 1967.

48. S. H. Durrain and H. Staras, "Multipath Problems in Communications Between Low Altitude Spacecraft and Stationary Satellites", RCA Review, May 1968.

49. A. B. Glenn, "Fading From Irregular Surfaces for Line-Of-Sight Communications", IEE Trans. on AES, Vol. AES 4, Mar. 1968.

Security Classification

DOCUMENT CONTROL DATA - R & D

(Security classification of title, body of abstract and indexing annotation must be entered when the overall report is classified)

1. ORIGINATING ACTIVITY (Corporate author)	2a. REPORT SECURITY CLASSIFICATION
Grumman Aerospace Corporation Bethpage, New York, 11714	UNCLASSIFIED 2b. GROUP

3. REPORT TITLE

FINAL REPORT, SYSTEM 621B USER EQUIPMENT DEFINITION AND EXPERIMENTS PROGRAM, PHASE II FIELD TESTS.

4. DESCRIPTIVE NOTES (Type of report and inclusive dates)

FINAL REPORT 11 Jan 1971 to 11 April 1973

5. AUTHOR(S) (First name, middle initial, last name)

John J. Courtney, Jr. — Paul Richards — Robert Regis (HC)
Ralph Laho — Michael Moore — Bert Glazer (MRL)
Ivan Kadar — Michael Neglia

6. REPORT DATE	7a. TOTAL NO. OF PAGES	7b. NO. OF REFS
11 April 1973		

8a. CONTRACT OR GRANT NO	9a. ORIGINATOR'S REPORT NUMBER(S)
FO 4701-71-C0176 b. PROJECT NO. SYSTEM 621B c. d.	Vol. I. - None Vol. II. - None Vol. III. - None 9b. OTHER REPORT NO(S) (Any other numbers that may be assigned this report) SAMSO TR 73-65

10. DISTRIBUTION STATEMENT

Distribution limited to U. S. Government Agencies only; Test and Evaluation, February 1973. Other requests for this document must be referred to HQ SAMSO/XRN.

11. SUPPLEMENTARY NOTES	12. SPONSORING MILITARY ACTIVITY
The distribution of this report is limited because it contains technology requiring disclosure only within the Department of Defense.	Space and Missile System Organization (XRLO) P.O. Box 92960, Worldway Postal Center Los Angeles, California, 90009

13. ABSTRACT

System 621B is a concept for a global satellite - based precision navigation system designed to meet the requirements of land, sea and air military forces in an advantageous cost effective manner. One of the most important elements in this system is the user receiver. This report summarizes a series of flight and ground tests conducted at the White Sands Missile Range to evaluate the performance of a four-channel receiver in typical flight and field environments in order to solidify confidence in the predicted performance of System 621B receivers.

DD FORM 1 NOV 68 1473

Security Classification

14. KEY WORDS	LINK A		LINK B		LINK C	
	ROLE	WT	ROLE	WT	ROLE	WT
Receiver Test						
Flight Test of Navigation Receiver						
Ground Equipment for Receiver Test						
Flight Test Data Processing						
Airborne Installation						
Antenna Design and Installation						
Flight Test Data Analysis						
Multipath Testing						